UNIVERSITÀ DELLA CALABRIA

Università degli Studi della Calabria

Dipartimento di Farmacia e Scienze della Salute e della Nutrizione

Dottorato di ricerca in "Medicina Traslazionale"

XXIX ciclo

Development, accreditation and application of a confirmatory method for the determination of mercury in biological matrices: results of a human biomonitoring study.

Settore scientifico: BIO/13

Coordinatore:
Ch.mo Prof. Sebastiano Andò

Tutor
Prof. Vincenzo Pezzi

Dottorando
Dott. Francesco Domanico

TABLE OF CONTENTS

<u>Determination of mercury through TDA-AAS TECHNIQUE for Human Biomonitoring activity.</u>

RATIONALE

During the first part of my PhD program, carried out in the "Biologia Cellulare ed Applicata" laboratory of University of Calabria directed by Prof. Vincenzo Pezzi, investigated the role of functional cross-talk between IGF - II / IGF1R and estrogen receptors in Adrenocortical Carcinoma (ACC) growth. In particular the role of G Protein Coupled Estrogen Receptor (GPER) in ACC growth. In the second part of the program I was included in the project of the Ministry of Health "Osservatorio per l'ILVA" through a partnership concluded between University of Calabria and National Institute for Health (ISS) in Rome. We developed and credited an analytical method for the determination of mercury through the TDA-AAS technique (Thermal Decomposition Amalgamation Atomic Absorption Spectrometry). This method used a mercury direct automatic analyzer DMA-80TRICELL (Srl Milestone, Sorisole, Italy) and it was applied for Human Biomonitoring activity expected by project.

GPER agonist G-1 decreases adrenocortical carcinoma (ACC) cell growth in vitro and in vivo

ACC is a very rare tumor accounting for 0.7-2.0 cases/million people per year with an increased incidence in the first and fourth-fifth decades of life. By gender, females are the most affected (55-60%) (Else et al., 2014). The cornerstones in the pathogenesis of ACC are considered to be the genetic alterations of the IGF-2, p53 and β-catenin molecular pathways (Barlaskar et al., 2007; Ragazzon et al., 2011). More than 85% of ACC showed allelic losses (LOH) at the TP53 locus (17p13)(Bertherat and Bertagna 2009). Additionally, other genes, such as ZNFR3, identified by a genome-wide study, appear potentially involved in the tumorigenesis of ACC (Assié et al., 2014).

Most frequently genetic alterations (90 % of cases) (Barlaskar et al. 2008) associated to ACC is the loss of region imprinted on locus 11p15 resulting in excess of insulin growth factor II (IGFII) expression. IGFII effects are mediated through its receptor IGF1R resulting in activation of the PI3K/AKT/mTOR cascade, the RAS/MAPK and the PLC/PKC pathways (Pollak, 2008), this demonstrate the important role of IGF system in ACC. However, Adrenocortical cancer is a disease extremely heterogeneous and this new pharmacological approach could not be enough for the therapy of all forms of ACC. To improve diagnosis, prognostic evaluation and treatment of different types of tumours is important understand the pathophysiology. Professor Pezzi's group have demonstrated that ACCs are characterized by ERα up-regulation and aromatase (the enzyme

involved in the production of estrogens using androgens as substrate) over-expression (Barzon et al 2008). They highlight that estradiol improves proliferation in cell line H295R, whereas antiestrogens upregulate ERβ and inhibit ACC cell growth (Montanaro et al., 2005). It is known that tamoxifen and its metabolite 4-hydroxytamoxifen not only exercise antiestrogenic activity. OHT, in fact, is able to modulate the downstream pathway of GPR30 (Montanaro et al., 2005; Vivacqua et al., 2006a). This receptor, when activated by OHT, mean rapid molecular signaling of non-genomic type similar to those induced by estradiol (Lappano et al.,. 2013; Prossnitz et al., 2009; Vivacquaet al., 2006a.) which include the mobilization of intracellular Ca^{2+}, stores and activation of mitogens activated protein kinase (MAPK) and the involvement of pathway-responsive of phosphoinositide 3-kinase (PI3K) (Prossnitz et al., 2009; Ariazi et al., 2010). GPER can modulate growth of hormonally responsive cancer cells (Vivacqua, et al.,2006b) and it exhibits prognostic utility in endometrial (Smith et al., 2007), ovarian (Smith et al., 2009), and breast cancer (Filardo et al., 2006). A non-steroidal, high-affinity GPER agonist G-1 (1-[4-(6-bromobenzo [1, 3]dioxol-5yl)-3a, 4, 5, 9b-tetrahydro-3H-cyclopenta-[c]quinolin-8-yl]-ethanone) has been used to distinguish GPER-mediated estrogen responses from those mediated by classic estrogen receptors (Bologa et al., 2006)). G-1 biological effects appear cell type specific and dependent on the ERs expression pattern (Chimentoet al. 2013a; Chimento et al., 2013b; Chimento et al.2012; Chimento et al., 2010; Chimentoet al., 2011). Using G-1, we investigated the role of GPER activation on ACC growth.

Determination of mercury through TDA-AAS TECHNIQUE for Human Biomonitoring activity

Mercury (Hg) is a dangerous heavy metal and its presence in the environment and in the human food chain is a matter of increasing concern. Metallic mercury is liquid at room temperature but mercury vapor are more dangerous than liquid form. Hg bind different elements forming inorganic mercureos compounds (Hg^+) or mercuric compounds ($Hg2^+$). In this way Hg moves in to the environment following the normal breakdown of minerals in rocks and soil due to exposure to wind and water, natural degassing of the earth's crust, evaporation of the oceans and volcanic activity (Hsiao et al., 2011; Sun et al., 2013). A good part of this metal derived from anthropogenic sources increased by human activities since the start of the industrial era (Mohmand et al., 2015).Among these are included the emissions derived from gold mining and the fusion of metals (gold, copper, zinc), coal combustion, incinerators and chlor-alkali industries. Existing three forms of this metal: organic, mostly as methyl-mercury (MeHg), inorganic and elemental. MeHg enters the food chain

through fish who takes it through the plankton. This biomagnification determines human exposure to the metal through the consumption of this type of products. The general population may be result exposed to mercury through diet, through the work (occupationally exposure) and in accidental way with medical equipment and amalgam fillings (accidentally exposure). Mercury is toxic and have not physiologic function in human body. Acute and chronic exposure to Hg can rise a wide range of effects, e.g., inattention, memory disturbance, learning problems, impairment of social behaviour, low intelligence quotient and other serious health consequences (Stein et al., 2002). Mercury vapor at high concentration inhalation may cause corrosive bronchitis and acute interstitial pneumonia with following clinical symptoms: neurasthenia, tremor, increased swelling of the thyroid and uptake of iodine, gingivitis tachycardia, hematological disorders and increased urinary excretion of the metal. Regarding to inorganic mercury the kidney is the main target organ. High doses of the metal are toxic for cells of the renal tubules, while, low doses chronic exposure can induce glomerular immunological pathology. Exposed can subjects show a reversible proteinuria.

In human the principal problems of MeHg exposure is the neurotoxicity. Methyl-mercury, in fact, is able to crossing blood–brain barrier by an amino acid carrier and readily accumulates in the brain (Kerper et al., 1992) as well as it is able to cross the placenta and accumulates in fetal blood and brain. Clinical manifestation include paresthesia, ataxia, neurasthenia loss of sight and hearing, tremor and difficulty in speaking. Toxicity can even lead to death as a result of cerebral edema with destruction of the gray matter and gliosis determined by brain atrophy. The high affinity of the divalent mercury for sulfhydryl groups of proteins is a major mechanism of damage non-specific and / or cell death. They are, however, involved more general mechanisms like neurotransmitter production and secretion, uptake and metabolism, cell signaling, protein, DNA and RNA synthesis, respiratory and energy-generating systems, the neuronal migration, cell division and the formation of microtubules (Castoldi et al., 2001; Clarkson et al., 1993; WHO, 1990). MeHg characteristics in term of biomagnification, ability to enter in food chain and its toxicokinetics make this species the most dangerous for human health. To quantified MeHg in the subjects we used as biomarker the hair. This choice was made because sulfur-containing proteins rich in the hair bind to MeHg (WHO, 1990). Once incorporated, Hg does not return to the blood, thus, it provides a good long-term marker of exposure. Moreover, hair is a biological specimen that is easily and noninvasively collected, with minimal cost, and it is easily stored and transported to the laboratory for analysis.

Mercury concentration is generally evaluated by different techniques such as the cold vapor atomic fluorescence spectroscopy (CV-AFS) (Adlnasab et al., 2014.; Brombach et al., 2015; Aranda et al., 2009), cold vapor atomic absorption spectroscopy (CV-AAS) (Balarama Khrisna and Karunasagar, 2015), inductively coupled plasma atomic emission spectrometry (ICP-AES) (Bidari et al., 2012)

and inductively coupled plasma mass spectrometry (ICP-MS) (Lin et al., 2015). All these techniques are sensitive, precise and supply reliable and reproducible data but involving pretreatment sample with contamination risk. The use of the thermal decomposition amalgamation atomic absorption spectrometry (TDA-AAS) allows to decrease the preparative steps number and contamination risk, in addition to this, it reduce the time and cost of analysis. In this context, a TDA-AAS instrument was adopted, in according to US-EPA 7473 method. This is a certified method containing general information on how to perform an analytical procedure or technique which a laboratory can use as a basic starting point for generating its own detailed standard operating procedure (SOP). It was created a confirmatory method based on EPA7473 to satisfy the requirements of quality system (UNI CEI EN ISO / IEC 17025). They were conducted tests in order to assess the performance qualities as regards repeatability, accuracy, limit of detection and quantification (LoD and LoQ). Furthermore to respect UNI CEI EN ISO / IEC 17025 we identified all the components of uncertainty and further provided a reasonable estimate of their contribution.

Then we used this confirmatory method in population study, involved 300 healthy individuals living in an urban area of South Italy, for the determination of Hg in hair and urine using a Direct Mercury Analyzer® (DMA-80 Tricell; Milestone Inc., Italy). Our population study is a part of the biomonitoring campaign planned by the Ministry of Health in the project "Osservatorio per l'ILVA".

GPER agonist G-1 decreases adrenocortical carcinoma (ACC) cell growth in vitro and in vivo

Background

Adrenocortical cancers

ACC is a neoplastic disease with a poor prognosis. Current studies in this field have indicated the need for a multidisciplinary approach in the management of this tumor (Creemers et al., 2016; Stigliano et al., 2016). Surgery remains the most effective treatment choice for the primary tumor or for the removal of isolated metastases (Else et al ., 2014; Crucitti et al., 1996). The experience that at least one-third of patients show loco-regional recurrence or distant metastases even after a radical surgical excision introduced the concept of adjuvant therapy in these patients (Donatini et al., 2014). Despite an extensive surgical resection, the survival rate of these patients is estimated as ~50% after 5 years (Vaughan, 2004). Although these data support the need for an adjuvant cancer therapy. At present, mitotane represents the only drug approved in Europe and in the United States for ACC treatment; but opinions regarding its use are still highly discordant (Huang and Fojo, 2008). Tumors that originate from the adrenal cortex can be divided into benign adenomas and malignant adenocarcinomas that can be associated to an endocrine component (Allolio and Fassnacht, 2006). ACC in fact can be asymptomatic, it can be manifest with a mass (Brennan, 1987) or it can be characterized by endocrine syndrome. Generally ACC presented an immature steroidogenesis with hormonal precursor excess but, 60% of all ACC patients presented signs and symptoms ("functional tumors")(Schulick and Brennan, 1999a; Schulick and Brennan, 1999b) related to type of hormone produced in excess:

• Cushing's syndrome, caused by hypersecretion of cortisol;

• Conn's syndrome, caused by aldosterone hypersecretion;

• hirsutism and virilization, caused by hypersecretion of androgens

Obliviously it is clear that differential diagnosis between adrenocortical adenoma and ACC is of crucial clinical relevance, because the prognosis and clinical management of benign and malignant adrenocortical tumors is entirely different. It is very difficult to establish malignancy adrenal tumors based on its size with the available imaging techniques. Currently in use guidelines recommended to remove adrenal tumors with a diameter of >6 cm, because they presented a risk of malignancy >25% (Aron et al., 2012). Hormonal features can also be used in diagnosis, for example recent data using urinary steroid hormone metabolomics showed characteristic patterns of steroid secretion and metabolism in ACC samples (Arltet al., 2011). Novel markers of malignancy are intensively searched using bioinformatics approaches to define an early and specific differential diagnosis between ACC and ACA since the histological diagnosis of malignancy is often difficult (Patalano et al., 2009).

Epidemiology

ACC is a rare solid tumor (Kebebew et al., 2006; Wajchenberg et al., 2000) with an incidence of 1–2 per million population (Allolioet al., 2003; Dackiw et al., 2001; Wajchenberg et al., 2000) as opposed to adrenal incidentalomas that have a prevalence of at least 3% in a population >50 years of age (ACC constitute <5% of all adrenal incidentalomas) (Barzon et al., 2003; Bovioet al., 2006; Grumbach et al., 2003; Mansmann et al., 2004; Song et al., 2007). ACC affects women more commonly than men with a ratio of 1.5:1 (Bilimoria et al., 2008; Dy, 2013; Koschkeret al., 2006; Roman, 2006; Wooten and King, 1993). Females with ACC are more likely to have functional tumors while men with ACC have bimodal age distribution, with a first peak in childhood (<5 years) and a second higher peak in the fourth and fifth decades with non-functional tumors (Brennan, 1987; Cohn et al., 1986; Koschker et al., 2006; Schulick and Brennan, 1999; Wajchenberg et al., 2000).

Adrenocortical adenoma

The adrenocortical adenoma is a benign neoplasm of adrenal cortical cells. The type of hormone secreted influenced the dimensions:

- adenoma with hyperaldosteronism is usually unilateral and of yellowish color, around 1.5 cm of size and is not encapsulated;
- adenoma with hypercortisolism is unilateral, has dimensions of about 4 cm, is yellow-brown and is encapsulated;
- adenoma with virilization is unilateral, has dimensions of about 5 cm, is red-brown and is encapsulated.

The color of the tumour is due to the stored lipid (mainly cholesterol), from which the cortical hormones are synthesized. The adrenocortical adenoma can present with primary aldosteronism (overproduction of the aldosterone by the adrenal gland) or Cushing's syndrome (signs and symptoms associated to exposure to high levels of cortisol). Only a very small percentage of these tumors leads to Cushing's syndrome, in fact, most of they are casually findings at post mortem examination commonly; Most adrenocortical adenomas produced no significant metabolic disorder.

Adrenocortical carcinoma

ACC is a rare and highly aggressive tumor. We can histologically distinguish: solid or trabecular areas with fibrous bands interposed between the tumor nodules, necrosis, the presence of large cells with vacuolated cytoplasm, nucleus atypical and hyperchromatic, prominent nucleoli, frequent mitosis, vascular and capsular invasion. It is highly aggressive: about 60% of patients have

metastases at diagnosis, with a 5-year survival rate of 8% for recurrent and inoperable disease. In the case of endocrine cancer, it is associated with Cushing's syndrome. The therapeutic approach of choice for adrenocortical carcinoma is surgery conducted only after appropriate preoperative diagnostic tests, including biochemical evaluation and imaging. Suspicious features to consider for ACC are: tumors size >4 cm, functional tumor, radiologic characteristics. Surgery however is not always practicable, for example the case in which the tumor was strongly adherent to the kidney, such as to look like a single mass, although histological examination has then denied the spread to the renal parenchyma. The case in which the surgery resection is not possible or not satisfactory a chemotherapeutic treatment was associated to operation (Fig.1). The recommended first-line cytotoxic treatment regimens are etoposide, doxorubicin, cisplatin plus mitotane (Berruti et al., 2005), or streptozotocin plus mitotane (Khan et al., 2000).
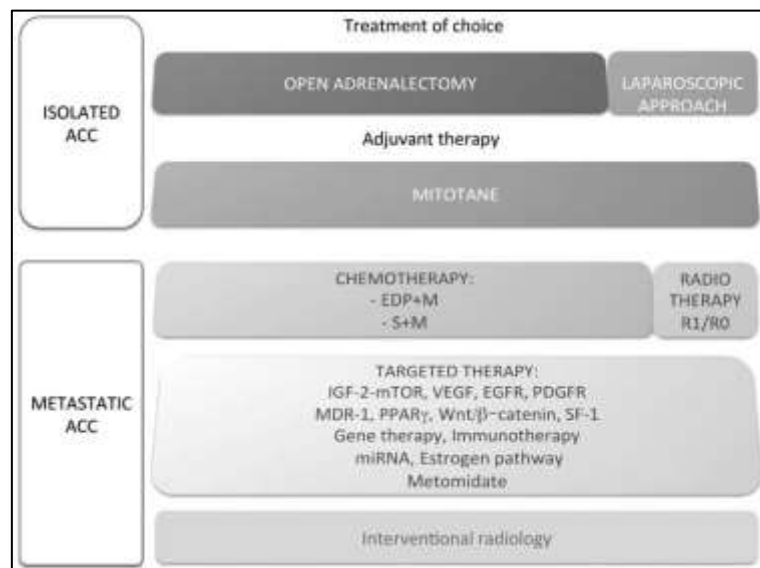
Figure 1 Treatments and molecular targets in isolated cortical carcinoma and metastatic (ACC)

 Mitotane are the only drug approved by the U.S. Food and Drug Administration and European Medicine Executive Agency for treatment of ACC (Schteingart et al., 2005). Mitotane is a derivative of the insecticide dichlorodiphenyldichloroethane (DDT) with adrenolytic and cytotoxic activity toward the fasciculata and reticularis adrenal areas. It inhibits steroidogenic pathways acting mainly at the level of the cholesterol side chain cleavage enzymes CYP11A1 and CYP11B1 (Lin et al., 2012; Lehmann et al., 2013). Mitotane metabolites (o',p-DDA and o',p- DDE, respectively) are the products of a hydroxylation that occurs in the liver and of which o',p-DDA represents the active form (van Slooten et al., 1984). It has indeed been shown, that o',p-DDA measurements reflect the mitotane response in treated patients (Hermsen et al., 2011). In most patients mitotane abolish steroid secretion but, since uninhibited hormone secretion might worsen

significantly quality of life and may even be life threatening. For its action the mitotane treatment required an endocrine symptoms control, with adrenostatic drugs (metyrapone, etomidate). Is required also a follow-up, that is repeated every 3 months for the first two years, including abdominal CT or MRI and hormonal markers, and kept on for at least 10 yr. Treatments with cisplatin and etoposide in combination with mitotane are placed among the most active for in advanced cancer. Several inhibitors of steroidogenesis were used to control deleterious effects of elevated hormone levels in ACC patients. During treatment with any of the steroidogenesis inhibitors, patients need to be regularly evaluated for adrenal insufficiency and should be regarded as adrenal-insufficient in times of physical stress (febrile illness or significant injury/surgery). Inhibition of steroidogenic pathway and adrenolytic effects are involved in control of hormone levels caused by Mitotane treatment. Usually ketoconazole and metyrapone are used to control glucocorticoid excess. Ketoconazole inhibits CYP17A1, CYP11A1, and also CYP11B1. During treatment with ketoconazole, are recommended monitoring of liver enzymes because it is an inhibitor of different hepatic drug metabolizing enzymes (eg, CYP3A4, CYP2C9, and CYP1A2) of which it could be altered the drug interaction. Another powerful steroidogenesis inhibitor at the level of CYP11B1 is metyrapone (Hartzband et al., 1988) that through inhibition of CYP11B1, increases adrenal androgens levels with worsening symptoms related to hyperandrogenemia. In subject with androgen-secreting tumors and mineralocorticoid- secreting tumors spironolactone can be used to control the effect on hormones. As with other malignancies, local control of ACC is important for effecting disease cure and for improving symptomatic outcomes. Furthermore radiotherapy, that usually was considered ineffective, have demonstrated in several recent studies to offer a significant improvement in disease control in both the adjuvant and palliative settings (Fassnacht et al., 2006; Hermsen et al., 2010). These improvement unfortunately has not been universally demonstrated (Habra et al., 2013). In recent years, considerable advances toward understanding the pathogenesis of ACT have been made using different strategies :

1.   Identification of genetic alterations in rare familial syndromes and evaluation of whether the same defects are present in sporadic tumors.

2.   Investigation of signaling pathways that were proved important in other tumors types.

3.   Employment of high-throughput techniques such as genome wide expression profiling, methylation profiling and microRNA profiling to interrogate novel signaling pathways.

4.   Studies with animal models with one or more genetic defects in known signaling pathways

Pathogenesis

The molecular mechanisms involved in adrenocortical tumorogenesis are still under study beacuse poorly understood. Recent study are focused on alterations of insuline-like growth factor (IGF) system associated with these tumors. Most common alteration (90% of malignant adrenocortical tumors) is in the 11p15 region, that contain the IGF-II gene maps (Gicquel et al., 2001) (Figure 2) The tumors with these abnormalities exhibit strong overexpression of IGF-II gene (Csernus et al., 1999) and large amounts of IGF-II protein (Gicquel et al., 2001; Listrat et al., 1999). In particular, in ACC, it possible note a overproduction of The type 1 IGF receptor (Janssen et al., 1997; Wolf et al., 1997) and the IGF-binding protein-2 (IGFB-2) (Boulle et al., 1998) These evidence show the involvement of the IGF system in adrenocortical tumor progression. The IGF system comprises numerous elements such as IGFs, IGF-I and IGF-II, small polypeptides produced in various tissues.
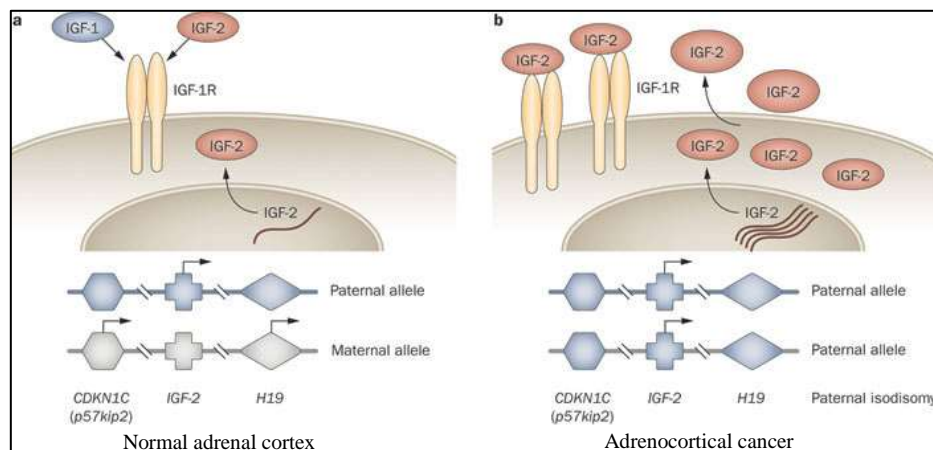
Fig. 2. Alterations of 11p15 locus and insulin-like growth factor II (IGF-II) over-expression in adrenocortical cancer (ACC)

This system have endocrine and auto/paracrine modes of action (Gockerman et al., 1995). Type IGF-I receptor mediates most effects of the IGFs while IGF-II/mannose-6-phosphate (IGF-II M6P) have a function of internalization and degradation of IGF-II (Clemmons et al., 1995; Gockerman et al., 1995). Both IGF-I both IGF-II can bind with high affinity IGFBPs that modulate positively or negatively the effects of IGFs depending on their abundance, their affinity for the growth factors and their cellular localization. Different study confirm the involvement of IGF-II in tumorogenesis of Wilms' tumors, hepatomas, colon carcinomas and pheochromocytomas (Karnieli et al., 1996) and in the same way IGF-II may also be involved in adrenocortical tumors.

Another mutation more frequently in adrenocortical carcinoma was detected on p53 gene (McNicol et al., 1997). Moreover, germ line mutations of p53 predispose to childhood adrenocortical cancer (Sameshima et al., 1992) (Wagner et al., 1994).These mutation were found more frequently also in other malignant tumors (Reinke V, 1997).

Another metabolic pathway involved Wnt-signaling that has recently been identified as a regulator of different endocrine functions. Wnt proteins are secreted glycoproteins that bind to the N-terminal extra-cellular cysteine-rich domain of the Frizzled (Fz) receptor family and to lipoprotein receptor-related protein (LRP) co-receptors (low density LRP). Frizzled receptors are G-protein-coupled seven-transmembrane receptors. It was possible distinguishes canonical (i.e. beta-catenin) and non-canonical Wnt-signaling based on the involvement of the transcriptional co-activator beta-catenin. Wnt Binding to both receptors activates the canonical Wnt-signaling pathway. Wnt, in fact, by binding a complex containing adenomatous polyposis coli (APC) and axin determine an inhibition of glycogen synthase kinase-3 (GSK3B) with stabilization of β-catenin. Subsequently, β-catenin, a transcriptional co-activator, translocates to the nucleus to activate T-cell factor (TCF)/lymphoid enhancer factor (LEF) transcription factors on canonical Wnt target-genes.

Furthermore a mutation involved in the inactivation of the type 1 MEN1 germline is found in approximately 90% of families with multiple endocrine neoplasia type 1 (MEN1) of these 25-40% presents adrenocortical tumors and / or hyperplasia (Kjellman et al., 1999a; Yano et al., 1989)

The mutation of MEN1 gene is very rare in ACC (Wales MM, 1995; Yano et al., 1989), opposed to hyperplasia that was found in patients with MEN1 who have hypersecretion of ACTH (Cushing's syndrome).

Role of ERα and ERβ activation on tumor development

A correlation between estrogen and tumor development was been suggested by epidemiological evidence and experimental studies. Adrenal tumors, in particular those secreting, are more frequent in women and the use of estrogen-progestin would seem to be a risk factor for tumor development. The presence of a cross-talk has been reported between the IGF system and estrogens in several tumoral cells. Both estrogens both IGF system are able to activate the same pathway through the action of estrogen receptors (Hamelers and Steenbergh, 2003). It has been largely demonstrated that the effects of estrogens are mediated by the ERα and ERβ, which act as transcription factors (Nilsson et al., 2001). H295R proliferation seems to be supported by an autocrine mechanism mediated by E2 through its receptors (Sirianni et al., 2012).

The assessment of response to estrogen receptor antagonists (such as ICI 182 780 and OHT (4-OH tamoxifen)) confirms the E2 involvement in H295R cell proliferation. This showed a dose-dependent inhibition of basal and E2-dependent cell proliferation. In particular, OHT induced morphological changes characteristic of apoptosis up-regulating the expression of FasL and inducing autocrine activation of caspases. ICI, while, caused a cytostatic effect that could be explained by the inhibitory effects exerted by ICI on IGF signaling pathway.   Pathway that is

strongly activated in H295R through the IGFIR by autocrine IGF-II action (Sirianni et al., 2012). ICI mediated inhibition of cell growth is not solely attributable to competition for the estrogen receptor but also to the interruption of the IGF signaling pathway (Sirianni et al., 2012).

ERα and ERβ belonging to steroid/thyroid hormone superfamily of nuclear receptors, and share a common structural architecture (Evans, 1988; Katzenellenbogen and Katzenellenbogen, 1996; Tsai and O'Malley, 1994). These receptor have three independent but interacting functional domains: the NH2-terminal or A/B domain, the C or DNA-binding domain, and the D/E/F or ligand-binding domain. Al these domains interact with each other. Binding of estrogens to ER triggers conformational changes in the receptor influencing the rate of transcription of estrogen-regulated genes. These steps include receptor dimerization, receptor-DNA interaction, recruitment of and interaction with coactivators and others transcription factors, over and above formation of a preinitiation complex (Katzenellenbogen and Katzenellenbogen, 1996; McKenna et al., 1999). Another striking difference between the two receptors is their distinctive responses to the synthetic antiestrogens tamoxifen, raloxifene, and ICI-164,384.In particular on an ERE-based reporter gene, these ligands are partial E2 agonists with ERα but are pure E2 antagonists with ERβ (Batistuzzo de Medeiros et al., 1997; McDonnell et al., 1995; McInerney et al., 1998). On these interactions COOH-terminal, E/F-, or ligand-binding domain (LBD) intermediates ligand binding with consequently receptor dimerization, nuclear translocation, and transactivation of target gene expression (Eudy et al., 1998; Giguere et al., 1988; Tsai and O'Malley, 1994). Crystallographic studies with the LBDs of ERα and ERβ revealed that the position of helix 12 is altered by binding of ligands. When the ERα LBD is complexed with the agonists, E2 or diethylstilbestrol (DES), helix 12 is positioned over the ligand-binding pocket and forms the surface for recruitment and interaction of coactivators (Shiau et al., 1998; Wurtz et al., 1996). In contrast, in the ERα- and ERβ-LBD complexes with raloxifene (Pike et al., 1999) or the ERα-LBD 4-OH-tamoxifen complex (Shiau et al., 1998), helix 12 is displaced from its agonist position over the ligand-binding cavity Hence different ligands induce different receptor conformations (McDonnell et al., 1995; Paech et al., 1997) and the positioning of helix 12 is the key event that permits discrimination between estrogen agonists (E2 and DES) and antagonists (raloxifene and 4-OH-tamoxifen). Typical tumoral condition show levels of ERβ significantly lower, conversely ERα up-regulation and aromatase over-expression. In addition, the expression of ER was correlated with the expression of nuclear hormone receptors, suggesting a correlation in the modulation of ER. Finally these evidence suggest that estrogen produced locally by aromatase can induce the proliferation of adrenocortical cells through autocrine and paracrine mechanisms and offer new perspectives on the potential use of anti-

estrogens and aromatase inhibitors as therapeutic agents against adrenocortical carcinoma (Barzon et al., 2008).

G Protein Coupled Estrogen Receptor: GPER and its ligand

Estrogen supports different biochemical pathways that were distinguished in rapid or "pregenomic" events (second messenger and protein/lipid kinase activation) that occur within minutes of estrogen exposure and delayed or genomic transcriptional responses that have more a slowly mechanism of action. Estrogen receptors (ER) belong to the nuclear steroid hormone receptor superfamily. We can distinguishes ERα and ERβ, which function as hormone inducible transcription factors with estrogen dependent gene transactivation. Tamoxifen (TAM) a selective estrogen receptors modulators was designed to block estrogen-ER binding, and it was widely and effectively clinically used in the treatment of breast cancer. An active metabolite of TAM, the hydroxytamoxifen, is capable to activate a transmembrane estrogen receptor named GPER. This seven-transmembrane G-protein-coupled receptor (GPCR) is able to mediate rapid estrogen signaling in different cell types (Prossnitz and Maggiolini, 2009). The signaling mechanisms employed by GPER that allow stimulation of adenylyl cyclase and release of membrane tethered epidermal growth factor (EGF) are not typical to GPER but are common to many other GPCR (Filardo and Thomas; 2005). In the past, numerous studies, have demonstrated estrogen signaling in GPER positive, ER negative cells indicate that GPER can act as a "stand alone" receptor. ER and GPER are correlated in different signaling mechanisms in reproductive cancer, but their action are also indipendent for several measures such as Er and GPER show independent expression in breast tumors and in cultured breast cancer cells lines(Filardo et al., 2006; Revankar et al., 2005.). Furthermore they have different binding affinities for various estrogens and are differentially activated by them (Blair et al., 1999) and some of GPER agonists are ER antagonists (Filardo 2011).

GPER-dependent cellular functions

GPER was an orphan member of the 7-transmembrane receptor family (Carmeci et al., 1997; O'Dowd et al., 1998; Owman et al., 1996; Takada et al., 1997). Based on the amino acid sequence homology, GPER bore the most similarity to the chemokine subfamily of GPCRs. Matching expression of GPER in a number of ER-positive (MCF7) and ER-negative (MDA-MB-231) cell lines and tissue revealed a strong positive correlation between ER and GPER expression, highlighting a link to physiologic responses into estrogen-responsive tissues and cancers (Carmeci et al., 1997). The role of GPER in the rapid activation of MAPKs by estrogen in breast cancer cells was investigated (Filardo et al., 2000). The correlation between GPER and functional response to

estrogen was demonstrated by Estrogen-mediated activation of Erk 1/2 in ER-negative cells as well as in GPER-transfected cell. However the pathway that involved this receptor was used by the ER antagonist, ICI 182, 780, for MAPK activation. Study results suggested that ER-negative cells could maintain responsiveness to estrogen through the expression of GPER (Filardo, 2002). Over the past years, a small number of papers related to GPER reported upregulating of GPER expression by progestin in MCF-7 cells (Ahola et al., 2002), expression that is critical for growth inhibition. This process was progestin-mediated and is involved in part in ERK inactivation (Ahola et al., 2002). A second phase of GPER-dependent signaling suggested that GPER promotes estrogen-mediated inhibition of oxidative stress-induced apoptosis by promoting Bcl-2 expression (Kanda and Watanabe, 2003b), promotes cell growth by stimulating of cyclin D expression (Kanda and Watanabe, 2004) and upregulates nerve growth factor production in macrophages through c-fos induction (Kanda and Watanabe, 2003a). Upregulation of c-fos by estrogen and phytoestrogens demonstrated also in breast cancer cells (Maggiolini 2004). It is noted that GPER not directly initiated the observed effects but is correlated with responsiveness to estrogen. Data confirmed by different reports that providing evidence on the capacity of binding of tritiated estrogen to membrane of SKBr3 and GPER-transfected HEK cells (Thomas et al., 2005). However GPER-transfected cell membrane treated with estrogen also activates GTP-binding proteins and the production of cAMP. The binding affinity and co-localization of a fluorescent estrogen to GPER both in GPER-transfected cells both in endogenously cells demonstrated that the binding affinity of GPER represented 10 fold higher value than that determined for ERα (Revankar et al., 2005). GPER that, for the large amount, was localized to intracellular membranes, predominantly in the endoplasmic reticulum, as demonstrated by expression of a GFP-tagged GPER as well as antibody staining of endogenously expressed GPER. These evidences suggesting a novel site of action for GPER function. Both ER and GPER are capable of activating PI3K in response to estrogen treatment, the two receptors utilize distinct signaling pathways and respond differentially to tamoxifen (Revankar et al., 2005). Additional studies demonstrated, in fact, that GPER, but not ERα, was activated by tamoxifen to stimulate PI3K activity. Finally, although estrogen-mediated activation of PI3K could also be mediated by ERα, this mechanism did not involve EGFR transactivation, which was required for GPER.

Identification and characterization of GPER-selective ligands

In depth review of GPER ligand binding properties the ER antagonist/SERMs tamoxifen and ICI182/870 have been shown to act as GPER agonists (Filardo et al., 2000; Revankar et al., 2005). Bologa et al. screened a library of approximately 10,000 compounds for chemical similarity to

estrogen and the top 100 compound were tested for GPER activity (Bologa et al., 2006). A compound termed G-1 displayed an agonist activity against GPER. The peculiarity of this compound was that it resulted inactive against classical estrogen receptors and thus represented the first selective GPER ligand. Different studies revealed that G-1 was capable of eliciting calcium mobilization as well as PI3K activation in cells expressing GPER but not in cells expressing either ERα and ERβ (Bologa et al., 2006). Furthermore, G-1, like estrogen, mediated an inhibition of chemotaxis towards EGF/serum in both MCF-7, which express classical ERs and GPER, and SKBr3 cells, which express only GPER. Other groups, sub sequentially, have utilized G-1 to examine the role of GPER in multiple systems because in different cell contexts, the pathways utilized by estrogen may vary depending on the complement of receptors expressed (Sathya et al., 2015; Yan et al., 2015). Pang et al, confirmed a role of GPER in the control of meiotic arrest (Pang et al., 2008). The role of GPER was examined in urothelial cell proliferation, where estrogen have bimodal mechanism of action, at low concentration stimulates cell proliferation through the classical estrogen receptors while the response is reduced at high concentrations (Teng et al., 2008). Urothelial cells were also shown to express high levels of GPER, raising the question as to the specific roles of individual estrogen receptors in these cells. In these cells, in fact, G-1 stimulation inhibited cell proliferation, conversely to the classics effects of estrogen. The inhibitory effects of estrogen on cell proliferation correlate with GPER as demonstrated by overexpression of GPER inhibited, estrogen-induced cell proliferation. Furthermore, G-1 failed to induce c-fos, c-jun or cyclin D1 expression, and GPR30 overexpression abolished estrogen-induced c-fos, c-jun or cyclin D1 expression whereas GPR30 downregulation improved expression of the same genes. These results suggested that the classical estrogen receptor stimulating proliferation while GPER inhibit proliferation via downregulation of the AP-1 components c-fos and c-jun with decreases in cyclin D1 expression. The role of GPER in the mechanical hyperalgesia was examined through PKC activation proving that G-1 and not classical ER agonists activated PKC in neurons of dissociated dorsal root ganglia (Kuhn et al., 2008). Another study have investigated the contribution of membrane estrogen receptors in the estrogen-mediated modulation of dopamine transporters in nerve growth factor differentiated PC12 pheochromocytoma cells (Alyea et al., 2008). Depletion studies, using siRNA revealed that ERα depletion blocked estrogen-mediated efflux, GPER depletion increase efflux while ERβ depletion having no effects. G-1 administered alone had no effect on efflux but co-administration with estrogen resulted in substantial inhibition of the estrogen response. These data are symptomatic of an antagonist role of GPER compare to stimulatory effect of ERα. One of the major feedback targets for estrogen in the brain is the gonadotropin-releasing hormone (GnRH) neurons, which regulate gonadal function and fertility in mammals. G-1 does not

show any effect on the calcium dynamics of GnRH neurons, while estrogen and ERα selective agonists displayed activity (Romano et al., 2008). Experiments performed in vivo with G-1 to examine the effect on mammary and uterine tissue show that, estrogen, but not G-1, regulated expression of Wnt-4, Frizzled-2, IGF-1 or cycline E1 in these tissues(Otto et al., 2009). G-1 failed to induce ductal growth and endbud formation in the mammary gland. It was unclear from such study if appropriate conditions were employed or if GPER may exhibit altered kinetics or responses from those primarily evoked by classical estrogen receptors. Other two studies characterized GPER knockout mice but in one case revealed no obvious defects in reproductive organs (Otto et al., 2009) 22and in the other revealed alterations in glucose tolerance, bone growth, blood pressure and serum insulin-like growth factor-I levels (Martensson et al., 2009). In this last study, aged female GPER knockout mice were hyperglycemic with impaired glucose tolerance, associated with decreased insulin expression and release, both in vivo and in isolated pancreatic islets. Recent publications described the capacity of G-1 to induce vasodilatation with resulting decreases in blood pressure (Haas et al., 2009) as well as the treatment with this agonist ameliorate the effects of multiple sclerosis in an animal model of autoimmune encephalomyelitis (Wang et al., 2009). In both studies, G-1 activity was absent in GPER knockout mice, confirming the physiological activity of G-1 through GPER. In some cases for estrogen-mediated activity, GPER and ERs work in concert, as in estrogen induced thymic atrophy. This evidence was demonstrated using a GPER knockout mice and G-1 (Wang et al., 2008). Kamanga-Sollo et al in their study concluded that, whereas GPER mediates the estrogen-stimulated increase in IGF-I mRNA, ERα mediates the proliferative effect (Kamanga-Sollo et al., 2008). They examined the mechanism involved in the stimulation of IGF-I mRNA and muscle growth, using bovine muscle satellite cell culture. Of the therapeutic anti-estrogens, ICI182,780 (a selective estrogen receptor down-regulator, SERD) was first demonstrated to interact with GPER, but surprisingly, as opposed to its antagonistic action towards ERα/β, ICI182,780 acted as an agonist towards GPER (Filardo et al., 2000). Similarly, an active metabolite of tamoxifen, 4-hydroxytamoxifen (selective estrogen receptor modulator, SERM) acts as a GPER agonist (Vivacqua et al., 2006b), and recently raloxifene has also been demonstrated to activate GPER in cells deficient for ERα (Petrie et al., 2013). Different synthetic compounds known to have estrogenic effects have also been demonstrated to bind and/or activate GPER, including atrazine (Albanito et al., 2008a), bisphenol A (Chevalier et al., 2012; Dong et al., 2011; Sheng et al., 2013), daidzein (Kajta et al., 2013), zearalonone, nonphenol, kepone, p,p'-DDT, o,p'-DDE and 2,2′,5′,-PCB-4-OH (Thomas and Dong, 2006). Finally, also a number of phytoestrogens display agonist activity towards GPER, including genistein (Maggiolini et al., 2004; Vivacqua et al., 2006a),

quercetin (Maggiolini et al., 2004), equol (Rowlands et al., 2011), resveratrol (Dong et al., 2013), oleuropein, and hydroxytyrosol (Chimento et al., 2013b).

Transcriptional activations mediated by GPER

Rapid signaling events mediated by GPER can also lead to the activation of transcriptional machinery of estrogens with the ligand-dependent genomic model of ER activity. E2, in fact, through GPER, upregulates nerve growth factor inducing by c-fos expression via cAMP in macrophages (Kanda and Watanabe, 2003a; Kanda and Watanabe, 2003b). The same research group, however, demonstrated that E2 induces cyclin D2 and Bcl-2 expression via protein kinase A-mediated CREB phosphorylation in Keratinocytes (Kanda and Watanabe, 2004); E2, in fact, reduces hepatic injury after trauma-hemorrhage by upregulating Bcl-2 expression with a GPER and PKA-dependent pathway (Hsieh et al., 2007). Supplementary evidences of GPER-dependent transcriptional activation by E2 in ER-positive MCF-7 and ER-negative SKBr3 breast cancer cells were given by C-fos expression, determined using an early molecular sensor for estrogen activity (Maggiolini et al., 2004). The study proved that GPER signaling requires EGFR and happens through rapid ERK 1/2 phosphorylation in triggering the genomic response to estrogen particularly in tumor cells devoid of ERs. E2, the phytoestrogen genistein and the 4-hydroxylated metabolite of tamoxifen (OHT) induced the expression of c-fos through the GPER/EGFR/ERK signaling pathway and also induced proliferation of thyroid tumor cells lacking ER (ARO cells) or cells expressing a non-transcriptionally active variant of ERα (FRO and WRO cells) (Vivacqua et al., 2006a). The GPER pathway, hence, may represent a new window to examine the classical ER-mediated biological thyroid cell response. The discovery of G-1, represented a key experiment to study its activity (Bologa et al., 2006). Taking advantage of the lack of activity of G-1 on the classical ER and using ovarian cancer cells that express both ERα and GPER, was observed that G-1, like E2, up-regulated diverse estrogen-responsive genes including c-fos, pS2 and cyclins A, D1 and E; however, it wasn't able to increase the ERα-target gene PR, which only responded to E2 treatment. The study was conducted using ER-negative and GPER-positive SKBr3 cells, where G-1 like E2 stimulated c-fos expression, but had no effect on PR expression (Albanito et al., 2008 b). Hence GPER, probably together with ERα, mediates the transcriptional activation of the other genes, while estrogen-activated PR expression occurs specifically through ERα. In addition, was demonstrated that exist an E2 and G-1 common pathway that mediates the genomic response.in ovarian cancer cells, in particular in the transcriptional activation of c-fos . Otherwise, knocking down GPER or ERα revealed a cross-talk between these estrogen receptors in the stimulation of cfos by G-1 and E2. From these data it is reasonable to argue that the evaluation of estrogenic activity of phyto- and

xenoestrogens should be extended to their potential ability to activate GPER signaling together with the classic effects exerted through the classical ER-mediated genomic response. A physiological role for GPER-mediated transcriptional responses through cross-talk with ERα was founded in mouse spermatogonia GC-1 cells, used to investigate the estrogen-mediated regulation of testicular function (Sirianni et al., 2008). The potential involvement of an estrogen-binding receptor, GPER, in estrogen signaling was investigated showing that E2 and G-1 activate the EGFR/ERK pathway causing the stimulation of c-fos and cyclin D1 expression as well as GC-1 cell growth. Conversely, using ICI182,780 or silencing GPER expression, the proliferative effects induced by E2 and G-1 were abrogated. The results obtained are consistent with a study in which demonstrated that E2, through the activity of a Gi protein, could induce rapid activation of ERK1/2 and PKA signaling pathways, which are involved in the proliferation of human germ cell tumors (Bouskine et al., 2008). Finally it is well known that tamoxifen can act as full agonist of GPER (Lappano et al., 2013; Vivacqua et al., 2006a) and GPER can mediate rapid E2-induced non-genomic signaling events. These events includes stimulation of adenylyl cyclase, mobilization of intracellular calcium ($Ca2+$) stores and activation of mitogen-activated protein kinase (MAPK) and phosphoinositide 3-kinase (PI3K) signaling pathways (Ariazi et al., 2010; Prossnitz and Barton, 2009). For all these reasons GPER exhibits prognostic utility in different cell lines.

Aim of the study

In the study we investigated the effect of G-1 an agonist of G Protein Coupled Estrogen Receptor (GPER) on ACC growth..

Materials and methods

Cell culture and tissues

H295R cells were obtained from Dr W.E. Rainey (University of Michigan at Ann Arbor, USA) (Rainey et al., 1994). Cells were cultured cultured in Dulbecco's modified Eagle's medium/Ham's F12 (DMEM/F12; 1:1; Eurobio, Les Ulis, France) supplemented with 1% ITS Liquid Media Supplement (100×; Sigma), 10% calf serum and antibiotics (Eurobio), at 37 °C in an atmosphere of humidified air containing 5% CO2. Cell monolayers were sub cultured onto 100 mm dishes for phosphatase activity and laddering assay (8×106 cells/plate), 60 mm dishes for protein and RNA extraction (4×106 cells/plate) and 24 well culture dishes for proliferation experiments (2×105 cells/well) and grown for 2 days. Prior to experiments, cells were starved overnight in DMEM/F-12 medium without phenol red and containing antibiotics. Cells were treated with (±)-1-[(3aR*, 4S*, 9bS*)-4-(6-Bromo-1, 3-benzodioxol- 5-yl)-3a, 4, 5, 9b-tetrahydro-3H-cyclopenta[c]quinolin-8-yl]-ethanone (G-1) (1 µM) (Tocris Bioscience, Bristol, UK) in DMEM/F-12 containing FBS-DCC 2, 5% (fetal bovine serum dextran-coated charcoal-treated). Inhibitors PD98059 (PD) (10 µM) (Calbiochem, Merck KGaA, Darmstadt, Germany) was used 1 h prior to G-1. Adrenocortical tumors, removed at surgery, and normal adrenal cortex, macroscopically dissected from adrenal glands of kidney donors, were collected at the hospital-based Divisions of the University of Padua (Italy). Tissue samples were obtained with the approval of local ethics committees and consent from patients, in accordance with the Declaration of Helsinki guidelines as revised in 1983. Diagnosis of malignancy was performed according to the histopathologic criteria proposed by Weiss et al. (Weiss et al., 1989) and the modification proposed by Aubert et al. (Aubert et al., 2002). Clinical data of the six ACC patients included in this study are not showed. Patient C6 terminated mitotane treatment six months after beginning of therapy for severe gastrointestinal side effects. Patients C1 and C2 were treated with chemotherapy EAP protocol (etoposide, doxorubicin, and cisplatin) + mitotane.

RNA extraction, reverse transcription and real time PCR

TRizol RNA isolation system (Invitrogen, Carlsbad, CA, USA) was used to extract total RNA from H295R, SKBR3 and ACCs. Each RNA sample was treated with DNase I (Invitrogen), and purity and integrity of the RNA were confirmed spectroscopically and by gel electrophoresis before use. One microgram of total RNA was reverse transcribed in a final volume of 30 µl using the ImProm-II Reverse transcription system kit (Promega Italia S.r.l., Milano, Italia); cDNA was diluted 1:2 in nuclease-free water, aliquoted, and stored at − 20°C. The nucleotide sequences for GPER amplification were forward, 5′-CGCTCTTCCTGCAGGTCAA-3′, and reverse, 5′-ATGTAGCGGTCGAAGCTCATC-3′ ; the nucleotide sequences for GAPDH amplification were

forward, 5′-CCCACTCCTCCACCTTTGAC-3′, and reverse, 5′-TGTTGCTGTAGCCAAATTCGTT-3′. PCR reactions were performed in the iCycler iQ Detection System (Bio-Rad Laboratories S.r.l., Milano, Italia) using 0.1 μmol/L of each primer, in a total volume of 30 μl reaction mixture following the manufacturer's recommendations. SYBR Green Universal PCR Master Mix (Bio-Rad) with the dissociation protocol was used for gene amplification; negative controls contained water instead of first-strand cDNA. Each sample was normalized to its GAPDH content. The relative gene expression levels were normalized to a calibrator (normal tissue for ACC tissues or SKBR3 for H295R cells). Final results were expressed as n-fold differences in gene expression relative to GAPDH and calibrator, calculated using the ΔΔCt method as previously shown (Sirianni et al., 2009).

Western Blot analysis

Fifty μg of protein was subjected to western blot analysis (Sirianni et al., 2007). Blots were incubated overnight at 4°C with antibodies against GPER, Cyclin E (CCNE), Cyclin B1 (CCNB1), phospho-Rb, Cytochrome c, Bax, Bcl-2, Parp1, pERK1/2-ERK2 (all from Santa Cruz Biotechnology, Santa Cruz CA, USA). Membranes were incubated with horseradish peroxidase (HRP)- conjugated secondary antibodies (Amersham Pharmacia Biotech, Piscataway, NJ) and immunoreactive bands were visualized with the ECL western blotting detection system (Amersham Pharmacia Biotech, Piscataway, NJ). To assure equal loading of proteins, membranes were stripped and incubated overnight with Glyceraldehyde 3-phosphate dehydrogenase (GAPDH) antibody (Santa Cruz Biotechnology).

Histopathological and Immunohistochemical analysis

Tumors were fixed in 4% neutral buffered formalin, embedded in paraffin, sectioned at 5 and stained with hematoxylin and eosin, as suggested by the manufacturer (Bio-Optica, Milan, Italy). Paraffin-embedded sections, 5 mm thick, were mounted on slides precoated with poly-lysine, and then they were deparaffinized and dehydrated (seven to eight serial sections). Immunohistochemical experiments were performed using mouse monoclonal Ki-67 primary antibody at 4°C over-night (Dako Italia Spa, Milano, Italy). Then, a biotinylated goat-anti-mouse IgG was applied for 1h at room temperature, to form the avidin biotin-horseradish peroxidase complex (Vector Laboratories, CA, USA). Immunoreactivity was visualized by using the diaminobenzi-dine chromogen (Vector Laboratories). Counterstaining was carried out with hematoxylin (Bio-Optica, Milano, Italy). The primary antibody was replaced by normal rabbit serum in negative control sections.

Cytochrome c detection

Cells were treated for 24 h, fractioned and processed for Cytochrome c detection as previously reported (Chimento et al., 2012). Briefly, cells were harvested by centrifugation at 2500 rpm for 10 min at 4°C. Pellets were resuspended in 50 µl of sucrose buffer (250 mM sucrose; 10 Mm Hepes; 10 mM KCl; 1.5 mM MgCl2; 1 mM EDTA; 1 mM EGTA) (all from Sigma-Aldrich, Milano, Italy) containing 20 µg/ml aprotinin, 20 µg/ml leupeptin, 1 mM PMSF and 0.05% digitonine (Sigma-Aldrich). Cells were incubated for 20 min at 4°C and then centrifuged at 13,000 rpm for 15 min at 4°C. Supernatants containing cytosolic protein fraction were transferred to new tubes and the resulting mitochondrial pellets were resuspended in 50 µl of lysis buffer (1% Triton X-100; 1 mM EDTA; 1 mM EGTA;

10 mM Tris-HCl, pH 7.4) (all from Sigma-Aldrich) containing 20 µg/ml aprotinin, 20 µg/ml leupeptin, 1 mM PMSF (Sigma-Aldrich) and then centrifuged at 13,000 rpm for 10 min at 4°C. Equal amounts of proteins were resolved by 11% SDS/polyacrylamide gel as indicated in the Western blot analysis paragraph.

Cell cycle analysis and evaluation of cell death

Subconfluent monolayers growing in 60 mm plates were depleted of serum for 24 h and treated for an additional 24 h with G-1. The cells were harvested by trypsinization and resuspended with 0.5 ml of Propidium Iodide solution (PI) (100 µg/ml) (Sigma-Aldrich) after treatment with RNase A (20 µg/ml). The DNA content was measured using a FACScan flow cytometer (Becton Dickinson, Mountain View, CA, USA) and the data acquired using CellQuest software. Cell cycle profiles were determined using ModFit LT program. Subconfluent monolayers growing in 60 mm plates were depleted of serum for 24 h and treated for 24 and 48 h with G-1. Trypsinized cells were incubated with Ligation Buffer (10 mM Hepes (pH = 7.4), 150 mM NaCl, 5 mM KCl, 1 mM MgCl2 and 1.8 mM CaCl2) containing Annexin-V-FITC (1:5000) (Santa Cruz) and with Propidium Iodide. Twenty minutes post-incubation at room temperature (RT) protected from light, samples were examined in a FACSCalibur cytometer (Becton Dickinson, Milano, Italy). Results were analyzed using CellQuest program.

Caspases 9 and 3/7 Activity Assay

H295R cells after treatments were subjected to caspases 9 and 3/7 activity measurement with Caspase- Glo 9 and 3/7 assay kits (Promega) and modified protocol. Briefly, the proluminescent

substrate containing LEHD or DEVD sequences (sequences are in a single-letter amino acid code) are respectively cleaved by Caspases 9 and 3/7. After caspases cleavage, a substrate for luciferase (aminoluciferin) is released resulting in luciferase reaction luminescent signal production. Cells were trypsinized, harvested and then suspended in DMEM-F12 before being incubated with an equal volume of Caspase-Glo reagent (40 μl) at 37°C for 1 h. The luminescence of each sample was measured in a plate-reading luminometer (Gen5 2.01) with Synergy H1 Hybrid Reader..

TUNEL assay

Cells were grown on glass coverslips, treated for 24 h and then washed with PBS and fixed in 4% formaldehyde for 15 min at room temperature. Fixed cells were washed with PBS and then soaked for 20 min with 0.25% of Triton X-100 in PBS. After two washes in deionized water, they were stained using the Click-iT® TUNEL Alexa Fluor® Imaging Assay (Invitrogen) according to the manufacturer's protocol. Co-staining with Hoechst33342 was performed to analyze the nuclear morphology of the cells after the treatment. Cell nuclei were observed and imaged under an inverted fluorescence microscope (200X magnification).

Determination of DNA fragmentation

To determine the occurrence of DNA fragmentation, total DNA was extracted from control and G-1 (1 μM) treated (48h) cells as previously described (Chimento et al., 2012). The attached and detached cells floating in the medium were collected by scraping and centrifuging (1500 rpm for 5 min at 4 _C). Pellets were washed three times with PBS and then resuspended in DNAladdering lysis buffer (10% NP40, 200 mMEDTA, 0.2 MTris–HCl pH 7.5). Lysates were centrifuged at 3000 rpm for 5 min at 4 °C. The recovered DNA was incubated with RNase A (final 5 lg/ll) in 1% SDS for 2 h at 56 °C. After addition of proteinase K (final 2.5 lg/ll) samples were incubated for an additional 3 h at 37 °C. DNA precipitation was performed using ethanol/ammonium acetate precipitation O/N at -80 °C. The following day samples were centrifuged at 12,000 rpm for 20 min at 4 _C and washed with 80% ice-cold ethanol. DNA pellets were resuspended in nuclease-free water. Equal amounts of DNA were analyzed by electrophoresis on a 2% agarose gel stained with ethidium bromide (Sigma–Aldrich).

Assessment of cell proliferation

[3H]Thymidine incorporation assay. H295R cell proliferation after G-1 treatment was directly evaluated as previously described (Sirianni et al., 2010). Cells were cultured in complete medium in 24 well plates (200,000 cells/well) for 24 h, then treated in serum-free medium for 48 h. Control

cells were treated with the same amount of vehicle alone (dimethylsulfoxide), which never exceeded the concentration of 0.01% (vol/vol). [3H]thymidine incorporation was evaluated after a 6 h incubation period with 1 lCi [3H]thymidine per well (Perkin–Elmer Life Sciences, Boston, MA, USA). Cells were washed once with 10% trichloroacetic acid, twice with 5% trichloroacetic acid, and lysed in 1 ml 0.1 N NaOH at 37 °C for 30 min. The total suspension was added to 5 ml optifluor fluid and radioactivity determined in a b-counter. Each experiment was performed in triplicate and results are expressed as percent (%) of basal.

The effect of G-1 on cell viability was measured using 3-[4,5-Dimethylthiaoly]-2,5-diphenyltetrazolium bromide (MTT) assay as previously described (Sirianni et al., 2012). Briefly, cells were treated for different times as indicated in figure legends. At the end of each time point fresh MTT (Sigma-Aldrich), re-suspended in PBS, was added to each well (final concentration 0.33 mg/ml). After 30 minutes incubation, cells were lysed with 1 ml of DMSO (Sigma-Aldrich). Each experiment was performed in triplicate and the optical density was measured at 570 nm in a spectrophotometer.

Gene silencing experiments

For the gene silencing experiments, cells were plated in 12 well plates (1 × 105 cells/well) for proliferation experiments or in 6 well plates (2 × 105 cells/well) for Western blot analysis; cells were transfected with control vector (shRNA) or shGPER in 2, 5% DCC-FBS medium using lipofectamine 2000 transfection reagent (Invitrogen) according to the manufacturer's recommendations for a total of 72 h. For proliferation experiments cells were transfected for 24 h and then treated for 48 h before performing MTT assay.

Xenograft model

Four-week-old nu/nu − Forkhead box N1nu female mice were obtained from Charles River Laboratories Italia (Calco, Lecco, Italy). All animals were maintained in groups of five or less and quarantined for two weeks. Mice were kept on a 12 h/12 h light/dark regimen and allowed access to food and water ad libitum. H295R cells, 6 × 106, suspended in 100 μl PBS (Dulbecco's Phosphate Buffered Saline), were combined with 30 μl of Matrigel (4 mg/ml) (Becton Dickinson) and injected subcutaneously in the shoulder of each animal. Resulting tumors were measured at regular intervals using a caliper, and tumor volume was calculated as previously described (Seshadri et al., 2007), using the formula: $V = 0.52 (L \times W^2)$, where L is the longest axis of the tumor and W is perpendicular to the long axis. Mice were treated 21 days after cell injection, when tumors had reached an average volume of about 200 mm3. Animals were randomly assigned to be treated with

vehicle or G-1 (Tocris Bioscience) at a concentration of 2 mg/kg/daily. Drug tolerability was assessed in tumor-bearing mice in terms of: a) lethal toxicity, i.e. any death in treated mice occurring before any death in control mice; b) body weight loss percentage $= 100 - [($body weight on day x/body weight on day 1$) \times 100]$, where x represents a day during the treatment period [66, 67]. Animals were sacrificed by cervical dislocation 42 days after cell injection. All animal procedures were approved by Local Ethics Committee for Animal Research.

Scoring system

The immunostained slides of tumor samples were evaluated by light microscopy using the Allred Score (Allred et al., 1998) which combines a proportion score and an intensity score. A proportion score was assigned representing the estimated proportion of positively stained tumor cells (0 = none; 1 = 1/100; 2 = 1/100 to < 1/10; 3 = 1/10 to < 1/3; 4 = 1/3 to 2/3; 5 = > 2/3). An intensity score was assigned by the average estimated intensity of staining in positive cells (0 = none; 1 = weak; 2 = moderate; 3 = strong). Proportion score and intensity score were added to obtain a total score that ranged from 0 to 8. A minimum of 100 cells were evaluated in each slide. Six to seven serial sections were scored in a blinded manner for each sample.

Data analysis and statistical methods

All experiments were performed at least three times. Data were expressed as mean values + standard error (SE), statistical significance between control (basal) and treated samples was analyzed using GraphPad Prism 5.0 (GraphPad Software, Inc.; La Jolla, CA) software. Control and treated groups were compared using the analysis of variance (ANOVA) with Bonferroni or Dunn's post hoc testing. A comparison of individual treatments was also performed, using Student's t test. Significance was defined as $p < 0.05$.

Results

H295R cell growth inhibited by G-1 treatment in vitro and in vivo

We examined GPER expression in human ACCs and in H295R cells by western blot analysis (Fig. 3. A) and real time RT-PCR (Fig. 3. B-C). Data demonstrated that GPER is expressed in normal adrenal, in human ACCs and in H295R cells at different levels. G-1 effects on cell viability and proliferation were tested using increasing concentrations (0.01-0.1-1µM) for different times (24-48-72 h) (Fig. 3. D-E). Among different doses tested only 1µM caused a time-dependent reduction in H295R cell growth. Doses higher than 1µM did not show any more pronounced effect (data not shown). Knocking down of GPER gene expression, using a specific shRNA, (shGPER) was assessed by western blot analysis and revealed a substantial decrease in protein content compared to the control shRNA (insert, Fig. 3. F). However, GPER silencing was able to only partially abrogate the inhibitory effects exerted by G-1 on H295R cell proliferation (Fig. 3. F).
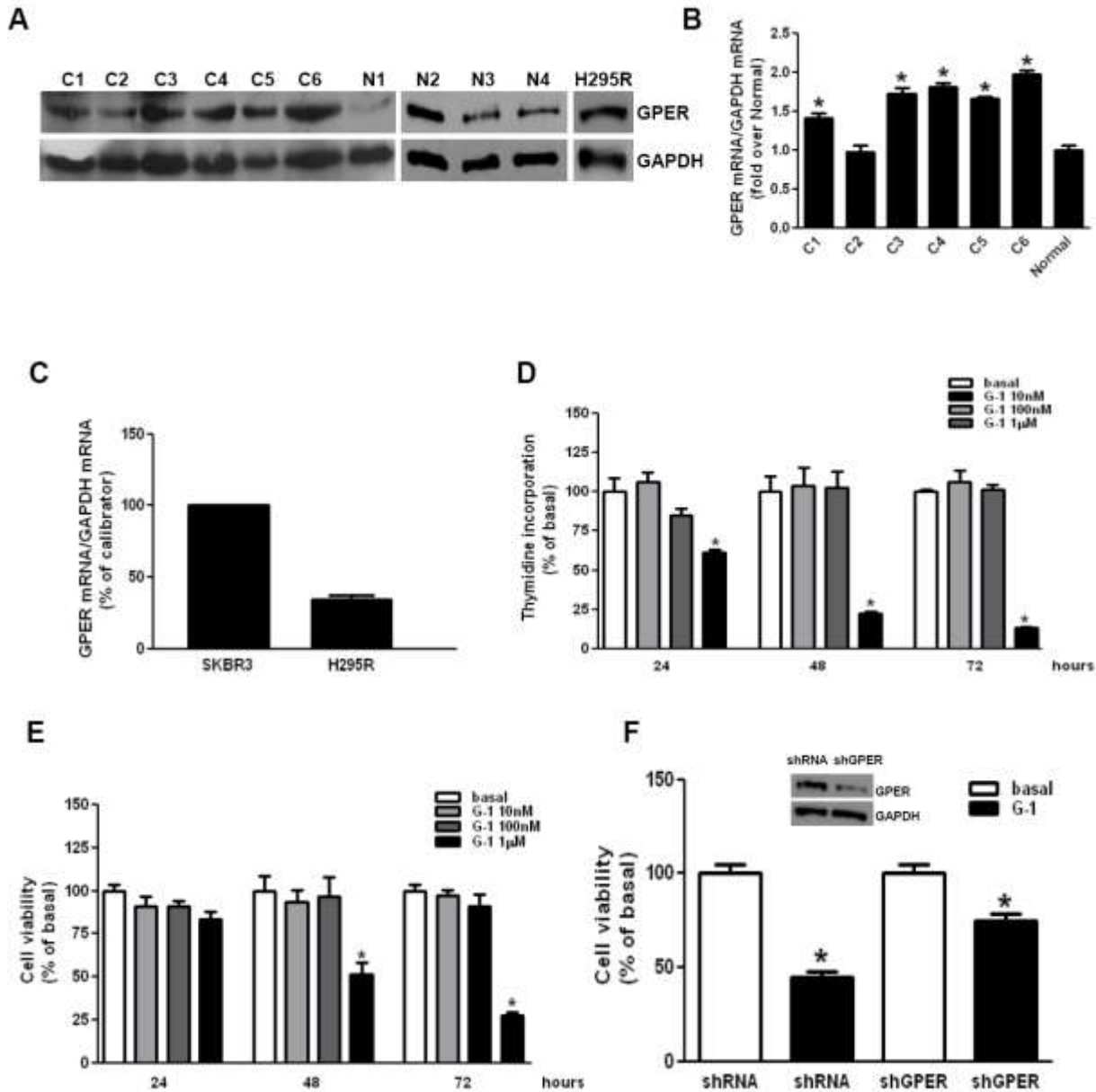
Figure 3: G-1 treatment decreases H295R cell growth *in vitro*. (A), Western blot analysis of GPER was performed on 50 µg of total proteins extracted from normal adrenal, ACCs and H295R cells. GAPDH was used as a loading control. (B-C), GPER mRNA expression in normal adrenal and ACCs (B), H295R and SKBR3 (positive control) cells (C) was analyzed by real time RT-PCR. Each sample was normalized to its GAPDH RNA content. Final results are expressed as n-fold differences of gene expression relative to calibrator. Data represent the mean+SE of values from at least three separate RNA samples; *, $P<0.05$, versus calibrator). (D-E), H295R cells were treated with G-1 (0.01-1µM) for different times (24, 48 and 72 h). Cell proliferation was evaluated by [^{3}H]Thymidine incorporation (D) and MTT (E) assays. Results were expressed as mean+SE of three independent experiments each performed in triplicate. Statistically significant differences are indicated (*, $P<0.05$ versus basal). (F) MTT assay was performed on H295R cells, which were previously transfected for 72 h in the presence of control vector (shRNA) or shGPER. Twenty-four hours after transfection cells were treated in 2.5 % DCC-FBS medium for 48 h with G-1 (1µM). Results were expressed as mean+SE of three independent experiments each performed in triplicate. (*p < 0.05 versus basal). The insert shows a Western blotting assay on H295R protein extracts evaluating the expression of GPER receptor in the presence of shRNA or of shGPER. GAPDH was used as a loading control.
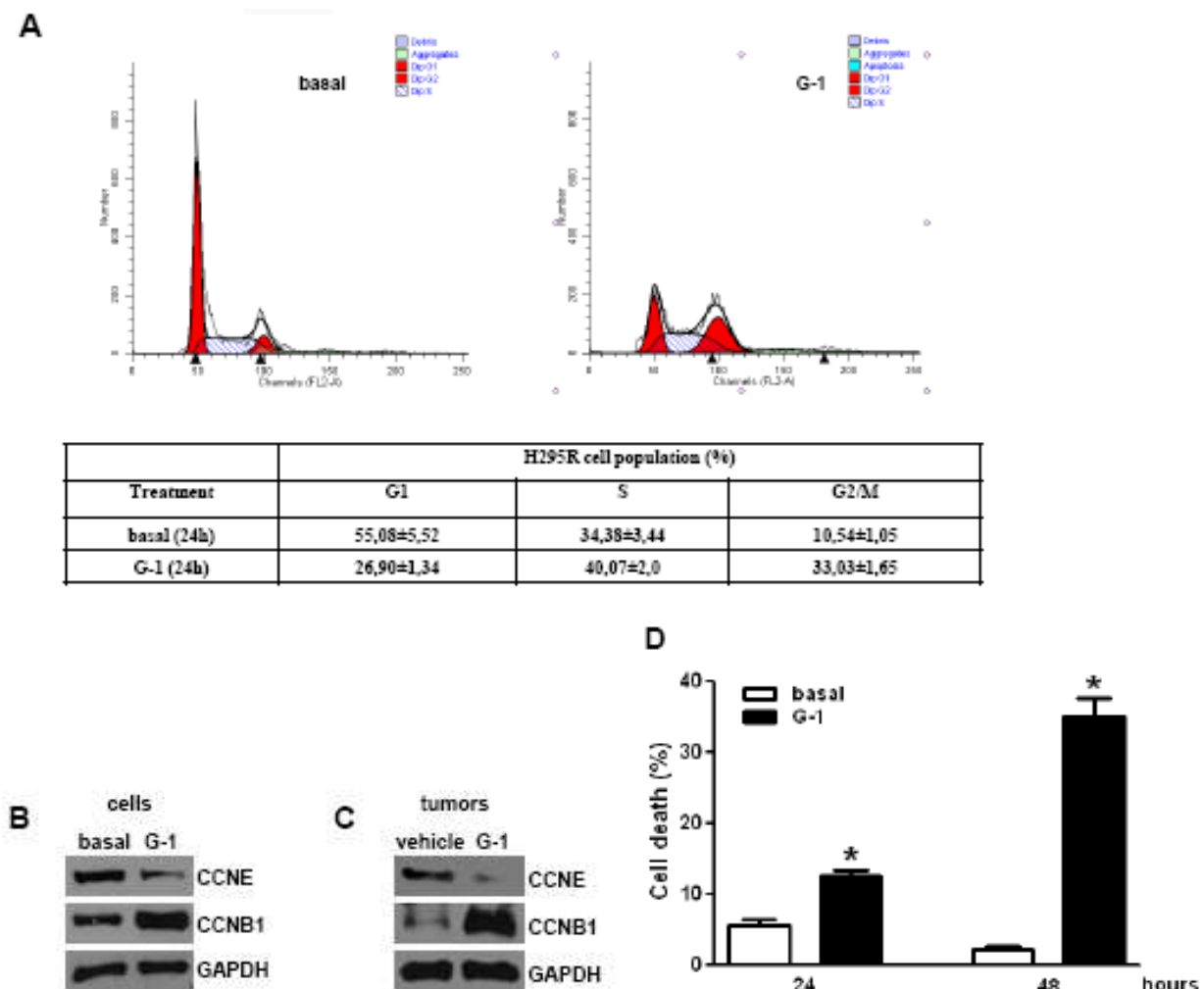
Twenty one days after tumor grafting all mice developed a detectable tumor and were randomized to be treated with either vehicle or G-1. G-1 administration produced a statistically significant decrease in tumor volume from day 14 post treatment (Fig. 4. A). The drug was well tolerated without lethal toxicity or body weight loss during treatment (data not shown). Multislices T2-W MRI indicated larger tumor volume in vehicle treated animals compared to tumors from G-1 treated mice. Hyperintense large cystic area and haemorrahagic regions, that appear as dark areas in the tumor sections, were present in vehicle treated animals (Fig. 4. B). Grafted tumors harvested after three-week treatment with G-1 showed a significant decrease in tumor weight compared to vehicle treated animals (Fig. 4. C). Only G-1 treated tumors revealed some picnotic nuclei through Hematoxylin and eosin staining (Fig. 4. D). Ki-67 immunostaimning was significantly lower in G-1-treated tumors compared to control mice (value score control: 6, 6 ± 0, 89 (SD); value score G-1 treated cells: 3, 1 ± 0.55 * (SD) (*p < 0.05) (Fig. 4. E). Cell cycle analysis of H295R cells after 24 h of G-1 treatment demonstrated a cell cycle arrest in the G2 phase(Fig 5. A). This effect was further confirmed by a change in the expression of cyclins, after G-1 treatment (Fig. 5. B). Specifically, by western analysis we observed that G-1 treatment caused a decrease in Cyclin E (CCNE), while Cyclin B1 (CCNB1), involved in the regulation of G2 phase, was increased. CCNE and CCNB1 had similar expression pattern in protein samples extracted from xenografts tumors (Fig. 5. C). Collectively these events support the idea of cells exiting G1 but remaining stuck in G2 phase. In agreement with the observation that inappropriate accumulation of B type cyclins is associated with the initiation of apoptotic pathways(Ling et al., 2002). We found that G-1 caused cell death by apoptosis. Cells were treated for 24 or 48 h with vehicle or G-1, incubated with an Annexin-V specific antibody and sorted by flow cytometry. As shown in Figure 5. D the number of dead cells increased in a time dependent manner reaching about 40% of apoptotic cells 48 h after G-1 treatment (Fig. 5. D).

Figure 4: G-1 treatment decreases H295R cell growth _in vivo_. (A), 6 x 10^{6} H295R cells were injected subcutaneously in the flank region of immunocompromized mice and the resulting tumors were grown to an average of 200 mm[3] twenty one days after inoculation. Tumor volumes were calculated, as indicated in Materials and Methods. Values represent the mean+SE of measured tumor volume over time in the control group (filled circles, n=10) and in the G-1-treated group (filled triangles, n=10). Data represent pooled values from two independent experiments. (*P<0.05 versus control at the same day of treatment). (B), _In vivo_ coronal T2-weighted spin-echo MR image of primary ACCs. Examples of multi-slices T2-W MRI (section thickness of 1 mm) tumors from vehicle treated mice (control tumors) show a larger volume compared to tumors from G-1 treated mice. Hyperintense large cystic area and haemorrhagic regions that appear as dark areas in the tumor sections, are present in the control tumors. (C), After 3-week treatment tumors were harvested and weighed. Values represent the mean+SE of measured tumor weight (n=10) (*, P<0.05 versus vehicle). (D), Hematoxylin and eosin stained histologic images of H295R xenograft tumors. (E), Representative pictures of Ki-67 immunohistochemical staining of H295R xenograft tumors. NC, negative control.

G-1trattment causes cell cycle arrest and cell death in H295R

H295R cell cycle analysis showed an arrest in the G_2 phase after 24 h of G-1 treatment (Fig. 5. A). This event was confirmed by a variation of cyclins expression, after G-1 treatment (Fig. 5. B). We observed, by western analysis, in fact, a decrease in Cyclin E (CCNE) after G-1 treatment. In the same condition Cyclin B1 (CCNB1) expression, involved in the regulation of G_2 phase, was increased. Both CCNE and CCNB1 in protein samples extracted from xenografts tumors showed similar expression pattern (Fig. 5. C).

Treatment	H295R cell population (%)		
	G1	S	G2/M
basal (24h)	55,08±5,52	34,38±3,44	10,54±1,05
G-1 (24h)	26,90±1,34	40,07±2,0	33,03±1,65

Figure 5: Effects of G-1 treatment on cell cycle distribution and on cell death. (A), H295R cells were synchronized in serum-free media for 24 h and then exposed to vehicle (basal) or G-1 (1 μM) for the indicated times. The distribution of H295R cells in the cycle was determined by Flow Cytometry using Propidium Iodide stained nuclei. Table shows the distribution of H295R cell population (%) in the various phases of cell cycle. (B-C), Western blot analyses of Cyclin E (CCNE) and Cyclin B1 (CCNB1) were performed equal amounts of total proteins extracted from H295R cells treated with G-1 (1 μM) for 24 h (B) and xenografts tumors (C). Blots are representative of three independent experiments with similar results. GAPDH was used as a loading control. (D), Subconfluent H295R monolayers starved for 24h were treated for the indicated times with G-1 (1 μM). Then cells were stained with Annexin V/ FITC plus PI and examined by flow cytometer. Graph represents the percentage of cell death at the different times of treatment. (*, P <0.05 versus basal).

G-1 causes cell nuclei morphological changes, DNA damage and apoptosis

DNA fragmentation confirmed G-1 ability to trigger apoptosis in H295R cells. TUNEL staining demonstrated the presence of increased positive cells in the samples treated with G-1 (Fig. 6. A). Moreover, Hoechst staining proved that untreated H295R cells had round nuclei with regular contours while nuclei from G-1 treated cells appeared shrunken, irregularly shaped or degraded with condensed DNA. DNA extracted from G-1 treated H295R , through DNA gel electrophoresis cells, revealed a classic laddering pattern of inter-nucleosomal DNA fragmentation that was absent in control cells (Fig. 6. B). This event was associated with an increase in Parp-1 cleavage (Fig. 6. C), with increased Bax and decreased Bcl-2 expression (Fig. 6. D). Data obtained from tumors samples by western blot analysis overlap with those obtained in H295R cells (Fig. 6. E). Triggering intrinsic of apoptotic mechanism causes Cytochrome c (Cyt C) release from mitochondria into the cytosol (Oberst et al., 2008). Therefore we fractionated G-1 treated H295R cell lysates into cytosolic and mitochondrial fractions and evaluated Cytochrome c release by western blot analysis (Fig. 6. F). As expected Cytochrome c levels increased in the cytosolic fraction of treated samples while decreased in the mitochondrial compartment. This Cytochrome c released from mitochondria into the cytosol triggers caspase activation; in fact after G-1 treatment we detected active Caspase 9 (Fig. 6. G) as well as the executioner Caspase 3/7 (Fig. 6. H).
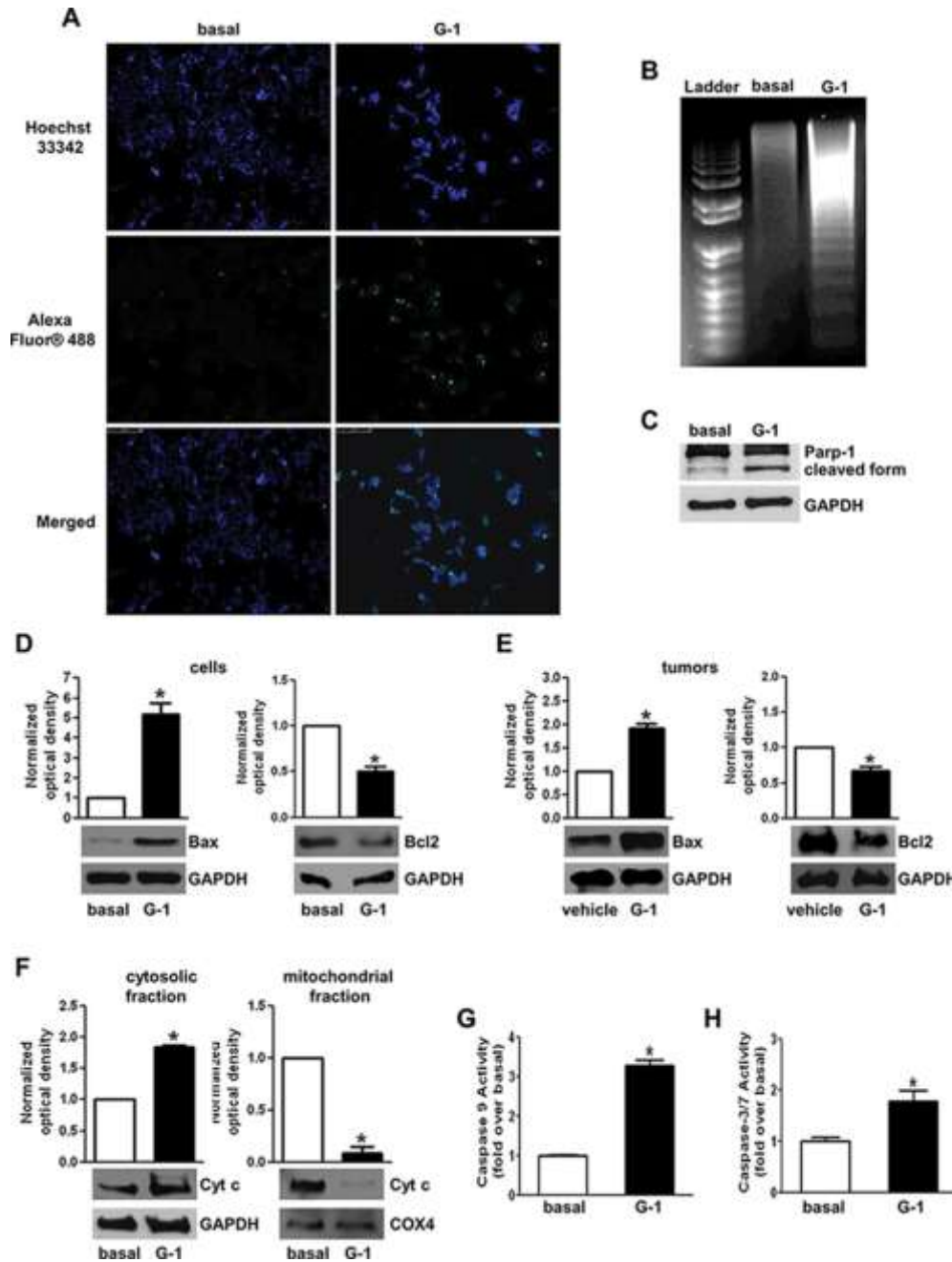
Figure 6: G-1 treatment induces apoptosis in H295R cells. (A) Cells were left untreated (basal) or treated with G-1 (1 μM) for 24 h; after treatment cells were fixed with paraformaldehyde and processed for TUNEL staining. Nuclei counterstaining was performed using Hoechst 33342. Fluorescent signal was observed under a fluorescent microscope (magnification 200X). Images are from a representative experiment. (B) After 48 h treatment DNA was extracted from cells and analyzed on a 1.5% agarose gel. Images are from a representative experiment.(C–F). H295R cells were treated with G-1 (1 μM) for 24 h. Western blot analyses of Parp-1 (C), Bax and Bcl-2 (D). Cytochrome c (F) were performed on equal amounts of total proteins. Blots are representative of three independent experiments with similar results. Bax and Bcl-2 were analyzed on total proteins extracted from xenograft tumors (E). GAPDH was used as a loading. G-H. H295R cells were treated with G-1 (1 μM) for 24 h. Caspase 9 (G) and caspase 3/7 (H) activity was determined by a luminescent assay. Results were expressed as percentage of enzyme activity. Graphs represent mean + SE of three independent experiments each performed in triplicate. Statistically significant differences are indicated (*$P < 0.05$ versus basal).

G1 treatment causes sustained ERK1/2 phosphorylation

To define the molecular mechanism involved with G-1-induced apoptosis, we investigated the activation of MAPK family members extracellular signal-regulated kinase 1/2 (ERK1/2), which have been demonstrated to be involved in apoptosis if activated for a prolonged time (Chen et al., 2005). As shown in Figure 7. A, G-1 treatment activated ERK1/2 in a time-dependent manner as seen by the increased levels of their phosphorylation status. Activation started after 30-min of G-1 treatment and persisted for up to 24 h (Fig. 7. A). ShGPER, that partially reversed G-1 effects on cell proliferation (Fig. 3. E) did not affect ERK1/2 activation (Fig. 7. B). Involvement of ERK1/2 in G-1-induced apoptosis of adrenocortical cancer cells was confirmed by the observation that MEK1 inhibitor, PD98059, prevented the up-regulatory effect exerted by G-1 on Bax expression (Fig. 7. C).
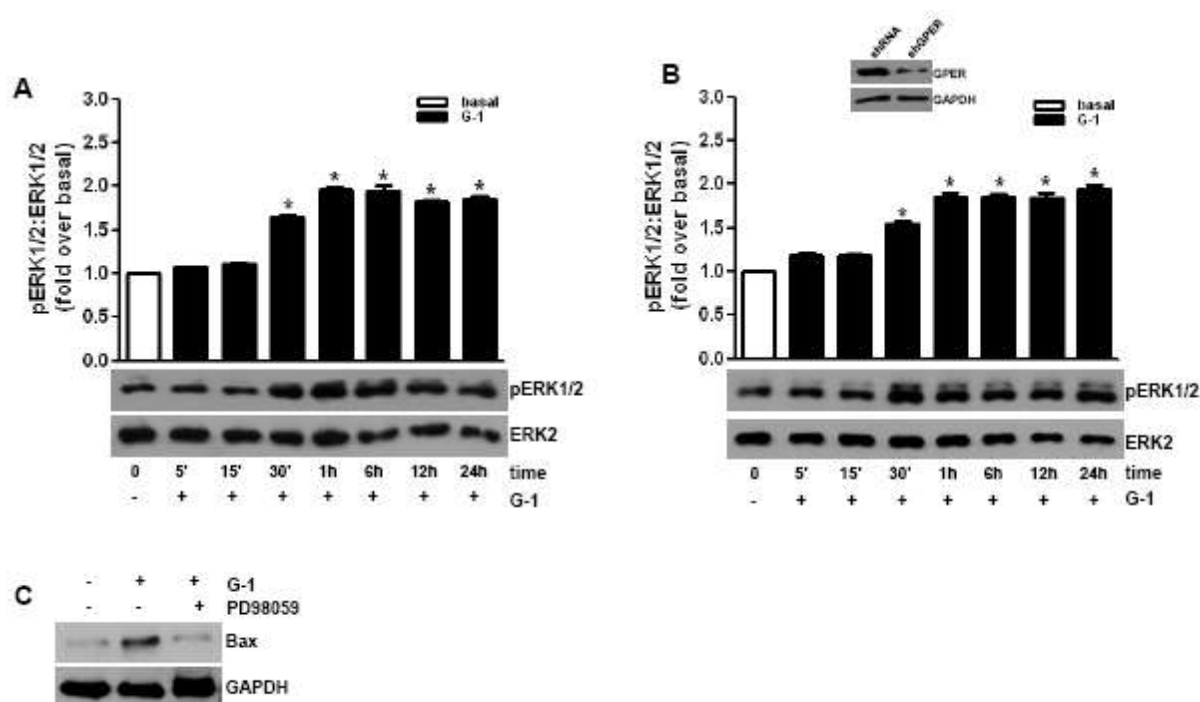
Figure 7: G-1-induced MAPK activation correlates with an increased protein expression of proapoptotic Bax. H295R cells were transfected with shRNA (A) or shGPER (B) for 72 h. Forty-eight hours after transfection cells were untreated (0) or treated for at the indicated time with G-1 (1μM). Western blot analyses of pERK1/2 were performed on 10 μg of total proteins. ERK1/2 was used as a loading control. Blots are representative of three independent experiments with similar results. The insert in Fig. 5. B shows a Western blot on H295R protein extracts evaluating the expression of GPER receptor in the presence of shcontrol or of shGPER. GAPDH was used as a loading control. (A-B up panels) Graphs represent means of normalized optical densities from three experiments, bars represent SE. *p < 0.05 versus basal. (C), H295R cells were treated for 24 h with vehicle (-) or G-1 (1 μM) alone or combined with PD98059 (10 μM). Western blot analysis of Bax was performed on equal amounts of total proteins. GAPDH was used as a loading control. Blots are representative of three independent experiments with similar results.

Discussion

GPER agonist G-1 decreases adrenocortical carcinoma (ACC) cell growth

In this thesis we confirmed the role of estrogenic ligand of GPER, named G-1, into inhibition of H295R cells both *in vitro* both *in vivo* through xenograft model. From these evidences we investigated the potential role of GPER in this event. We confirmed GPER expression both in H295R both in normal adrenal and ACC samples. This first analysis not indicate any expression levels difference. Recent studies, have shown that activation of GPER initiates signaling cascades are associated with both proliferation (Albanito et al., 2008a; Vivacqua et al., 2006b) and apoptosis (Chen et al., 2005; Chimento et al., 2013a) depending on the cell type. GPER activation have conflicting effects on cell proliferation of ERs negative and ERs positive breast cancer cells (Ariazi et al., 2010). In particular when ERs are expressed, activation of GPER leads to inhibition of cell proliferation. On the contrary, activation of GPER leads to an increase in cell proliferation when cells are ERs negative (Ariazi et al., 2010). We demonstrated that micromolar concentrations of G-1 decrease H295R cell proliferation in vitro, significantly reduce ACC tumor volume in vivo and cause a marked decrease in the expression of the nuclear proliferation antigen Ki-67. Flow cytometry analysis, in fact, revealed that G-1 treatment causes changes in cellular distribution within the different phases of cell cycle. Cell cycle progression is regulated by complexes containing cyclins and cyclin dependent kinases (CDKs) (John et al., 2001). We observed that, after G-1 treatment, expression of G1 phase cyclin CCNE was reduced, while G2 phase cyclin CCNB1 was increased. Cyclin levels indicates that H295R cells do not bypass G2 checkpoint. Similar behavior was observed for prostate cancer cells. In these cells GPER activation by G-1 1 µM treatment caused cell cycle arrest in G2 phase (Chan et al., 2010). Arrest in G2 phase and apoptotic cell death was confirmed by staining for Annexin-V, with nuclei morphological changes and appearance of DNA ladder pattern. Apoptosis can be induced by extrinsic (Kim et al., 2006) and intrinsic mechanisms (Fadeel and Orrenius, 2005); intrinsic mechanism is controlled by bcl-2 family proteins (Cory and Adams, 2002) through pro- (Bax, Bad, Bak, Bid) and anti-apoptotic (Bcl-2, Bcl-xl) proteins. Proteins that modulate the execution phase of the cell death pathway. In particular Bax exert pro apoptotic activity allowing Cytochrome c translocation from the mitochondria to the cytosol (Antonsson et al., 2000). Cytochrome c then binds to apoptotic protease-activating factor-1 (Apaf-1) (Wang, 2001), which in turn associates with Procaspase 9 resulting in the activation of its enzymatic activity (Kuida et al., 1998) responsible for the proteolytic activation of executioner Caspase 3 (Wilson, 1998). Caspase 3 is involved in the cleavage of a set of proteins including Poly-(ADP) ribose polymerase-1 (Parp-1) (Soldani and Scovassi, 2002). Bcl-2, instead, exerts in part its anti-apoptotic activity, by inhibiting the translocation of Bax to the mitochondria (Wang, 2001). Changes in expression and/or activation of

all the above mentioned biochemical markers of mitochondrial apoptotic pathway were observed in H295R cells in response to G-1 treatment. Part of GPER signaling are MAPK family members ERK1/2 (Lappano et al., 2013). Despite the well-defined role of ERK1/2 activation in proliferative pathways (Meloche and Pouyssegur, 2007), sustained ERK1/2 phosphorylation is also involved in apoptotic events (Chen et al., 2005; Chimento et al., 2013a; Ramos, 2008). In particular is important that duration of ERK activation in promoting cell death can be different depending on cell type and stimuli. G-1 caused sustained ERK1/2 activation in H295R, this event was concomitant with apoptosis, since chemical inhibition of MEK1/2 using PD98059 abrogated G-1 ability to induce the expression of proapoptotic factor Bax. ERK1/2 activity, in fact, can be associated with upregulation of proapoptotic members of the Bcl-2 family, such as Bax (Chen et al., 2010; Tan and Chiu, 2013; Tong et al., 2011). Moreover, ERK activity directly affect mitochondrial function in different way (Cagnol and Chambard, 2010) such as decreasing mitochondrial respiration (Nowak, 2002; Nowak et al., 2006) and mitochondrial membrane potential (Kim et al., 2003; Nowak et al., 2006), causing mitochondrial membrane disruption and Cytochrome c release (Kim et al., 2003; Li et al., 2005; Zhang et al., 2004). Interestingly, GPER silencing was not able to prevent G-1 induced ERK phosphorylation, underlying the existence of alternative targets for G-1. These targets, similarly to GPER, are able to activate ERK1/2 signaling, however for a prolonged period, and clearly deserve further investigation. Other papers evidenced inhibitory effects exerted by G-1 on the growth of different tumor cell types in a GPER independent manner [55–57], but a precise mechanism has not been defined. Although further studies are needed to clarify the molecular mechanisms behind G-1-dependent effects, this molecule could be a viable alternative to the current limited treatment options and therapeutic efficacy for adrenocortical cancer.

In conclusion, we demonstrated that treatment of H295R cells with G-1 reduced tumor growth in vitro and in vivo through a mechanism involving not only GPER activation. G-1 clearly causes cell-cycle arrest at the G2 phase and apoptosis through a mechanism that requires sustained ERK1/2 activation. Our previously published results highlighting the ability of OHT, a known GPER agonist and ESR1 antagonist, to reduce ACC cell growth, together with the present findings indicating the inhibitory effects exerted by G-1, open up new perspectives for the development of therapies with molecules modulating estrogen receptors action for the treatment of ACC.

Determination of mercury through TDA-AAS TECHNIQUE for Human Biomonitoring activity

Background

Mercury

Heavy metals are essential components of Earth's crust. Heavy metals are generally defined as metals with relatively high densities, atomic weights, or atomic numbers. Some heavy metals are either essential nutrients (typically iron, cobalt, copper and zinc), or relatively harmless (such as ruthenium, silver, and indium), but can be toxic in larger amounts or certain forms (Fergusson, 1990). Other heavy metals, such as cadmium, mercury and lead, are highly poisonous (Tchounwou et al., 2012). In China, Egypt, Greece and Rome has been recorded the use of mercury (Hg) in manufacturing and medical purposes since classical times. Parallel, poisoning by Hg has also been reported since at 2000 years ago. Plinio il Vecchio (23-79 AD), in fact, in Naturalis Historia, refers to cinnabar (HgS) poisoning among miners at Almaden, Spain (Rackham, 1952). Historically, Hg poisoning was a consequence of iatrogenic and occupational activity as documented in 18th century by Ramazinni that described the occupational diseases developed by workers exposed to Hg (Goldwater, 1936). Mercury, especially in elemental and inorganic form continued to be widely used in industrial applications as in medical treatments. In 16th century, in fact, mercurous chloride or calomel (Hg_2Cl_2) was introduced as a treatment for syphilis (De Laguna, 1955.) and furthermore Hg use has also extended into 20th century. It was present in different preparations such as antisyphilitic, antihelminthic, diuretic, and many others including also Chinese herbal medicines(Ernst and Coon, 2001). Some of these preparations exceed the maximum concentrations permitted by regulatory bodies (World Health Organization 1991). Dental mercury amalgam, which releases low amounts of elemental Hg vapor was first recorded (600 AD) in China; safety theme of mercury amalgam has long been a source of controversy (Dodes, 2001; Clarkson, 2002). Between 1932 and 1968, the Chisso Corporation dumped an estimated 27 tons of Hg compounds in Minamata Bay. Minamata is a small Japanese town where the release of high levels of methylmercury (MeHg) as industrial waste into local waterways induced environmental contamination and consequent population exposure through consumption of contaminated fish and shellfish . The devastating health effects subsequently became known as "Minamata disease" a developmental conditions at high dose characterized by infantile cerebral palsy, congenital abnormalities, ataxia, paralysis, hearing and vision loss, and other symptoms related to entity of exposure. WHO (World Health Organization) estimates that at least 50,000 people have been affected and more than 2000 cases of Minamata disease have been certified as result of the incident.
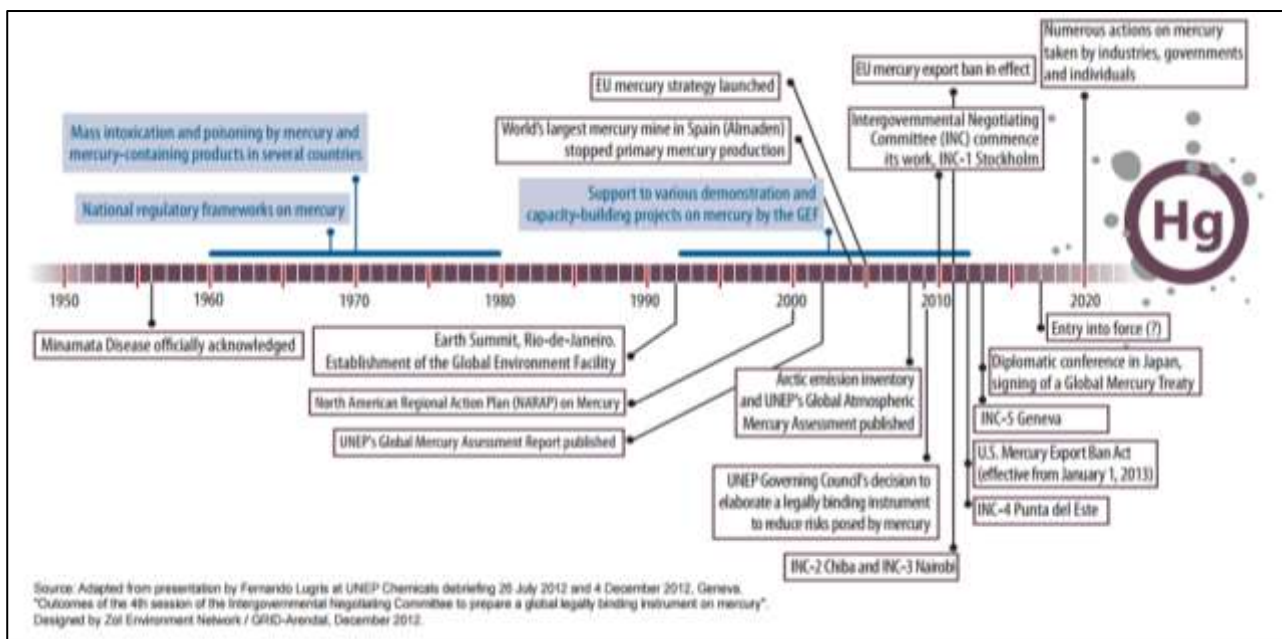
Figure 8: Global Mercury events timeline (http://www.unep.org/PDF/PressReleases/Mercury_TimeToAct.pdf).

On January 19, 2013, The Minamata Convention on Mercury was agreed upon at the fifth session of the Intergovernmental Negotiating Committee in Geneva, Switzerland (Fig. 8). It is a global treaty to safeguard human health and the environment from the adverse effects of Hg. The first step of the convention is the reduction of Hg emission and eradication of potential source of exposure through a ban on new mercury mines, the phase-out of existing ones, control measures on air emissions, and the international regulation of the informal sector for artisanal and small-scale gold mining (http://www.mercuryconvention.org/Convention)

Mercury cycling

Hg is a heavy metal noted for its potential toxicity, especially in environmental contexts. The same amount has existed on the planet since the earth was formed; however, natural and anthropogenic activities can redistribute this element between atmosphere, soil and water through a combination of transport and transformations. During the industrial times, as result of its uses, the amount of Hg mobilized and released into the atmosphere has increased compared to the pre-industrial levels. This metal has been indeed employed in a wide array of applications (i.e., manufacturing, dentistry, metallurgy) thanks to its unique physico-chemical properties (i.e., high specific gravity, low electrical resistance, constant volume of expansion) (see Table 1).

PROPERTIES	USES
Liquid metal	Barometers, blood pressure cuffs
Expands/contracts with temperature	Thermometers
Conducts electricity	Switches, fluorescent bulbs,electrolytic production of chlorine
Amalgamates with other metals	Dental fillings, gold purification
Kills bacteria and fungi	Disinfectants, preservatives, vaccines

Table 1: Properties and Uses Of Mercury.

Hg, emitted to the atmosphere from a variety of point and diffuse sources, is transported in the air and deposited to the earth where it was redistributed between water and soil (Fig. 9). It also enters the environment through discharges to water from various industries or dental clinics and ends up in the sewage sludge that is used as agricultural fertilizer. Mercury cycling and partitioning between different environmental compartments are phenomena that depend on numerous environmental key factors as:

- The chemical and physical form of Hg in air that influence the depositional fluxes
- Wet deposition, the primary mechanism for transferring Hg and its compounds from atmosphere to aquatic and terrestrial ecosystem (except for arid regions where particle dry deposition fluxes may be significant)
- Dissolved and/or particulate Hg forms in aquatic ecosystems and chemical/microbial transformation to MeHg Contaminated sediments at the bottom of surface waters that can serve as aHg reservoir, with mercury recycling back into the aquatic ecosystem for decades or longer.
- Due to its long retention time in soil, Hg may continue to be released to surface waters and other media for long periods of time.
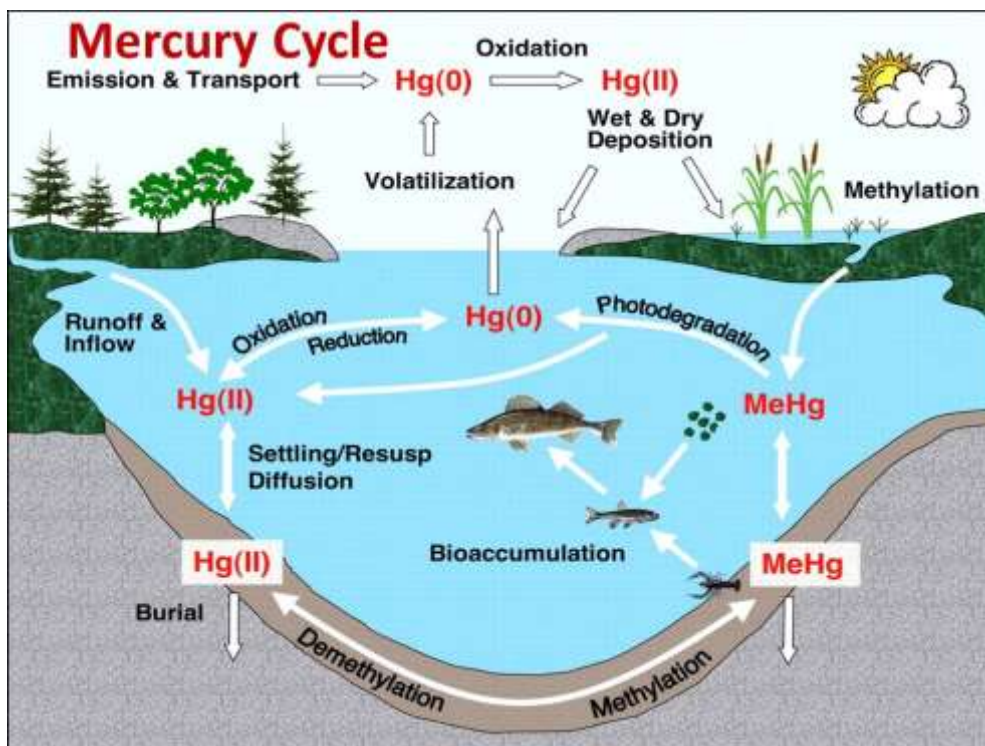
Figure 9: Mechanisms involved in the global mercury cycle.

The different processes affecting the global cycle of Hg, among which the mechanisms driving the methylation and bioaccumulation pathways in the aquatic food chain, are not completely understood.

Mercury is emitted in atmosphere in two main forms: elemental vapor (Hg0) and gaseous divalent (Hg(II)). Chemical and physical characteristics of the two main forms of Hg drive the chemical and physical interactions with other atmospheric contaminants (Pacyna and Keeler 1995; Petersen et al., 1998; Pirrone et al., 2000; Munthe et al., 2000; Munthe et al., 2001) and the transport of this metal. Elemental Hg vapor is relatively inert to chemical reactions with other atmospheric constituents, and is only thinly soluble in pure water with an atmospheric residence time of approximately one year (Slemr et al., 1979). Once released to the atmosphere, elemental Hg can be dispersed and transported for long distances before being deposited to the earth. In the presence of liquid water in the atmosphere (fog or cloud water or precipitation), in fact, small amounts of Hg^0 are dissolved and can be oxidized to Hg(II) species in the aqueous phase by ozone (Munthe, 1992) or OH radicals (Gårdfeldt et al., 2001). These reactions occur at a significantly higher rate in the aqueous phase than in the gas phase. Instead reactions with dissolved sulphur dioxide and OH radicals were involved in the back-reduction to Hg^0 and subsequent transfer back to the gas phase. The rate of reduction is to some extent governed by the complexation chemistry of Hg(II) in the liquid phase

Routes of exposure

The ambient air and dental fillings represent the two major sources of human exposure to the vapor of metallic Hg in adult (WHO, 1997).Hg from dental amalgam may contribute from 0 to more than 75% of the total daily Hg exposure, depending on the number of amalgam fillings. The amalgam used in dental fillings contains approximately 50% metallic Hg that is released from the surface of the filling due to corrosion or chewing or grinding motions. However, exist other sources of exposure to metallic Hg vapors such as breathing contaminated air around hazardous waste sites, waste incinerators, or power plants that burn Hg-containing fuels. Most outdoor air is not likely to contain levels that would be harmful, and exposure to Hg compounds at hazardous waste sites is much more likely to happen from handling contaminated soil (i.e., children playing in or eating contaminated surface soil), drinking well-water, or eating fish from contaminated waters near those sites (Tab.2) . High consumption of fish represents a source of exposure to MeHg; people may be exposed to higher levels of this compound if they have a diet high in fish, shellfish, or marine mammals (whales, seals, dolphins, and walruses) living in Hg-contaminated waters (Tab. 3). MeHg accumulates up the food chain, so that fish at the top of the food chain will have the most Hg in their tissues through a process called bio-magnification. Other foods containing higher levels of Hg include wild game, such as wild birds and mammals (bear) that eat large amounts of contaminated fish. Through eating meat or fat from marine mammals including whales, dolphins and walruses, people, especially in the most northern climates, may be exposed to high levels of Hg.

Metallic Hg is used in a variety of household products and industrial items, including thermostats, fluorescent light bulbs, barometers, glass thermometers, and some blood pressure devices. When these devices, that generally does not pose a risk, is damaged or broken Hg vapors are released. People can be exposed to Hg vapors also from the use of fungicides that contain Hg or from swallowing or applying to the skin outdated medicinal products (laxatives, worming medications, and teething powders) that contain mercurous chloride. Exposure may also occurs from the improper or excessive use of other chemicals containing Hg, such as skin-lightening creams and some topical antiseptic or disinfectant agents (mercurochrome and thimerosal). Less important aren't religious practices that may include the use of metallic Hg such as Santeria, Voodoo and Espiritismo. Prenatal Hg exposure and its fetotoxic effects may be of particular concern. Hg exposures begin at the point of conception but the exposure to this metal continues throughout the life stages - infancy, childhood, and adolescence. There are numerous sources that have been recognized of special significance during pregnancy as dietary intake of fish, shellfish or marine mammals and also Hg vapors released from maternal dental amalgams (WHO, 1997). During pregnancy, the maternal exposure to Hg could result in irreversible damage especially to the

nervous system of fetus with behavioral, cognitive patterns and motor skills alterations (Rice and Barone, 2000). Exposure to Hg may result in effects on other systems in which prolonged developmental processes are required such as the immune system and reproduction. Because of the highly efficient gastrointestinal absorption and physiological immaturity in addition to a larger consumption of foods to support their growth, children can be considered at higher risk than adults (Dorea and Donangelo, 2005; WHO, 1996). Infants may be exposed to Hg compounds first via breast milk consumption (i.e., on a body weight basis food consumption of infants are higher than older children) (see Tab.4) and then to exposures to specific practices and products, such as teething powders, soaps, and organo-mercurials used in medicines (World Health Organization, 2010). Both organic and inorganic Hg occur in breast milk, and in addition to diet, elevated levels of Hg could originate via occupational exposures and also dental amalgams of pregnant women (Bose-O'Reilly et al., 2008). Due to the mammary gland efficiency, in fact, both the forms of Hg were transferred from maternal blood to breast milk. This transport is more rapid for inorganic Hg than for MeHg as showed by several studies in which maternal dental amalgams (i.e., inorganic Hg) are more closely correlated with breast milk Hg concentrations, than maternal MeHg concentrations. The preferential partition of inorganic Hg to breast milk is correlated with the association between plasma Hg and breast milk; as MeHg is preferentially partitioned to erythrocytes rather than plasma, plasma is relatively enriched in inorganic Hg (Bjornberg et al., 2005).When they grow sources of exposure for children are different and occur by accident (e.g., from broken thermometers, fluorescent light bulbs and other pressure gauges or liquid metal used in school laboratories), from specific products (e.g., Hg-containing paints), from take-home exposure from occupationally exposed adults or through use of cosmetics (e.g., skin-lightening creams and soaps) containing Hg salts (Bose-O'Reilly et al., 2010; Xu J et al., 2016; Scheepers et al., 2014). Regard to exposure in workplaces, children are not typically exposed but some former industrial facilities, contaminated by Hg and subsequently converted to residences or childcare facilities, can lead to significant elemental Hg exposure (ATSDR, 2007). As regard organic Hg, MeHg intoxication in children may result from diet while ethylmercury (EtHg) exclusively from vaccines. EtHg, in fact, has been used as a topical antiseptic and as antifungal agent in multi-dose vaccine vials given to children as thimerosal (which contains 49.6% of EtHg by weight) (Ronchetti et al., 2006; Guzzi et al., 2012; Stajich et al., 2000). For this reason, thimerosal has been removed from most vaccines in the United States. In the EU the lack of precise regulations is a concern because the adverse effects of high-dose EtHg are thought to be similar to high-dose MeHg (Allen et al., 2004). The window of exposure may still be a critical factor for children entering puberty and adolescence. A wide range of effects on endocrine system (e.g., specific cytotoxicity in endocrine tissues, changes in hormone concentrations,

interactions with sex hormones and regulation of enzymes within the steroidogenesis pathway) were established during puberty but adverse neurological effects may also occur in older children and adolescents (Grandjean, et al., 2004; Tan et al., 2009). These evidences reflect the cumulative influence of different factors and sources to which adolescents may be exposed. In conclusion, children can be exposed to Hg in a number of ways such that their exposures exceed those of most adults, and , actions are required to reduce the threat and to promote the healthy development of the world's children. (World Health Organization, 2010).

Source of exposure	Elemental mercury vapor	Inorganic mercury compounds	Methylmercury
Air	0.030 (0.024)	0.002 (0.001)	0.008 (0.0064)
Food			
Fish	0	0.600 (0.042)	2.4 (2.3)
Non-fish	0	3.6 (0.25)	0
Drinking water	0	0.050 (0.0035)	0
Dental amalgams	3.8–21 (3–17)	0	0
Total	3.9–21 (3–17)	4.3 (0.3)	2.41 (2.31)

Note: Values given are the estimated average daily intake (in µg/day) for adults in the general population who are not occupationally exposed to mercury; the figures in parentheses represent the estimated amount retained in the body of an adult.

Source: WHO 1990, 1991

Table 2: Estimated average daily intake and retention of total Hg and Hg compounds in the general population (Available at URL: https://www.atsdr.cdc.gov/toxprofiles/tp46.pdf).

Consumption rate (g/day)	Description	Population	Reference
170	95 %ile (adult)	Umatilla, Nez Perce, Yakima, and Warm Springs Tribes of Columbia River Basin Washington	CRITFC 1994
140	90 %ile (adult)	Subsistence fisher (default value)	EPA 1995k
109	Mean (adult)	Native Alaskans in 11 separate communities	Nobmann et al. 1992
63	95 %ile (adult)	Wisconsin anglers (10 counties) includes both recreationally and commercially caught fish	Fiore 1989
59	Mean (adult)	Umatilla, Nez Perce, Yakima, and Warm Springs Tribes of Columbia River Basin Washington	CRITFC 1994
37	95 %ile (adult)	Wisconsin anglers (10 counties) includes only recreationally caught fish	Fiore 1989
34	75 %ile (adult)	Wisconsin recreational anglers	Fiore 1989
30	Mean (adult)	Recreational fisher (default value)	EPA 1995k
28	Mean (adult)	New York anglers	Connelly 1990
26	Mean (adult)	Wisconsin anglers (10 counties) includes both recreationally and commercially caught fish	Fiore 1989
20	Mean (child 5 years and younger)	Umatilla, Nez Perce, Yakima, and Warm Springs Tribes of Columbia River Basin Washington	CRITFC 1994
12	Mean (adult)	Wisconsin anglers (10 counties) includes only recreationally caught fish	Fiore 1989
6.5	Mean (adults)	General U.S. population	EPA 1995k

Source: EPA 1996e

Table 3: Fish consumption rates of various populations including general population and recreational and subsistence fishers (Available at URL: https://www.atsdr.cdc.gov/toxprofiles/tp46.pdf).

Population	Year	Number of samples (% positive)	Total Hg content in whole milk (ppb)*	Reference
Minamata, Japan (contaminated seafood)	1968	–	63	Fujita and Takabatake 1977
Iraq (contaminated grain)	1972	44	<200[b]	Bakir et al. 1973
Tokyo, Japan (urban population)	1974	34	3.6±2.2 (0.4–9.8)	Fujita and Takabatake 1977
Iowa, USA (general population without abnormal exposure)	1975	32 (44%)	0.9±0.23	Pitkin et al. 1976
Alaska, USA (coastal population) (interior population) (urban population)	1975	1155	7.6±2.7 3.2±0.8 3.3±0.5	Galster 1976
Madrid, Spain	1981	20 (100%)	9.5±5.5 (0.9–19)	Baluja et al. 1982
Sweden (15 women fish consumers)	1980s	NA	0.2–6.3	Skerfving 1988
Sweden (fish consumers with an average of 12 amalgam fillings)	1990s	30	0.6±0.4[c] (0.1–2.0)	Oskarsson et al. 1996
Faroe Islands (88 women who consumed pilot whale meat)	1990s	100	median 2.45 maximum 8.7	Grandjean et al. 1995

* Results are expressed as means ±S.D unless otherwise noted. Ranges are shown in parentheses.

[b] Of the total mercury, 40% was inorganic mercury; 60% was methylmercury.

[c] Of the total mercury 51% was inorganic; 49% was organic mercury.

Table 4. Total Hg concentration in human breast milk (Available at URL: https://www.atsdr.cdc.gov/toxprofiles/tp46.pdf).

Toxicokinetic

Toxicokinetic of Hg depends by its form and varies considerably. Sources of exposure, critical target organs, toxicokinetic, distribution, biotransformation, and excretion of each Hg species are different. Elemental Hg is oxidized to mercuric inorganic form. (Barregard et al., 1992; Hursh et al., 1980; International Agency for Research on Cancer (IARC), 1993). Inorganic Hg, instead, was complexed with reduced glutathione containing thiol group, while MeHg formed complex both with glutathione both with cysteine or was oxidized to mercuric inorganic forms (demethylation process) in tissues (Harris et al., 2003). The formation of complexes with thiol- containing small molecules plays a major role in the process of transport and distribution in the body. MeHg was absorbed through gastrointestinal tract and enter the bloodstream from which it is distributed to other tissues included the brain (Vahter et al., 1994; Zarebaet al., 2007) Experiments showed that MeHg entry into endothelial cells of the blood-brain barrier as a cysteine complex thanks to a neutral amino acid carrier (Kerper, et al., 1992; Simmons-Willis et al., 2002). The structure of MeHg-cysteine, in fact, closely remember methionine and the carrier process is so selective that only the L-optical enantiomorph is transported. In the central nervous system (CNS) MeHg is transported across the blood-brain barrier by an amino acid carrier and accumulates "*in situ*" where it undergoes to slow dealkylation to inorganic Hg (Aschner and Clarkson, 1988). Toxicity of MeHg is expressed by two principal mechanisms showed in Fig. 10. Regarding the first mechanism, in the extracellular environment, MeHg inhibits glutamate uptake and some amino acids that are associated with the

synthesis of astrocytic glutathione (GSH). Accumulation of glutamate in the extracellular space and the resulting excessive activation of N-methyl-D-aspartate (NMDA) receptor can result in excitotoxicity and cell death. The second proposed mechanism is the impaired cytoplasmatic Ca^{2+} homeostasis and the release of ROS, metabolic inhibition that leads to impaired ATP production, lipid peroxidation and nuclear damage. Furthermore MeHg can provoke microtubules chain disruption decreasing vesicular migration or genotoxicity (Do Nascimento et al., 2008). MeHg shows the same mechanism of absorption also in the gastrointestinal tract and liver. Here MeHg combines with reduced glutathione using a glutathione carriers (Ballatori and Clarkson, 1985; Ballatoriet al., 1955) to form a complex that is secreted into bile. Hence glutathione is hydrolyzed to its constituent amino acids, releasing the MeHg-cysteine complex. The latter part is reabsorbed in the gallbladder into the bloodstream and, in part, secreted into intestinal tract along with any unhydrolysed glutathione complex. Once in the intestinal tract, an amount was reabsorbed into the portal circulation as the cysteine complex and an amount is demethylated by intestinal microflora. Demethylation process can occur also in other organ as demonstrated by Suda and Hirayama (Suda and Hirayama, 1992) that reported the liver microsomes are also capable of demethylating MeHg perhaps via the action of NADPH-cytocrome P-450 reductase.

The result of the metabolic processes is that most of inorganic Hg produced as previous described is excreted in feces.
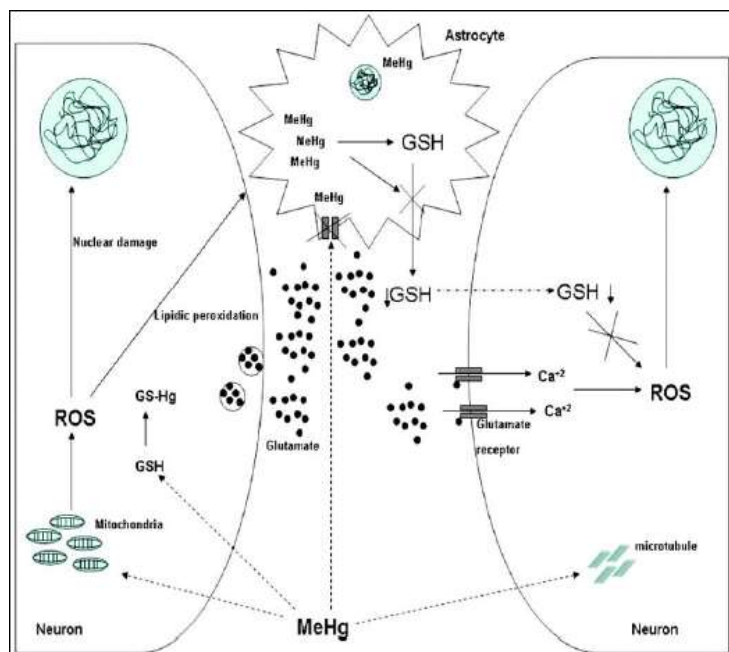

Figure 10: A schematic model of some of the currently proposed mechanisms for cellular damage induced by MeHg in the CNS.

Regarding EtHg the only source of human exposure is thimerosal (inside vaccines). After thimerosal injection, EtHg is released and interacts with thiol-containing proteins and low-molecular-weight thiols, mainly cysteine and reduced glutathione. Thimerosal also releases its non-Hg moiety (thiosalicylate) which presents no significant toxic effects (Tan and Parkin, 2000; Reader and Lines, 1983). The EtHg–cysteine complex can be exported from muscle cells either by plasma membrane transport proteins, via mimicry processes, or through exchange reactions with the plasma membrane thiol-containing proteins, while the EtHg complexed with GSH can be exported only via exchange. The exported EtHg-cysteine complexes then can exchange with generic plasma thiol proteins, with low-molecular weight thiols (Figure. 11) or with albumin. The metabolism of EtHg to cationic Hg drastically alter the fate of Hg in the body. EtHg is more rapidly degraded to Hg^{2+} and for equivalent doses, less Hg will be found in the brain after EtHg exposure as compared to MeHg. The excretion of EtHg resulted more rapid than MeHg from infant blood (Pichichero et al., 2008). Finally EtHg appears to be approximately similar to MeHg in terms of distribution to blood and for excretion route (feces), but there are a difference in tissue deposition and rate of metabolism to inorganic Hg.
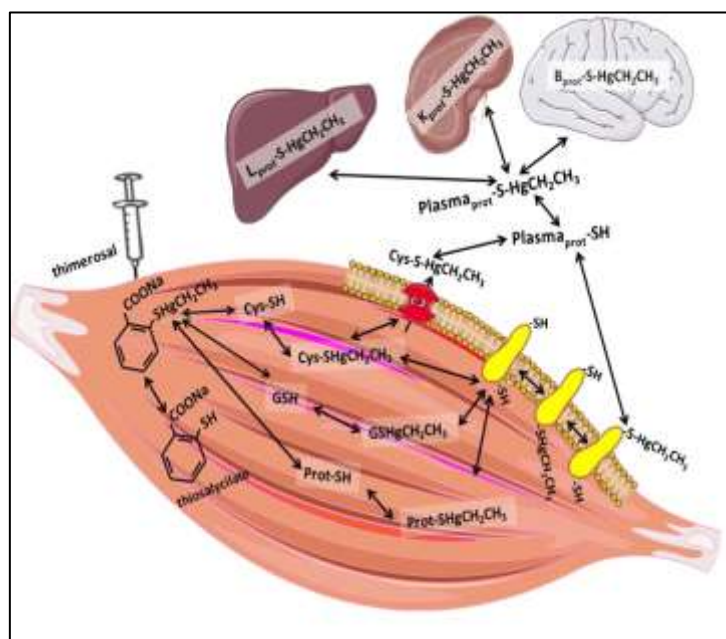
Figure 11: Schematic representation of intramuscular EtHg administration as thimerosal.

Inorganic Hg, instead, accumulates principally in the kidney and in lesser amount in the liver. Inorganic Hg absorption can occur through topic absorption consequence of the use of skin creams, medications, and soaps. The mechanism of deposition in the body is poorly understood, presumably two glutathione molecules attaches Hg cation to form a structure exported from liver cells by

glutathione carriers. Furthermore reduced glutathione play an important role in the renal handling of Hg. It is the principal responsible of renal uptake of Hg, in fact, inhibition of the enzyme gamma-glutamyltranspeptidase (gamma GT), which degrades glutathione, causes a marked reduction of uptake and a large increase on urinary excretion of Hg (De Ceaurriz et al., 1994;Tanaka et al., 1990; Berndt et al., 1985). These evidences demonstrated that inorganic Hg is secreted by proximal tubular cells into tubular lumen as a glutathione complex (Tanaka-Kagawa et al., 1990). This complex is then degraded by gamma GT and Hg is subsequently reabsorbed into renal cells probably as Hg-cysteine complex via the large neutral amino acid transporter (Wei et al., 1999). Higher doses cause collapse of kidney function and extensive corrosive damage to the gastrointestinal tract, stomatitis and gastroenteritis. Lower doses cause selective damage to the kidneys especially in the proximal tube though the biochemical mechanisms of renal toxicity are unknown (Rahola et al., 1973; Hattula and Rahola, 1975). Many reports have also indicated that Hg, especially divalent inorganic form, determine autoimmune diseases both in animals and humans (Pollard and Hultman, 1997) influencing different cellular processes such as inhibition of enzyme function and blockade of cellular receptors or ion channel (McCabe et al., 2005).

Elemental Hg is absorbed by lungs through inhaling, passed to bloodstream and distributed to most tissues where it binds sulfhydryl groups. In tissues MeHg is oxidized to mercurous and mercuric inorganic forms (Clarkson and Magos , 2006; Hursh et al 1976; Halbach and Clarkson 1978). Oxidation process takes place by catalase-hydrogen peroxide pathway. The protein first forms an adduct with hydrogen peroxide to form a catalase compound and then reacts with an atom of Hg to form mercuric mercury. The same pathway is involved in re-oxidation of vapor generated by mercuric mercury reduction. The role of this cycle is not well understood and it isn't determinant for Hg elimination, conversely it plays a role in the mobility of this metal. Regard symptoms, acute inhalation exposure, at high concentrations, may induce respiratory distress including dyspnea. Chronic exposuremay induce symptoms at the CNS including tremors, delusions, memory loss and neurocognitive disorders (Eide and 1983; Syversen and Kaur 2012). Hg is known to be a toxic element for humans and the environment. The International Agency for Research on Cancer (IARC) classified the methylated compounds of Hg as a possible human carcinogen (Group 2B) while metallic and inorganic Hg compounds as unclassifiable with regard to carcinogenicity in humans (Group 3) (IARC (International Agency for Research on Cancer; Available:http://monographs.iarc.fr/ENG/Classification/ClassificationsAlphaOrder.pdf).

Occupational limits have been established for both forms of Hg, elemental and inorganic: the American Conference of Government Industrial Hygienists (ACGIH) fixed a Threshold Limit Value (TLV) – Time Weighted Average (TWA) equal to 0.025 mg/m^3, a BEI (Biological Exposure

Index) of 35 μg/g of creatinine for total Hg in urine and a BEI of 15 μg/L for inorganic Hg in blood (ACGIH (American Conference of Government Industrial Hygienists), 1996).

Human Biomonitoring

Human biomonitoring (HBM) allows to measure human exposure to chemicals by measuring either the substances themselves, their metabolites or markers of subsequent health effects in body fluids or matrices (blood, urine, saliva, serum, breast milk, teeth, nails, hair). Information on human exposure can then be linked to data on sources and epidemiological surveys, in order to inform research on the exposure-response relationships in humans (http://www.eea.europa.eu/themes/human/human-biomonitoring) (Angerer et al., 2006). The HBM can evaluate both recent and past exposure to chemicals and follow the evolution in time of entity of exposure (Schulz et al., 2007b; Wittsiepe et al., 2000). The HBM has a great value to identify population groups at high risk as children, vulnerable to certain pollutants or able to transform parental compounds into toxic metabolites more than adults (Becker et al., 2007). Through HBM it is possible to establish reference values (RVs) for certain substances in the general population and assess the exposure of vulnerable groups as children and elderly, highlighting priorities for research and reviewing the effectiveness of regulatory and legislative measures adopted. For reliable HBM data is necessary to respect severe quality criteria in the different process steps such as the selection of individuals, sampling, control of the variability, analytical and statistical processing of results (Nordberg et al., 1992). All these activities are aimed to develop, standardize and validate sampling protocols and analytical methods as pivotal for the reliability, comparability and transferability of HBM results. The use of HBM to identify spatial and temporal trends in human exposures to chemicals has contributed successfully to initiate policy measures and to create preventive campaigns for the health of the general population and susceptible groups . Examples of national HBM surveys are the US National Health and Nutrition Examination Survey (NHANES) (https://www.cdc.gov/nchs/nhanes/). , the French National Survey on Nutrition and Health (ENNS) (Fréry et al., 2012), the PROBE Italian HBM survey (Pino et al., 2012), the Flemish Environment and Health Study (FLESH) (Schoeters et al., 2012), and the German Environmental Survey (GerES). These HBM surveys intended to define the exposure of the general population and/or susceptible groups to various types of pollutants and combine also subjects' interviews and physical examinations (http://www.umweltbundesamt.de/gesundheit-e/survey/index.htm; Schulz et al., 2007b; Schulz et al., 2009). On the basis of the GerES campaigns, the German Commission has established RVs (Table.3) and HBMI and HBM-II biological limits for different chemicals, different biological matrices and different subgroups of population (Table.5) (Schulz et al., 2007b).

Parameter and matrix (reference)	Population group (age range)	Study period	RV
Mercury in urine (Wilhelm et al., 2004; Schulz et al., 2007a)	Children without dental amalgam fillings (3–14 years)	2003–2006	0.4 µg/l
	Adults without dental amalgam fillings (18–69 years)	1997–1999	1.0 µg/l
Mercury in blood (Wilhelm et al., 2004; Schulz et al., 2009)	Children who ate fish ≤ 3 times per month (3–14 years)	2003–2006	0.8 µg/l
	Adults who ate fish ≤ 3 times per month (18–69 years)	1997–1999	2.0 µg/l
[a]: Uncertainty of analysis must be taken into account.			

Table 5: Reference values (RV_{95}) for Hg in biological fluids.

Parameter and medium	Population group (age range)	HBM I value	HBM II value
Mercury in urine (Schulz et al., 2007a)	Children and adults	7 µg/l	25 µg/l
		5 µg/g creatinine	20 µg/g creatinine
Mercury in blood (Schulz et al., 2007c)	Children and adults*	5 µg/l	15 µg/l
* Derived from women of reproductive age. The value is recommended for other groups			

Table 6: Human biomonitoring (HBM) values for mercury in urine or blood.

The RVs for chemical substances in human matrices (e.g., blood, urine) are derived statistically from a series of measurements, and represent the basic exposure of the general population. They can be expressed as the 95th percentile of the level of the substance in biological samples from a representative group of the general population.

The HBM values are health-related biological exposure limit values; in particular the HBM-I value corresponds to the substance concentration in sample below which there is no risk of adverse effects for the population, while the HBM-II represents the value above which it is present a risk of adverse effects (Ewers et al., 1999). A substance concentration between HBM-I and HBM-II values represents an alert level and biological data must be confirmed by further measurements. A concentration value above the HBM-II is regarded as level of intervention, and immediate actions should be performed.

Biomarker

A biomarker is defined as a cellular, biochemical or molecular alteration that is measurable in biological media such as human tissues, cells, or fluids (http://crsbasilea.inti.gov.ar/pdf/mercurio/MarceloConti-MercuryBiomarkers.ppt). It represents the grade of exposure of the population to environmental contaminants and the temporal trends. Once chemical is absorbed in the body, in fact, it can be excreted without transformation or be metabolized and then excreted or stored in various tissues or bones. All these processes are influenced by the physicochemical properties of the contaminant which influence also the selection of the appropriate matrix. The ideal biological matrix should be easily accessible, available in an adequate amount for analysis, sampled with the less invasive procedure that does not present risks to the subject. Critical factors for biomarker selection are also the clinical end-point and the prognostic value of the biomarker itself.. Other essential characteristics of a suitable biomarker are its validity and reliability. Validity is defined to be the extent to which it measures what it is intended to measure (e.g. the exposure, the effect, the disease or the susceptibility), and it is expressed by two indices: the sensitivity (ability to detect a signal at a low concentration and highlight also the minor variations) and specificity (ability to be characteristic of that particular event). The reliability of a biomarker refers to the degree to which the results obtained by a measurement procedure can be replicated Laboratory personnel, laboratory methods, storage, transport procedures may all affect the reliability of the biomarkers used. Furthermore a biomarker should be readily available and its inclusion in the study should be feasible, also in terms of financial resources. Biologic stability is also critical particularly if the biomarker is to be stored for any length of time. Knowledge of the time that elapses between exposure and sampling is essential in choosing a biomarker. A biomarker characterized by a short half-life only reflect recent exposure but can result valid if the exposure is constant over time. Conversely, for a biomarker with long half-life, the internal dose increased in time and age or time of exposure are determinant factors. Utility of biomarkers are maximized with long half-life contaminants in order to monitor months or

years of previous exposures . Short half-life chemicals are usually measured in urine while long half-life chemicals are quantified in blood. Contaminants that are liposoluble are best measured in matrices with a high content of fat (e.g. adipose tissue and breast milk). It should be also considered that many chemical compounds express a biphasic or polyphasic pharmacokinetics (various compartments and various half-lives): assuming one compartment and a single half-life for the biomarker can lead to errors in the interpretation of the obtained concentration.

There are several different categories of biomarkers, that measure exposure, effect and susceptibility. Each is useful for answering different questions.

A **biomarkers of exposure:** indicator of the exposure to a specific substance, highlighting also possible variations in time;

- A **biomarkers of effect:** indicator of pre-clinical abnormalities or possible or established health effects associated to the exposure to a specific substance or its metabolite;

- A b**iomarkers of susceptibility:** indicator of an inherent or acquired susceptibility to respond to the exposure to a specific substance or its metabolite Biomarker of exposure reflects an individual's current body burden, which is a function of recent and/or past exposure.

Interpretation of biomarkers of exposure requires knowledge of when and how the exposure occurred in the study population group and the toxic potential for that exposure. In assessing the appropriateness of a particular biomarker of exposure, it is important to consider three factors: how well the biomarker predict the external exposure; how well the biomarker correlates with the dose at the site of toxicity and how well the biomarker inform regarding variations in external exposure. In this study the levels of Hg in urine and hair were used as biomarker of exposure to Hg in an Italian children population with the final aim to evaluate possible associations with neurobehavioral and cognitive deficiencies. The human exposure to Hg can be generally assessed through determination of its level in blood and urine, but also hair can be used as biomarkers of exposure. Typically, the levels of Hg in blood and urine represent the total Hg, thus including both inorganic and organic Hg. The WHO estimated an average concentration of total blood Hg for the general population of 8 mg/L, however this value can increase to 200 g/L in case of high consumption of fish (ATSDR (Agency of Toxic Substances and Disease Registry), 1999). Typical concentrations of total Hg in urine vary between 4 and 5 µg/L and reflect mainly exposure to inorganic Hg and also a little fraction of demethylated MeHg. The latest US campaign (NHANES) reports for total Hg a GM (geometric mean) value of 0,703 µg/L in blood and 0,367 µg/L (creatinine corrected) in urine (Fourth National Report on Human Exposure to Environmental Chemicals, 2015). In Italy, for the

general population have been reported ranges between 3,49 and 6,36 g / L in blood and 1.32 to 2.1 mg/L in serum (Alimonti et al., 2005; Alimonti et al., 2009; Minoia et al., 1990) and between 1.15 and 3.5 mg/L in urine (Apostoli et al., 2002; Soleo et al., 2003).

Hair

Generally, Hg concentration in   hair is 250 to 300-fold higher than that in blood, because sulfur-containing proteins rich in the hair bind to MeHg (World Health Organization, 1990). Once incorporated, Hg does not return to the blood, thus, it provides a good long-term marker of exposure. Although inorganic as well organic Hg is incorporated in the hair structure, among fish consumers MeHg constitutes at least 80% of the total Hg. Therefore, hair total Hg is widely used as a biomarker for evaluating exposure to MeHg at all exposure levels (including fetal exposure) (McDowell et al., 2004; National Research Council, 2000). In addition, hair is a biological specimen that is easily and noninvasively collected, with minimal cost, and easy to store and transport to the laboratory for analysis. However, considerable attention to laboratory quality assurance and quality control is required to produce reliable analytic results (World Health Organization, 2010). In contrast to blood concentration - which provides no clear information about the magnitude or timing of the exposures - the hair concentration has the advantages of being able to integrate exposure over a known time. Such information is based on two assumptions: 1) growing hair shafts incorporate Hg in proportion to the concentration of Hg in the blood; 2) hair shafts grow at a constant rate that does not vary significantly among individuals. The first assumptions is necessary for establishing a quantitative relationship between hair Hg concentration and MeHg intake; the blood Hg concentration being an intermediate kinetic compartmentThe second issue is necessary for establishing the relationship between location along the hair strand and the time of exposure (National Research Council, 2000). An average growth rate of 1.1 cm per month for scalp hair is commonly assumed. Thus, a 9-cm length of maternal hair can correspond to ca. 8 months of gestation and maternal hair can be used as a biomarker of fetal exposure. (Grandjean et al., 1992). Notwithstanding several factors such as ethnicity, age, gender, and color may affect the hair growth rate and MeHg incorporation, leading to temporal uncertainty and exposure misclassification (Sakamoto et al., 2004; Grandjean et al., 2002), Grandejan et al. (2002) observed that segmental hair analysis has the potential to provide information about exposure during specific portions (e.g., trimesters) of gestation, but uncertainties related to hair-growth rate make difficult the identification of segments corresponding to periods as short than a single trimester. Despite those limitations, several attempts have been undertaken to determine guidance levels (e.g., benchmark doses, BMD) based on hair Hg levels. The BMDs determined on the basis

of the greatest follow-up studies (i.e., Seychelles, New Zealand and Faroes cohorts) indicated that a level of 4–25 µg/g measured in maternal hair may carry a risk to the infant (Budtz-Jorgensenet al., 2000; Crumpet al., 2000; Van Wijngaarden et al., 2006). However sources of uncertainty (e.g., assumptions about the shape of the dose–response curve, the choice of the cut-off as a benchmark response, and decisions on the critical endpoints) make that level currently under discussion; anyway a linear relationships between 1 µg/g increase in maternal hair Hg concentration and 0.18 point reduction in children's IQ were well established (Axelrad et al., 2007). Furthermore, a recent study, involving analysis of data from studies of developmental neurotoxicity at low Hg exposure levels, estimated a lower biological limit (0.58 µg/g) in hair (Grandjean et al., 2007; Bellanger et al., 2013).

Urine

The major form of Hg in urine is inorganic Hg. Therefore, total Hg concentration in this matrix reflects the amount of inorganic Hg accumulated in kidney (which is a good biomarker for evaluating exposure to inorganic Hg and Hg vapor), and also as an indicator of Hg body burden (World Health Organization, 1995). Urine represents the best biomarker of long-term low-level exposure because urinary Hg is derived directly from those deposited in the kidney tissue, which serves as the main deposit site during chronic Hg exposure (Clarkson and Magos, 2006). If possible, inorganic Hg exposure can be measured by determining urinary Hg concentration preferably using a 24-hour urine collection. Results greater than 10 or 20 µg/L could lead to excessive exposure, while neurologic signs may appear at values greater than 100 µg/L, but also at much lower levels (down to 5-10 µg/L) (Bose-O'Reillyet al., 2010). However, if the Hg exposure has been intermittent or variable in intensity, Hg concentration in urine does not necessarily correlate with chronicity or severity of toxic effects (Goldman and Shannon, 2001). Due to its relatively short half time, urine Hg level is useful only when measured soon after a short term and high-level exposure to inorganic Hg or Hg vapor (i.e., the values tend to return to normal below 5 µg/L within days after the end of the exposure) (Park and Zheng, 2012). The primary target organs of elemental Hg are the brain and kidney. Unlike inorganic Hg, elemental Hg is lipid soluble and can cross the blood-brain barrier. After absorption, it is rapidly converted to inorganic Hg and excreted in urine, thus also a long-term elemental Hg exposure is well represented by the presence of Hg in this matrix (Bose-O'Reilly et al., 2010). Again the blood level could be useful when measured soon after the exposure, because blood Hg levels peak sooner than urine levels. The concentration of Hg in urine, hence, is a good indicator of a long-term integrated exposure, respect

to blood that is a good indicator of recent exposure (Pirrone et al., available at URL: http://www.iia.cnr.it/project/position-paper-on-mercury).

Regulations and guidelines

The limit values established by the institutions must take into account the different types of exposure including environmental (soil, deep and surface water), labor and alimentary. Regard biological matrix the Italian Society References Values (S.I.V.R.) established for Hg RVs of 4,5 µg/L in blood, 1,5 µg/L in serum and 5,0 µg/L in urine (S.I.V.R., 2011). All the previously mentioned values are calculated for the general adult population. Concerning air, instead the time-weighted average (TLV-TWA) for workers exposed during the eight working hours is set by the ACGIH (ACGIH, 2001) at 25 µg/m^3. Regard to the limits for soil the law that sets a limit for Hg farmland can be deduced by Legislative Decree. n ° 99 of 27/01/1992 - Implementation of Directive 86/278 / EEC on environmental protection, in particular of the soil. The fixed value for Hg is 1 µg/g in soil. The Presidential Decree 515/1982 fixed at 1 µg/L the limit for water intended for drinking, while the FAO document (FAO, 1985) fixed at 10 g/L the limit for water intended for livestock. Specific is the state of the art regarding food limits. The Food and Drug Administration (FDA) sets at 1 µg/g the maximum allowable Hg value in fish and seeds of wheat (U.S. FOOD AND DRUG ADMINISTRATION, 2000). Although it is specific for the mentioned foods, this limit may reasonably indicate, in the absence of another, a reference level of attention.

Analytical methods

Many of the analytical methods used for environmental samples are the methods approved by federal agencies and organizations such as the Environmental Protection Agency (EPA) and the National Institute for Occupational Safety and Health (NIOSH) or those that are approved by groups such as the Association of Official Analytical Chemists (AOAC) and the American Public Health Association (APHA). Additionally, analytical methods can be included, if adequately modified, to obtain lower detection limits and to improve accuracy and precision. The analysis of Hg in biological and environmental samples is difficult due to different organic and inorganic forms of the metal that may be present. This problem is usually overcome by reducing all the metal in the sample to its elemental form prior to analysis but this method is not suitable when information about the single Hg forms is desired. Furthermore Hg is relatively volatile and, therefore, easily lost during sample preparation and analysis. Nevertheless several methods have been settled for determining trace amounts of Hg in biological and environmental samples. Moreover, careful attention must be paid to involuntary contamination of the sample with Hg, especially when very low concentration is determined. Most common methods have used atomic absorption spectrometry

(AAS), atomic fluorescence spectrometry (AFS), or neutron activation analysis (NAA). In addition, methods based on mass spectrometry (MS), spectrophotometry, and anodic stripping voltammetry (ASV) have also been established. Among previously mentioned techniques the cold vapor (CV) AAS is the most widely used. The same technique is the first used to determine Hg in blood and serum (Friese et al., 1990; Ngim et al., 1988; Vermeir et al., 1988; Vermeir et al., 1989; Vesterberg, 1991). Both direct reduction of sample (Friese et al., 1990; Ngim et al., 1988) and pre-digestion followed by reduction (Oskarsson et al., 1996.; Vermeir et al., 1988; Vermeir et al., 1989) produced good accuracy and precision. Pre-digestion showed best results when samples were heated in a closed teflon container in a microwave oven and pre-concentrated on gold-coated sand (Vermeir et al., 1989). A complimentary method to CVAAS for total Hg determination in blood is electrothermal atomic absorption (ETAAS) (Emteborg et al., 1992) that showed good sensitivity and excellent recoveries. Also for analysis of urinary Hg the most used method is CVAAS (Akagi et al., 1995; Friese et al., 1990; Ngim et al., 1988; Oskarsson et al., 1996; Ping and Dasgupta, 1989; Ping and Dasgupta, 1990;Vesterberg, 1991). CVAAS showed good sensitivity (low-ppt), recovery (>76%) and precision (<10%) of relative standard deviation [%RSD]. ; furthermore can be used on either digested or undigested samples (Friese et al., 1990; Ngim et al., 1988; Ping and Dasgupta, 1989; Ping and Dasgupta, 1990). An alternative to CVAAS, for total Hg determination in blood and urine, can be inductively coupled plasma-atomic emission spectroscopy (ICP-AES) or ICP-mass spectrometry (Buneaux et al., 1992; Kalamegham and Ash,1992). These methods are sensitive and show good recoveries (>90%) and precision (<17% coefficient of variation [%CV]). Every technique has different figures of merits in the determination of Hg, in terms of different limit of detection, linearity range, accuracy, precision, applicability (number of samples analyzed) and specificity reported. Despite the mentioned advantages, the above mentioned analytical techniques also have drawbacks; they are time-consuming and involved potentially contaminating sample pre-treatment (in some the Hg in the sample is reduced to the elemental state and in others the pre-digestion of the sample is required prior to reduction). At all phases of sample preparation and analysis, the possibility of contamination from environmental Hg must be considered. An alternative approach which can measure total Hg directly is available in commercial instrumentation: Direct Mercury Analyzer (DMA-80). The DMA-80 techniques integrate sample combustion, pre-concentration of Hg by amalgamation with gold, and atomic absorption spectrometry (AAS). The peculiarities of TDA-AAS are: (1) rapid technique that eliminates reagent waste; (2) no sample pretreatment is needed (3); lower possibility of contamination; and (4) no matrix effect.

Aims of the study

1. To develop and accredited a confirmatory method based on the standardized US EPA Method 7473 to mercury detection through TDA-AAS TECHNIQUE in biological fluids and tissues (urine and hair) for Human Biomonitoring activity.

2. To assess and define exposure to Hg in fluids and tissues (urine and hair) of children aged 6-12 years living in an urban area of southern Italy and a control group. The goal of this part of study is to identify possible disparities in Hg exposure and evaluate possible associations with deficiencies in the neurobehavioral and cognitive sphere of children.

Materials and methods

Methodologies

To ensure the quality of this study and compare it to others at European level we adopted harmonized procedures for Hg determination, appropriate biomarkers, dedicated instruments for the analysis and reliable sampling protocols. The study, in fact, has been divided into various steps:

-analysis of the scientific literature and fine tuning of the study design

-preparation of any materials for the Ethics Committee

- definition of the criteria for eligibility

-training sessions with pediatricians, school principals, teachers and parents

-distribution of the information regarding the aim of the study, agreement consensus to personal data processing, and screening questionnaires to be filled out by the pediatrician

- training for the harmonization of procedures to collect, transport and storage the samples;

- neuropsychological tests - development and validation of laboratory methods for the quantification of Hg;

- determination of Hg in urine and hair of the population;

- Stratification of data by sex, age, socioeconomic status and neuropsychological test scores.

Identification of the sample population is achieved through the adoption of strict eligibility criteria based on age group, sex, geographical area of residence, general health status of children and mothers, use of drugs, socioeconomic status, educational level, dietary habits, sports, etc. This selection was made in order to keep under control confounding factors and to allow data stratification to highlight differences in children susceptibility (Needham et al., 2007).

Sampling

The population included 300 healthy children living in a urban area of South Italy. The enrollment of subjects was performed in the Primary School. Hair and urine were collected by qualified medical personnel. To obtain more information about children and mothers neuropsychological tests were performed by psychologists. Subjects were interviewed to obtain detailed information on family, dietary habits, lifestyle and potential exposures. Neuropsychological, cognitive and behavioral tests were also performed by qualified personnel. The study protocol was approved by the Institutional Ethical Committee of the Italian National Institute for Health. After verification of membership cards and the screening questionnaire, a list of suitable subjects was produced, balanced by area, age and gender. Eligibility criteria were: the subject recruited must be born and grew steadily in neighborhood of interest at the same time the mother's pregnancy stably conducted in the residence at the time of recruitment.

Subject with the following characteristics were excluded:

- total parenteral nutrition prior

- family history of neurodegenerative diseases

- taking medications (active on the nervous system)

- inadequately corrected visual defects

- neurological disorders

- metabolic, endocrine, kidney, liver and biliary tract diseases

-neuropsychiatric disorders.

To each suitable children a progressive identification code alpha numeric was attributed to guarantee the anonymous treatment of data. Hair samples were cut from the sub-occipital zone of the head at ca. 1 cm from the scalp using dedicated scissors and free powder gloves in order to limit Hg contamination. The samples were collected in individual plastic bags and stored in a desiccator kept in the dark before analysis. Regard to urine the only recommendation was to avoid the consumption of fish the day before urine collection because it could weaken the results on Hg. The morning urine samples were collected in a 100 ml Kartell® and stored at -20°C till the analysis.

Questionnaire eating habits

The interviews with parents and teachers were carried out in a dedicated room and during school hours. By the questionnaire, dietary habits as the weekly consumption of certain foods for mothers and children were investigated. The data allow to estimate the oral intake of Hg and better understand the possible sources of Hg exposure. Furthermore, other factors as socio-economic variables, demographic and life-style habits were investigated both for mothers and children.

Treatment of the samples

To avoid external contamination due to environmental dirt and dust, sweat and desquamation of the skin, as well as detergents and cosmetic treatments, hair samples were submitted to adequate rinses in order to eliminate possible external Hg contamination. The procedure adopted in this study is based on the following steps: i), three rinses (10 minutes each) under continuous stirring in a mixture of 3:1 (v/v) ethyl ether/acetone (Sigma-Aldrich, St. Louis, MO, USA) to remove the sweat; ii), soaking under stirring for 1 h in 5% sodium ethylenediaminetetracetic acid (Sigma-Aldrich) solution to bind the chemical elements present on hair surface; iii), final rinse with high purity deionized water (EASY-pure UV, PBI, Milan, Italy). Samples were then placed to dry at 80°C overnight, and after drying, two aliquots were taken from each hair sample. The first aliquot (25 mg) was used for direct analysis of Hg by the DMA-80 TRICELL and the second one was stored in

a biological bank. Regard urine samples, after thawing at room temperature, an amount of 100 μL was taken directly from Kartell® and transferred into appropriate quartz boat.

Technique

The principle on which is based the Hg analysis is the atomic absorption spectrometry (AAS). This technique, although destructive, appears to be the quickest and most effective for the determination of Hg in hair. In this matrix, in fact, the Hg present is derived almost exclusively from food and remains trapped within the matrix itself. It is evaluated the absorption of an electromagnetic radiation after it passes through a medium in which the sample is present in the form of atoms. When the atom absorb the electromagnetic energy of an adequate intensity, it reaches an higher energy level and an excited state resulting less stable. From this excited state, the atom decays rapidly and energy is purchased in the form of radiation. In the AAS single beam, the beam emitted by the source passes through the atomization system, which contains the sample in form of atomic gas and arrives at the monochromator; then monochromatic radiation arrives at the detector. The light from the source is modulated (pulsed) by means of a chopper, in order to distinguish the light emitted from the lamp by the light emitted from the atom excited.

DMA-80Tricell

Milestone's DMA-80 TRICELL is a direct Hg analyzer which uses the principle of thermal decomposition, amalgamation and atomic absorption spectrometry (TDA-AAS). The Hg is released from the sample through thermal decomposition. This eliminates the need for any sample preparation and, subsequently, handling of hazardous chemicals. Because no sample preparation is required, the typical bottleneck in the analytical laboratory is eliminated. Therefore, time (only 5 minutes per sample) and cost of the analysis are reduced in comparison with traditional Hg techniques, such as CV-AAS, ICP-AES or ICP-MS. Analytical determinations were performed via an integrated AAS set to the Hg absorption wavelength ($\lambda \approx 253.65$ nm). In the lamp, the Hg vapor discharge emits predominantly UV radiation ($\lambda \approx 253.7$ nm) converted into visible radiation by the phosphors deposited on the inside of the tube to absorb UV and emit visible radiation (frequency transducers). The three reading cells, with different optical path, allow to analyze the metal as a function of the concentration present in the sample. The DMA-80 TRICELL has no matrix effect and it can analyze both solid and liquid matrices with equal precision. DMA-80 TRICELL can be used with environmental, geochemical, petrochemical, food and feed, clinical and polymer samples.

The instrument is fully compliant with US EPA method 7473 and with ASTM method D-6722-01. The method used is reported Fig. 12.

Hair are weighed into quartz boats, and then transferred from the analytical balance to the DMA-80 TRICELL, equipped with an autosampler. Samples are first dried and then thermally decomposed through oxygen-fluxes in furnace. Mercury and other combustion products are released from the sample and they are carried to the catalyst section, where nitrogen and sulfur oxides, as well as halogens and other interfering compounds, are eliminated. Mercury is selectively trapped through gold amalgamation. Combustion by-products are flushed off. The amalgamator is heated and Hg is rapidly released. Mercury is flown via the carrier gas into a unique block with a tri-cell arrangement, positioned along the optical path of the AAS, where it is quantitatively measured. Time, temperature and air flow of all these steps process are regulated by our optimized method (Fig. 12). Schematic representation of instrument is reported Figure 13.

DMA-80 TRICELL	
Air flow (mL min^{-1})	200
Drying	350 °C for 60 s
Decomposition and catalysis	650 °C for 180 s
Purge time 1	60 s
Amalgamator	650 °C for 12 s
Purge time 2	60 s

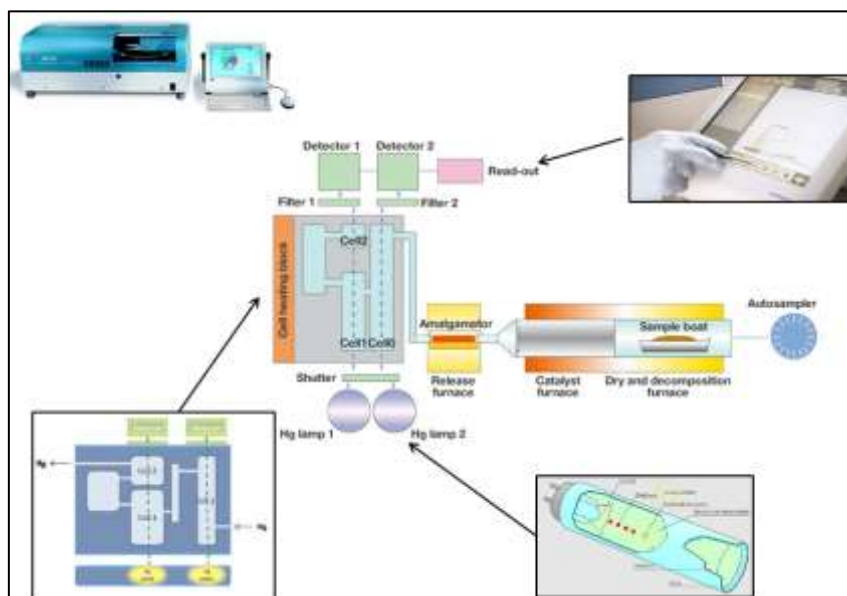**Figure 12: Instrumental setting method.**

Figure 13: DMA-80 structure.

The DMA-80 TRICELL produces independent results from the matrix because it is calibrated with standard aqueous samples. It can analyze both organic and inorganic samples, so different matrices can be analyzed using a single method. The instrument does not suffer from any memory effect, because the software is equipped with the "Autoblank" feature through which the user can set a satisfactory level of blanks. If blank levels are not satisfactory , the instrument automatically starts the vacuum cycle until the required level is obtained. This feature ensures stability in time (even for months) of the analysis and calibration.

Validation method

Our laboratory operates in a quality control system (UNI CEI EN ISOIEC 17025) and developed a confirmatory method for the determination of Hg based on the US EPA Method 7473 ("Mercury in solids and solutions with thermal decomposition, amalgamation and atomic absorption spectrometry"). Guidelines followed to develop, validate and accreditate the confirmatory method are reported on table 7.
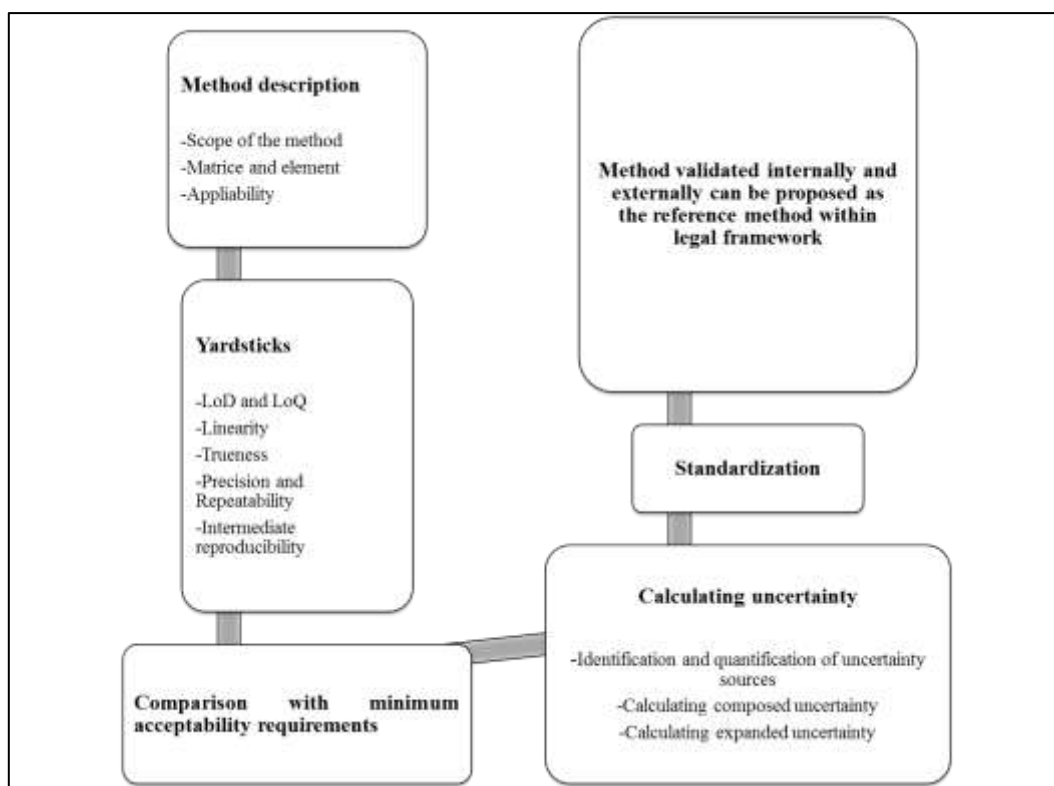
Table 7: Operation procedure to validate and crediting confirmatory method

The method was validated in-house according to previous published papers (Bocca et al., 2010; Bocca et al., 2011a; Bocca et al., 2011b) and internationally recognized regulations (CITAC, EURACHEM, 2002; ISO 5725:2004). The validation provides an estimate of the performances of the method and the factors that may affect the uncertainty associated with the results, as required by the UNI CEI EN ISOIEC 17025: 2005. The method performances estimated were repeatability, accuracy, sensitivity, limit of detection (LoD) and limit of quantification (LoQ). The validation data were then assessed against minimum acceptability requirements predefined by the laboratory and on the basis of tests of significance. Performances of the method, in fact, depend on the environmental laboratory conditions, instrument status, skill of the personnel as well as quality of materials and reagents used. For this reason, an internal operating procedure (IOP) was laid down in order to strictly define all the procedural steps for the determination of Hg in urine and hair by the DMA-80 TRICELL analyzer. The method ("Determination of mercury in biological matrices") was accredited by the Italian accreditation body (Accredia) and continuously monitored during the Accredia annual visits.

Exposure assessment via biomonitoring

Biological samples were collected in schools . Urine samples were stored at -20 degrees °C temporarily at the local ASL unit. Hair samples were collected at the occipital region of the scalp; stainless steel scissors were avoided in order to reduce external contamination. Hg was analyzed in hair and urine samples using the confirmatory method "Determination of mercury in biological matrices".

Extrapolation of results

To put biomonitoring data in a context of risk assessment, concentrations of Hg in hair and urine were compared with the HBM-I and HBM-II biological limit values developed by the German Commission of human biomonitoring (Schulz et al., 2011). Another comparing biological limit is the "Biomonitoring Equivalent" (BE). In the EPA calculation, using the "reference dose", the BE corresponds to the concentration of the contaminant in the biological sample at which people can be exposed for the lifetime without having toxic effects. In addition the BE_{POD} (POD, Point Of Departure) has been defined as the upper limit of BE. Concentrations below the BE are considered safe for the health, those between BE and BE_{POD} have a medium priority, while those exceeding BE_{POD} require actions to reduce the exposure (LaKind et al., 2008). The biomonitoring data can be also compared with RVs which represent the basic exposure of the general population to the contaminant ; among them, VRs obtained from the US National Health and Nutrition Examination

Survey (NHANES, 2015) and the German Environmental Survey for Children (GERES IV, 2008) carried out in 2003-06

Results

Accrediting method

We developed and accredited a confirmatory method based on the standardized US EPA Method 7473 ("Mercury in solids and solutions with thermal decomposition, amalgamation and atomic absorption spectrometry"). The method for the determination of Hg through the TDA-AAS technique (Thermal Decomposition Amalgamation-Atomic Absorption Spectrometry) used the DMA-80 TRICELL Hg analyzer. Laboratory worked in a quality control system according to UNI CEI EN ISO IEC 17025. To define all the procedural steps an internal operating procedure (IOP) was laid down containing pretreatment and analytical procedures and performances of the method. The first parameters calculated were LoD and LoQ. The calculation of these limits was carried out by analyzing ten times the absorbance of a blank and a blank fortified with Hg (spike) and applying the 3σ criterion for LoD (0.065 µg/L) and the 10σ criterion for LoQ (0.218 µg/L). The linearity range of the calibration curves in each of the three different reading cells was also evaluated; the linearity was measured between 0.1 ng and 200 ng of Hg and it showed a correlation coefficient R^2 better than 0.999 (Fig.14)
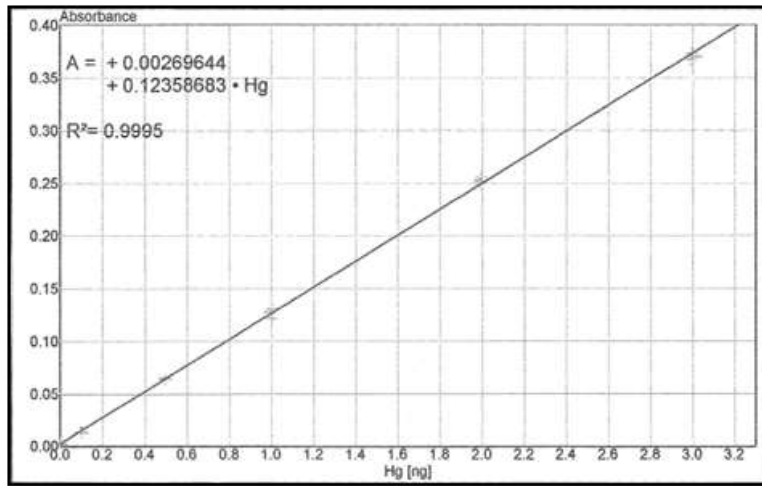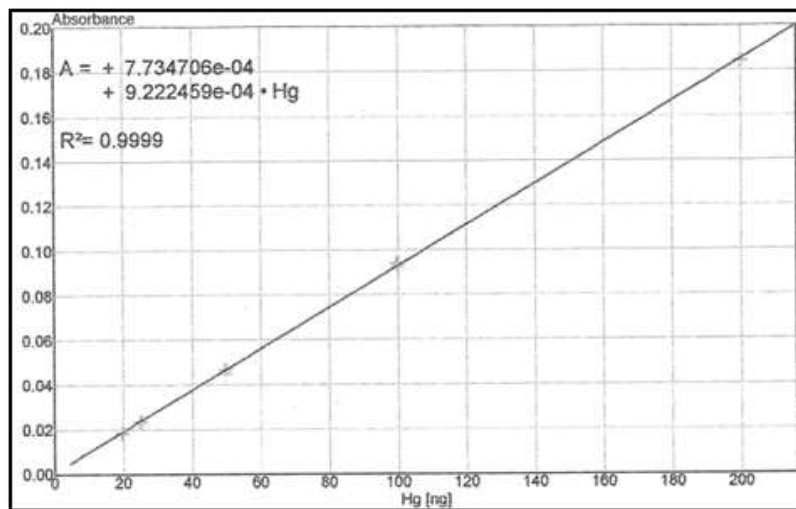
a)
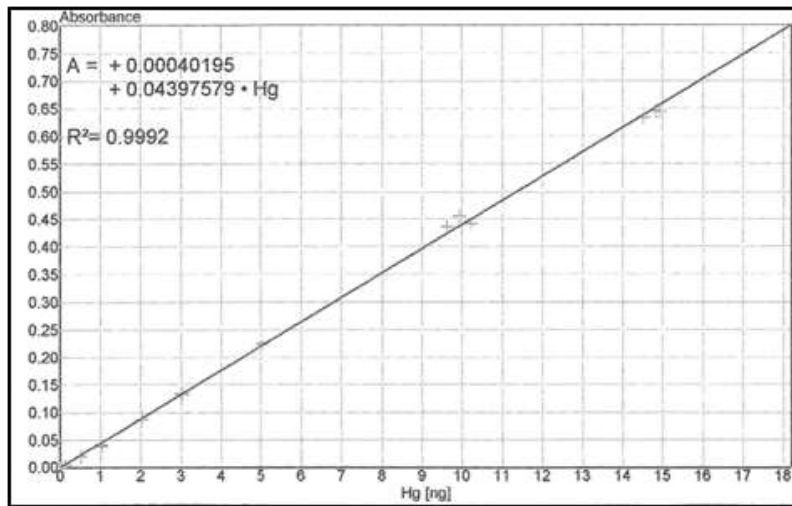
b)

c)

Figure 14: Linearity range (a) Cell 0, (b) Cell1 and (c) Cell2.

The repeatability was determined at different concentration levels to cover the entire assay range. Correlation coefficients (between concentration in µg/L and absorbance) were equal to $R^2 = 0.9916$ for 0 and 1 cell while $R^2 = 0.8072$ for the cell 2. Equation obtained served to evaluate the repeatability limit of the method (Fig.15)

PROFILO RIPETIBILITA' cell 0 e 1	
Limite di ripetibilità (r) *µg/L*	Media *µg/L*
0,06	0,12
0,13	1,02
0,57	3,15
1,15	5,54
2,40	10,98
3,65	19,18
y = 0,1957x + 0,0212	

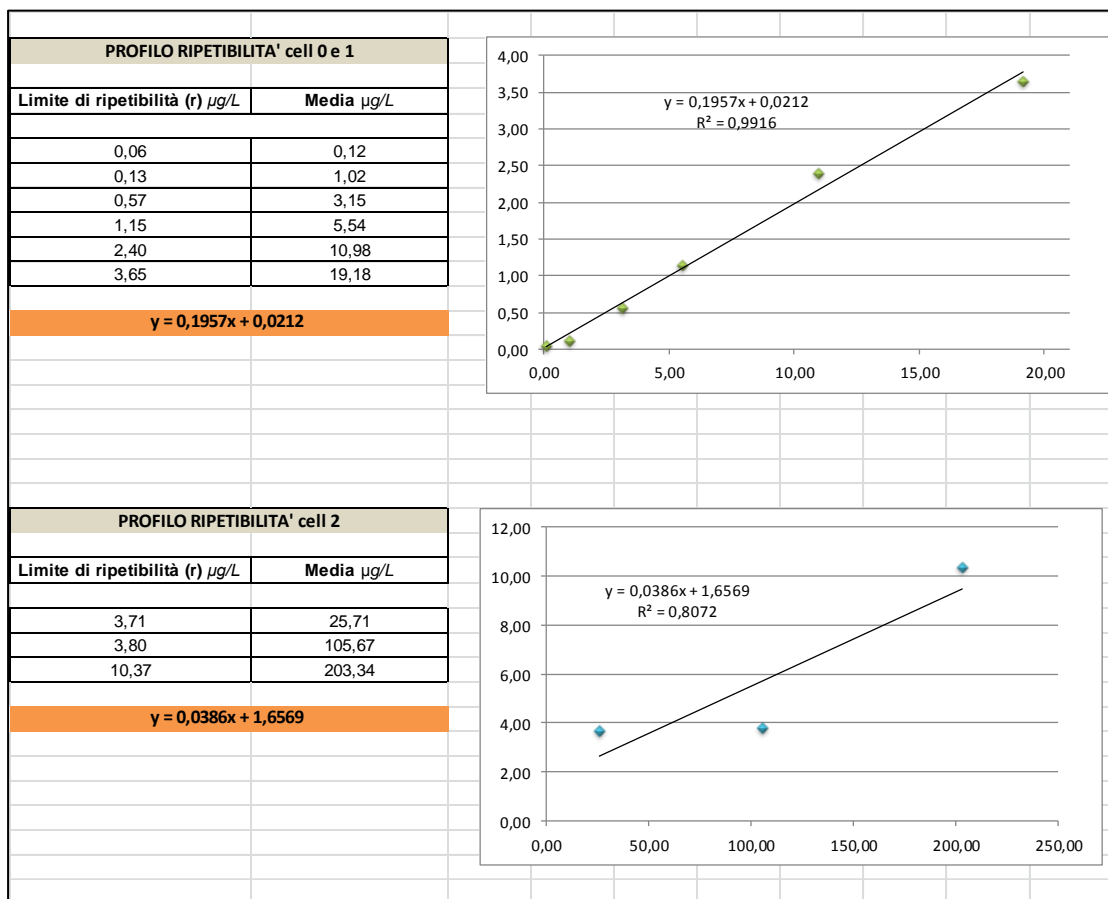| PROFILO RIPETIBILITA' cell 2	
Limite di ripetibilità (r) *µg/L*	Media *µg/L*
3,71	25,71
3,80	105,67
10,37	203,34
y = 0,0386x + 1,6569	

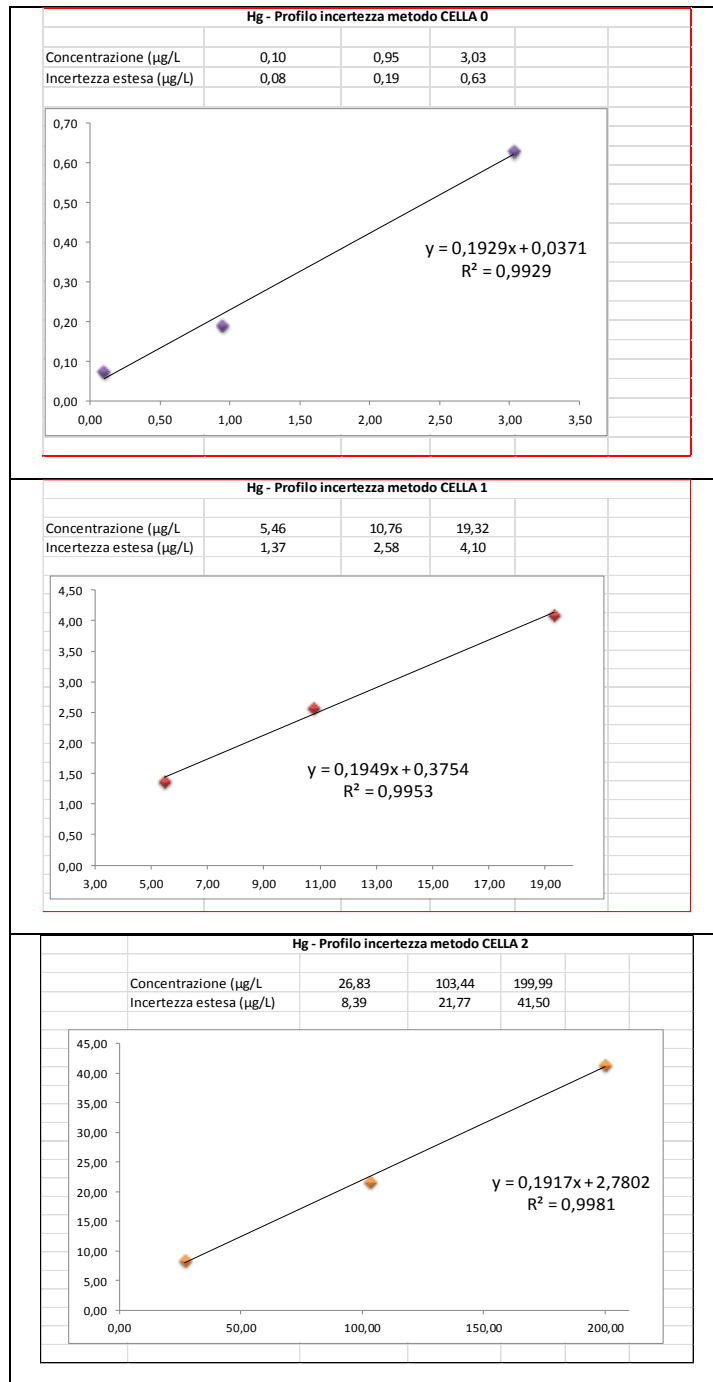Figure 15: Repeatability profile in three reading cells.

The acceptability criterion of the results was the difference of Hg concentration in the control sample (Hg fortified water solution) analyzed in duplicate, which must be less than the repeatability limit declared in the method.

Another parameter evaluated was the accuracy assessed using a certified reference material (Seronorm Trace Elements Serum, SERO AS) containing a certified value of Hg, analyzed ten times in the same day. The average value found was 43.79 µg/L with a standard deviation of 0.91 µg/L. The trueness percentage, calculated by dividing the average concentration observed and the certified concentration provided by the manufacturer (39.8 µg/L ± 8 µg/L) was equal to 110%.

Another parameter calculated was the sensitivity ; a sensitivity equal to 0.153 was obtained for 10 µg Hg/L. Uncertainty of measurements was also evaluated, as required by the UNI CEI EN ISOIEC 17025. The expanded uncertainty (u_{est}) provides the interval that may be expected to encompass a large fraction of the distribution of values that could reasonably be attributed to the measurand. The estimation of measurement uncertainty and expressions were performed accordingly to accepted international guidelines (Barwick and Ellison, 2000; UNI CEI ENV 13005: 2000; EUROLAB Technical Report No. 1 / 2007, ISO 21748: 2010;). The u_{est} is obtained by multiplying the combined standard uncertainty (u_{comp}), for the coverage factor k. The choice of the factor k depends on the desired confidence level. We initially identified all the uncertainty components and then provided a reasonable estimate of their contribution considering a confidence level of about 95%, k = 2 (QUAM: 2000.1) (Fig.16). The expanded uncertainty profile is obtained plotting concentration and expanded uncertainty associated with the known concentration. The equation obtained from the profile is useful for evaluating the expanded uncertainty associated with a concentration obtained in the analysis of unknown samples (Fig.17). The contributions to the combined uncertainty (u_{comp}) are various. The sources of uncertainty are not all independent of each other, but some of them are related. Therefore, the uncertainty of measurement calculation process is simplified by grouping some sources of uncertainty and quantifying the uncertainty due to the grouped components. The principal contributes to the combined uncertainty (u_{comp}) are the uncertainty of the calibration curve, preparation of solutions, use of the balance (weighing), and trueness and intermediate repeatability.

		Hg							
		Cella 0			Cella 1			Cella 2		
STIMA INCERTEZZA METODO	0,1 ng	1 ng	3 ng	5 ng	10 ng	20 ng	25 ng	100 ng	200 ng
Incertezza % di ripetibilità intermedia (uR)	25,6%	2,4%	3,3%	2,9%	5,6%	3,8%	2,1%	2,5%	2,7%
gradi di libertà (uR)	25	26	26	20	20	20	17	29	29
Incertezza % di esattezza (tru)	10,1%	10,1%	10,1%	10,1%	10,1%	10,1%	10,1%	10,1%	10,1%
gradi di libertà (u$_r$)	9	9	9	9	9	9	9	9	9
Incertezza % Reg	27,84%	2,49%	0,97%	7,35%	3,38%	1,94%	12,15%	2,69%	1,65%
Incertezza Peso	2,11%	0,23%	0,08%	0,05%	2,17%	1,14%	0,90%	0,23%	0,12%
Incertezza Volume	0,8%	0,8%	0,8%	0,8%	0,7%	0,7%	0,7%	0,7%	0,7%
Incertezza % composta (u$_c$)	39%	10%	11%	13%	12%	11%	16%	11%	11%
Gradi di liberta effettivi	137	9005	2766	7308	467	1363	58554	10394	6695
Fattore di copertura (k)	1,98	1,96	1,96	1,96	1,97	1,96	1,96	1,96	1,96
Incertezza estesa (U%)	78%	20%	21%	25%	24%	22%	31%	21%	21%
Concentrazione media (µg/L)	0,10	0,95	3,03	5,46	10,76	19,32	26,83	103,44	199,99
Inc. estesa (U, µg/L)	0,08	0,19	0,63	1,37	2,58	4,18	8,39	21,77	41,5

Figure 16: Uncertainty components and their contribution.

Hg - Profilo incertezza metodo CELLA 0

Concentrazione (µg/L)	0,10	0,95	3,03
Incertezza estesa (µg/L)	0,08	0,19	0,63

$y = 0{,}1929x + 0{,}0371$
$R^2 = 0{,}9929$

Hg - Profilo incertezza metodo CELLA 1

Concentrazione (µg/L)	5,46	10,76	19,32
Incertezza estesa (µg/L)	1,37	2,58	4,10

$y = 0{,}1949x + 0{,}3754$
$R^2 = 0{,}9953$

Hg - Profilo incertezza metodo CELLA 2

Concentrazione (µg/L)	26,83	103,44	199,99
Incertezza estesa (µg/L)	8,39	21,77	41,50

$y = 0{,}1917x + 2{,}7802$
$R^2 = 0{,}9981$

Figure 17: Uncertainty profiles and their equation.

Sample selection and recruitment strategies

300 children were studied living in different areas located at different kilometers from the industrial area: between 1 and 5 Km; between 5 and 10 km and between 10 and 15 Km. Of these 62% agreed to participate while 23 subjects refused. Furthermore 33 subjects were excluded because geographical and clinical requisites were lacking and 78 were not involved because in excess respect to request. Of 312 selected subjects, 20 were excluded *in itinere* producing a final number

of 292 children enrolled. All the subjects of this study aged between 6 and 12 years and lived in a coastal city of south Italy that present different industrial settings. The area of interest has been affected for decades by the impact of industrial emissions on the environment and health of workers and citizens. Urine is used as biomarker of consolidated exposure to inorganic Hg while hair analysis provides a good estimate of exposure to MeHg through consumption of food, in particular fish and shellfish (Miklavčič et al.,2011; Kern L. Nuttall, 2006; Çamur D et al., 2016). Hair is the best biomarker of MeHg exposure because it contains sulfhydryl groups for which MeHg cations have high affinity. MeHg can bind to hair strands during hair formation (Grandjean et al. 1999). The analysis of two different matrices allowed us to discriminate between the different forms of Hg (inorganic and organic Hg) to children may be exposed. The mean hair Hg concentration, in few studies, results in the range of 0.3 to 1.0 µg/g (EPA 1997) while if the diet population is based on high fish consumption the Hg levels are more higher (Grandjean et al. 1992; Cernichiari et al. 1995). For Hg in hair (MeHg) there are no toxicity limit values. Some studies have reported median values ranging from 70 ng/g determined in Brazil to 430 ng/g of South Korea, up to 750 ng/g in Spain; the median of our data (472 ng/g) is comparable to the Korean study (Carneiro et al., 2011; Beněs et al., 2003; Park et al., 2007). Furthermore for hair HBM values did not exist. Table 8 show Hg biomonitoring data of the general population. The median (472 ng/g) of the population could be influenced by fish consumption. In fact this habits influences Hg intake and body burden in subjects. Regarding gender, Hg hair levels were found higher in females than in males. This phenomenon occurs because the sampling was carried out in summer when the boys have short hair. To be precise, we analyzed the same amount of sample both for girls and boys but in girls, more longer hair samples, reflect a period of exposure was more longer than in boys considering the hair grow (c.a. 1 cm per month).

We used urine to determine inorganic Hg and it showed lower levels than in hair; this can be due also to other potential sources different from anthropogenic sources, as dental amalgam fillings (Kern L. Nuttall 2004; WHO (World Health Organization), 2003; Allen Countera and Leo Buchanan, 2004). The results shown in Table 8 summarize the Hg concentrations in the two matrices, also subgrouping for gender. Data obtained in children were similar to those found in the general population. We have found the amount of Hg in hair (MeHg) higher than that in urine (I-Hg), because urinary Hg is mainly an indicator of the inorganic Hg form. In 76 children (26% of the children population) urinary Hg was found to be below the LOQ of the technique; the remaining children showed urine Hg concentrations below the HBM-I limit value (7 ng/ml) so, no action is required. The average Hg values are slightly higher for females (see table 9) than males (see table 10). Analyzing the data as a function of the distance from the industrial area (Tab.11) we observed

that children living in the more remote areas showed higher Hg values. These values could be affected by socio-economic conditions. The more distant areas coincide with a population of upper middle class that can consume a particular diet, including a high fish consumption. Because about 70% of the urinary Hg could come from MeHg metabolized (Sherman et al., 2013) , we verified if exist a correlation between Hg concentration in urine and the metal concentration in hair. As showed Fig.18 plotting hair Hg levels vs. urine Hg levels, no correlation was found. Possibly, other factors impact on the Hg level in the study subjects. Further studies will enable to identify alternative sources of Hg exposure and possible variables that may influence the Hg body burden in children.

Total population		MEAN	SD	MEDIAN	GM	P5	P95
Urine	292	0,67	1,78	0,37	0,26	0,016	1,81
Hair	292	643	616,7	472	454,7004	107,6	1925,7

Table 8: Levels of Hg in urine and hair of 299 subjects. Concentrations in ng/ml (urine) ng/g (hair).

Female population		MEAN	SD	MEDIAN	GM	P5	P95
Urine	155	0,77	2,38	0,36	0,24	0,0003	1,97
Hair	155	630	631,3	477	449,1	102,8	2025,44

Table 9: Data male study population. Concentrations in ng/ml (urine) ng/g (hair).

Male population		MEAN	SD	MEDIAN	GM	P5	P95
Urine	137	0,56	0,63	0,38	0,29	0,039	1,49
Hair	137	657	601,7	468	461,1	114,8	1810,82

Table 10: Data female study population. Concentrations in ng/ml (urine) ng/g (hair).
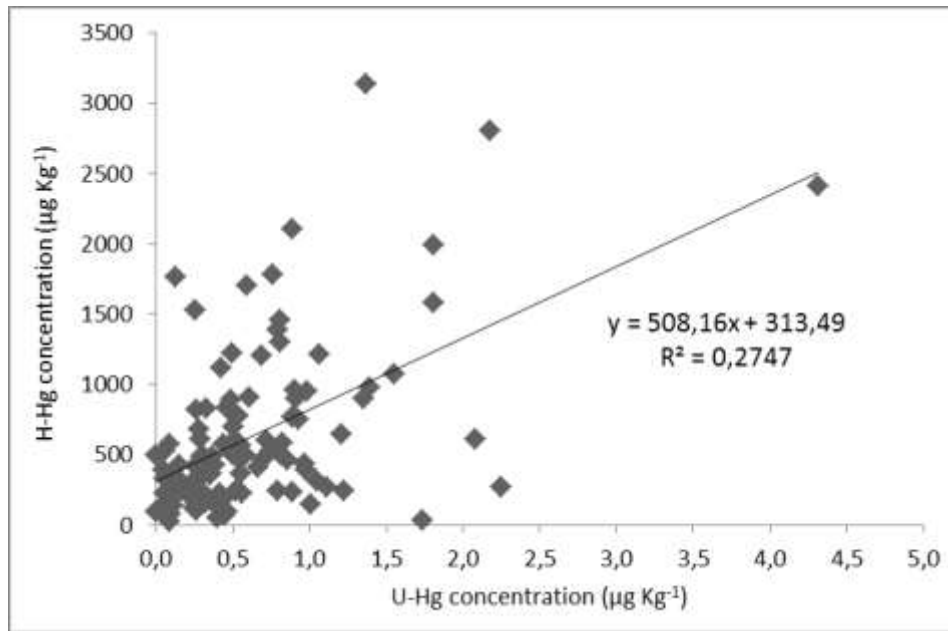
Figure 18: Correlation between urine and hair Hg concentration (ng/g).

	Total no.292	From 0 to 5 Km No. 96	From 5 to 10 Km No.100	From 10 to 15 Km No.96
Urinary Hg ng/mL	0.37 (0.0001-28.3)	0.30 (0.0001-2.5)	0.42 (0.0001-2.1)	0.47 (0.0001-28.3)
Hair Hg ng/g	472 (21.2-4357)	388.2 (49.5-2299)	419 (21.2-3091)	580 (50.3-4357)

Table 11: Biomarkers by increasing distances from the source (results expressed as median value with minimum and maximum value).

Discussion

The neurodevelopmental disorders, particularly autism, syndrome of attention deficit and hyperactivity (Attention Deficit Hyperactiviy Disorder- ADHD), learning and behavioral disorders are increasing globally and in Italy. The international scientific literature outlines possible environmental determinants that may, together with the genetic predisposition, increase neurodevelopmental disorders. They include heavy metals as Hg. The geographical area of interest has been subjected for decades to the impact of industrial emissions on the environment and health of workers and citizens. However, they had not been studied before the possible neurological effects of mercury exposure in children living in that area.

A confirmatory method was developed and validated in house and accredited according to the UNI CEI EN ISOIEC 17025 to perform the analysis of Hg in urine and hair of children living around an industrial area in South Italy. The analytical performances demonstrated that technique is sensitive, precise and supply reliable data. Furthermore the use of the DMA-80 TRICELL might be preferable to other techniques for a number of reasons, such as the reduction of the sample manipulation with minor risk of contamination, less time consuming due to the absence of the acid digestion cycle, cheaper analyses and the absence of matrix effects that could interfere with the measurement.

The study investigated 300 children aged 6-12 years. The children were examined by a team of psychologists with extensive experience for a full assessment of neurobehavioral functions. Variables concerning the state socio-economic and cultural level of the families were taken into account mercury concentrations in hair and urine (Table.8) are under the alert biological level with values lower of ca. three order of magnitude. Even if 70% of the urinary Hg could come from MeHg metabolized in adults (Sherman et al., 2013), we didn't find a correlation between Hg concentration in urine and Hg levels in hair as showed in Figure 18. This difference can be due to the age of the studied subjects (6 to 12 years).
Children, are not little adults, their unique physiology can influence the extent of their exposure because they have immature metabolic pathways that are differentiating and growing (Bose-O'Reillyet al., 2010). Some studies, however, demonstrate that in urine there is mostly inorganic Hg while in hair the metal is typically represented by MeHg (Clarkson and Magos, 2006; Cernichiari et al., 1995). The median value of Hg in hair (476 ng/g) is comparable to or even lower than that measured in other national and international studies for exposed and non-exposed subjects of comparable age. Regarding urinary Hg (inorganic and/or metallic), 221 subjects had a Hg level below the LoQ value while the remaining 78 children have concentrations of less than 7 ng/mL, i.e. at the HBM-I limit value.

Further research is needed to overcome the current limitations, by examining a high number of cases. Retrospective comparative evaluation of these data will allow to reconstruct the levels of exposure to Hg over the last 15 years and create cumulative indices according to the new integrated exposomic assessment (Cui et al., 2016). Moreover it will be possible to make actions to reduce Hg exposure in target areas and to relate the current health indicators of exposure levels experienced in earlier eras.

References

ACGIH (American Conference of Government Industrial Hygienists), 7th ed. 2001.

ACGIH (American Conference of Government Industrial Hygienists). Threshold limit values for chemical substances and physical agents and biological exposure indices for 1996. Cincinnati, OH: American Conference of Governmental Industrial Hygienists; 1996.

Adlnasab, L., Ebrahimzadeh, H., Asgharinezhad, A.A., Aghdam, M.N., Dehghani, A., Esmaeilpour, S. (2014). A preconcentration procedure for determination of ultra-trace mercury (II) in environmental samples employing continuous-flow cold vapor atomic absorption spectrometry. Food Anal Methods 7(3):616–628; C-C.

Ahola, T.M., N. Alkio, T. Manninen, and T. Ylikomi. 2002. Progestin and G protein-coupled receptor 30 inhibit mitogen-activated protein kinase activity in MCF-7 breast cancer cells. Endocrinology. 143:4620-4626.

Akagi, H., Malm, O., Branches, F. J.P., et al. 1995. Human exposure to mercury due to gold mining in the Tapajos river basin, Amazon, Brazil: Speciation of mercury in human hair, blood and urine. Water Air and Soil Pollution 80(1-4):85-9.

Albanito, L., D. Sisci, S. Aquila, E. Brunelli, A. Vivacqua, A. Madeo, R. Lappano, D.P. Pandey, D. Picard, L. Mauro, S. Ando, and M. Maggiolini. 2008b. Epidermal growth factor induces G protein-coupled receptor 30 expression in estrogen receptor-negative breast cancer cells. Endocrinology. 149:3799-3808.

Albanito, L., R. Lappano, A. Madeo, A. Chimento, E.R. Prossnitz, A.R. Cappello, V. Dolce, S. Abonante, V. Pezzi, and M. Maggiolini. 2008a. G-protein-coupled receptor 30 and estrogen receptor-alpha are involved in the proliferative effects induced by atrazine in ovarian cancer cells. Environmental health perspectives. 116:1648-1655.

Alimonti, A., Bocca, B., Mannella, E., Petrucci, F., Zennaro, F., Cotichini, R., D'Ippolito, C., Agresti, A., Caimi, S., Forte, G.; Assessment of reference values for selected elements in a healthy urban population. Ann Ist Super Sanità 2005;41(2):181-7.

Alimonti, A., Bocca, B., Mattei, D., Lamazza, A., Fiori, E., De Masi, E., Pino, A., Forte, G.; Composition of essential and non-essential elements in tissues and body fluids of healthy subjects and patients with colorectal polyps. Int J Environ Health 2009;3(2):224-37.

Allen Countera, S., Leo Buchanan, H., Mercury exposure in children: a review, Toxicology and Applied Pharmacology 198 (2004) 209– 230.

Allolio, B., and M. Fassnacht. 2006. Adrenocortical Carcinoma: Clinical Update. Journal of Clinical Endocrinology Metabolism. 91:2027-2037.

Allolio, B., M. Reincke, W. Arlt, U. Deuss, W. Winkelmann, and L. Siekmann. 1989. Suramin for treatment of adrenocortical carcinoma. Lancet. 2:277.

Allred, D.C., J.M. Harvey, M. Berardo, and G.M. Clark. 1998. Prognostic and predictive factors in breast cancer by immunohistochemical analysis. Modern pathology : an official journal of the United States and Canadian Academy of Pathology, Inc. 11:155-168.

Alyea, R.A., S.E. Laurence, S.H. Kim, B.S. Katzenellenbogen, J.A. Katzenellenbogen, and C.S. Watson. 2008. The roles of membrane estrogen receptor subtypes in modulating dopamine transporters in PC-12 cells. Journal of neurochemistry. 106:1525-1533.

Angerer, J., Bird, M.G., Burke, T.A., Doerrer, N.G., Needham, L., Robison, S.H., et al. 2006. Strategic biomonitoring initiatives: moving the science forward. ToxicolSci 93:3–10.

Antonsson, B., S. Montessuit, S. Lauper, R. Eskes, and J.C. Martinou. 2000. Bax oligomerization is required for channel-forming activity in liposomes and to trigger cytochrome c release from mitochondria. The Biochemical journal. 345 Pt 2:271-278.

Apostoli, P., Cortesi, I., Mangili, Elia, G., Drago, I., Gagliardi, T., Soleo, L., Valente, T., Sciarra, G.F., Aprea, C., Ronchi, A., Minoia, C.; Assessment of reference values for mercury in urine: the results of an Italian polycentric study. Sci Total Environ 2002;289(1-3):13-24.

Aranda, P.R., Gil, R.A., Moyano, S., Vito, I.D. and Martinez, L.D.. Preconcentration, speciation, and determination of key elements in biological samples in Latin America. J. Hazard. Mater., 2009, 161, 1399–1403.

Ariazi, E.A., E. Brailoiu, S. Yerrum, H.A. Shupp, M.J. Slifker, H.E. Cunliffe, M.A. Black, A.L. Donato, J.B. Arterburn, T.I. Oprea, E.R. Prossnitz, N.J. Dun, and V.C. Jordan. 2010. The G protein-coupled receptor GPR30 inhibits proliferation of estrogen receptor-positive breast cancer cells. Cancer research. 70:1184-1194.

Arlt, W., M. Biehl, A.E. Taylor, S. Hahner, R. Libe, B.A. Hughes, P. Schneider, D.J. Smith, H. Stiekema, N. Krone, E. Porfiri, G. Opocher, J. Bertherat, F. Mantero, B. Allolio, M. Terzolo, P. Nightingale, C.H. Shackleton, X. Bertagna, M. Fassnacht, and P.M. Stewart. 2011. Urine steroid metabolomics as a biomarker tool for detecting malignancy in adrenal tumors. The Journal of clinical endocrinology and metabolism. 96:3775-3784.

Aron, D., M. Terzolo, and T.J. Cawood. 2012. Adrenal incidentalomas. Best practice & research. Clinical endocrinology & metabolism. 26:69-82.

Aschner, M. , Clarkson, T.W., Uptake of methylmercury in the rat brain: effects of amino acids, Brain Res. 462 (1) (1988) 31–39.

Assié, G., Letouzé, E., Fassnacht, M., Jouinot, A., Luscap, W., Barreau, O., Omeiri, H., Rodriguez, S., Perlemoine, K., René-Corail, F., et al: Integrated genomic characterization of adrenocortical carcinoma. Nat Genet 46: 607-612, 2014.

ATSDR (Agency of Toxic Substances and Disease Registry). Toxicological profile for mercury Atlanta, Georgia US: Department of Health and Human Services, Public Health Service; 1999.

ATSDR Agency for Toxic Substances and Disease Registry. 2007. Health consultation: Mercury exposure investigation using serial urine testing and medical records review, Kiddie Kollege. Available from: http://www.state.nj.us/health/eoh/cehsweb/kiddiekollege/documents/kiddiekollegehc.pdf.

Aubert, S., A. Wacrenier, X. Leroy, P. Devos, B. Carnaille, C. Proye, J.L. Wemeau, M. Lecomte-Houcke, and E. Leteurtre. 2002. Weiss system revisited: a clinicopathologic and immunohistochemical study of 49 adrenocortical tumors. The American journal of surgical pathology. 26:1612-1619.

Axelrad, D,A., Bellinger, D.C., Ryan, L.M., Woodruff, T.J.; Dose–response relationship of prenatal mercury exposure and IQ: an integrative analysis of epidemiologic data. Environ. Health Perspect. 2007, 115, 609–615.

Balarama Khrisna, M.V. and Karunasagar, D., Robust ultrasound assisted extraction approach using dilute TMAH solutions for the speciation of mercury in fish and plant materials by cold vapour atomic absorption spectrometry (CVAAS).Anal. Methods, 2015, 7, 1997–2005.

Ballatori, N., and Clarkson, T.W. (1985). Biliary secretion of glutathione and of glutathione-metal complexes.Fundam. Appl. Toxicol. 5(5):816-31.

Ballatori, N., Gatmaitan, Z., and Truong, A.T. (1955).Impaired biliary excretion and whole body elimination of methylmercury in rats with congenital defect in biliary glutathione excretion. Hepatology 22(5):1469-73.

Barlaskar, F.M., A.C. Spalding, J.H. Heaton, R. Kuick, A.C. Kim, D.G. Thomas, T.J. Giordano, E. Ben-Josef, and G.D. Hammer. 2009. Preclinical targeting of the type I insulin-like growth factor receptor in adrenocortical carcinoma. The Journal of clinical endocrinology and metabolism. 94:204-212.

Barlaskar, FM. and Hammer, G.D.; The molecular genetics of adrenocortical carcinoma. Rev Endocr Metab Disord 8: 343-348, 2007.

Barregard, L., Sallsten, G., Schutz, A., Attewell, R., Skerfving, S., Jarvholm, B.; Kinetics of mercury in blood and urine after brief occupational exposure. Arch Environ Health 1992;7(3):176-184.

Barwick & Ellison; Estimating measurement uncertainty using a cause and effect and reconciliation approach;† Measurement uncertainty estimates compared with collaborative trial expectation‡;Analytical Communications 35(11):377-383; January 1998, 2000.

Barzon, L., G. Masi, M. Pacenti, M. Trevisan, F. Fallo, A. Remo, G. Martignoni, D. Montanaro, V. Pezzi, and G. Pal. 2008. Expression of aromatase and estrogen receptors in human adrenocortical tumors. Virchows Archiv. 452:181-191.

Barzon, L., N. Sonino, F. Fallo, G. Palu, and M. Boscaro. 2003. Prevalence and natural history of adrenal incidentalomas. European journal of endocrinology / European Federation of Endocrine Societies. 149:273-285.

Batistuzzo de Medeiros, S.R., G. Krey, A.K. Hihi, and W. Wahli. 1997. Functional interactions between the estrogen receptor and the transcription activator Sp1 regulate the estrogen-dependent transcriptional activity of the vitellogenin A1 io promoter. The Journal of biological chemistry. 272:18250-18260.

Becker, K., Conrad, A., Kirsch, N., Kolossa-Gehring, M.; German Environmental Survey (GerES): Human biomonitoring as a tool to identify exposure pathways. Int J Hyg Environ Health 2007;210:267-9.

Bellanger, M., Pichery, C., Aerts, D., Berglund, M., Castaño, A., Cejchanová, M., et al. Economic benefits of methylmercury exposure control in Europe: monetary value of neurotoxicity prevention. Environ. Health 2013,12, 3.

Beněs, B., Sladká, J., Spěváčková, V., Šmíd, J., Determination of normal concentration levels of Cd, Cr Cu, Hg, Pb, Se and Zn in hair of the child population in the Czech Republic. Cent. Eur. J. Public Health 2003; 11: 184–186.

Bennett, C.N., S.E. Ross, K.A. Longo, L. Bajnok, N. Hemati, K.W. Johnson, S.D. Harrison, and O.A. MacDougald. 2002. Regulation of Wnt signaling during adipogenesis. The Journal of biological chemistry. 277:30998-31004.

Berndt, W.O., Baggett, J.M., Blacker, A., and Houser, M.(1985). Renal glutathione and mercury uptake by kidney. Fundam. Appl. Toxicol. 5(5):832-9.

Berruti, A., M. Terzolo, P. Sperone, A. Pia, S. Della Casa, D.J. Gross, C. Carnaghi, P. Casali, F. Porpiglia, F. Mantero, G. Reimondo, A. Angeli, and L. Dogliotti. 2005. Etoposide, doxorubicin and cisplatin plus mitotane in the treatment of advanced adrenocortical carcinoma: a large prospective phase II trial. Endocrine-related cancer. 12:657-666.

Bertherat, J., and X. Bertagna. 2009. Pathogenesis of adrenocortical cancer. Best practice & research. Clinical endocrinology & metabolism. 23:261-271.

Bidari, A., Ganjali, M.R., Assadi, Y., Kiani, A., Norouzi, P.; Assay of total mercury in commercial food supplements of marine origin by means of DLLME/ICP-AES, Food Anal. Methods 5 (2012) 695–701.

Bilimoria, K.Y., W.T. Shen, D. Elaraj, D.J. Bentrem, D.J. Winchester, E. Kebebew, and C. Sturgeon. 2008. Adrenocortical carcinoma in the United States: treatment utilization and prognostic factors. Cancer. 113:3130-3136.

Bjornberg, K.A., Vahter, M., Berglund, B., Niklasson, B., Blennow, M., Sandborgh-Englund, G.; Transport of methylmercury and inorganic mercury to the fetus and breast-fed infant. Environ Health Perspect. 2005; 113:1381–5.

Blair, R.M., Fang, H., Branham, W.S., Hass, B.S., Dial, S.L., Moland, C.L., Tong, W., Shi, L., Perkins, R.D., Sheehan, D.M. 1999. The estrogen receptor relative binding affinities of 188 natural and xenochemicals: structural diversity of ligands. Toxic Sci 54:138–153.

Bocca, B., Mattei, D., Pino, A., Alimonti, A.; Uncertainty evaluation in the analysis of biological samples by sector field inductively coupled plasma mass spectrometry. Part A: measurements of Be, Cd, Hg, Ir, Pb, Pd, Pt, Rh, Sb, U, Tl and W in human serum. Rapid Commun Mass Spectrom 2010;24:2363-9

Bocca, B., Mattei, D., Pino, A., Alimonti, A.; Uncertainty evaluation in the analysis of biological samples by sector field inductively coupled plasma mass spectrometry. Part B: measurements of As, Co, Cr, Mn, Mo, Ni, Sn and V in human serum. Rapid Commun Mass Spectrom 2011a;25:453-8.

Bocca, B., Mattei, D., Pino, A., Alimonti, A.; Uncertainty evaluation in the analysis of biological samples by sector field inductively coupled plasma mass spectrometry. Part B: measurements of As, Co, Cr, Mn, Mo, Ni, Sn and V in human serum. Rapid Communication in Mass Spectrometry 2011b; 25: 453-458.

Bologa, C.G., C.M. Revankar, S.M. Young, B.S. Edwards, J.B. Arterburn, A.S. Kiselyov, M.A. Parker, S.E. Tkachenko, N.P. Savchuck, L.A. Sklar, T.I. Oprea, and E.R. Prossnitz. 2006. Virtual and biomolecular screening converge on a selective agonist for GPR30. Nature chemical biology. 2:207-212.

Bose-O'Reilly, S., McCarty, K.M., Steckling, N., Lettmeier, B.; Mercury Exposure and Children's Health. Curr. Probl. Pediatr. Adolesc. Health Care 2010, 40(8), 186–215.

Bose-O'Reilly, S., Lettmeier, B., Roider, G., Siebert, U., Drasch, G.; Mercury in breast milk - a health hazard for infants in gold mining areas?; Int J Hyg Environ Health. 2008 Oct;211(5-6):615-23.

Boulle, N., A. Logie, C. Gicquel, L. Perin, and Y. Le Bouc. 1998. Increased levels of insulin-like growth factor II (IGF-II) and IGF-binding protein-2 are associated with malignancy in sporadic adrenocortical tumors. The Journal of clinical endocrinology and metabolism. 83:1713-1720.

Bouskine, A., M. Nebout, B. Mograbi, F. Brucker-Davis, C. Roger, and P. Fenichel. 2008. Estrogens promote human testicular germ cell cancer through a membrane-mediated activation of extracellular regulated kinase and protein kinase A. Endocrinology. 149:565-573.

Bovio, S., A. Cataldi, G. Reimondo, P. Sperone, S. Novello, A. Berruti, P. Borasio, C. Fava, L. Dogliotti, G.V. Scagliotti, A. Angeli, and M. Terzolo. 2006. Prevalence of adrenal incidentaloma in a contemporary computerized tomography series. Journal of endocrinological investigation. 29:298-302.

Brennan, M.F. 1987. Adrenocortical carcinoma. CA: a cancer journal for clinicians. 37:348-365;

Brombach, B. Chen, W.T. Corns, J. Feldmann and E. M. Krupp, Methylmercury in water samples at the pg/L level by online preconcentration liquid chromatography cold vapor-atomic fluorescence spectrometry, Spectrochimica Acta Part B, 105, 2015, 103–108.

Budtz-Jorgensen, E., Grandjean, P., Keiding, N., White, R.F., Weihe, P.; Bench-mark dose calculations of methylmercury-associated neurobehavioural deficits. Toxicol. Lett. 2000, 112(13), 193–199.

Buneaux, F., Buisine, A., Bourdon, S., et al. 1992. Continuous-flow quantification of total mercury in whole blood, plasma, erythrocytes and urine by inductively coupled plasma atomic-emission spectroscopy. J Anal Toxicol 16(2):99-101.

Cagnol, S., and J.C. Chambard. 2010. ERK and cell death: mechanisms of ERK-induced cell death--apoptosis, autophagy and senescence. The FEBS journal. 277:2-21.

Caldwell, K.L., et al., 2009. Total blood mercury concentrations in the U.S. population: 1999–2006. Int. J. Hyg. Environ. Health 212,588–598.

Çamur, D., Güler, Ç., Vaizoğlu, S.A., Özdilek, B.; Determining mercury levels in anchovy and in individuals with different fish consumption habits, together with their neurological effects. ToxicolInd Health. 2016 Jul;32(7):1215-23.

Carmeci, C., E.C. deConinck, T. Lawton, D.A. Bloch, and R.J. Weigel. 1997. Analysis of estrogen receptor messenger RNA in breast carcinomas from archival specimens is predictive of tumor biology. The American journal of pathology. 150:1563-1570.

Carneiro, M. F., Moresco, M. B., Chagas G. R., de Oliveira Souza, V. C., Rhoden C. R., and Barbosa, F. 2011. Assessment of trace elements in scalp hair of a young urban population in Brazil. Biol. Trace Elem. Res. 143:815–824.

Castoldi, A. F., Coccini, T., Ceccatelli, S., Manzo, L.; Neurotoxicity and molecular effects of methylmercury; Brain Res Bull. 2001 May 15;55(2):197-203.

Cernichiari, E.; Brewer, G.J., Myers, D.O. Marsh, L.W., Lapham, C., Cox, Shamlaye, C.F., Berlin, M., Davidson P.W. and Clarkson T.W. 1995. Monitoring methylmercury during pregnancy: Maternal hair predicts fetal brain exposure. Neuro Toxicology 16:705-710.

Chan, Q.K., H.M. Lam, C.F. Ng, A.Y. Lee, E.S. Chan, H.K. Ng, S.M. Ho, and K.M. Lau. 2010. Activation of GPR30 inhibits the growth of prostate cancer cells through sustained activation of Erk1/2, c-jun/c-fos-dependent upregulation of p21, and induction of G(2) cell-cycle arrest. Cell death and differentiation. 17:1511-1523.

Chen, J.R., L.I. Plotkin, J.I. Aguirre, L. Han, R.L. Jilka, S. Kousteni, T. Bellido, and S.C. Manolagas. 2005. Transient versus sustained phosphorylation and nuclear accumulation of ERKs underlie anti-versus pro-apoptotic effects of estrogens. The Journal of biological chemistry. 280:4632-4638.

Chevalier, N., A. Bouskine, and P. Fenichel. 2012. Bisphenol A promotes testicular seminoma cell proliferation through GPER/GPR30. International journal of cancer. Journal international du cancer. 130:241-242.

Chimento, A., I. Casaburi, C. Rosano, P. Avena, A. De Luca, C. Campana, E. Martire, M.F. Santolla, M. Maggiolini, V. Pezzi, and R. Sirianni. 2013b. Oleuropein and hydroxytyrosol activate GPER/ GPR30-dependent pathways leading to apoptosis of ER-negative SKBR3 breast cancer cells. Molecular nutrition & food research.

Chimento, A., I. Casaburi, M. Bartucci, M. Patrizii, R. Dattilo, P. Avena, S. Ando, V. Pezzi, and R. Sirianni. 2013a. Selective GPER activation decreases proliferation and activates apoptosis in tumor Leydig cells. Cell death & disease. 4:e747.

Chimento, A., R. Sirianni, C. Delalande, D. Silandre, C. Bois, S. Ando, M. Maggiolini, S. Carreau, and V. Pezzi. 2010. 17 beta-estradiol activates rapid signaling pathways involved in rat pachytene spermatocytes apoptosis through GPR30 and ER alpha. Molecular and cellular endocrinology. 320:136-144.

Chimento, A., R. Sirianni, F. Zolea, C. Bois, C. Delalande, S. Ando, M. Maggiolini, S. Aquila, S. Carreau, and V. Pezzi. 2011. Gper and ESRs are expressed in rat round spermatids and mediate oestrogen-dependent rapid pathways modulating expression of cyclin B1 and Bax. International journal of andrology. 34:420-429.

Chimento, A., R. Sirianni, I. Casaburi, C. Ruggiero, M. Maggiolini, S. Ando, and V. Pezzi. 2012. 17beta-Estradiol activates GPER- and ESR1-dependent pathways inducing apoptosis in GC-2 cells, a mouse spermatocyte-derived cell line. Molecular and cellular endocrinology. 355:49-59.

CITAC, EURACHEM, 2002; Available at URL: https://www.eurachem.org/images/stories/Guides/pdf/Eurachem_CITAC_QAC_2016_EN.pdf .

Clarkson, T.W., Magos, L.; The toxicology of mercury and its chemical compounds. Crit Rev Toxicol 2006;36: 609-662 16973445.

Clarkson, T.W.; Mercury: major issues in environmental health; Environ. Health Perspect., 1993, 100, 31–38; WHO, Environmental Health Criteria 101: Methylmercury, World Health Organization, Geneva, 1990.

Clemmons, D.R., W.H. Busby, T. Arai, T.J. Nam, J.B. Clarke, J.I. Jones, and D.K. Ankrapp. 1995. Role of insulin-like growth factor binding proteins in the control of IGF actions. Progress in growth factor research. 6:357-366.

Cohn, K., L. Gottesman, and M. Brennan. 1986. Adrenocortical carcinoma. Surgery. 100:1170-1177.

Cory, S., and J.M. Adams. 2002. The Bcl2 family: regulators of the cellular life-or-death switch. Nature reviews. Cancer. 2:647-656.

Counter A.S., and Buchanan L.H.; Mercury exposure in children: a review;Toxicology and Applied Pharmacology 198 (2004) 209 – 230.

Creemers, S.G., Hofland, L.J., Korpershoek, E., Franssen, G.J., Van Kemenade, F.J., De Herder, W.W. and Feelders, R.A.; Future directions in the diagnosis and medical treatment of adrenocortical carcinoma. Endocr Relat Cancer 23: R43-R69, 2016.

Crucitti, F., R. Bellantone, A. Ferrante, M. Boscherini, and P. Crucitti. 1996. The Italian Registry for Adrenal Cortical Carcinoma: analysis of a multiinstitutional series of 129 patients. The ACC Italian Registry Study Group. Surgery. 119:161-170.

Crump, K.S., Van Landingham, C., Shamlaye, C., Cox, C., Davidson, P.W., Myers, G.J., Clarkson, T.W.; Benchmark concentrations for methylmercury obtained from the Seychelles Child Development Study. Environ. Health Perspect. 2000, 18(3), 257-263.

Csernus, V.J., A.V. Schally, H. Kiaris, and P. Armatis. 1999. Inhibition of growth, production of insulin-like growth factor-II (IGF-II), and expression of IGF-II mRNA of human cancer cell lines by antagonistic analogs of growth hormone-releasing hormone in vitro. Proceedings of the National Academy of Sciences of the United States of America. 96:3098-3103.

Cui, Y., Balshaw, D.M., Kwok, R.K., Thompson, C.L., Collman, G.W., Birnbaum, L.S.; The Exposome: Embracing the Complexity for Discovery in Environmental Health.Environ Health Perspect. 2016 Aug 1;124(8):A137-40.

Dackiw, A.P., J.E. Lee, R.F. Gagel, and D.B. Evans. 2001. Adrenal cortical carcinoma. World journal of surgery. 25:914-926.

De Ceaurriz, J., Payan, J.P., Morel, G., Brondeau, M.T. (1994). Role of extracellular glutathione and gamma-glutamyltranspeptidase in the disposition and kidney toxicity of inorganic mercury in rats. J. Appl. Toxicol. 14(3):201-6.

De Laguna, A. 1955. PedacioDioscoridesAnazarbeo, Acerca de la Materia Medicinal y de los venenos mortiferos. Libro V, Cap. LXIX: Del Azogue, (Juan Latio, Anvers, Belgium). pp. 540-542;Sigerest, H.E. 1996. Four Treatises of Theophrastus von Hohenheim Called Paracelsus (The Johns Hopkins University Press: Baltimore, MD, USA).

Do Nascimento, J.L.M., Oliveira, K.R.M., Crespo- Lopez, M.E., Macchi, B.M., Maues, L.A.L., Pinheiro, M.C.N., Luiz Carlos L. Silveira, L.C.L. and Herculano, A.M. 2008. Methylmercury neurotoxicity and antioxidant defenses. Indian J. Med. Res. 128: 373-382.

Dodes, J.E. 2001. The amalgam controversy: An evidence-based analysis. JADA 132: 348-356; Clarkson, R.W. 2002. The three modern faces of mercury. Environ. Health Perspect. 110: 11-23.

Donatini, G., Caiazzo, R., Do Cao, C., Aubert, S., Zerrweck, C., El-Kathib, Z., Gauthier, T., Leteurtre, E., Wemeau, J.L., Vantyghem, M.C., et al: Long-term survival after adrenalectomy for stage I/II adrenocortical carcinoma (ACC): A retrospective comparative cohort study of laparoscopic versus open approach. Ann Surg Oncol 21: 284-291, 2014.

Dong, S., S. Terasaka, and R. Kiyama. 2011. Bisphenol A induces a rapid activation of Erk1/2 through GPR30 in human breast cancer cells. Environ Pollut. 159:212-218.

Dong, W.H., J.C. Chen, Y.L. He, J.J. Xu, and Y.A. Mei. 2013. Resveratrol inhibits K(v)2.2 currents through the estrogen receptor GPR30-mediated PKC pathway. American journal of physiology. Cell physiology. 305:C547-557.

Dorea, J.G., Donangelo, C.M.; Early (in uterus and infant) exposure to mercury and lead.ClinNutr. 2006 Jun;25(3):369-76. Epub 2005 Nov 22.

Dy, S.M. 2013. Measuring the quality of palliative care and supportive oncology: principles and practice. The journal of supportive oncology. 11:160-164.

Eide, I., Syversen, T.L.; Relationship between catalase activity and uptake of elemental mercury by rat brain. ActaPharmacolToxicol (Copenh) 1983;52:217–23.

Else, T., Kim, A.C., Sabolch, A., Raymond, V.M., Kandathil, A., Caoili, E.M., Jolly, S., Miller, B.S., Giordano, T.J. and Hammer, G.D.: Adrenocortical carcinoma. Endocr Rev 35: 282-326, 2014.

Emteborg, H., Bulska, E., Frech, W., et al. 1992. Determination of total mercury in human whole blood by electrothermal atomic absorption spectrometry following extraction. J Anal Atomic Spectrum 7(2):405-408.

Ernst, E. and Coon, C.T. 2001. Heavy metals in traditional Chinese medicines: a systemic review. Clin. Pharmacol. Ther. 70: 497-504.

Eudy, J.D., S. Yao, M.D. Weston, M. Ma-Edmonds, C.B. Talmadge, J.J. Cheng, W.J. Kimberling, and J. Sumegi. 1998. Isolation of a gene encoding a novel member of the nuclear receptor superfamily from the critical region of Usher syndrome type IIa at 1q41. Genomics. 50:382-384.

EUROLAB Technical Report No. 1 / 2007, ISO 21748: 2010.

Evans, R.M. 1988. The steroid and thyroid hormone receptor superfamily. Science. 240:889-895.

Ewers, H., Krause, C., Schulz, C., Wilhelm, M.; Reference values and human biological monitoring values for environmental toxins. Int Arch Occup Environ Health 1999;72:255-60

Fadeel, B., and S. Orrenius. 2005. Apoptosis: a basic biological phenomenon with wide-ranging implications in human disease. Journal of internal medicine. 258:479-517.

FAO Paper 29 Rev 1; Roma 1985.

Fassnacht, M., S. Hahner, B. Polat, A.C. Koschker, W. Kenn, M. Flentje, and B. Allolio. 2006. Efficacy of adjuvant radiotherapy of the tumor bed on local recurrence of adrenocortical carcinoma. The Journal of clinical endocrinology and metabolism. 91:4501-4504.

Fergusson, J.E. The Heavy Elements: Chemistry, Environmental Impact and Health Effects. Oxford: Pergamon Press; 1990.

Filardo, E.J. 2002. Epidermal growth factor receptor (EGFR) transactivation by estrogen via the G-protein-coupled receptor, GPR30: a novel signaling pathway with potential significance for breast cancer. The Journal of steroid biochemistry and molecular biology. 80:231-238.

Filardo, E.J. 2011. GPER and ER: estrogen receptors with distinct biological roles in breast cancer. Immun Endoc Metab Agents in Med Chem 11:00–002.

Filardo, E.J., C.T. Graeber, J.A. Quinn, M.B. Resnick, D. Giri, R.A. DeLellis, M.M. Steinhoff, and E. Sabo. 2006. Distribution of GPR30, a seven membrane-spanning estrogen receptor, in primary breast cancer and its association with clinicopathologic determinants of tumor progression. Clinical cancer research : an official journal of the American Association for Cancer Research. 12:6359-6366.

Filardo, E.J., J.A. Quinn, K.I. Bland, and A.R. Frackelton, Jr. 2000. Estrogen-induced activation of Erk-1 and Erk-2 requires the G protein-coupled receptor homolog, GPR30, and occurs via trans-activation of the epidermal growth factor receptor through release of HB-EGF. Mol Endocrinol. 14:1649-1660.

Filardo, E.J., Thomas, P. 2005. GPR30: a seven-transmembrane-spanning estrogen receptor that triggers EGF release. Trends Endocrinol Metab 16:362–367.

Fourth National Report on Human Exposure to Environmental Chemicals, Updated Tables, February 2015 Available at URL: https://www.cdc.gov/biomonitoring/pdf/FourthReport_UpdatedTables_Feb2015.pdf).

Fréry, N., Vandentorren, S., Etchevers, A., Fillol, C.; Highlights of recent studies and future plans for the French human biomonitoring (HBM) programme; Int J Hyg Environ Health. 2012 Feb;215(2):127-32.

Friese, K.H., Roschig, M., Wuenscher, G.; et al. 1990. A new calibration method for the determination of trace amounts of mercury in air and biological materials. Fresenius J Anal Chem 337(8):860-866.

Gårdfeldt, K., Sommar, J., Strömberg, D., Feng , X. 2001. Oxidation of atomic mercury by hydroxyl radicals and photoinduceddecomposition of methylmercury species in the aqueous phase. AtmosphericEnvironment 35, 3039-3047.

Gicquel, C., N. Boulle, A. Logie, N. Bourcigaux, V. Gaston, and Y. Le Bouc. 2001. [Involvement of the IGF system in the pathogenesis of adrenocortical tumors]. Annales d'endocrinologie. 62:189-192.

Giguere, V., N. Yang, P. Segui, and R.M. Evans. 1988. Identification of a new class of steroid hormone receptors. Nature. 331:91-94.

Gockerman, A., T. Prevette, J.I. Jones, and D.R. Clemmons. 1995. Insulin-like growth factor (IGF)-binding proteins inhibit the smooth muscle cell migration responses to IGF-I and IGF-II. Endocrinology. 136:4168-4173.

Goldman, L.R., Shannon, M.W.; Committee on Environmental Health, American Academy of Pediatrics. Technical report: mercury in the environment: implications for pediatricians. Pediatrics. 2001; 108:197–205.

Goldwater, L.J. 1936. From Hippocrates to Ramazini: early history of industrial medicine. Ann. Med. Hist. 8: 27-35.

Grandjean, P., Budtz-Jørgensen, E., White, R.F., Jørgensen, P.J., Weihe, P., Debes, F., Keiding, N.; Methylmercury exposure biomarkers as indicators of neurotoxicity in children aged 7 years. Am J Epidemiol. 1999 Aug 1;150(3):301-5.

Grandjean, P., Jørgensen, P.J., Weihe, P.; Validity of mercury exposure biomarkers. In Biomarkers of Environmentally Associated Disease Wilson, S.H.; Suk, W.A., Eds.; CRC Press: Boca Raton, FL, 2002, pp. 235-247.

Grandjean, P., Murata, K., Budtz-Jørgensen, E., Weihe, P. (2004): Cardiac autonomic activity in methylmercury neurotoxicity: 14-year follow-up of a Faroese birth cohort. The Journal of Pediatrics. 144 (2): 169-176.

Grandjean, P., Weihe, P., Jorgensen, P.J., Clarkson, T., Cernichiari, E., Videro, T.; Impact of maternal seafood diet on fetal exposure to mercury, selenium, and lead. Arch. Environ. Health 1992, 47, 185–195.

Grandjean, P.; Methylmercury toxicity and functional programming. Reprod. Toxicol. 2007, 23, 414–20.

Grumbach, M.M., B.M. Biller, G.D. Braunstein, K.K. Campbell, J.A. Carney, P.A. Godley, E.L. Harris, J.K. Lee, Y.C. Oertel, M.C. Posner, J.A. Schlechte, and H.S. Wieand. 2003. Management of the clinically inapparent adrenal mass ("incidentaloma"). Annals of internal medicine. 138:424-429.

Guzzi, G., Pigatto, P.D.; Spadari, F. and La Porta, C.A.M.; Effect of thimerosal, methylmercury, and mercuric chloride in Jurkat T Cell Line, InterdiscipToxicol. 2012 Sep; 5(3): 159–161.

Haas, E., I. Bhattacharya, E. Brailoiu, M. Damjanovic, G.C. Brailoiu, X. Gao, L. Mueller-Guerre, N.A. Marjon, A. Gut, R. Minotti, M.R. Meyer, K. Amann, E. Ammann, A. Perez-Dominguez, M. Genoni, D.J. Clegg, N.J. Dun, T.C. Resta, E.R. Prossnitz, and M. Barton. 2009. Regulatory role of G protein-coupled estrogen receptor for vascular function and obesity. Circulation research. 104:288-291.

Habra, M.A., S. Ejaz, L. Feng, P. Das, F. Deniz, E.G. Grubbs, A. Phan, S.G. Waguespack, M. Ayala-Ramirez, C. Jimenez, N.D. Perrier, J.E. Lee, and R. Vassilopoulou-Sellin. 2013. A retrospective cohort analysis of the efficacy of adjuvant radiotherapy after primary surgical resection in patients with adrenocortical carcinoma. The Journal of clinical endocrinology and metabolism. 98:192-197.

Halbach, S., Clarkson, T.W.; Enzymatic oxidation of mercury vapor by erythrocytes. BiochimBiophysActa 1978;523:522–31.

Hamelers, I.H., and P.H. Steenbergh. 2003. Interactions between estrogen and insulin-like growth factor signaling pathways in human breast tumor cells. Endocrine-related cancer. 10:331-345.

Harris, H.H., Pickering, I.J., and George, G.N. (2003). The chemical form of mercury in fish. Science 301(5637):1203.

Hartzband, P.I., A.J. Van Herle, L. Sorger, and D. Cope. 1988. Assessment of hypothalamic-pituitary-adrenal (HPA) axis dysfunction: comparison of ACTH stimulation, insulin-hypoglycemia and metyrapone. Journal of endocrinological investigation. 11:769-776.

Hattula T, Rahola T. The distribution and biological half-time of 203Hg in the human body according to a modified whole-body counting technique. Environ PhysiolBiochem 1975;5:252–7.

Hermsen, I.G., Fassnacht, M., Terzolo, M., Houterman, S., den Hartigh, J., Leboulleux, S., Daffara, F., Berruti, A., Chadarevian, R., Schlumberger, M., et al: Plasma concentrations of o,p'DDD, o,p'DDA, and o,p'DDE as predictors of tumor response to mitotane in adrenocortical carcinoma: Results of a retrospective ENS@T multicenter study. J Clin Endocrinol Metab 96: 1844‑1851, 2011.

Hermsen, I.G., Y.E. Groenen, M.W. Dercksen, J. Theuws, and H.R. Haak. 2010. Response to radiation therapy in adrenocortical carcinoma. Journal of endocrinological investigation. 33:712-714.

Hsiao, H.W., Ullrich, S.M., Tanton, T.W., 2011. Burdens of mercury in residents of Temirtau, Kazakhstan: I: hair mercury concentrations and factors of elevated hair mercury levels. Sci. Total Environ. 409 (11), 2272–2280.

Hsieh, Y.C., H.P. Yu, M. Frink, T. Suzuki, M.A. Choudhry, M.G. Schwacha, and I.H. Chaudry. 2007. G protein-coupled receptor 30-dependent protein kinase A pathway is critical in nongenomic effects of estrogen in attenuating liver injury after trauma-hemorrhage. The American journal of pathology. 170:1210-1218.

Huang H and Fojo T: Adjuvant mitotane for adrenocortical cancer - a recurring controversy. J Clin Endocrinol Metab 93: 3730-3732, 2008.

Hursh, J.B., Cherian , M.G., Clarkson, T.W., Vostal, J.J., Mallie, R.V.; Clearance of mercury (HG-197, HG-203) vapor inhaled by human subjects. Arch Environ Health 1976;31:302–9.

Hursh, J.B., Greenwood, M.R., Clarkson, T.W., Allen, J., Demuth, S.; The effect of ethanol on the fate of mercury vapor inhaled by man. J PharmacolExpTher 1980;214(3):520-527.

IARC (International Agency for Research on Cancer; Available:http://monographs.iarc.fr/ENG/Classification/ClassificationsAlphaOrder.pdf

International Agency for Research on Cancer (IARC). IARC Monographs on the Evaluation of Risks to Humans. Volume 58. Beryllium, Cadmium, Mercury, and Exposures in the Glass Manufacturing industry. 1993. Available at URL: http:// monographs.iarc.fr/ENG/Monographs/vol58/index.php. 7/15/09 .

iSchroeder, W. H.; Munthe, J., (1998) Atmospheric Mercury – An Overview. Atmospheric Environment 29, 809-822.

ISO 5725:2004, Available at URL: http://www.iss.it/binary/meta/cont/Procedura_Operativa_005.pdf .

Janssen, J.A., M.L. Jacobs, F.H. Derkx, R.F. Weber, A.J. van der Lely, and S.W. Lamberts. 1997. Free and total insulin-like growth factor I (IGF-I), IGF-binding protein-1 (IGFBP-1), and IGFBP-3 and their relationships to the presence of diabetic retinopathy and glomerular hyperfiltration in insulin-dependent diabetes mellitus. The Journal of clinical endocrinology and metabolism. 82:2809-2815.

John, P.C., M. Mews, and R. Moore. 2001. Cyclin/Cdk complexes: their involvement in cell cycle progression and mitotic division. Protoplasma. 216:119-142.

Kajta, M., J. Rzemieniec, E. Litwa, W. Lason, M. Lenartowicz, W. Krzeptowski, and A.K. Wojtowicz. 2013. The key involvement of estrogen receptor beta and G-protein-coupled receptor 30 in the neuroprotective action of daidzein. Neuroscience. 238:345-360.

Kalamegham, R., Ash, K.O.; 1992. A simple ICP-MS procedure for the determination of total mercury in whole blood and urine. J Clin Lab Anal 6(4):190-193

Kamanga-Sollo, E., White, M.E., Chung, K.Y., Johnson, B.J., Dayton, W.R.; Potential role of G-protein-coupled receptor 30 (GPR30) in estradiol-17beta-stimulated IGF-I mRNA expression in bovine satellite cell cultures. Domest Anim Endocrinol. 2008;35:254–262

Kanda, N., and S. Watanabe. 2003a. 17Beta-estradiol enhances the production of nerve growth factor in THP-1-derived macrophages or peripheral blood monocyte-derived macrophages. The Journal of investigative dermatology. 121:771-780.

Kanda, N., and S. Watanabe. 2003b. 17beta-estradiol inhibits oxidative stress-induced apoptosis in keratinocytes by promoting Bcl-2 expression. The Journal of investigative dermatology. 121:1500-1509.

Kanda, N., and S. Watanabe. 2004. 17beta-estradiol stimulates the growth of human keratinocytes by inducing cyclin D2 expression. The Journal of investigative dermatology. 123:319-328.

Karnieli, E., H. Werner, F.J. Rauscher, 3rd, L.E. Benjamin, and D. LeRoith. 1996. The IGF-I receptor gene promoter is a molecular target for the Ewing's sarcoma-Wilms' tumor 1 fusion protein. The Journal of biological chemistry. 271:19304-19309.

Katzenellenbogen, J.A., and B.S. Katzenellenbogen. 1996. Nuclear hormone receptors: ligand-activated regulators of transcription and diverse cell responses. Chemistry & biology. 3:529-536.

Kebebew, E., E. Reiff, Q.Y. Duh, O.H. Clark, and A. McMillan. 2006. Extent of disease at presentation and outcome for adrenocortical carcinoma: have we made progress? World journal of surgery. 30:872-878.

Kern L. Nuttall, Review: Interpreting Mercury in Blood and Urine of Individual Patients, Annals of Clinical & Laboratory Science, vol. 34, no. 3, 2004.

Kern L. Nuttall; Interpreting Hair Mercury Levels in Individual Patients. Annals of Clinical & Laboratory Science, vol. 36, no.3, 2006.

Kerper , L. E., Ballatori, N., Clarkson, T. W.; Methylmercury transport across the blood-brain barrier by an amino acid carrier; American Journal of Physiology - Regulatory, Integrative and Comparative Physiology May 1992, 262 (5) R761-R765.

Khan, T.S., H. Imam, C. Juhlin, B. Skogseid, S. Grondal, S. Tibblin, E. Wilander, K. Oberg, and B. Eriksson. 2000. Streptozocin and o,p'DDD in the treatment of adrenocortical cancer patients: long-term survival in its adjuvant use. Annals of oncology : official journal of the European Society for Medical Oncology / ESMO. 11:1281-1287.

Kim, G.S., J.S. Hong, S.W. Kim, J.M. Koh, C.S. An, J.Y. Choi, and S.L. Cheng. 2003. Leptin induces apoptosis via ERK/cPLA2/cytochrome c pathway in human bone marrow stromal cells. The Journal of biological chemistry. 278:21920-21929.

Kim, R., M. Emi, K. Tanabe, S. Murakami, Y. Uchida, and K. Arihiro. 2006. Regulation and interplay of apoptotic and non-apoptotic cell death. The Journal of pathology. 208:319-326.

Kjellman, M., L. Roshani, B.T. Teh, O.-P. Kallioniemi, A. Höög, S. Gray, L.-O. Farnebo, M. Holst, M. Bäckdahl, and C. Larsson. 1999a. Genotyping of Adrenocortical Tumors: Very Frequent Deletions of the MEN1 Locus in 11q13 and of a 1-Centimorgan Region in 2p16. Journal of Clinical Endocrinology & Metabolism. 84:730-735.

Koch, H.M., Preuss, R., Angerer, J.; Di(2-ethylhexyl)phthalate (DEHP): human metabolism and internal exposure - an update and latest results. Int J Androl 2006;29:155-65

Koschker, A.C., M. Fassnacht, S. Hahner, D. Weismann, and B. Allolio. 2006. Adrenocortical carcinoma -- improving patient care by establishing new structures. Experimental and clinical endocrinology & diabetes : official journal, German Society of Endocrinology [and] German Diabetes Association. 114:45-51.

Kuhn, J., O.A. Dina, C. Goswami, V. Suckow, J.D. Levine, and T. Hucho. 2008. GPR30 estrogen receptor agonists induce mechanical hyperalgesia in the rat. The European journal of neuroscience. 27:1700-1709.

LaKind, J.S., Aylward, L.L., Brunk, C., DiZio, S., Dourson, M., Goldstien, D.A., Kilpatrick, M.E., Krewski, D., Bartels, M.J., Barton, H.A., Boogaard, P.J., Lipscomb, J., Krishnan, K., Nordberg, M., Okino, M., Tan, Y-M., Viau, C., Yager, J.W., Hays, S.M., 2008. Guidelines for the communication of Biomonitoring Eqivalents: Report from the Biomonitoring Equivalents Expert Workshop. Regul. Toxicol. Pharmacol. 51, S16–S26.

Lappano, R., P. De Marco, E.M. De Francesco, A. Chimento, V. Pezzi, and M. Maggiolini. 2013. Cross-talk between GPER and growth factor signaling. The Journal of steroid biochemistry and molecular biology.

Lehmann, T.P., T. Wrzesinski, and P.P. Jagodzinski. 2013. The effect of mitotane on viability, steroidogenesis and gene expression in NCIH295R adrenocortical cells. Molecular medicine reports. 7:893-900.

Li, D.W., J.P. Liu, Y.W. Mao, H. Xiang, J. Wang, W.Y. Ma, Z. Dong, H.M. Pike, R.E. Brown, and J.C. Reed. 2005. Calcium-activated RAF/MEK/ERK signaling pathway mediates p53-dependent apoptosis and is abrogated by alpha B-crystallin through inhibition of RAS activation. Molecular biology of the cell. 16:4437-4453.

Lin, C.W., Chang, Y.H. and Pu, H.F.; Mitotane exhibits dual effects on steroidogenic enzymes gene transcription under basal and cAMP-stimulating microenvironments in NCI-H295 cells. Toxicology 298: 14-23, 2012.

Lin, H., Yuan, D., Lu, B., Huang, S., Sun, L., Zhang, F. and Gao, Y., Isotopic composition analysis of dissolved mercury in seawater with purge and trap preconcentration and a modified Hg introduction device for MC-ICP-MS. J. Anal. At. Spectrom., 2015, 30, 353–359.

Ling, Y.H., J.D. Jiang, J.F. Holland, and R. Perez-Soler. 2002. Arsenic trioxide produces polymerization of microtubules and mitotic arrest before apoptosis in human tumor cell lines. Molecular pharmacology. 62:529-538.

Listrat, A., L. Belair, B. Picard, N. Boulle, Y. Geay, J. Djiane, and H. Jammes. 1999. Insulin-like growth factor II (IGF-II) mRNA expression during skeletal muscle development of double-muscled and normal bovine foetuses. Reproduction, nutrition, development. 39:113-124.

Maggiolini, M., A. Vivacqua, G. Fasanella, A.G. Recchia, D. Sisci, V. Pezzi, D. Montanaro, A.M. Musti, D. Picard, and S. Ando. 2004. The G protein-coupled receptor GPR30 mediates c-fos up-regulation by 17beta-estradiol and phytoestrogens in breast cancer cells. The Journal of biological chemistry. 279:27008-27016.

Mansmann, G., J. Lau, E. Balk, M. Rothberg, Y. Miyachi, and S.R. Bornstein. 2004. The clinically inapparent adrenal mass: update in diagnosis and management. Endocrine reviews. 25:309-340.

Martensson, U.E., S.A. Salehi, S. Windahl, M.F. Gomez, K. Sward, J. Daszkiewicz-Nilsson, A. Wendt, N. Andersson, P. Hellstrand, P.O. Grande, C. Owman, C.J. Rosen, M.L. Adamo, I. Lundquist, P. Rorsman, B.O. Nilsson, C. Ohlsson, B. Olde, and L.M. Leeb-Lundberg. 2009. Deletion of the G protein-coupled receptor 30 impairs glucose tolerance, reduces bone growth, increases blood pressure, and eliminates estradiol-stimulated insulin release in female mice. Endocrinology. 150:687-698.

McCabe, M.J. Jr, Eckles, K.G., Langdon, M., Clarkson, T.W., Whitekus, M.J., Rosenspire, A.J.; Attenuation of CD95-induced apoptosis by inorganic mercury: caspase-3 is not a direct target of low levels of Hg2+. Toxicol Lett. 2005 Jan 15;155(1):161-70.

McDonnell, D.P., D.L. Clemm, T. Hermann, M.E. Goldman, and J.W. Pike. 1995. Analysis of estrogen receptor function in vitro reveals three distinct classes of antiestrogens. Molecular endocrinology. 9:659-669.

McDowell, M.A.; Dillon, C.F.; Osterloh, J.; Bolger, P.M.; Pellizzari, E.; Fernando, R.; Montes de Oca, R.; Schober, S.E.; Sinks, T.; Jones, R.L.; et al. Hair mercury levels in U.S. children and women of childbearing age: Reference range data from NHANES 1999–2000. Environ. Health Perspect. 2004, 112, 1165–1171.

McInerney, E.M., K.E. Weis, J. Sun, S. Mosselman, and B.S. Katzenellenbogen. 1998. Transcription activation by the human estrogen receptor subtype beta (ER beta) studied with ER beta and ER alpha receptor chimeras. Endocrinology. 139:4513-4522.

McKenna, N.J., J. Xu, Z. Nawaz, S.Y. Tsai, M.J. Tsai, and B.W. O'Malley. 1999. Nuclear receptor coactivators: multiple enzymes, multiple complexes, multiple functions. The Journal of steroid biochemistry and molecular biology. 69:3-12.

McNicol, A.M., C.E. Nolan, A.J. Struthers, M.A. Farquharson, J. Hermans, and H.R. Haak. 1997. Expression of p53 in adrenocortical tumours: clinicopathological correlations. The Journal of Pathology. 181:146-152.

Meloche, S., and J. Pouyssegur. 2007. The ERK1/2 mitogen-activated protein kinase pathway as a master regulator of the G1- to S-phase transition. Oncogene. 26:3227-3239.

Miklavcˇicˇ, A., Cuderman, P., Mazej, D., SnojTratnik, J., Krsnik, M., Planinˇsek, P., Osredkar, J., Horvat, M.; Biomarkers of low-level mercury exposure through fish consumption in pregnant and lactating Slovenian women. Environmental Research111(2011)1201–1207.

Minoia, C., Sabbioni, E., Apostoli, P., Pietra, R., Pozzoli, L., Gallorini, M., Nicolaou, G., Alessio, L., Capodaglio, E.; Trace element reference values in tissues from inhabitants of the European Community. I. A study of 46 elements in urine, blood and serum of Italian subjects. Sci Total Environ 1990;95:89-105.

Mohmand, J., Eqani, S.A.M.A.S., Fasola, M., Alamdar, A., Ali, N., Mustafa, I., Liu, P., Peng, S., Shen, H., 2015. Human exposures to toxic metals via contaminated dust: bioaccumulation trends and risk assessment. Chemosphere 132, 142–151.

Montanaro, D., M. Maggiolini, A.G. Recchia, R. Sirianni, S. Aquila, L. Barzon, F. Fallo, S. Ando, and V. Pezzi. 2005. Antiestrogens upregulate estrogen receptor beta expression and inhibit adrenocortical H295R cell proliferation. Journal of molecular endocrinology. 35:245-256.

Munthe, J. The aqueous oxidation of elemental mercury by ozone. Atmospheric Environment 26A, 1461 - 1468, 1992.

Munthe, J., Kindbom, K., Kruger, O., Petersen, G., Pacyna, J.M. and Iverfeldt, Å.(2001): Emission, deposition, and atmospheric pathways of mercury in Sweden, accepted for Water, Air and Soil Pollution.

Munthe, J., Wangberg, I., Pirrone, N., Iverfeld, A., Ferrara, R., Ebinghaus, R., Feng., R., Gerdfelt, K., Keeler, G.J., Lanzillotta, E., Lindberg, S.E., Lu, J., Mamane, Y., Nucaro, E., Prestbo, E., Schmolke, S., Schroder, W.H., Sommar, J., Sprovieri, F., Stevens, R.K., Stratton, W., Tuncel, G., Urba, A. (2000) Intercomparison of Methods for Sampling and Analysis of Atmospheric Mercury Species. Atmos. Environ. 35, 3007-3017.

National Research Council, 2000. Committee on Toxicology of Methylmercury. Washington DC.

Needham, L.L., Calafat, A.M., Barr, D.; Uses and issues of Biomonitoring. Int J Hyg Environ Health 2007;210:229-38.

Ngim, C.H., Foo, S.C., Phoon, W.O.; 1988. Atomic absorption spectrophotometric determination of mercury in undigested biological samples. Ind Health 26(3):173-178.

Nilsson, S., S. Makela, E. Treuter, M. Tujague, J. Thomsen, G. Andersson, E. Enmark, K. Pettersson, M. Warner, and J.A. Gustafsson. 2001. Mechanisms of estrogen action. Physiological reviews. 81:1535-1565.

Nordberg, G., Brune, D., Gerhardsson, L., Grandjean, P., Vesterberg, O., Wester, P,O.; The ICOH and IUPAC international programme for establishing reference values of metals. Sci Total Environ 1992;120:17- 21.

Nowak, G. 2002. Protein kinase C-alpha and ERK1/2 mediate mitochondrial dysfunction, decreases in active Na+ transport, and cisplatin-induced apoptosis in renal cells. The Journal of biological chemistry. 277:43377-43388.

Nowak, G., G.L. Clifton, M.L. Godwin, and D. Bakajsova. 2006. Activation of ERK1/2 pathway mediates oxidant-induced decreases in mitochondrial function in renal cells. American journal of physiology. Renal physiology. 291:F840-855.

Oberst, A., C. Bender, and D.R. Green. 2008. Living with death: the evolution of the mitochondrial pathway of apoptosis in animals. Cell death and differentiation. 15:1139-1146.

O'Dowd, B.F., T. Nguyen, A. Marchese, R. Cheng, K.R. Lynch, H.H. Heng, L.F. Kolakowski, Jr., and S.R. George. 1998. Discovery of three novel G-protein-coupled receptor genes. Genomics. 47:310-313.

Oskarsson, A., Schutz, A., Skerfving, S., et al. 1996. Total and inorganic mercury in breast milk and blood in relation to fish consumption and amalgam fillings in lactating women. Arch Environ Health. 51(3): 234-241.

Otto, C., I. Fuchs, G. Kauselmann, H. Kern, B. Zevnik, P. Andreasen, G. Schwarz, H. Altmann, M. Klewer, M. Schoor, R. Vonk, and K.H. Fritzemeier. 2009. GPR30 does not mediate estrogenic responses in reproductive organs in mice. Biology of reproduction. 80:34-41.

Owman, C., P. Blay, C. Nilsson, and S.J. Lolait. 1996. Cloning of human cDNA encoding a novel heptahelix receptor expressed in Burkitt's lymphoma and widely distributed in brain and peripheral tissues. Biochemical and biophysical research communications. 228:285-292.

Pacyna J. M. and Keeler G., (1995) Sources of mercury in the Arctic. Water Air Soil Pollut., 80, 621-632.

Paech, K., P. Webb, G.G. Kuiper, S. Nilsson, J. Gustafsson, P.J. Kushner, and T.S. Scanlan. 1997. Differential ligand activation of estrogen receptors ERalpha and ERbeta at AP1 sites. Science. 277:1508-1510.

Pang, Y., J. Dong, and P. Thomas. 2008. Estrogen signaling characteristics of Atlantic croaker G protein-coupled receptor 30 (GPR30) and evidence it is involved in maintenance of oocyte meiotic arrest. Endocrinology. 149:3410-3426.

Park, H-S., Shin, K-O., Kim, J-S.; Assessment of reference values for hair minerals of Korean preschool children. Biol. Trace Elem. Res. 2007; 116: 119–130.

Park, J-D., Zheng, W.; Human Exposure and Health Effects of Inorganic and Elemental Mercury. Journal of Preventive Medicine and Public Health 2012; 45(6): 344-352.

Patalano, A., V. Brancato, and F. Mantero. 2009. Adrenocortical cancer treatment. Hormone research. 71 Suppl 1:99-104.

Petersen, G., J. Munthe, K. Pleijel, R. Bloxam, and A. Vinod Kumar (1998) A comprehensive eulerian modeling framework for airborne mercury species: Development and testing of the tropospheric chemistry module (TCM). Atmospheric Environment, 29, 829-843.

Petrie, W.K., M.K. Dennis, C. Hu, D. Dai, J.B. Arterburn, H.O. Smith, H.J. Hathaway, and E.R. Prossnitz. 2013. G protein-coupled estrogen receptor-selective ligands modulate endometrial tumor growth. Obstetrics and gynecology international. 2013:472720.

Pichichero, M.E.; Gentile, A.; Giglio, N.; Umido, V.; Clarkson, T.; Cernichiari, E.; Zareba, G.; Gotelli, C.; Gotelli, M.; Yan, L.; et al. Mercury levels in newborns and infants after receipt of thimerosal-containing vaccines. Pediatrics 2008, 121, 208–214).

Pike, A.C., A.M. Brzozowski, R.E. Hubbard, T. Bonn, A.G. Thorsell, O. Engstrom, J. Ljunggren, J.A. Gustafsson, and M. Carlquist. 1999. Structure of the ligand-binding domain of oestrogen receptor beta in the presence of a partial agonist and a full antagonist. The EMBO journal. 18:4608-4618.

Ping, L., Dasgupta, P.K.; 1990. Determination of urinary mercury with an automated micro batch analyzer. Anal Chem 62(1):85-88;Vesterberg O. 1991. Automatic method for quantitation of mercury in blood, plasma and urine. J BiochemBiophys Methods 23(3):227-236.

Ping, L., Dasgupta, PK.; 1989. Determination of total mercury in water and urine by a gold film sensor following Fenton's reagent digestion. Anal Chem 61(11):1230-1235.

Pino, A., Amato, A., Alimonti, A., Mattei, D., Bocca, B.; Human biomonitoring for metals in Italian urban adolescents: data from Latium Region. Int. J. Hygiene Environ. Health 2012, 215(2), 185–190

Pirrone et al. Position Paper on Mercury: http://www.iia.cnr.it/project/position-paper-on-mercury.

Pirrone, N., Hedgecock, I., Forlano, L. (2000) The Role of the Ambient Aerosol in the Atmospheric Processing of Semi-Volatile Contaminants: A Parameterised Numerical Model (GASPAR). Journal of Geophysical Research, 105, D8, 9773-9790.

Pollak M. Insulin and insulin-like growth factor signalling in neoplasia. Nature reviews Cancer. 2008; 8:915–928.

Pollard, K.M., Hultman, P.; Effects of mercury on the immune system. Met Ions Biol Syst. 1997;34:421-40.

Prossnitz, E.R., and M. Barton. 2009. Signaling, physiological functions and clinical relevance of the G protein-coupled estrogen receptor GPER. Prostaglandins & other lipid mediators. 89:89-97.

Prossnitz, E.R., and M. Maggiolini. 2009. Mechanisms of estrogen signaling and gene expression via GPR30. Molecular and cellular endocrinology. 308:32-38.

Rackham, H., 1952. Pliny: Natural history (English trans.), Loeb Classical ser., W. Heinemann, London.

Ragazzon B, Assié G and Bertherat J: Transcriptome analysis of adrenocortical cancers: From molecular classification to the identification of new treatments. Endocr Relat Cancer 18: R15-R27, 2011.

Rahola, T., Hattula, T., Korolainen, A., Miettinen, J.K.; Elimination of free and protein-bound ionic mercury (203Hg2+) in man. Ann Clin Res 1973;5:214–9.

Rainey, W.E., I.M. Bird, and J.I. Mason. 1994. The NCI-H295 cell line: a pluripotent model for human adrenocortical studies. Molecular and cellular endocrinology. 100:45-50.

Ramos, J.W. 2008. The regulation of extracellular signal-regulated kinase (ERK) in mammalian cells. The international journal of biochemistry & cell biology. 40:2707-2719.

Reader, M.J., and Lines, C.B. (1983). Decomposition of thimerosal in aqueous solution and its determination by high-performance liquid chromatography. J. Pharm. Sci. 72(12):1406-9.

Reinke V, L.G. 1997. Differential activation of p53 targets in cells treated with ultraviolet radiation that undergo both apoptosis and growth arrest. Radiat. Res. 148.

Revankar, C.M., D.F. Cimino, L.A. Sklar, J.B. Arterburn, and E.R. Prossnitz. 2005. A transmembrane intracellular estrogen receptor mediates rapid cell signaling. Science. 307:1625-1630.

Rice, D.; Barone, S Jr. Critical periods of vulnerability for the developing nervous system: evidence from humans and animal models. Environ. Health Perspect. 2000, 108(3), 511–339.

Roman, S. 2006. Adrenocortical carcinoma. Current opinion in oncology. 18:36-42.

Romano, N., K. Lee, I.M. Abraham, C.L. Jasoni, and A.E. Herbison. 2008. Nonclassical estrogen modulation of presynaptic GABA terminals modulates calcium dynamics in gonadotropin-releasing hormone neurons. Endocrinology. 149:5335-5344.

Ronchetti; R., Zuurbier, M., Jesenak, M., Koppe, J.G., Ahmed, U.F., Ceccatelli, S. and Villa,M.P.; Children's health and mercury exposure, Acta Pædiatrica, 2006; 95 Suppl 453: 36-44.

Rowlands, D.J., S. Chapple, R.C. Siow, and G.E. Mann. 2011. Equol-stimulated mitochondrial reactive oxygen species activate endothelial nitric oxide synthase and redox signaling in endothelial cells: roles for F-actin and GPR30. Hypertension. 57:833-840.

S.I.V.R., LIST OF THIRD REFERENCE VALUES FOR ELEMENTS, ORGANIC COMPOUNDS AND THEIR METABOLITES, EDITION 2011.Available at URL:http://fad.saepe.it/approfondimenti/Valori_di_riferimento_LISTA_SIVR_2011.0.pdf .

Sakamoto, M., Kubota, M., Liu, X.J., Murata, K., Nakai, K., Satoh, H.; Maternal and fetal mercury and n-3 polyunsaturated fatty acids as a risk and benefit of fish consumption to fetus. Environ. Sci. Technol. 2004, 38, 3860-3863.

Sameshima, Y., Y. Tsunematsu, S. Watanabe, T. Tsukamoto, K. Kawa-ha, Y. Hirata, H. Mizoguchi, T. Sugimura, M. Terada, and J. Yokota. 1992. Detection of Novel Germ-line p53 Mutations in Diverse-Cancer-Prone Families Identifiled by Selecting Patients With Childhood Adrencortical Carcinoma. Journal of the National Cancer Institute. 84:703-707.

Sathya, S., S. Sudhagar, and B.S. Lakshmi. 2015. Estrogen suppresses breast cancer proliferation through GPER / p38 MAPK axis during hypoxia. Molecular and cellular endocrinology. 417:200-210.

Scheepers, P.T., van Ballegooij-Gevers, M., Jans, H.; Biological monitoring involving children exposed to mercury from a barometer in a private residence. Toxicol Lett. 2014 Dec 15;231(3):365-73.

Schoeters, G., Den Hond, E., Colles, A., Loots, I., Morrens, B., Keune, H., et al. Concept of the Flemish human biomonitoring programme. Int. J. Hyg. Environ. Health 2012, 215(2), 102–108.

Schteingart, D.E., G.M. Doherty, P.G. Gauger, T.J. Giordano, G.D. Hammer, M. Korobkin, and F.P. Worden. 2005. Management of patients with adrenal cancer: recommendations of an international consensus conference. Endocrine-related cancer. 12:667-680.

Schulick, R.D., and M.F. Brennan. 1999. Adrenocortical carcinoma. World journal of urology. 17:26-34; Schulick, R.D., and M.F. Brennan. 1999b. Long-term survival after complete resection and repeat resection in patients with adrenocortical carcinoma. Annals of surgical oncology. 6:719-726.

Schulz, C., Angerer, J., Ewers, U., Heudorf, U., Wilhelm, M.; Human Biomonitoring Commission of the German Federal Environment Agency. Revised and new reference values for environmental pollutants in urine or blood of children in Germany derived from the German environmental survey on children 2003-2006 (GerES IV). Int. J. Hyg. Environ. Health 2009, 212, 637-647.

Schulz, C., Angerer, J., Ewers, U., Kolossa-Gehring, M.; The German Human Biomonitoring Commission. Int J Hyg Environ Health 2007a ;210:375-84.

Schulz, C., Butte, W., 2007. Revised reference value for pentachlorophenol in morning urine. Int. J. Hyg. Environ. Health 210, 741–744.

Schulz, C., Conrad, A., Becker, K., Kolossa-Gehring, K., Seiwert, M.; 20 years of German Environmental Survey (GerES): human biomonitoring and trends over time. Int J Hyg Environ Health 2007b;210:271-97.

Schulz, C., Conrad, A., Becker, K., Kolossa-Gehring, M., Seiwert, M., Seifert, B.; Twenty years of the German Environmental Survey (GerES): Human biomonitoring – temporal and spatial (West Germany/East Germany) differences in population exposure. Int. J. Hyg. Environ. Health 2007c, 210(3–4), 271–297.

Schulz, C., et al., 2007d. The German human biomonitoring commission. Int. J. Hyg. Environ. Health 210, 373–382.

Schulz, C., et al., 2012. Reprint of"Update of the reference and HBM values derived by the German Human Biomonitoring Commission". Int. J. Hyg. Environ. Health 215,150–158.

Schulz, C., Wilhelm, M., Heudorf, U., Kolossa-Gehring, M.; Update of the reference and HBM values derived by the German Human Biomonitoring Commission. Int. J. Hyg. Env. Health 2011;215: 26– 35.

Seshadri, M., J.A. Spernyak, P.G. Maiery, R.T. Cheney, R. Mazurchuk, and D.A. Bellnier. 2007. Visualizing the acute effects of vascular-targeted therapy in vivo using intravital microscopy and magnetic resonance imaging: correlation with endothelial apoptosis, cytokine induction, and treatment outcome. Neoplasia. 9:128-135.

Sheng, Z.G., W. Huang, Y.X. Liu, and B.Z. Zhu. 2013. Bisphenol A at a low concentration boosts mouse spermatogonial cell proliferation by inducing the G protein-coupled receptor 30 expression. Toxicology and applied pharmacology. 267:88-94.

Sherman, L.S., Blum, J.D., Franzblau, A., Basu, N.; New insight into biomarkers of human mercury exposure using naturally occurring mercury stable isotopes. Environ Sci Technol. 2013 Apr 2;47(7):3403-9.

Shiau, A.K., D. Barstad, P.M. Loria, L. Cheng, P.J. Kushner, D.A. Agard, and G.L. Greene. 1998. The structural basis of estrogen receptor/coactivator recognition and the antagonism of this interaction by tamoxifen. Cell. 95:927-937.

Simmons-Willis, T.A., Koh, A.S., Clarkson, T.W., and Ballatori, N.(2002).Transport of a neurotoxicant by molecular mimicry: the methylmercury-L-cysteine complex is a substrate for human L-type large neutral amino acid transporter (LAT) 1 and LAT2.Biochem J. 367(Pt 1):239-46.

Sirianni, R., A. Chimento, A. De Luca, F. Zolea, A. Carpino, V. Rago, M. Maggiolini, S. Ando, and V. Pezzi. 2009. Inhibition of cyclooxygenase-2 down-regulates aromatase activity and decreases proliferation of Leydig tumor cells. The Journal of biological chemistry. 284:28905-28916.

Sirianni, R., A. Chimento, A. De Luca, I. Casaburi, P. Rizza, A. Onofrio, D. Iacopetta, F. Puoci, S. Ando, M. Maggiolini, and V. Pezzi. 2010. Oleuropein and hydroxytyrosol inhibit MCF-7 breast cancer cell proliferation interfering with ERK1/2 activation. Molecular nutrition & food research. 54:833-840.

Sirianni, R., A. Chimento, C. Ruggiero, A. De Luca, R. Lappano, S. Ando, M. Maggiolini, and V. Pezzi. 2008. The novel estrogen receptor, G protein-coupled receptor 30, mediates the proliferative effects induced by 17beta-estradiol on mouse spermatogonial GC-1 cell line. Endocrinology. 149:5043-5051.

Sirianni, R., A. Chimento, R. Malivindi, I. Mazzitelli, S. Ando, and V. Pezzi. 2007. Insulin-like growth factor-I, regulating aromatase expression through steroidogenic factor 1, supports estrogen-dependent tumor Leydig cell proliferation. Cancer research. 67:8368-8377.

Sirianni, R., F. Zolea, A. Chimento, C. Ruggiero, L. Cerquetti, F. Fallo, C. Pilon, G. Arnaldi, G. Carpinelli, A. Stigliano, and V. Pezzi. 2012. Targeting estrogen receptor-alpha reduces adrenocortical cancer (ACC) cell growth in vitro and in vivo: potential therapeutic role of

selective estrogen receptor modulators (SERMs) for ACC treatment. The Journal of clinical endocrinology and metabolism. 97:E2238-2250.

Slemr, F.; Seiler, W.; Eberling, C.; Roggendorf, P. (1979) Analyt. Chim. Acta, 110, 35-47; Lindqvist, O., and H. Rodhe, Atmospheric mercury -a review, Tellus, Ser. B, 37, 136-159, 1985.

Smith, H.O., H. Arias-Pulido, D.Y. Kuo, T. Howard, C.R. Qualls, S.J. Lee, C.F. Verschraegen, H.J. Hathaway, N.E. Joste, and E.R. Prossnitz. 2009. GPR30 predicts poor survival for ovarian cancer. Gynecologic oncology. 114:465-471.

Smith, H.O., K.K. Leslie, M. Singh, C.R. Qualls, C.M. Revankar, N.E. Joste, and E.R. Prossnitz. 2007. GPR30: a novel indicator of poor survival for endometrial carcinoma. American journal of obstetrics and gynecology. 196:386 e381-389; discussion 386 e389-311.

Soleo, L., Elia, G., Russo, A., Schiavulli, N., Lasorsa, G., Mangili, A., Gilberti, E., Ronchi, A., Balducci, C., Minoia, C., Aprea, C., Sciarra, G.F., Valente, T., Fenga, C.; Valori di riferimento del mercurio urinario nella popolazione italiana. G Ital Med Lav Erg 2003;25(1):107-13.

Song, J.H., F.S. Chaudhry, and W.W. Mayo-Smith. 2007. The incidental indeterminate adrenal mass on CT (> 10 H) in patients without cancer: is further imaging necessary? Follow-up of 321 consecutive indeterminate adrenal masses. AJR. American journal of roentgenology. 189:1119-1123.

Stajich, G.V., Lopez, G.P., Harry, S.W., Sexson, W.R.; Iatrogenic exposure to mercury after hepatitis B vaccination in preterm infants. J Pediatr 2000 May;136(5):679-81.

Stein, J., Schettler, T., Wallinga, D., Valenti, M.; In harm's way: Toxic threats to child development.Dev. Behav. Pediatr. 2002, 23, S13–S22.

Stigliano A, Chiodini I, Giordano R, Faggiano A, Canu L, Della Casa S, Loli P, Luconi M, Mantero F and Terzolo M: Management of adrenocortical carcinoma: A consensus statement of the Italian Society of Endocrinology (SIE). J Endocrinol Invest 39: 103-121, 2016.

Suda, I., and Hirayama, K. (1992). Degradation of methyl and ethyl mercury into inorganic mercury by hydroxyl radical produced from rat liver microsomes.Arch Toxicol.66(6):398-402.

Sun, G., Li, Z., Bi, X., Chen, Y., Lu, S., Yuan, X., 2013. Distribution, sources and health risk assessment of mercury in kindergarten dust. Atmos. Environ. 73, 169–176.

Syversen, T., Kaur, P.; The toxicology of mercury and its compounds, J. Trace Elem. Med. Biol. 26 (4) (2012) 215–226.

Takada, Y., C. Kato, S. Kondo, R. Korenaga, and J. Ando. 1997. Cloning of cDNAs encoding G protein-coupled receptor expressed in human endothelial cells exposed to fluid shear stress. Biochemical and biophysical research communications. 240:737-741.

Tan SW, Meiller JC, Mahaffey KR. The endocrine effects of mercury in humans and wildlife. Crit Rev Toxicol 2009; 39:228-69.

Tan, M., Parkin, J.E.(2000). Route of decomposition of thiomersal (thimerosal). Int J Pharm. 208(1-2):23-34; Reader, M.J., and Lines, C.B. (1983). Decomposition of thimerosal in aqueous solution and its determination by high-performance liquid chromatography. J. Pharm. Sci. 72(12):1406-9.

Tanaka, T., Naganuma, A., and Imura, N. (1990). Role of gamma-glutamyltranspeptidase in renal uptake and toxicity of inorganic mercury in mice.Toxicology 60(3):187-98.

Tanaka-Kagawa, T., Naganuma, A., and Imura, N. (1990). Tubular secretion and reabsorption of mercury compounds in mouse kidney. J. Pharmacol. Exp. Ther. 264(2):776-82.

Tchounwou, P.B., Yedjou, C.G., Anita K Patlolla, and Dwayne J Sutton. Heavy Metals Toxicity and the Environment.EXS. 2012 ; 101: 133–164.

Teng, J., Z.Y. Wang, E.R. Prossnitz, and D.E. Bjorling. 2008. The G protein-coupled receptor GPR30 inhibits human urothelial cell proliferation. Endocrinology. 149:4024-4034.

Thomas, P., and J. Dong. 2006. Binding and activation of the seven-transmembrane estrogen receptor GPR30 by environmental estrogens: a potential novel mechanism of endocrine disruption. The Journal of steroid biochemistry and molecular biology. 102:175-179.

Thomas, P., Y. Pang, E.J. Filardo, and J. Dong. 2005. Identity of an estrogen membrane receptor coupled to a G protein in human breast cancer cells. Endocrinology. 146:624-632.

Tong, J.S., Q.H. Zhang, X. Huang, X.Q. Fu, S.T. Qi, Y.P. Wang, Y. Hou, J. Sheng, and Q.Y. Sun. 2011. Icaritin causes sustained ERK1/2 activation and induces apoptosis in human endometrial cancer cells. PloS one. 6:e16781.

Tsai, M.J., and B.W. O'Malley. 1994. Molecular mechanisms of action of steroid/thyroid receptor superfamily members. Annual review of biochemistry. 63:451-486.

U.S. EPA 1997. Criteria Pollutants (Greenbook). National Ambient Air Quality Standards. U.S. Environmental Protection Agency, Office of Air and Radiation.

U.S. FOOD AND DRUG ADMINISTRATION - Industry Activities Staff Booklet - August 2000: Action levels for poisonous or deleterious substances in human food and animal feed - http://www.cfsan.fda.gov/~lrd/fdaact.html

UNI CEI ENV 13005: 2000, Available at URL: http://www.inrim.it/events/insegnanti/doc/Modulo_3-Norma_UNI-CEI_ENV_13005.pdf .

Vahter, M., Mottet, N.K., Friberg, L., Lind, B., Shen, D.D., Burbacher, T.; Speciation of mercury in the primate blood and brain following long-term exposure to methyl mercury. ToxicolApplPharmacol 1994;124:221-229.

van Slooten, H., Moolenaar, A.J., van Seters, A.P. and Smeenk, D.; The treatment of adrenocortical carcinoma with o,p'-DDD: Prognostic implications of serum level monitoring. Eur J Cancer Clin Oncol 20: 47-53, 1984.

Van Wijngaarden, E., Beck, C., Shamlaye, C.F., Cernichiari, E., Davidson, P.W., Myers, G.J., Clarkson, T.W.; Benchmark concentrations for methyl mercury obtained from the 9-year follow-up of the Seychelles Child Development Study. Neurotoxicology 2006, 27, 702–709.

Vaughan ED Jr: Diseases of the adrenal gland. Med Clin North Am 88: 443-466, 2004.

Vermeir, G., Vandecasteele, C., Dams, R.; 1989. Microwave dissolution for the determination of mercury in biological samples. Anal ChimActa 220(1):257-261.

Vermeir, G., Vandecasteele, C., Temmerman, E., et al. 1988. Determination of mercury in biological materials by CV (cold-vapour) AAS after wet digestion. MikrochimActa 3:305-313.

Vesterberg, O.; 1991. Automatic method for quantitation of mercury in blood, plasma and urine. J BiochemBiophys Methods 23(3):227-236.

Vivacqua, A., D. Bonofiglio, A.G. Recchia, A.M. Musti, D. Picard, S. Ando, and M. Maggiolini. 2006b. The G protein-coupled receptor GPR30 mediates the proliferative effects induced by 17beta-estradiol and hydroxytamoxifen in endometrial cancer cells. Mol Endocrinol. 20:631-646.

Vivacqua, A., D. Bonofiglio, L. Albanito, A. Madeo, V. Rago, A. Carpino, A.M. Musti, D. Picard, S. Ando, and M. Maggiolini. 2006a. 17beta-estradiol, genistein, and 4-hydroxytamoxifen induce the proliferation of thyroid cancer cells through the g protein-coupled receptor GPR30. Molecular pharmacology. 70:1414-1423.

Wagner, J., C. Portwine, K. Rabin, J.-M. Leclerc, S.A. Narod, and D. Malkin. 1994. High Frequency of Germline p53 Mutations in Childhood Adrenocortical Cancer. Journal of the National Cancer Institute. 86:1707-1710.

Wajchenberg, B.L., M.A. Albergaria Pereira, B.B. Medonca, A.C. Latronico, P. Campos Carneiro, V.A. Alves, M.C. Zerbini, B. Liberman, G. Carlos Gomes, and M.A. Kirschner. 2000. Adrenocortical carcinoma: clinical and laboratory observations. Cancer. 88:711-736.

Wales MM, B.M., el Deiry W, Nelkin BD, Issa JP, Cavenee WK, Kuerbitz SJ, Baylin SB 1995. P53 activates expression of HIC-1, a new candidate tumour suppressor gene on 17p13.3. Nature Madicine. 1:570-577.

Wang, C., B. Dehghani, I.J. Magrisso, E.A. Rick, E. Bonhomme, D.B. Cody, L.A. Elenich, S. Subramanian, S.J. Murphy, M.J. Kelly, J.S. Rosenbaum, A.A. Vandenbark, and H. Offner. 2008. GPR30 contributes to estrogen-induced thymic atrophy. Mol Endocrinol. 22:636-648.

Wang, C., B. Dehghani, Y. Li, L.J. Kaler, T. Proctor, A.A. Vandenbark, and H. Offner. 2009. Membrane estrogen receptor regulates experimental autoimmune encephalomyelitis through up-regulation of programmed death 1. J Immunol. 182:3294-3303.

Wang, X. 2001. The expanding role of mitochondria in apoptosis. Genes & development. 15:2922-2933.

Wei, H., Qiu, L., Divine, K.K., Ashbaugh, M.D., McIntyre, L.C. Jr, Fernando, Q., Gandolfi, A.J.; Toxicity and transport of three synthesized mercury-thiol-complexes in isolated rabbit renal proximal tubule suspensions. Drug ChemToxicol. 1999 May;22(2):323-41.

Weiss, L.M., L.J. Medeiros, and A.L. Vickery, Jr. 1989. Pathologic features of prognostic significance in adrenocortical carcinoma. The American journal of surgical pathology. 13:202-206.

WHO (World Health Organization), 2003, expert committee on food additives, Sixty-first meeting Rome,10–19June2003;

WHO. (1997). WHO consensus statement on dental amalgam. FDI World Dental Federation. FDI World 6(6):9

WHO. Lead, cadmium and mercury. In: Trace Elements in Human Nutrition and Health. Geneva: WHO; 1996

Wilhelm, M., Ewers, U., Schulz, C., 2004. Revised and new reference values for some trace elements in blood and urine for human biomonitoring in environmental medicine. Int. J. Hyg. Environ. Health 207, 69–73.

Wittsiepe, J., Schrey, P., Ewers, U., Selenka, F., Wilhelm, M.; Decrease of PCDD/F levels in human blood from Germany over the past ten years (1989-1998). Chemosphere 2000;40:1103-11.

Wolf, E., P.M. Jehle, M.M. Weber, H. Sauerwein, A. Daxenberger, B.H. Breier, U. Besenfelder, L. Frenyo, and G. Brem. 1997. Human insulin-like growth factor I (IGF-I) produced in the mammary glands of transgenic rabbits: yield, receptor binding, mitogenic activity, and effects on IGF-binding proteins. Endocrinology. 138:307-313.

Wooten, M.D., and D.K. King. 1993. Adrenal cortical carcinoma. Epidemiology and treatment with mitotane and a review of the literature. Cancer. 72:3145-3155.

World Health Organization (WHO) (1995) Bridging the gaps. Available: http://www.who.int/whr/1995/en/whr95_en.pdf .

World Health Organization (WHO) (2010) Children's exposure to mercury compounds. Available: http://www.who.int/phe/news/Mercury-flyer.pdf .

World Health Organization 1991. Inorganic Mercury, Volume 118. Distribution and Sales Service, International Program on Chemical Safety, Geneva, Switzerland.

World Health Organization. Environmental Health Criteria 101: Methylmercury. Geneva: WHO; 1990

Wurtz, J.M., W. Bourguet, J.P. Renaud, V. Vivat, P. Chambon, D. Moras, and H. Gronemeyer. 1996. A canonical structure for the ligand-binding domain of nuclear receptors. Nature structural biology. 3:206.

Xu, J., Yan, CH., Hu, H., Wu, M.Q., Shen, X.M.; Prenatal Maternal Occupational Exposure and Postnatal Child Exposure to Elemental Mercury. PediatrEmerg Care. 2016 Mar;32(3):175-9.

Yan, Y., X. Jiang, Y. Zhao, H. Wen, and G. Liu. 2015. Role of GPER on proliferation, migration and invasion in ligand-independent manner in human ovarian cancer cell line SKOV3. Cell biochemistry and function.

Yano, T., M. Linehan, P. Angland, M.I. Lerman, L.N. Daniel, C.A. Stein, C.N. Roberston, R. LaRocca, and B. Zbar. 1989. Genetic Changes in Human Adrenocortical Carcinomas. Journal of the National Cancer Institute. 81:518-519.

Zareba, G., Cernichiari, E., Hojo, R. , Nitt, S.M., Weiss, B., Mumtaz, M.M., Jones, D.E., Clarkson, T.W.; Thimerosal distribution and metabolism in neonatal mice: comparison with methyl mercury, J. Appl. Toxicol. 27 (5) (2007) 511–518.

Zhang, C.L., L.J. Wu, H.J. Zuo, S. Tashiro, S. Onodera, and T. Ikejima. 2004. Cytochrome c release from oridonin-treated apoptotic A375-S2 cells is dependent on p53 and extracellular signal-regulated kinase activation. Journal of pharmacological sciences. 96:155-163.

AUTHOR OF 4 FULL PAPERS

Brunelli E, **Domanico F**, La Russa D, Pellegrino D. SEX DIFFERENCES IN CIRCULATING OXIDATIVE STRESS BIOMARKERS. Current Drug Targets.2014;15(8):811-5

Casaburi I, Avena P, De Luca A, Chimento A , Sirianni R , Malivindi R , Rago V, Fiorillo M, **Domanico F**, Campana C, Cappello AR, Sotgia F, Lisanti M, Pezzi V. ESTROGEN RELATED RECEPTOR A (ERRA) A PROMISING TARGET FOR THE THERAPY OF ADRENOCORTICAL CARCINOMA (ACC). 2015 Sep 22;6(28):25135-48. doi: 10.18632/oncotarget.4722

Chimento A, Sirianni R, Casaburi I, Zolea F, Rizza P, Avena P, Malivindi R, De Luca A, Campana C, Martire E, **Domanico F**, Fallo F, Carpinelli G, Cerquetti L, Amendola D, Stigliano A, Pezzi V. GPER AGONIST G-1 DECREASES ADRENOCORTICAL CARCINOMA (ACC) CELL GROWTH IN VITRO AND IN VIVO. Oncotarget. 2015 Aug 7;6(22):19190-203

Domanico F, Forte G, Majorani C, Senofonte O, Petrucci F, Pezzi V, Alimonti A; COMPARISON BETWEEN THERMAL DECOMPOSITION AMALGAMATION ATOMIC ABSORPTION SPECTROMETRY AND INDUCTIVELY COUPLED PLASMA MASS SPECTROMETRY FOR THE DETERMINATION OF MERCURY IN HAIR. Journal of Trace Elements in Medicine and Biology, DOI: 10.1016/j.jtemb.2016.09.008

PARTICIPATION CONFERENCES WITH ABSTRACTS

Domanico F, Forte G, Majorani C, Senofonte O, Petrucci F, Pezzi V, Alimonti A; COMPARISONBETWEENTHERMALDECOMPOSITIONAMALGAMATIONATOMICABSORPTION SPECTROMETRY AND INDUCTIVELY COUPLED PLASMA MASS SPECTROMETRY FOR THE DETERMINATION OF MERCURY IN HAIR; "New horizons on trace elements and minerals role in human and animal health" 6th International Symposium Catania 26-28 Maggio 2016. (Oral relation)

Majorani C, **Domanico F**, Senofonte O, Petrucci F, Pezzi V, Alimonti A; CONFIRMATORY METHOD FOR MERCURY DETERMINATION IN BIOLOGICAL SAMPLES BY AMALGAMATION-ATOMIC ABSORPTION SPECTROMETRY; "New horizons on trace elements and minerals role in human and animal health" 6th International Symposium Catania 26-28 Maggio 2016.

Sex Differences in Oxidative Stress Biomarkers

Elvira Brunelli[1], Francesco Domanico[2], Daniele La Russa[1] and Daniela Pellegrino[1,*]

Departments of [1]Biology, Ecology and Earth Sciences (DiBEST) and [2]Pharmacy, Health and Nutritional Sciences, University of Calabria, Italy

Abstract: Although an increased oxidative stress has been associated with several pathologies, predictive value of circulating oxidative stress biomarkers remains poorly understood. It has been demonstrated that several pathologies underestimated in women, including cardiovascular diseases, develop differently by gender. In this study, conducted on 195 healthy volunteers, we assessed the putative gender difference in prooxidant and antioxidant status. Our results were successful in demonstrating a significant difference in oxidative stress between sexes, whereas no difference was found in the plasma antioxidant barrier efficiency. To assess whether this difference was due to hormonal status (i.e. estrogen levels), female samples were divided into pre-menopausal and post-menopausal groups. No significant difference emerged for both biomarkers. Despite the well-known antioxidant estrogen role, women in this study presented a higher oxidative status than males. This suggests that there is a difference in the production and metabolic deactivation of reactive oxygen metabolite.

Keywords: Antioxidant capacity, gender differences, healthy subject, oxidative stress, predictive biomarkers, reactive oxygen species.

INTRODUCTION

Oxidative stress is referred to the disproportion between reactive oxygen species and antioxidant system to detoxify or to repair cells. Reactive oxygen species can be beneficial, as they are used by the immune system as a defense mechanism and they are also key elements in cellular signaling [1]. Although oxidation reactions are essential for life, they can also be damaging in the case of insufficient antioxidant levels or inhibition of antioxidant enzymes [2, 3]. In humans, enhanced oxidative stress has been associated with several pathologies, including diabetes [4] and cardiovascular diseases [5, 6] but the prognostic importance of circulating oxidative stress biomarkers remains poorly understood [7]. Furthermore, a number of studies have shown that in recent years several pathologies have been underestimated in women and that these diseases develop differently by gender [8]. Gender-based differences are also reported in both redox signals and alterations with reference to human pathological conditions [9 and references therein].

In recent times a number of experimental evidences have highlighted sex differences in the progression of pathologies related to redox state alterations, including diabetes and cardiovascular disease [10, 11]; however, it remains unclear whether these differences in gender are associated with redox states changes [9]. The available data on oxidative stress differences between sexes are mainly focused on pathological conditions, but it is also important to know the situation of healthy subjects to well explore the mechanisms

underlying this phenomenon. The purpose of this study was to explore the putative sex/hormonal status differences on prooxidant and antioxidant conditions, valued in healthy subjects by analysis of circulating oxidative stress biomarkers.

SUBJECTS AND METHODS

Subjects

The study was conducted during 2013 on 195 healthy Italian volunteers (work-suitable) of both sexes and aged between 25 and 70 years (120 males, mean age: 51.16 ± 11.4 years and 75 female subjects, mean age: 46.35 ± 9.8 years) recruited among University of Calabria staffs during the annual visit performed by UNICAL Prevention and Protection Service. These volunteers were subjected to a "health check" by filling in a form (information on health status and lifestyle), by physical measurements (body mass index, systolic and diastolic blood pressure), and by a blood test (blood glucose, lipoprotein panel, pro-oxidant and antioxidant status). All subjects were studied in the morning and in a fasting state.

Blood samples were taken from the antecubital vein and immediately centrifuged (2500 g for 15 min at 4°C) and the plasma obtained was stored at 4°C until measurements. Baseline characteristics of the cohort are shown in Table **1**. These data are comparable to the results of the second population survey of Cardiovascular Epidemiologic Observatory (Progetto cuore- Istituto Superiore Sanità- Italy) relative to a population sample from Calabria monitored in the period 2008-2012.

Oxidative Stress Measurements

We performed oxidative stress determination by using photometric measurement kits and a free radical analyzer

*Address correspondence to this author at the Departments of Biology, Ecology and Earth Sciences (DiBEST), University of Calabria, 87030 Arcavacata di Rende, Cosenza, Italy; Tel: +39-0984-493007; Fax: +39-0984-493271; E-mail: danielapellegrino@unical.it

system provided with spectrophotometric device reader (FREE Carpe Diem, Diacron International, Grosseto, Italy). To avoid auto-oxidation phenomenon that can occur on samples left at room temperature or which have been freeze-thawed, all analyses were performed on ice-stored samples within maximum 6 hours of venous blood collection.

Table 1.   Baseline characteristics of the cohort according to gender (data are expressed as mean±SD).

	Males (n=120)	**Females (n=75)**
Age (years)	51.16±11.4	46.35±9.8
BMI	26.77±3.73	23.152±3.16
Systolic blood pressure	126.84±13.78	113.21±14.78
Diastolic blood pressure	77.87±7.99	70.07±8.88
Blood glucose	102.61±21.90	88.22±7.69
Total cholesterol	206.66±42.40	204.92±45.35
HDL cholesterol	48.69±14.10	61.06±11.78
LDL cholesterol	135.83±31.76	130.82±36.75
Triglycerides	129.05±71.00	79.48±32.19
Smokers	21(18%)	13(18%)

Here we used Diacron reactive oxygen metabolite (dROM), and biological antioxidant potential (BAP) tests to evaluate plasma levels of reactive oxygen metabolites and antioxidant capacity.

The d-ROMs test help to determine the oxidant ability of a plasma sample measuring the presence of Reactive Oxygen Metabolites derivatives, in particular hydroperoxides. By means of an appropriate acidic buffer, transition metal ions (essentially iron), originating by protein, are converted to alkoxy and peroxy radicals that react with hydroperoxides thus forming new radicals; aromatic amine (N,N-diethyl-paraphenylene-diamine) react with these new radicals originating a colored cation radical spectrophotometrically detect-

able at 505 nm [12, 13]. Results are expressed in Carratelli Units (UC; 1UC=0.8 mg/L of hydrogen peroxide) [12, 13].

The BAP test provides an overall measure of the biological antioxidant potential measuring the blood concentration of antioxidants (such as bilirubin, uric acid, vitamins C and E and proteins) capable of reducing the iron from ferric to the ferrous form; in fact, when the plasma is mixed with a colored solution (ferric chloride and thiocyanate) a decoloration occurs whose intensity is related to the ability of the plasma to reduce the ions of iron [14, 15]. The intensity of decoloration is spectrophotometrically detectable at 505 nm. Results are expressed in µmol /L of the reduced ferric ions. Table **2** shows the reference values for both tests.

Statistical Analysis

Data have been analyzed using GraphPad/Prism version 5.01 statistical software (SAS Institute, Abacus Concept, Inc., Berkeley, CA, USA). Differences between groups were examined using the Unpaired t-test, or the Mann-Whitney test, or the Dunn's test, or the ANOVA test. Data are expressed as the mean ± standard deviation.

Ethics Statement

All investigations have been conducted according to the Declaration of Helsinki principles, and have been approved by the Ethical Committee of the University of Calabria. All subjects have provided written informed consent that, as guarantor, is retained by the corresponding author.
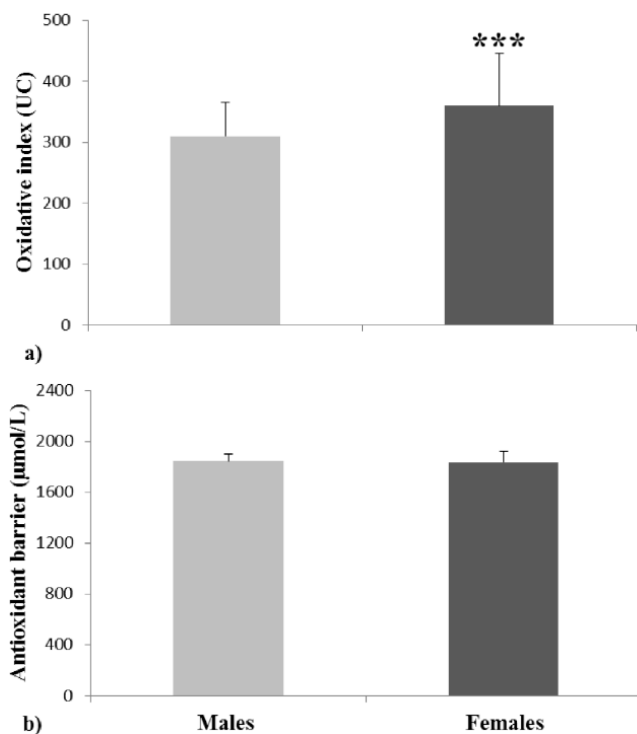
RESULTS

The study population consists of 195 subjects (120 males, and 75 females) aged between 25 and 70 years (25-35 n=23; 36-45, n=44; 46-55, n=52; 56-70, n=76). Among females, 47 women (62%) were in a pre-menopausal status, and not using hormonal contraceptives, and 28 women (38%) were in a post-menopausal status and not subjected to hormone replacement therapy. By comparing the dROMs test results, we found a significant difference (Mann-Whitney test, p<0.001) between males and females in the values of oxidative stress (Fig. **1a**). In particular, females present higher ROM values (359.93±85) that are within the range of me-

Table 2.   Reference values of dROMs test (a) and BAP test (b).

a			**b**	
ROMs	**ROMs**	**Oxidative Stress**	**µmol/L**	**Antioxidant Barrier**
(UC)	*(mg H_2O_2/dL)*	*(Severity)*		*(Efficacy)*
250-300	20.08-24.00	normal range	>2200	optimum value
301-320	24.08-25.60	border-line range	2200-2000	border-line range
321-340	25.68-27.20	low level oxidative stress	2000-1800	slight deficiency status
341-400	27.28-32.00	middle level oxidative stress	1800-1600	deficiency status
401-500	32.08-40.00	high level oxidative stress	1600-1400	high deficiency status
>500	>40,00	very high level oxidative stress	<1400	very high deficiency status

dium oxidative stress, while males show ROM values close to the normal values (309.61±55.38; borderline level). For what concern the antioxidant barrier efficacy, no significant differences were observed between sexes (Unpaired t-test; Fig. **1b**), even if a slightly higher value (1896.32±361.59) was detected in females compared to males (1847±308.54). In both cases, the antioxidant barrier effectiveness results at a slight deficiency level. In another parallel study we conducted on rats, no difference was observed between males and females (unpublished data). In order to assess whether the differences between sexes in humans were due to the hormonal status (i.e. estrogen levels), female samples were divided into two groups: pre-menopausal (n=47) and post-menopausal (n=28) women. Comparing these two groups no significant difference was observed in the values of both oxidative stress (Mann Whitney test) and efficacy of antioxidant barrier (Unpaired t- test; Table **3**). Indeed, the ROM values of both groups fall in the range of medium oxidative stress; similar results also occur for the effectiveness of the antioxidant barrier which stood in a range of slight deficiency (Table **3**).

years which only include both pre-and post-menopausal females. Even if the differences between pre- and post-menopausal females are not significant (Mann-Whitney test), a greater ROM values can be observed in pre-menopausal (386±112; n=16) as compared to post-menopausal (373±51.38; n=10) women.

Table 3. Values of dROMs and BAP test in pre-menopausal and post-menopausal females (data are expressed as mean±SD).

	Pre-Menopausal	Post-Menopausal
	Females (n=47)	**Females (n=28)**
dROMs test *(UC)*	359.66±98.78	360.39±56.37
BAP test (μmol/L)	1889.59±377.166	1907.61±340.259

A constant reduction of antioxidant barrier efficacy was observed in males with increasing age (Fig. **2b**). This reduction is significant only in the higher age group (56-70 years; Dunnet test, *p<0.05). In females, an age-related decrease, which was not statistically significant, could be observed in the 46-55 years group, where the values reach the minimum (Fig. **2b**).

Fig. (1). Values of dROMs (a) and BAP (b) test in in males and females (data are expressed as mean±SD; ***p<0.001).

We also analyzed the trend of both oxidative stress and antioxidant barrier efficacy in relation to age. We divided the study population in four age groups according to gender (25-35 years: 11 males and 12 females; 36-45 years: 26 males and 18 females; 46-55 years: 26 males and 26 females; 56-70 years: 57 males and 19 females). As shown in Fig. (**2a**), in males the ROM values remain at a constant level in all groups, while in females there is a marked and significant increase in oxidative stress with the increasing of age; high values were detected particularly in the age groups 35-45 and 46-55 (Dunn's test, p<0.005). To evaluate potential relationships with hormonal status, we analyzed the group 46-55

Fig. (2). Values of dROMs (a) and BAP (b) test in males and females by age (data are expressed as mean±SD; *p<0.05; **p<0.005).

Concerning smoking habits, we found no differences between males and females, nor between pre-menopausal and post-menopausal women (data not shown). However, it

should be noted that the smokers sample, despite equally distributed between sex, is very low and consists mainly of moderate smokers (less than ten cigarettes daily).

DISCUSSION

In the present study, conducted on a large healthy population, we were successful in demonstrating a significant gender difference in oxidative stress biomarkers. In particular, we found that females present a medium state of oxidative stress that is significantly higher compared to males. This data does not reflect what would be expected in considering the well-known antioxidant properties of the female hormones that are supposed to be the main contributors for numerous sex-gender differences, in the onset of several pathologies [16, 17]. A significantly higher oxidative index in women has already been highlighted in a previous study performed by using the same experimental protocol reported here [18]. Interestingly, we do not find differences between sexes in rats.

In a healthy population, it is not clear whether the levels of oxidative stress are significantly different between males and females in fact studies carried out on both animals and humans showed conflicting results [19, 20, 21]. Several studies have reported that men exhibit higher plasma levels of oxidative stress markers (isoprostanes and malondialdehyde) compared to women [22-24]; in contrast, another study reported that the same plasmatic markers were significantly higher in women [25]. These differences may be due to the different methods used to determine oxidative stress biomarkers in body fluids. In addition, sample handling is extremely important to estimate oxidative stress *in vivo* and may represent another important source for the conflicting results. In this perspective, we paid particular attention to the pre-analytical phase preserving blood samples on ice for at most six hours after collection.

In the last decade, several studies have focused on the potential link between high levels of oxidative stress observed in women and diseases such as atherosclerosis, coronary artery disease, cancer, and autoimmune syndromes [26 and references therein]. Although there are no unequivocal data, increasing evidences support the involvement of oxidative stress in the development/evolution of this type of diseases. Vignon-Zellweger and coworkers [27] suggested that sexual dimorphisms in mice cardiac dysfunction could be due to a sex difference in the expression pattern of proteins involved in oxidative stress and energy metabolism, in particular endothelin-1 and endothelial nitric oxide synthase (eNOS). A growing attention is paid to potential therapeutic options obtained through modulation of eNOS-derived ROS as superoxide anion production deriving by eNOS-uncoupling is one of the major underlying causes of vascular dysfunction and related pathology [28, 29]. At present, oxidative stress represents an important target for prevention and therapy in vascular disease as reviewed by Münzel and colleagues [30]. Moreover, several researches have suggested new pharmacological approach based on reduction of mitochondrial ROS in the prevention of both cardiac disease and diabetic complications [31, 32].

Gender-related differences in redox signals and redox alterations is a topic of great interest and relevance; which clarifies whether there are gender differences and it may help to identify the underlying mechanisms and the use of targeted pharmacological approaches.

For several diseases related to alterations of the redox status, gender differences have been reported during both diagnostic and prognostic phases but most studies were carried out in the context of human pathologic conditions [9]. On the contrary, our study was conducted on a healthy population where subjects, especially women, had lower rates of risk thus emphasizing the importance of assessing oxidative stress even in the absence of pathological conditions. To detect putative differences resulting from circulating estrogen concentration, we compared pre-menopausal and post-menopausal females. In women the importance of the hormone balance in the values of oxidative stress is also emphasized by physiological oxidative stress that occurs in pregnancy [33]. We revealed no significant differences between these two groups showing almost identical ROM values. These results are not in agreement with many literature data on both rats [34] and humans [16, 35], although some authors have reported no correlation between oxidative stress and post-menopausal state [18]. Furthermore, oxidative status in women may fluctuate during menstrual phases even if little information is available on that topic [18 and references therein]. The design of this study did not include hormone doses but it would be interesting to assess oxidative stress biomarkers in relation to the menstrual cycle. It would also be interesting to analyze a much larger sample and to examine post-menopausal women undergoing hormone replacement therapy.

For the antioxidant barrier efficacy, literature data indicate that, levels of anti-oxidants (such as GSH, catalase, and SOD) are significantly lower in males [36-38]. It has been hypothesized that estrogen receptor activation induced an overexpression of antioxidant enzymes [39]. We showed that no significant differences exist between sexes or pre- menopausal and post-menopausal females even if females have a greater BAP value probably due to an increased ROM stimulation. Although the cell ability to react against oxidative stress is essential for its homeostasis, our data do not indicate a significant enhancement of the antioxidant barrier in females as compensation for the higher levels of oxidative stress. Despite that the role of oxidative stress is well known in aging and age-related diseases, until now no specific markers related to age have been developed [40]. An interesting statement that emerges from our study is that the age dependent ROM values are evident only in females, while the values of oxidative stress remain constant in males. These ROM differences between sexes in our sample are well pronounced and do not seem to be related to other parameters such as BMI or lipid profile. It is interesting to note that only in the younger age group (25-35 years) there was no difference in the ROM values between males and females. In conclusion, we have shown that, in humans, baseline ROM levels are significantly higher in women than male and that this data is not linked to hormonal status. Clearly, additional studies are needed to further characterize gender differences related to oxidative stress as well as to investigate the mechanisms that underlie these differences. Lastly, our data highlight the importance of considering the existing differences between sexes regarding both prevention and therapy aspects.

CONFLICT OF INTEREST

The authors confirm that this article content has no conflict of interest.

ACKNOWLEDGEMENTS

REFERENCES

[1]   Forman FU, Ursinic F, Maiorinoc M. An overview of mechanisms of redox signaling. J Mol Cell Cardiol 2014; pii: S0022-2828(14)00038-8.

[2]   Halliwell B. Free radicals and antioxidants: updating a personal view. Nutr Rev 2012; 70: 257-65.

[3]   Rafieian-Kopaei M, Baradaran A, Rafieian M. Plants antioxidants: from laboratory to clinic. J Nephropathology 2013; 2: 152-3.

[4]   Arora MK, Singh UK. Oxidative stress: meeting multiple targets in pathogenesis of diabetic nephropathy. Curr Drug Targets 2014; 15: 531-8.

[5]   Madamanchi NR, Vendrov A, Runge MS. Oxidative stress and vascular disease. Arterioscler Thromb Vasc Biol 2005; 25: 29-38.

[6]   Singh U, Jialal I. Oxidative stress and atherosclerosis. Pathophysiology 2006; 13: 129-42.

[7]   Strobel NA, Fassett RG, Marsh SA, Coombes JS. Oxidative stress biomarkers as predictors of cardiovascular disease. Int J Cardiol 2011; 147: 191-201.

[8]   Mosca L, Barrett-Connor E, Wenger NK. Sex/gender differences in cardiovascular disease prevention: what a difference a decade makes. Circulation 2011; 124: 2145-54.

[9]   Malorni W, Campesi I, Straface E, Vella S, Franconi F. Redox features of the cell: a gender perspective. Antioxid Redox Signal 2007; 9: 1779-801.

[10]   Legato MJ, Gelzer A, Goland R, Ebner SA, Rajan S, Villagra V, Kosowski M. Gender-specific care of the patient with diabetes: review and recommendations. Gender Med 2006; 3: 131-58.

[11]   Mosca L, Manson JE, Sutherland SE, Langer RD, Manolio T, Barrett-Connor E. Cardiovascular disease in women: a statement for healthcare professionals from the American Heart Association Writing Group. Circulation 1997; 96: 2468-82.

[12]   Cornelli U, Terranova R, Luca S, Cornelli M, Alberti A. Bioavailability and antioxidant activity of some food supplements in men and women using the D-Roms test as a marker of oxidative stress. J Nutr 2001; 131: 3208-11.

[13]   Carratelli M, Porcaro L, Ruscica M, et al. Reactive oxygen metabolites and prooxidant status in children with Down's syndrome. Int J Clin Pharmacol Res 2001; 21: 79-84.

[14]   Martinovic J, Dopsaj V, Dopsaj MJ, et al. Long-term effects of oxidative stress in volleyball players. Int J Sports Med 2009; 30: 851-6.

[15]   Pasquini A, Luchetti E, Marchetti V, Cardini G, Iorio EL. Analytical performances of d-ROMs test and BAP test in canine plasma. Definition of the normal range in healthy Labrador dogs. Vet Res Commun 2008; 32: 137-43.

[16]   Miller AA, De Silva TM, Jackman KA, Sobey CG. Effect of gender and sex hormones on vascular oxidative stress. Clin Exp Pharmacol Physiol 2007; 34: 1037-43.

[17]   Pajovic SB, Saicic ZS. Modulation of antioxidant enzyme activities by sexual steroid hormones. Physiol Res. 2008; 57: 801-11.

[18]   Vassalle C, Novembrino C, Maffei S, et al. Determinants of oxidative stress related to gender: relevance of age and smoking habit. Clin Chem Lab Med 2011; 49: 1509-13.

[19]   Block G, Dietrich M, Norkus EP, et al. Factors associated with oxidative stress in human populations. Am J Epidemiol 2002; 156: 274-85.

[20]   Coudray C, Roussel AM, Mainard F, Arnaud J, Favier A. Lipid peroxidation level and antioxidant micronutrient status in a presaging population; correlation with chronic disease prevalence in a French epidemiological study (Nantes, France). J Am Coll Nutr 1997; 16: 584-91.

[21]   Sartori-Valinotti JC, Iliescu R, Fortepiani LA, Yanes LL, Reckelhoff JF. Sex differences in oxidative stress and the impact on blood pressure control and cardiovascular disease. Clin Exp Pharmacol Physiol 2007; 34: 938-45.

[22]   van Kesteren PJ, Kooistra T, Lansink M, et al. The effects of sex steroids on plasma levels of marker proteins of endothelial cell functioning. Thromb Haemost 1998; 79: 1029-33.

[23]   Ide T, Tsutsui H, Ohashi N, et al. Greater oxidative stress in healthy young men compared with pre-menopausal women. Arterioscler. Thromb Vasc Biol 2002; 22: 1239-42.

[24]   Nielsen F, Mikkelsen BB, Nielsen JB, Andersen HR, Grandjean P. Plasma malondialdehyde as biomarker for oxidative stress: reference interval and effects of life-style factors. Clin Chem 1997; 43: 1209-14.

[25]   Helmersson J, Mattsson P, Basu S. Prostaglandin F(2alpha) metabolite and F2-isoprostane excretion in migraine. Clin Sci 2002; 102: 39-43.

[26]   Kamhieh-Milz J, Salama A. Oxidative stress is predominant in female but not in male patients with autoimmune thrombocytopenia. Oxid Med Cell Longev 2014; 2014: 720347.

[27]   Vignon-Zellweger N, Relle K, Rahnenführer J, Schwab K, Hocher B, Theuring F. Endothelin-1 overexpression and endothelial nitric oxide synthase knock-out induce different pathological responses in the heart of male and female mice. Life Sci 2013; S0024-3205: 750-759.

[28]   Kietadisorn R, Juni RP, Moens AL. Tackling endothelial dysfunction by modulating NOS uncoupling: new insights into its pathogenesis and therapeutic possibilities. Am J Physiol Endocrinol Metab 2012; 302: E481-495.

[29]   Oliveira-Paula GH, Lacchini R, Tanus-Santos JE. Inducible nitric oxide synthase as a possible target in hypertension. Curr Drug Targets 2014; 15: 164-74.

[30]   Münzel T, Gori T, Bruno RM, Taddei S. Is oxidative stress a therapeutic target in cardiovascular disease? Eur Heart J 2010; 31: 2741-8.

[31]   Hernández-Reséndiz S, Buelna-Chontal M, Correa F, Zazueta C. Targeting mitochondria for cardiac protection. Curr Drug Targets 2013; 14: 586-600.

[32]   Araki E, Nishikawa T. Oxidative stress: A cause and therapeutic target of diabetic complications. J Diabetes Investig 2010; 1: 90-6.

[33]   Toescu V, Nuttall SL, Martin U, et al. Changes in plasma lipids and markers of oxidative stress in normal pregnancy and pregnancies complicated by diabetes. Clin Sci 2004; 106: 93-8.

[34]   Da Rocha JT, Pinton S, Mazzanti A, et al. Effects of diphenyl diselenide on lipid profile and hepatic oxidative stress parameters in ovariectomized female rats. J Pharm Pharmacol 2011; 63: 663-9.

[35]   Akçay T, Dinçer Y, Kayali R, Colgar U, Oral E, Cakatay U. Effects of hormone replacement therapy on lipid peroxides and oxidation system in post-menopausal women. J Toxicol Environ Health 2000; 59: 1-5.

[36]   Borras C, Sastre J, Garcia-Sal, D, Lloret A, Pallardo FV, Vina J. Mitochondria from females exhibit higher antioxidant gene expression and lower oxidative damage than males. Free Radic Biol Med 2003; 34: 546-52.

[37]   May RC. Gender, immunity and the regulation of longevity. Bioessays 2007; 29: 795-802.

[38]   Malorni W, Straface E, Matarrese P, et al. Redox state and gender differences in vascular smooth muscle cells. FEBS Lett 2008; 582:635-642.

[39]   Vina J, Borras C, Gambini J, Sastre J, Pallardo FV. Why females live longer than males? Importance of the upregulation of longevity-associated genes by oestrogenic compounds. FEBS Lett 2005; 579: 2541-5.

[40]   Murri M, Luque-Ramírez M, Insenser M, Ojeda-Ojeda M, Escobar-Morreale HF. Circulating markers of oxidative stress and polycystic ovary syndrome (PCOS): a systematic review and meta-analysis. Hum Reprod Update 2013; 19: 268-88.

GPER agonist G-1 decreases adrenocortical carcinoma (ACC) cell growth *in vitro* and *in vivo*

Adele Chimento[1,*], Rosa Sirianni[1,*], Ivan Casaburi[1,*], Fabiana Zolea[1], Pietro Rizza[1], Paola Avena[1], Rocco Malivindi[1], Arianna De Luca[1], Carmela Campana[1], Emilia Martire[1], Francesco Domanico[1], Francesco Fallo[2], Giulia Carpinelli[3], Lidia Cerquetti[4], Donatella Amendola[5], Antonio Stigliano[4], Vincenzo Pezzi[1]

[1]Department of Pharmacy, Health and Nutritional Sciences, University of Calabria, Arcavacata di Rende, Cosenza, Italy

[2]Department of Medicine-DIMED, University of Padova, Padova, Italy

[3]Department of Cell Biology and Neurosciences, National Institute of Health, Rome, Italy

[4]Department of Clinical and Molecular Medicine, Sant'Andrea Hospital, Faculty of Medicine and Psychology, Rome, Italy

[5]Research Center, San Pietro Hospital-Fatebenefratelli, Rome, Italy

[*]These authors have contributed equally to this work

Correspondence to:
Vincenzo Pezzi, **e-mail:** v.pezzi@unical.it

ABSTRACT

We have previously demonstrated that estrogen receptor (ER) alpha (ESR1) increases proliferation of adrenocortical carcinoma (ACC) through both an estrogen-dependent and -independent (induced by IGF-II/IGF1R pathways) manner. Then, the use of tamoxifen, a selective estrogen receptor modulator (SERM), appears effective in reducing ACC growth *in vitro* and *in vivo*. However, tamoxifen not only exerts antiestrogenic activity, but also acts as full agonist on the G protein-coupled estrogen receptor (GPER). Aim of this study was to investigate the effect of a non-steroidal GPER agonist G-1 in modulating ACC cell growth. We found that G-1 is able to exert a growth inhibitory effect on H295R cells both *in vitro* and, as xenograft model, *in vivo*. Treatment of H295R cells with G-1 induced cell cycle arrest, DNA damage and cell death by the activation of the intrinsic apoptotic mechanism. These events required sustained extracellular regulated kinase (ERK) 1/2 activation. Silencing of GPER by a specific shRNA partially reversed G-1-mediated cell growth inhibition without affecting ERK activation. These data suggest the existence of G-1 activated but GPER-independent effects that remain to be clarified. In conclusion, this study provides a rational to further study G-1 mechanism of action in order to include this drug as a treatment option to the limited therapy of ACC.

INTRODUCTION

Adrenocortical carcinoma (ACC) represents a rare malignancy with a very poor prognosis. Resectability is the prime determinant of prognosis. For patients with disseminated disease, chemotherapy options are few and lack sufficient efficacy. Mitotane, a cytotoxic drug with a not well documented mechanism of action [1], is the conventional therapy. The toxicity of mitotane has been a major limit to its suitability in the treatment of ACC

patients. Severe side-effects, of either the gastrointestinal or the nervous system, have been frequently reported, and many patients are not able to take the drug regularly [2, 3]. Recently, monoclonal antibodies targeting insulin-like growth factor (IGF) receptor (IGF1R) have been tested in clinical trials, however, they provided a limited effectiveness in refractory patients [4]. Rationale for targeting IGF1R comes from the observation that IGFII [5] is overexpressed in ACC. IGFII effects are mediated through its receptor IGF1R resulting in activation of the

PI3K/AKT/mTOR cascade, the RAS/MAPK and the PLC/PKC pathways [6]. We have recently demonstrated that activation of these pathways can be triggered by the estrogen receptor alpha (ESR1) [7], a gene overexpressed in ACC that mediates estrogen-dependent proliferative effects [7, 8]. Our *in vitro* experiments demonstrated that ESR1 knock down was more effective than an IGF1R antibody in controlling H295R cell proliferation [7]. Targeting ESR1 *in vivo* using tamoxifen, a selective estrogen receptor modulator (SERM), was effective in reducing H295R xenografts growth [7].

It is well known that tamoxifen and its active metabolite 4-hydroxytamoxifen (OHT), not only exert antiestrogenic activity [9], but also act as full agonist on the G protein-coupled estrogen receptor GPR30 (from the GPER gene) [10–14]. Then, can Tamoxifen effects depend on GPER activation? GPER can mediate rapid E2-induced non-genomic signaling events, including stimulation of adenylyl cyclase, mobilization of intracellular calcium (Ca^{2+}) stores and activation of mitogen-activated protein kinase (MAPK) and phosphoinositide 3-kinase (PI3K) signaling pathways [15–17]. GPER exhibits prognostic utility in endometrial [18], ovarian [19], and breast cancer [20] and can modulate growth of hormonally responsive cancer cells [10, 11, 21, 22]. Expression of GPER has been characterized in the outer zona glomerulosa (ZG) and in the medulla of the human adrenal [23], however its expression status in ACC is not known.

A non-steroidal, high-affinity GPER agonist G-1 (1-[4-(6-bromobenzo [1, 3]dioxol-5yl)-3a, 4, 5, 9b-tetrahydro-3H-cyclopenta-[c]quinolin-8-yl]-ethanone) has been developed to dissect GPER-mediated estrogen responses from those mediated by classic estrogen receptors [24]. The biological effects triggered by G-1 appear cell type specific and dependent on the ERs expression pattern [25–29]. By using G-1, in this study we wanted to investigate the effects of GPER activation on ACC growth.

RESULTS

G-1 treatment decreases H295R cell growth *in vitro* and *in vivo*

We first examined GPER expression in human ACCs and in H295R cells. By western blot analysis (Fig. 1A) and real time RT-PCR (Fig. 1B-1C) we demonstrated that GPER is expressed in normal adrenal, in human ACCs and in H295R cells at variable levels. Effects of G-1 on cell viability and proliferation were tested using increasing concentrations (0.01-0.1-1 μM) for different times (24-48-72 h) (Fig. 1D-1E). Of the different doses tested only 1 μM caused a time-dependent reduction in H295R cell growth. Doses higher than 1uM did not show any more pronounced effect (data not shown). Knocking down of GPER gene expression, using a specific shRNA, (shGPER) was assessed by western blot analysis and

revealed a substantial decrease in protein content compared to the control shRNA (insert, Fig. 1F). However, GPER silencing was able to only partially abrogate the inhibitory effects exerted by G-1 on H295R cell proliferation (Fig. 1F)

H295R cells were used to generate xenograft tumors in athymic nude mice. Twenty one days after tumor grafting all mice developed a detectable tumor and were randomized to be treated with either vehicle or G-1. G-1 administration produced a statistically significant decrease in tumor volume from day 14 post treatment (Fig. 2A). A trend of growth inhibition was observed thereafter. The drug was well tolerated without lethal toxicity or body weight loss during treatment (data not shown). Multi-slices T2-W MRI indicated larger tumor volume in vehicle treated animals compared to tumors from G-1 treated mice. Hyperintense large cystic area and haemorrahagic regions, that appear as dark areas in the tumor sections, were present in vehicle treated animals (Fig. 2B). Grafted tumors harvested after three-week treatment with G-1 showed a significant decrease in tumor weight compared to vehicle treated animals (Fig. 2C). Hematoxylin and eosin staining of xenograft tumors revealed some picnotic nuclei only in G-1 treated tumors (Fig. 2D). Ki-67 immunostaimning was significantly lower in G-1-treated tumors compared to control mice (value score control: 6, 6 ± 0, 89 (SD); value score G-1 treated cells: 3, 1 ± 0.55 * (SD) (*$p < 0.05$) (Fig. 2E).

G-1 induces H295R cell cycle arrest and cell death

Cell cycle analysis of H295R cells after 24 h of G-1 treatment demonstrated a cell cycle arrest in the G_2 phase (Fig 3A). This effect was further confirmed by a change in the expression of cyclins, after G-1 treatment (Fig. 3B). Specifically, by western analysis we observed that G-1 treatment caused a decrease in Cyclin E (CCNE), while Cyclin B1 (CCNB1), involved in the regulation of G_2 phase, was increased. CCNE and CCNB1 had similar expression pattern in protein samples extracted from xenografts tumors (Fig. 3C). Collectively these events support the idea of cells exiting G_1 but remaining stuck in G_2 phase. In agreement with the observation that inappropriate accumulation of B type cyclins is associated with the initiation of apoptotic pathways [30], we found that G-1 caused cell death by apoptosis. Cells were treated for 24 or 48 h with vehicle or G-1, incubated with an Annexin-V specific antibody and sorted by flow cytometry. As shown in Figure 3D the number of dead cells increased in a time dependent manner reaching about 40% of apoptotic cells 48 h after G-1 treatment (Fig. 3D).

G-1 causes cell nuclei morphological changes, DNA damage and apoptosis

G-1 ability to trigger apoptosis in H295R cells was further confirmed by evaluation of DNA fragmentation.
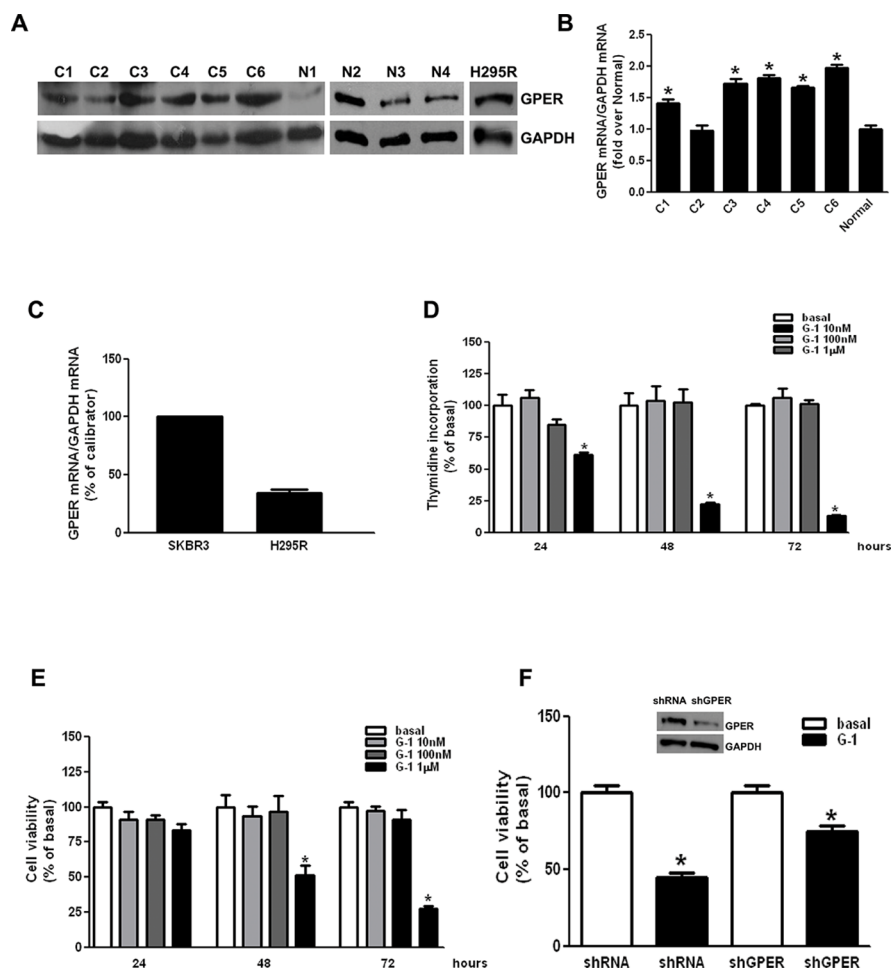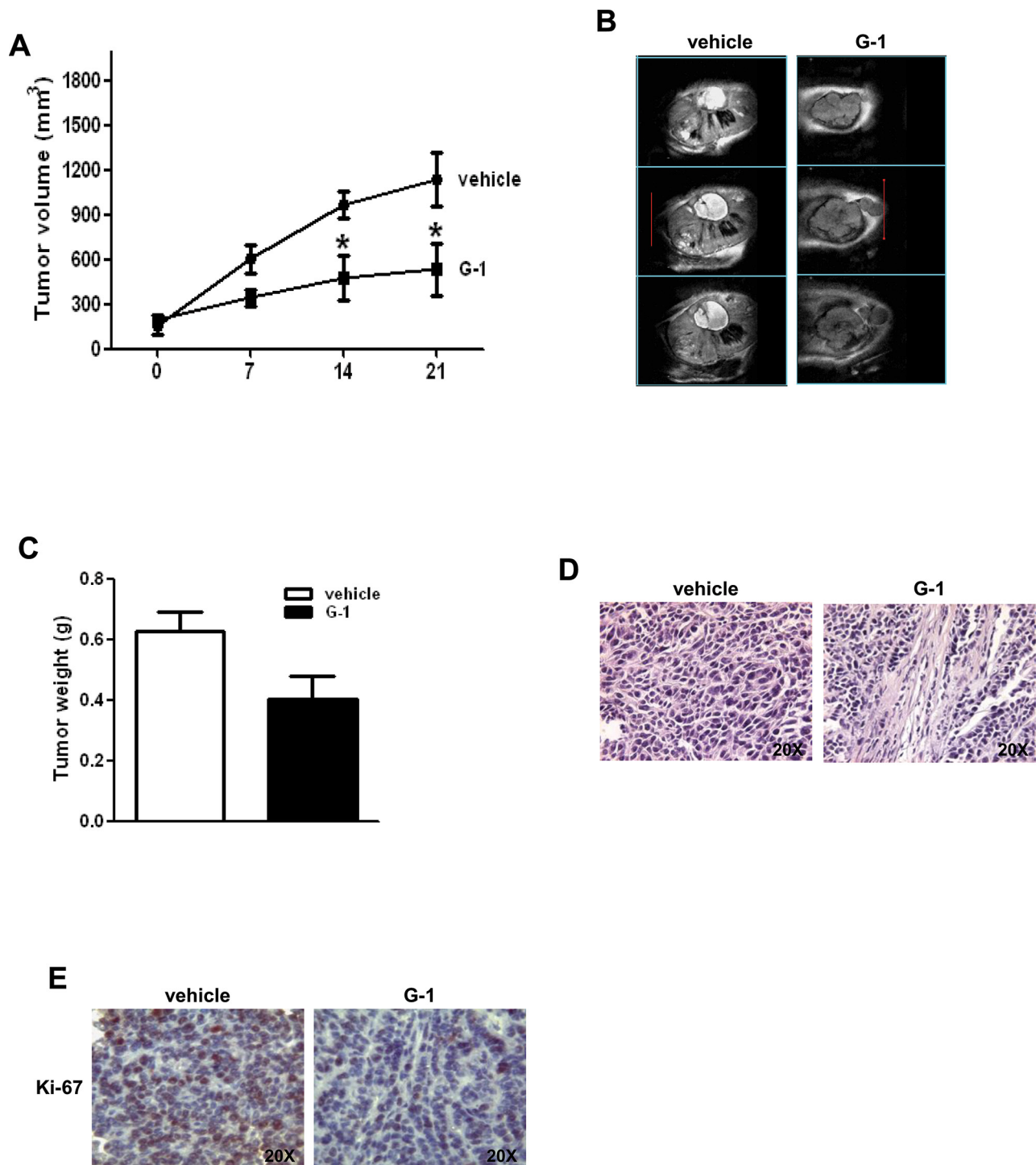
Figure 1: G-1 treatment decreases H295R cell growth *in vitro*. A. Western blot analysis of GPER was performed on 50 μg of total proteins extracted from normal adrenal, ACCs and H295R cells. GAPDH was used as a loading control. **B-C.** GPER mRNA expression in normal adrenal and ACCs (B), H295R and SKBR3 (positive control) cells (C) was analyzed by real time RT-PCR. Each sample was normalized to its GAPDH RNA content. Final results are expressed as n-fold differences of gene expression relative to calibrator. Data represent the mean + SE of values from at least three separate RNA samples; *$P < 0.05$, versus calibrator). **D-E.** H295R cells were treated with G-1 (0.01–1 μM) for different times (24, 48 and 72 h). Cell proliferation was evaluated by [³H]Thymidine incorporation (D) and MTT (E) assays. Results were expressed as mean + SE of three independent experiments each performed in triplicate. Statistically significant differences are indicated (*$P < 0.05$ versus basal). **F.** MTT assay was performed on H295R cells, which were previously transfected for 72 h in the presence of control vector (shRNA) or shGPER. Twenty-four hours after transfection cells were treated in 2.5% DCC-FBS medium for 48 h with G-1 (1 μM). Results were expressed as mean + SE of three independent experiments each performed in triplicate. (*$p < 0.05$ versus basal). The insert shows a Western blotting assay on H295R protein extracts evaluating the expression of GPER receptor in the presence of shRNA or of shGPER. GAPDH was used as a loading control.

TUNEL staining demonstrated the presence of increased positive cells in cells treated with G-1 (Fig. 4A). In addition, Hoechst staining evidenced that untreated H295R cells had round nuclei with regular contours; while nuclei from cells treated with G-1 appeared shrunken and irregularly shaped or degraded with condensed DNA. DNA gel electrophoresis extracted from G-1 treated H295R cells revealed a classic laddering pattern of internucleosomal DNA fragmentation that was absent in control cells (Fig. 4B). This event was associated with an increase in Parp-1 cleavage (Fig. 4C). The presence of G-1 increased Bax expression while decreased Bcl-2 (Fig. 4D). Similarly, data obtained from western blot analysis of tumors samples overlap with those obtained in H295R cells (Fig. 4E). When the intrinsic apoptotic mechanism is triggered, Cytochrome c (Cyt c) is released from the mitochondria into the cytosol [31]. Therefore we fractionated G-1 treated H295R cell lysates into cytosolic and mitochondrial fractions and evaluated Cytochrome c release by western blot analysis (Fig. 4F). Cytochrome c levels increased in the cytosolic fraction of treated samples while decreased in the mitochondrial compartment. Cytochrome c release from mitochondria into the cytosol triggers caspase activation. After G-1 treatment we detected active Caspase 9 (Fig. 4G) as well as the executioner Caspase 3/7 (Fig. 4H).
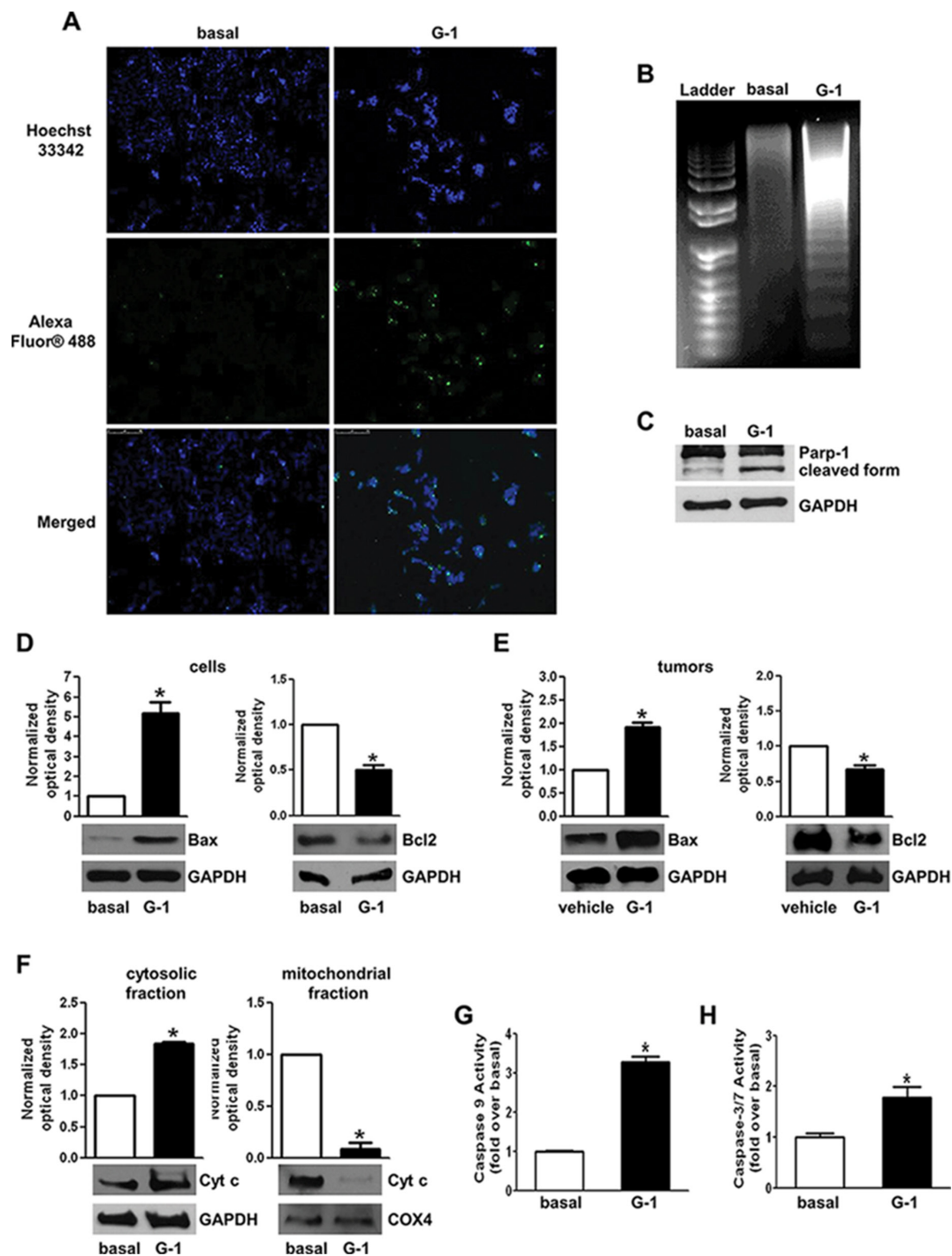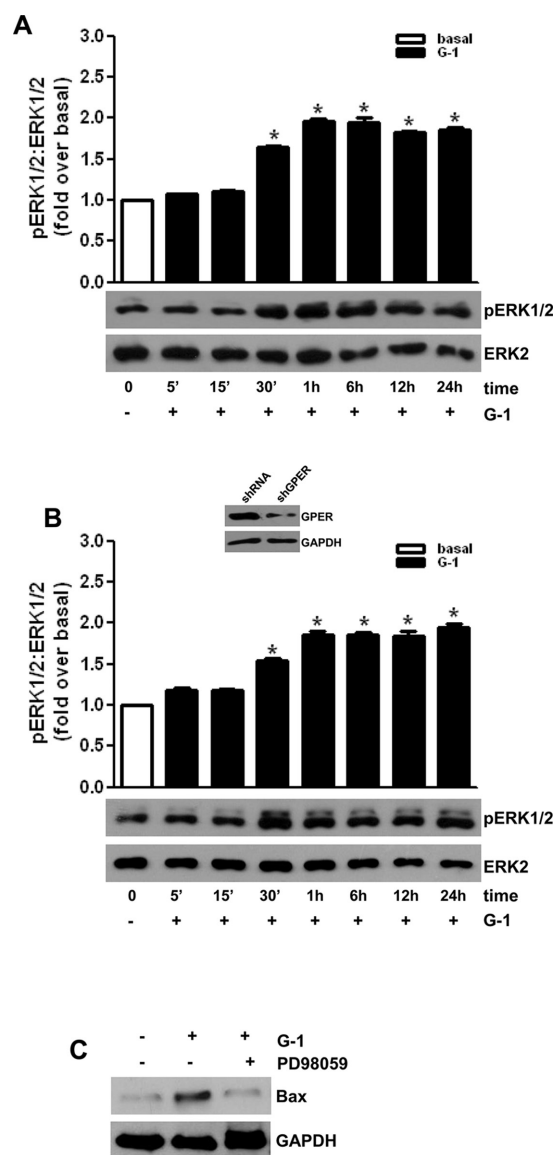
Figure 2: G-1 treatment decreases H295R cell growth *in vivo*. A. 6×10^6 H295R cells were injected subcutaneously in the flank region of immunocompromized mice and the resulting tumors were grown to an average of 200 mm³ twenty one days after inoculation. Tumor volumes were calculated, as indicated in Materials and Methods. Values represent the mean + SE of measured tumor volume over time in the control group (filled circles, *n* = 10) and in the G-1-treated group (filled triangles, *n* = 10). Data represent pooled values from two independent experiments. (*$P < 0.05$ versus control at the same day of treatment). **B.** *In vivo* coronal T2-weighted spin-echo MR image of primary ACCs. Examples of multi-slices T2-W MRI (section thickness of 1 mm) tumors from vehicle treated mice (control tumors) show a larger volume compared to tumors from G-1 treated mice. Hyperintense large cystic area and haemorrhagic regions that appear as dark areas in the tumor sections, are present in the control tumors. **C.** After 3-week treatment tumors were harvested and weighed. Values represent the mean + SE of measured tumor weight (*n* = 10) (* $P < 0.05$ versus vehicle). **D.** Hematoxylin and eosin stained histologic images of H295R xenograft tumors. **E.** Representative pictures of Ki-67 immunohistochemical staining of H295R xenograft tumors.

	H295R cell population (%)		
Treatment	G1	S	G2/M
basal (24h)	55,08±5,52	34,38±3,44	10,54±1,05
G-1 (24h)	26,90±1,34	40,07±2,0	33,03±1,65

Figure 3: Effects of G-1 treatment on cell cycle distribution and on cell death. A. H295R cells were synchronized in serum-free media for 24 h and then exposed to vehicle (basal) or G-1 (1 μM) for the indicated times. The distribution of H295R cells in the cycle was determined by Flow Cytometry using Propidium Iodide stained nuclei. Table shows the distribution of H295R cell population (%) in the various phases of cell cycle. **B-C.** Western blot analyses of Cyclin E (CCNE) and Cyclin B1 (CCNB1) were performed equal amounts of total proteins extracted from H295R cells treated with G-1 (1 μM) for 24 h (B) and xenografts tumors (C) Blots are representative of three independent experiments with similar results. GAPDH was used as a loading control. **D.** Subconfluent H295R monolayers starved for 24 h were treated for the indicated times with G-1 (1 μM). Then cells were stained with Annexin V/ FITC plus PI and examined by flow cytometer. Graph represents the percentage of cell death at the different times of treatment. (* $P < 0.05$ versus basal).

Figure 4: G-1 treatment induces apoptosis in H295R cells. A. Cells were left untreated (basal) or treated with G-1 (1 μM) for 24 h; after treatment cells were fixed with paraformaldehyde and processed for TUNEL staining. Nuclei counterstaining was performed using Hoechst 33342. Fluorescent signal was observed under a fluorescent microscope (magnification 200X). Images are from a representative experiment. **B.** After 48 h treatment DNA was extracted from cells and analyzed on a 1.5% agarose gel. Images are from a representative experiment. **C–F.** H295R cells were treated with G-1 (1 μM) for 24 h. Western blot analyses of Parp-1 (C), Bax and Bcl-2 (D). Cytochrome c (F) were performed on equal amounts of total proteins. Blots are representative of three independent experiments with similar results. Bax and Bcl-2 were analyzed on total proteins extracted from xenograft tumors (E). GAPDH was used as a loading. **G-H.** H295R cells were treated with G-1 (1 μM) for 24 h. Caspase 9 (G) and caspase 3/7 (H) activity was determined by a luminescent assay. Results were expressed as percentage of enzyme activity. Graphs represent mean + SE of three independent experiments each performed in triplicate. Statistically significant differences are indicated (*P < 0.05 versus basal).

Figure 5: G-1-induced MAPK activation correlates with an increased protein expression of proapoptotic Bax. H295R cells were transfected with shRNA **A.** or shGPER **B.** for 72 h. Forty-eight hours after transfection cells were untreated (0) or treated for at the indicated time with G-1 (1 μM). Western blot analyses of pERK1/2 were performed on 10 μg of total proteins. ERK1/2 was used as a loading control. Blots are representative of three independent experiments with similar results. The insert in (B) shows a Western blot on H295R protein extracts evaluating the expression of GPER receptor in the presence of shcontrol or of shGPER. GAPDH was used as a loading control. (A-B up panels) Graphs represent means of normalized optical densities from three experiments, bars represent SE. *$p < 0.05$ versus basal. **C.**, H295R cells were treated for 24 h with vehicle (−) or G-1 (1 μM) alone or combined with PD98059 (10 μM). Western blot analysis of Bax was performed on equal amounts of total proteins. GAPDH was used as a loading control. Blots are representative of three independent experiments with similar results.

G1 treatment causes sustained ERK1/2 phosphorylation

In order to define the molecular mechanism associated with G-1-induced apoptosis, we investigated the activation of MAPK family members extracellular signal-regulated kinase 1/2 (ERK1/2), which have been demonstrated to be involved in apoptosis if activated for a prolonged time [32]. As shown in Figure 5A, G-1 treatment activated ERK1/2 in a time-dependent manner as seen by the increased levels of their phosphorylation status. Activation started after 30-min of G-1 treatment and persisted for up to 24 h (Fig. 5A). ShGPER, that partially reversed G-1 effects on cell proliferation (Fig. 1E) did not affect ERK1/2 activation (Fig. 5B). Involvement of ERK1/2 in G-1-induced apoptosis of adrenocortical cancer cells was confirmed by the observation that MEK1 inhibitor, PD98059, prevented the up-regulatory effect exerted by G-1 on Bax expression (Fig. 5C).

DISCUSSION

Here, we demonstrated for the first time that a selective non estrogenic ligand of GPER named G-1 is able to inhibit H295R cell growth both *in vitro* and *in vivo* in a xenograft model. Starting from these results we investigated the potential role of GPER in this event.

First, we showed GPER expression both at transcriptional and post-transcriptional level in our ACC cell model represented by H295R cells as well as in normal adrenal and ACC samples. These first analyses aimed to assess only if GPER was expressed in normal and tumor adrenal and not to indicate any difference in expression levels, since overexpression of GPCR is not a common event in human diseases [20].

Recent studies have shown that activation of GPER initiates signaling cascades that, depending on the cell type, are associated with both proliferation [11, 33] and apoptosis [29, 32]. Ariazi et al. have highlighted the opposite effects played by GPER activation on cell proliferation of ERs negative and ERs positive breast cancer cells [17]. Specifically, when ERs are expressed, activation of GPER leads to inhibition of cell proliferation. On the contrary, when cells are ERs negative activation of GPER leads to an increase in cell proliferation [17]. Our work, demonstrated that micromolar concentrations of G-1 decrease H295R cell proliferation *in vitro*, significantly reduce ACC tumor volume *in vivo* and cause a marked decrease in the expression of the nuclear proliferation antigen Ki-67. Accordingly, flow cytometry analysis revealed that G-1 treatment causes changes in cellular distribution within the different phases of cell cycle. It is well established that cell cycle progression is dynamically and strictly regulated by complexes containing cyclins and cyclin dependent kinases (CDKs) [34]. Here, we found that after G-1 treatment expression of G_1 phase cyclin CCNE was reduced, while G_2 phase cyclin CCNB1 was increased. This observation indicates that H295R cells do not bypass G_2 checkpoint. Similar data were reported for prostate cancer cells, where GPER activation by 1 μM G-1 caused cell cycle arrest at the G_2 phase [35]. G_2 phase arrest was followed by apoptotic cell death as indicated by positive staining for Annexin-V, nuclei morphological changes and appearance of DNA ladder pattern.

Apoptosis can be induced by extrinsic [36] and intrinsic [37] mechanisms; the latter is strictly controlled by bcl-2 family of proteins [38] that consists of both pro- (Bax, Bad, Bak, Bid) and anti-apoptotic (Bcl-2, Bcl-xl) proteins able to modulate the execution phase of the cell death pathway. Bax exerts pro-apoptotic activity by allowing Cytochrome c translocation from the mitochondria to the cytosol [39]. Cytochrome c then binds to apoptotic protease-activating factor-1 (Apaf-1) [40], which in turn associates with Procaspase 9 resulting in the activation of its enzymatic activity [41], responsible for the proteolytic activation of executioner Caspase 3 [42].

The active Caspase 3 is then involved in the cleavage of a set of proteins including Poly-(ADP) ribose polymerase-1 (Parp-1) [43]. Bcl-2, instead, exerts its anti-apoptotic activity, at least in part, by inhibiting the translocation of Bax to the mitochondria [40]. Changes in expression and/or activation of all the above mentioned biochemical markers of mitochondrial apoptotic pathway were observed in H295R cells in response to G-1 treatment.

MAPK family members ERK1/2 are part of GPER signaling [14]. Despite the well-defined role of ERK1/2 activation in proliferative pathways [44], sustained ERK1/2 phosphorylation is involved in apoptotic events [29, 32, 45]. Cagnol and Chambard have summarized more than 50 publications showing a link between prolonged ERK activation and apoptosis [46]. Specifically it can be appreciated that duration of ERK activation in promoting cell death can be different depending on cell type and stimuli. G-1 caused sustained ERK1/2 activation in H295R, this event was clearly involved in the induction of apoptosis, since chemical inhibition of MEK1/2 using PD98059 abrogated G-1 ability to induce the expression of proapoptotic factor Bax. Several reports pointed out that ERK1/2 activity can be associated with upregulation of proapoptotic members of the Bcl-2 family, such as Bax [47–49]. Moreover, ERK activity has been shown to directly affect mitochondrial function [46] by decreasing mitochondrial respiration [50, 51] and mitochondrial membrane potential [51, 52], causing mitochondrial membrane disruption and Cytochrome c release [52–54].

Interestingly, GPER silencing was not able to prevent G-1 induced ERK phosphorylation, underlying the existence of alternative targets for G-1. These targets, similarly to GPER, are able to activate ERK1/2 signaling, however for a prolonged period, and clearly deserve further investigation.

Other papers evidenced inhibitory effects exerted by G-1 on the growth of different tumor cell types in a GPER independent manner [55–57], but a precise mechanism has not been defined. Although further studies are needed to clarify the molecular mechanisms behind G-1-dependent effects, this molecule could be a viable alternative to the current limited treatment options and therapeutic efficacy for adrenocortical cancer.

In conclusion, we demonstrated that treatment of H295R cells with G-1 reduced tumor growth *in vitro* and *in vivo* through a mechanism involving not only GPER activation. G-1 clearly causes cell-cycle arrest at the G_2 phase and apoptosis through a mechanism that requires sustained ERK1/2 activation. Our previously published results highlighting the ability of OHT, a known GPER agonist and ESR1 antagonist, to reduce ACC cell growth, together with the present findings indicating the inhibitory effects exerted by G-1, open up new perspectives for the development of therapies with molecules modulating estrogen receptors action for the treatment of ACC.

MATERIALS AND METHODS

Cell culture and tissues

H295R cells were obtained from Dr W.E. Rainey (University of Michigan at Ann Arbor, USA) [58]. Cells were cultured as previously described [9]. Cell monolayers were subcultured onto 100 mm dishes for phosphatase activity and laddering assay (8×10^6 cells/plate), 60 mm dishes for protein and RNA extraction (4×10^6 cells/plate) and 24 well culture dishes for proliferation experiments (2×10^5 cells/well) and grown for 2 days. Prior to experiments, cells were starved overnight in DMEM/F-12 medium without phenol red and containing antibiotics. Cells were treated with (±)-1-[(3aR*, 4S*, 9bS*)-4-(6-Bromo-1, 3-benzodioxol-5-yl)-3a, 4, 5, 9b-tetrahydro-3H-cyclopenta[c]quinolin-8-yl]-ethanone (G-1) (1 μM) (Tocris Bioscience, Bristol, UK) in DMEM/F-12 containing FBS-DCC 2, 5% (fetal bovine serum dextran-coated charcoal-treated). Inhibitors PD98059 (PD) (10 μM) (Calbiochem, Merck KGaA, Darmstadt, Germany) was used 1 h prior to G-1. Adrenocortical tumors, removed at surgery, and normal adrenal cortex, macroscopically dissected from adrenal glands of kidney donors, were collected at the hospital-based Divisions of the University of Padua (Italy). Tissue samples were obtained with the approval of local ethics committees and consent from patients, in accordance with the Declaration of Helsinki guidelines as revised in 1983. Diagnosis of malignancy was performed according to the histopathologic criteria proposed by Weiss et al. [59] and the modification proposed by Aubert et al. [60]. Clinical data of the six ACC patients included in this study are shown in Table 1. Patient C6 terminated mitotane treatment six months after beginning of therapy for severe gastrointestinal side effects. Patients C1 and C2 were treated with chemotherapy EAP protocol (etoposide, doxorubicin, and cisplatin) + mitotane.

RNA extraction, reverse transcription and real time PCR

TRizol RNA isolation system (Invitrogen, Carlsbad, CA, USA) was used to extract total RNA from H295R, SKBR3 and ACCs. Each RNA sample was treated with DNase I (Invitrogen), and purity and integrity of the RNA were confirmed spectroscopically and by gel electrophoresis before use. One microgram of total RNA was reverse transcribed in a final volume of 30 μl using the ImProm-II Reverse transcription system kit (Promega Italia S.r.l., Milano, Italia); cDNA was diluted 1:2 in nuclease-free water, aliquoted, and stored at − 20°C. The nucleotide sequences for GPER amplification were forward, 5′-CGCTCTTCCTGCAGGTCAA-3′, and reverse, 5′-ATGTAGCGGTCGAAGCTCATC-3′ ; the nucleotide sequences for GAPDH amplification were forward, 5′-CCCACTCCTCCACCTTTGAC-3′, and reverse, 5′-TGTTGCTGTAGCCAAATTCGTT-3′. PCR reactions were performed in the iCycler iQ Detection System (Bio-Rad Laboratories S.r.l., Milano, Italia) using 0.1 μmol/L of each primer, in a total volume of 30 μl reaction mixture following the manufacturer's recommendations. SYBR Green Universal PCR Master Mix (Bio-Rad) with the dissociation protocol was used for gene amplification; negative controls contained water instead of first-strand cDNA. Each sample was normalized to its GAPDH content. The relative gene expression levels were normalized to a calibrator (normal tissue for ACC tissues or SKBR3 for H295R cells). Final results were expressed as n-fold differences in gene expression relative to GAPDH and calibrator, calculated using the ΔΔCt method as previously shown [61].

Western blot analysis

Fifty μg of protein was subjected to western blot analysis [62]. Blots were incubated overnight at 4°C with antibodies against GPER, Cyclin E (CCNE), Cyclin B1 (CCNB1), phospho-Rb, Cytochrome c, Bax, Bcl-2, Parp1, pERK1/2-ERK2 (all from Santa Cruz Biotechnology, Santa Cruz CA, USA). Membranes were incubated with horseradish peroxidase (HRP)-conjugated secondary antibodies (Amersham Pharmacia Biotech, Piscataway, NJ) and immunoreactive bands were visualized with the ECL western blotting detection system (Amersham Pharmacia Biotech, Piscataway, NJ).

Table 1: Clinical data of the 6 ACC patients analyzed in this study

Sample ID	Age(years)	Gender	Stage at surgery	Syndrome	Weiss score	Size (cm)	Outcome
C1	41	M	IV	Cushing	9	16	Died, 1 year
C2	17	F	IV	Cushing	9	14	Died, 18 months
C3	43	F	III	None	4	9	Died, 8 years
C4	46	M	III	None	3	18	Remission, 7 years
C5	47	M	IV	Cushing	9	14	Died, 1 year
C6	57	M	II	SubclinicalCushing	5	14	Remission, 4 years

To assure equal loading of proteins, membranes were stripped and incubated overnight with Glyceraldehyde 3-phosphate dehydrogenase (GAPDH) antibody (Santa Cruz Biotechnology).

Histopathological analysis

Tumors were fixed in 4% formalin, sectioned at 5 μm and stained with hematoxylin and eosin, as suggested by the manufacturer (Bio-Optica, Milan, Italy).

Immunohistochemical analysis

Paraffin-embedded sections, 5 mm thick, were mounted on slides precoated with poly-lysine, and then they were deparaffinized and dehydrated (seven to eight serial sections). Immunohistochemical experiments were performed as described [63], using mouse monoclonal Ki-67 primary antibody at 4°C over-night (Dako Italia Spa, Milano, Italy). Then, a biotinylated goat-anti-mouse IgG was applied for 1 h at room temperature, to form the avidin biotin-horseradish peroxidase complex (Vector Laboratories, CA, USA). Immunoreactivity was visualized by using the diaminobenzi-dine chromogen (Vector Laboratories). Counterstaining was carried out with hematoxylin (Bio-Optica, Milano, Italy). The primary antibody was replaced by normal rabbit serum in negative control sections.

Cytochrome c detection

Cells were treated for 24 h, fractioned and processed for Cytochrome c detection as previously reported [26]. Briefly, cells were harvested by centrifugation at 2500 rpm for 10 min at 4°C. Pellets were resuspended in 50 μl of sucrose buffer (250 mM sucrose; 10 mM Hepes; 10 mM KCl; 1.5 mM MgCl2; 1 mM EDTA; 1 mM EGTA) (all from Sigma-Aldrich, Milano, Italy) containing 20 μg/ml aprotinin, 20 μg/ml leupeptin, 1 mM PMSF and 0.05% digitonine (Sigma-Aldrich). Cells were incubated for 20 min at 4°C and then centrifuged at 13,000 rpm for 15 min at 4°C. Supernatants containing cytosolic protein fraction were transferred to new tubes and the resulting mitochondrial pellets were resuspended in 50 μl of lysis buffer (1% Triton X-100; 1 mM EDTA; 1 mM EGTA; 10 mM Tris-HCl, pH 7.4) (all from Sigma-Aldrich) containing 20 μg/ml aprotinin, 20 μg/ml leupeptin, 1 mM PMSF (Sigma-Aldrich) and then centrifuged at 13,000 rpm for 10 min at 4°C. Equal amounts of proteins were resolved by 11% SDS/polyacrylamide gel as indicated in the Western blot analysis paragraph.

Cell cycle analysis and evaluation of cell death

Subconfluent monolayers growing in 60 mm plates were depleted of serum for 24 h and treated for an additional 24 h with G-1. The cells were harvested by trypsinization and resuspended with 0.5 ml of Propidium Iodide solution (PI) (100 μg/ml) (Sigma-Aldrich) after treatment with RNase A (20 μg/ml). The DNA content was measured using a FACScan flow cytometer (Becton Dickinson, Mountain View, CA, USA) and the data acquired using CellQuest software. Cell cycle profiles were determined using ModFit LT program. Subconfluent monolayers growing in 60 mm plates were depleted of serum for 24 h and treated for 24 and 48 h with G-1. Trypsinized cells were incubated with Ligation Buffer (10 mM Hepes (pH = 7.4), 150 mM NaCl, 5 mM KCl, 1 mM MgCl2 and 1.8 mM CaCl2) containing Annexin-V-FITC (1:5000) (Santa Cruz) and with Propidium Iodide. Twenty minutes post-incubation at room temperature (RT) protected from light, samples were examined in a FACSCalibur cytometer (Becton Dickinson, Milano, Italy). Results were analyzed using CellQuest program.

Caspases 9 and 3/7 activity assay

H295R cells after treatments were subjected to caspases 9 and 3/7 activity measurement with Caspase-Glo 9 and 3/7 assay kits (Promega) and modified protocol. Briefly, the proluminescent substrate containing LEHD or DEVD sequences (sequences are in a single-letter amino acid code) are respectively cleaved by Caspases 9 and 3/7. After caspases cleavage, a substrate for luciferase (aminoluciferin) is released resulting in luciferase reaction luminescent signal production. Cells were trypsinized, harvested and then suspended in DMEM-F12 before being incubated with an equal volume of Caspase-Glo reagent (40 μl) at 37°C for 1 h. The luminescence of each sample was measured in a plate-reading luminometer (Gen5 2.01) with Synergy H1 Hybrid Reader.

TUNEL (terminal deoxynucleotidyltransferase-mediated dUTP nick-end labelling) assay

Cells were grown on glass coverslips, treated for 24 h and then washed with PBS and fixed in 4% formaldehyde for 15 min at room temperature. Fixed cells were washed with PBS and then soaked for 20 min with 0.25% of Triton X-100 in PBS. After two washes in deionized water, they were stained using the Click-iT® TUNEL Alexa Fluor® Imaging Assay (Invitrogen) according to the manufacturer's protocol. Co-staining with Hoechst33342 was performed to analyze the nuclear morphology of the cells after the treatment. Cell nuclei were observed and imaged under an inverted fluorescence microscope (200X magnification).

Determination of DNA fragmentation

To determine the occurrence of DNA fragmentation, total DNA was extracted from control and G-1 (1 μM) treated (48 h) cells as previously described [26]. Equal amounts of DNA were analyzed

by electrophoresis on a 2% agarose gel stained with Ethidium Bromide (Sigma-Aldrich).

Assessment of cell proliferation

[³H]Thymidine incorporation assay

H295R cell proliferation after G-1 treatment was directly evaluated after a 6 h incubation with 1 μCi of [³H]thymidine (Perkin- Elmer Life Sciences, Boston, MA, USA) per well as previously described [64]. Each experiment was performed in triplicate and results are expressed as percent (%) of basal.

MTT assay

The effect of G-1 on cell viability was measured using 3-[4, 5-Dimethylthiaoly]-2, 5-diphenyltetrazolium bromide (MTT) assay as previously described [7]. Briefly, cells were treated for different times as indicated in figure legends. At the end of each time point fresh MTT (Sigma-Aldrich), re-suspended in PBS, was added to each well (final concentration 0.33 mg/ml). After 30 minutes incubation, cells were lysed with 1 ml of DMSO (Sigma-Aldrich). Each experiment was performed in triplicate and the optical density was measured at 570 nm in a spectrophotometer.

Gene silencing experiments

For the gene silencing experiments, cells were plated in 12 well plates (1×10^5 cells/well) for proliferation experiments or in 6 well plates (2×10^5 cells/well) for Western blot analysis; cells were transfected with control vector (shRNA) or shGPER in 2, 5% DCC-FBS medium using lipofectamine 2000 transfection reagent (Invitrogen) according to the manufacturer's recommendations for a total of 72 h. For proliferation experiments cells were transfected for 24 h and then treated for 48 h before performing MTT assay.

Xenograft model

Four-week-old nu/nu − Forkhead box N1^{nu} female mice were obtained from Charles River Laboratories Italia (Calco, Lecco, Italy). All animals were maintained in groups of five or less and quarantined for two weeks. Mice were kept on a 12 h/12 h light/dark regimen and allowed access to food and water *ad libitum*. H295R cells, 6×10^6, suspended in 100 μl PBS (Dulbecco's Phosphate Buffered Saline), were combined with 30 μl of Matrigel (4 mg/ml) (Becton Dickinson) and injected subcutaneously in the shoulder of each animal. Resulting tumors were measured at regular intervals using a caliper, and tumor volume was calculated as previously described [65], using the formula: $V = 0.52 (L \times W^2)$, where L is the longest axis of the tumor and W is perpendicular to the long axis. Mice were treated 21 days after cell injection, when tumors had reached an average volume of about 200 mm³. Animals were randomly assigned to be treated with vehicle or G-1 (Tocris Bioscience) at a concentration of 2 mg/kg/daily. Drug tolerability was assessed in tumor-bearing mice in terms of: a) lethal toxicity, i.e. any death in treated mice occurring before any death in control mice; b) body weight loss percentag$e = 100 − $ [(body weight on day x/body weight on day 1) $\times$ 100], where x represents a day during the treatment period [66, 67]. Animals were sacrificed by cervical dislocation 42 days after cell injection. All animal procedures were approved by Local Ethics Committee for Animal Research.

In vivo magnetic resonance analyses

Mice were anesthetized with 1–2% isofluorane in O2, 1 L/min (Forane, Abbott SpA, Latina, Italia) and underwent MRI/MRS study. MR analyses were performed at 4.7 T on Agilent Technologies system (Palo Alto, CA, USA). T2-weighted MRI was acquired using a spin echo sequence with the following parameters: TR/TE = 3000/70 ms, section thickness of 1.0 mm, number of acquisitions = 4, point resolution of 256 μm.

Scoring system

The immunostained slides of tumor samples were evaluated by light microscopy using the Allred Score [68] which combines a proportion score and an intensity score. A proportion score was assigned representing the estimated proportion of positively stained tumor cells (0 = none; 1 = 1/100; 2 = 1/100 to < 1/10; 3 = 1/10 to < 1/3; 4 = 1/3 to 2/3; 5 = > 2/3). An intensity score was assigned by the average estimated intensity of staining in positive cells (0 = none; 1 = weak; 2 = moderate; 3 = strong). Proportion score and intensity score were added to obtain a total score that ranged from 0 to 8. A minimum of 100 cells were evaluated in each slide. Six to seven serial sections were scored in a blinded manner for each sample.

Data analysis and statistical methods

All experiments were performed at least three times. Data were expressed as mean values + standard error (SE), statistical significance between control (basal) and treated samples was analyzed using GraphPad Prism 5.0 (GraphPad Software, Inc.; La Jolla, CA) software. Control and treated groups were compared using the analysis of variance (ANOVA) with Bonferroni or Dunn's post hoc testing. A comparison of individual treatments was also performed, using Student's *t* test. Significance was defined as $p < 0.05$.

CONFLICTS OF INTEREST

The authors declare no conflicts of interest.

REFERENCES

1. Lehmann TP, Wrzesinski T, Jagodzinski PP. The effect of mitotane on viability, steroidogenesis and gene expression in NCIH295R adrenocortical cells. Molecular medicine reports. 2013; 7:893–900.

2. Lubitz JA, Freeman L, Okun R. Mitotane use in inoperable adrenal cortical carcinoma. Journal of the American Medical Association. 1973; 223:1109–1112.

3. Barzilay JI, Pazianos AG. Adrenocortical carcinoma. The Urologic clinics of North America. 1989; 16:457–468.

4. Haluska P. Insulin-like growth factor pathway. Journal of thoracic oncology: official publication of the International Association for the Study of Lung Cancer. 2010; 5:S478–479.

5. Barlaskar FM, Spalding AC, Heaton JH, Kuick R, Kim AC, Thomas DG, Giordano TJ, Ben-Josef E, Hammer GD. Preclinical targeting of the type I insulin-like growth factor receptor in adrenocortical carcinoma. The Journal of clinical endocrinology and metabolism. 2009; 94:204–212.

6. Pollak M. Insulin and insulin-like growth factor signalling in neoplasia. Nature reviews Cancer. 2008; 8:915–928.

7. Sirianni R, Zolea F, Chimento A, Ruggiero C, Cerquetti L, Fallo F, Pilon C, Arnaldi G, Carpinelli G, Stigliano A, Pezzi V. Targeting estrogen receptor-alpha reduces adrenocortical cancer (ACC) cell growth *in vitro* and *in vivo*: potential therapeutic role of selective estrogen receptor modulators (SERMs) for ACC treatment. The Journal of clinical endocrinology and metabolism. 2012; 97:E2238–2250.

8. Barzon L, Masi G, Pacenti M, Trevisan M, Fallo F, Remo A, Martignoni G, Montanaro D, Pezzi V, Palu G. Expression of aromatase and estrogen receptors in human adrenocortical tumors. Virchows Archiv: an international journal of pathology. 2008; 452:181–191.

9. Montanaro D, Maggiolini M, Recchia AG, Sirianni R, Aquila S, Barzon L, Fallo F, Ando S, Pezzi V. Antiestrogens upregulate estrogen receptor beta expression and inhibit adrenocortical H295R cell proliferation. Journal of molecular endocrinology. 2005; 35:245–256.

10. Vivacqua A, Bonofiglio D, Albanito L, Madeo A, Rago V, Carpino A, Musti AM, Picard D, Ando S, Maggiolini M. 17beta-estradiol, genistein, and 4-hydroxytamoxifen induce the proliferation of thyroid cancer cells through the g protein-coupled receptor GPR30. Molecular pharmacology. 2006; 70:1414–1423.

11. Vivacqua A, Bonofiglio D, Recchia AG, Musti AM, Picard D, Ando S, Maggiolini M. The G protein-coupled receptor GPR30 mediates the proliferative effects induced by 17beta-estradiol and hydroxytamoxifen in endometrial cancer cells. Molecular Endocrinology. 2006; 20:631–646.

12. Li Y, Chen Y, Zhu ZX, Liu XH, Yang L, Wan L, Lei TW, Wang XD. 4-Hydroxytamoxifen-stimulated processing of cyclin E is mediated via G protein-coupled receptor 30 (GPR30) and accompanied by enhanced migration in MCF-7 breast cancer cells. Toxicology. 2013; 309:61–65.

13. Prossnitz ER, Maggiolini M. Mechanisms of estrogen signaling and gene expression via GPR30. Molecular and cellular endocrinology. 2009; 308:32–38.

14. Lappano R, De Marco P, De Francesco EM, Chimento A, Pezzi V, Maggiolini M. Cross-talk between GPER and growth factor signaling. The Journal of steroid biochemistry and molecular biology. 2013.

15. Prossnitz ER, Barton M. Signaling, physiological functions and clinical relevance of the G protein-coupled estrogen receptor GPER. Prostaglandins & other lipid mediators. 2009; 89:89–97.

16. Prossnitz ER, Arterburn JB, Smith HO, Oprea TI, Sklar LA, Hathaway HJ. Estrogen signaling through the transmembrane G protein-coupled receptor GPR30. Annual review of physiology. 2008; 70:165–190.

17. Ariazi EA, Brailoiu E, Yerrum S, Shupp HA, Slifker MJ, Cunliffe HE, Black MA, Donato AL, Arterburn JB, Oprea TI, Prossnitz ER, Dun NJ, Jordan VC. The G protein-coupled receptor GPR30 inhibits proliferation of estrogen receptor-positive breast cancer cells. Cancer research. 2010; 70:1184–1194.

18. Smith HO, Leslie KK, Singh M, Qualls CR, Revankar CM, Joste NE, Prossnitz ER. GPR30: a novel indicator of poor survival for endometrial carcinoma. American journal of obstetrics and gynecology. 2007; 196:386. e381–389, discussion e389–311.

19. Smith HO, Arias-Pulido H, Kuo DY, Howard T, Qualls CR, Lee SJ, Verschraegen CF, Hathaway HJ, Joste NE, Prossnitz ER. GPR30 predicts poor survival for ovarian cancer. Gynecologic oncology. 2009; 114:465–471.

20. Filardo EJ, Graeber CT, Quinn JA, Resnick MB, Giri D, DeLellis RA, Steinhoff MM, Sabo E. Distribution of GPR30, a seven membrane-spanning estrogen receptor, in primary breast cancer and its association with

clinicopathologic determinants of tumor progression. Clinical cancer research: an official journal of the American Association for Cancer Research. 2006; 12:6359–6366.

21. Albanito L, Madeo A, Lappano R, Vivacqua A, Rago V, Carpino A, Oprea TI, Prossnitz ER, Musti AM, Ando S, Maggiolini M. G protein-coupled receptor 30 (GPR30) mediates gene expression changes and growth response to 17beta-estradiol and selective GPR30 ligand G-1 in ovarian cancer cells. Cancer research. 2007; 67:1859–1866.

22. Thomas P, Pang Y, Filardo EJ, Dong J. Identity of an estrogen membrane receptor coupled to a G protein in human breast cancer cells. Endocrinology. 2005; 146:624–632.

23. Baquedano MS, Saraco N, Berensztein E, Pepe C, Bianchini M, Levy E, Goni J, Rivarola MA, Belgorosky A. Identification and developmental changes of aromatase and estrogen receptor expression in prepubertal and pubertal human adrenal tissues. The Journal of clinical endocrinology and metabolism. 2007; 92:2215–2222.

24. Bologa CG, Revankar CM, Young SM, Edwards BS, Arterburn JB, Kiselyov AS, Parker MA, Tkachenko SE, Savchuck NP, Sklar LA, Oprea TI, Prossnitz ER. Virtual and biomolecular screening converge on a selective agonist for GPR30. Nature chemical biology. 2006; 2:207–212.

25. Chimento A, Casaburi I, Rosano C, Avena P, De Luca A, Campana C, Martire E, Santolla MF, Maggiolini M, Pezzi V, Sirianni R. Oleuropein and hydroxytyrosol activate GPER/ GPR30-dependent pathways leading to apoptosis of ER-negative SKBR3 breast cancer cells. Molecular nutrition & food research. 2014; 58:478–489.

26. Chimento A, Sirianni R, Casaburi I, Ruggiero C, Maggiolini M, Ando S, Pezzi V. 17beta-Estradiol activates GPER- and ESR1-dependent pathways inducing apoptosis in GC-2 cells, a mouse spermatocyte-derived cell line. Molecular and cellular endocrinology. 2012; 355:49–59.

27. Chimento A, Sirianni R, Zolea F, Bois C, Delalande C, Ando S, Maggiolini M, Aquila S, Carreau S, Pezzi V. Gper and ESRs are expressed in rat round spermatids and mediate oestrogen-dependent rapid pathways modulating expression of cyclin B1 and Bax. International journal of andrology. 2011; 34:420–429.

28. Chimento A, Sirianni R, Delalande C, Silandre D, Bois C, Ando S, Maggiolini M, Carreau S, Pezzi V. 17 beta-estradiol activates rapid signaling pathways involved in rat pachytene spermatocytes apoptosis through GPR30 and ER alpha. Molecular and cellular endocrinology. 2010; 320:136–144.

29. Chimento A, Casaburi I, Bartucci M, Patrizii M, Dattilo R, Avena P, Ando S, Pezzi V, Sirianni R. Selective GPER activation decreases proliferation and activates apoptosis in tumor Leydig cells. Cell death & disease. 2013; 4:e747.

30. Ling YH, Jiang JD, Holland JF, Perez-Soler R. Arsenic trioxide produces polymerization of microtubules and mitotic arrest before apoptosis in human tumor cell lines. Molecular pharmacology. 2002; 62:529–538.

31. Oberst A, Bender C, Green DR. Living with death: the evolution of the mitochondrial pathway of apoptosis in animals. Cell death and differentiation. 2008; 15:1139–1146.

32. Chen JR, Plotkin LI, Aguirre JI, Han L, Jilka RL, Kousteni S, Bellido T, Manolagas SC. Transient versus sustained phosphorylation and nuclear accumulation of ERKs underlie anti-versus pro-apoptotic effects of estrogens. The Journal of biological chemistry. 2005; 280:4632–4638.

33. Albanito L, Lappano R, Madeo A, Chimento A, Prossnitz ER, Cappello AR, Dolce V, Abonante S, Pezzi V, Maggiolini M. G-protein-coupled receptor 30 and estrogen receptor-alpha are involved in the proliferative effects induced by atrazine in ovarian cancer cells. Environmental health perspectives. 2015; 123:493–9.

34. John PC, Mews M, Moore R. Cyclin/Cdk complexes: their involvement in cell cycle progression and mitotic division. Protoplasma. 2001; 216:119–142.

35. Chan QK, Lam HM, Ng CF, Lee AY, Chan ES, Ng HK, Ho SM, Lau KM. Activation of GPR30 inhibits the growth of prostate cancer cells through sustained activation of Erk1/2, c-jun/c-fos-dependent upregulation of p21, and induction of G(2) cell-cycle arrest. Cell death and differentiation. 2010; 17:1511–1523.

36. Kim R, Emi M, Tanabe K, Murakami S, Uchida Y, Arihiro K. Regulation and interplay of apoptotic and non-apoptotic cell death. The Journal of pathology. 2006; 208:319–326.

37. Fadeel B, Orrenius S. Apoptosis: a basic biological phenomenon with wide-ranging implications in human disease. Journal of internal medicine. 2005; 258:479–517.

38. Cory S, Adams JM. The Bcl family: regulators of the cellular life-or-death switch. Nature reviews Cancer. 2002; 2:647–656.

39. Antonsson B, Montessuit S, Lauper S, Eskes R, Martinou JC. Bax oligomerization is required for channel-forming activity in liposomes and to trigger cytochrome c release from mitochondria. The Biochemical journal. 2000; 2:271–278.

40. Wang X. The expanding role of mitochondria in apoptosis. Genes & development. 2001; 15:2922–2933.

41. Kuida K, Haydar TF, Kuan CY, Gu Y, Taya C, Karasuyama H, Su MS, Rakic P, Flavell RA. Reduced apoptosis and cytochrome c-mediated caspase activation in mice lacking caspase 9. Cell. 1998; 94:325–337.

42. Wilson MR. Apoptosis: unmasking the executioner. Cell death and differentiation. 1998; 5:646–652.

43. Soldani C, Scovassi AI. Poly(ADP-ribose) polymerase-1 cleavage during apoptosis: an update. Apoptosis: an international journal on programmed cell death. 2002; 7:321–328.

44. Meloche S, Pouyssegur J. The ERK1/2 mitogen-activated protein kinase pathway as a master regulator of the G1- to S-phase transition. Oncogene. 2007; 26:3227–3239.

45. Ramos JW. The regulation of extracellular signal-regulated kinase (ERK) in mammalian cells. The international journal of biochemistry & cell biology. 2008; 40:2707–2719.

46. Cagnol S, Chambard JC. ERK and cell death: mechanisms of ERK-induced cell death—apoptosis, autophagy and senescence. The FEBS journal. 2010; 277:2–21.

47. Chen MF, Qi L, Li Y, Zu XB, Dai YQ, Zhang P. Icaritin induces growth inhibition and apoptosis of human prostatic smooth muscle cells in an estrogen receptor-independent manner. Amino acids. 2010; 38:1505–1513.

48. Tong JS, Zhang QH, Huang X, Fu XQ, Qi ST, Wang YP, Hou Y, Sheng J, Sun QY. Icaritin causes sustained ERK1/2 activation and induces apoptosis in human endometrial cancer cells. PloS one. 2011; 6:e16781.

49. Tan BJ, Chiu GN. Role of oxidative stress, endoplasmic reticulum stress and ERK activation in triptolide-induced apoptosis. International journal of oncology. 2013; 42:1605–1612.

50. Nowak G. Protein kinase C-alpha and ERK1/2 mediate mitochondrial dysfunction, decreases in active Na+ transport, and cisplatin-induced apoptosis in renal cells. The Journal of biological chemistry. 2002; 277:43377–43388.

51. Nowak G, Clifton GL, Godwin ML, Bakajsova D. Activation of ERK1/2 pathway mediates oxidant-induced decreases in mitochondrial function in renal cells. American journal of physiology Renal physiology. 2006; 291:F840–855.

52. Kim GS, Hong JS, Kim SW, Koh JM, An CS, Choi JY, Cheng SL. Leptin induces apoptosis via ERK/cPLA2/cytochrome c pathway in human bone marrow stromal cells. The Journal of biological chemistry. 2003; 278:21920–21929.

53. Zhang CL, Wu LJ, Zuo HJ, Tashiro S, Onodera S, Ikejima T. Cytochrome c release from oridonin-treated apoptotic A375-S2 cells is dependent on p53 and extracellular signal-regulated kinase activation. Journal of pharmacological sciences. 2004; 96:155–163.

54. Li DW, Liu JP, Mao YW, Xiang H, Wang J, Ma WY, Dong Z, Pike HM, Brown RE, Reed JC. Calcium-activated RAF/MEK/ERK signaling pathway mediates p53-dependent apoptosis and is abrogated by alpha B-crystallin through inhibition of RAS activation. Molecular biology of the cell. 2005; 16:4437–4453.

55. Holm A, Grande PO, Luduena RF, Olde B, Prasad V, Leeb-Lundberg LM, Nilsson BO. The G protein-coupled oestrogen receptor 1 agonist G-1 disrupts endothelial cell microtubule structure in a receptor-independent manner. Molecular and cellular biochemistry. 2012; 366:239–249.

56. Gui Y, Shi Z, Wang Z, Li JJ, Xu C, Tian R, Song X, Walsh MP, Li D, Gao J, Zheng XL. The GPER Agonist G-1 Induces Mitotic Arrest and Apoptosis in Human Vascular Smooth Muscle Cells Independent of GPER. Journal of cellular physiology. 2015; 230:885–895.

57. Wang C, Lv X, Jiang C, Davis JS. The putative G-protein coupled estrogen receptor agonist G-1 suppresses proliferation of ovarian and breast cancer cells in a GPER-independent manner. American journal of translational research. 2012; 4:390–402.

58. Rainey WE, Bird IM, Mason JI. The NCI-H295 cell line: a pluripotent model for human adrenocortical studies. Molecular and cellular endocrinology. 1994; 100:45–50.

59. Weiss LM, Medeiros LJ, Vickery AL Jr. Pathologic features of prognostic significance in adrenocortical carcinoma. The American journal of surgical pathology. 1989; 13:202–206.

60. Aubert S, Wacrenier A, Leroy X, Devos P, Carnaille B, Proye C, Wemeau JL, Lecomte-Houcke M, Leteurtre E. Weiss system revisited: a clinicopathologic and immunohistochemical study of 49 adrenocortical tumors. The American journal of surgical pathology. 2002; 26:1612–1619.

61. Sirianni R, Chimento A, De Luca A, Zolea F, Carpino A, Rago V, Maggiolini M, Ando S, Pezzi V. Inhibition of cyclooxygenase-2 down-regulates aromatase activity and decreases proliferation of Leydig tumor cells. The Journal of biological chemistry. 2009; 284:28905–28916.

62. Sirianni R, Chimento A, Malivindi R, Mazzitelli I, Ando S, Pezzi V. Insulin-like growth factor-I, regulating aromatase expression through steroidogenic factor 1, supports estrogen-dependent tumor Leydig cell proliferation. Cancer research. 2007; 67:8368–8377.

63. Catalano S, Panza S, Malivindi R, Giordano C, Barone I, Bossi G, Lanzino M, Sirianni R, Mauro L, Sisci D, Bonofiglio D, Ando S. Inhibition of Leydig tumor growth by farnesoid X receptor activation: the *in vitro* and *in vivo* basis for a novel therapeutic strategy. International journal of cancer Journal international du cancer. 2013; 132:2237–2247.

64. Sirianni R, Chimento A, De Luca A, Casaburi I, Rizza P, Onofrio A, Iacopetta D, Puoci F, Ando S, Maggiolini M, Pezzi V. Oleuropein and hydroxytyrosol inhibit MCF-7 breast cancer cell proliferation interfering with ERK1/2 activation. Molecular nutrition & food research. 2010; 54:833–840.

65. Seshadri M, Spernyak JA, Maiery PG, Cheney RT, Mazurchuk R, Bellnier DA. Visualizing the acute effects of vascular-targeted therapy *in vivo* using intravital microscopy and magnetic resonance imaging: correlation with endothelial apoptosis, cytokine induction, and treatment outcome. Neoplasia. 2007; 9:128–135.

66. Johnson JI, Decker S, Zaharevitz D, Rubinstein LV, Venditti JM, Schepartz S, Kalyandrug S, Christian M, Arbuck S, Hollingshead M, Sausville EA. Relationships between drug activity in NCI preclinical *in vitro* and *in vivo* models and early clinical trials. British journal of cancer. 2001; 84:1424–1431.

67. Hollingshead MG. Antitumor efficacy testing in rodents. Journal of the National Cancer Institute. 2008; 100:1500–1510.

68. Allred DC, Harvey JM, Berardo M, Clark GM. Prognostic and predictive factors in breast cancer by immunohistochemical analysis. Modern pathology: an official journal of the United States and Canadian Academy of Pathology, Inc. 1998; 11:155–168.

Estrogen related receptor α (ERRα) a promising target for the therapy of adrenocortical carcinoma (ACC)

Ivan Casaburi[1,*], Paola Avena[1,*], Arianna De Luca[1,*], Adele Chimento[1], Rosa Sirianni[1], Rocco Malivindi[1], Vittoria Rago[1], Marco Fiorillo[1], Francesco Domanico[1], Carmela Campana[1], Anna Rita Cappello[1], Federica Sotgia[2], Michael P. Lisanti[2], Vincenzo Pezzi[1]

[1]Department of Pharmacy, Health and Nutritional Sciences, University of Calabria, Italy

[2]The Breakthrough Breast Cancer Research Unit and the Manchester Centre for Cellular Metabolism, Institute of Cancer Sciences, University of Manchester, UK

*These authors have contributed equally to this work

Correspondence to:
Vincenzo Pezzi, **e-mail:** v.pezzi@unical.it

ABSTRACT

The pathogenesis of the adrenocortical cancer (ACC) involves integration of molecular signals and the interplay of different downstream pathways (i.e. IGFII/IGF1R, β-catenin, Wnt, ESR1). This tumor is characterized by limited therapeutic options and unsuccessful treatments. A useful strategy to develop an effective therapy for ACC is to identify a common downstream target of these multiple pathways. A good candidate could be the transcription factor estrogen-related receptor alpha (ERRα) because of its ability to regulate energy metabolism, mitochondrial biogenesis and signalings related to cancer progression.

In this study we tested the effect of ERRα inverse agonist, XCT790, on the proliferation of H295R adrenocortical cancer cell line. Results from *in vitro* and *in vivo* experiments showed that XCT790 reduced H295R cell growth. The inhibitory effect was associated with impaired cell cycle progression which was not followed by any apoptotic event. Instead, incomplete autophagy and cell death by a necrotic processes, as a consequence of the cell energy failure, induced by pharmacological reduction of ERRα was evidenced.

Our results indicate that therapeutic strategies targeting key factors such as ERRα that control the activity and signaling of bioenergetics processes in high-energy demanding tumors could represent an innovative/alternative therapy for the treatment of ACC.

INTRODUCTION

Adrenocortical carcinoma (ACC) is a very rare and aggressive disease with a high risk of relapse after radical surgery. Treatment options in advanced, metastatic stages are limited, since cytotoxic chemotherapy options are poor and radiotherapy is mostly ineffective [1]. The drug mitotane (o, p′-dichlorodiphe nyldichloroethane (o, p′-DDD)) with its adrenolytic activity is the only adrenal specific drug that is currently used for ACC treatment. However, toxicity, narrow therapeutic window and side effects are the major limitation to its use as well as therapeutic success [2].

Given the high mortality and aggressiveness of ACC, more effective and specific treatment options are needed. Recently, monoclonal antibodies targeting insulin-like growth factor II (IGFII) receptor (IGF1R) have been tested in clinical trials, however they provided a limited effectiveness in refractory patients [3]. Rationale for targeting IGF1R comes from the observation that IGFII gene is overexpressed in ACC [4]. We have recently demonstrated that IGFII/IGF1R pathway can be activated by the estrogen receptor alpha (ESR1), a gene overexpressed in ACC that mediates estrogen-dependent proliferative effects [5, 6]. ESR1 knock down was more effective than an IGF1R antibody in reducing H295R cell

proliferation *in vitro* [5] and the selective estrogen receptor modulator (SERM) tamoxifen prevented the growth of H295R both *in vitro* [7] and as xenografts *in vivo* [5]. Thus, ESR1 could be a promising target to reduce ACC growth.

Indeed, a recent study [8], investigating a large cohort of advanced ACC, confirmed the presence of a large number of potentially targetable molecules involved in ACC progression. These observations confirm that ACC is an extremely heterogeneous disease and that its pathogenesis involves integration of signals and the interplay of downstream pathways. It is currently accepted that these changes are also associated with a profound reprogramming of cellular metabolism [9]. Consequently, one potential strategy to develop an effective therapy for ACC could be the identification of a common downstream target of multiple pathways capable of controlling expression and activity of various bioenergetic factors.

Estrogen Related Receptor α (ERRα) is an orphan member of the nuclear hormone receptor superfamily of transcription factors that has been identified on the basis of its high level of sequence identity to ERα and for which an endogenous ligand has yet to be defined [10]. ERRα functions downstream of the peroxisome proliferator-activated receptor gamma coactivator-1 alpha and beta (PGC-1α and PGC-1β) and regulates the expression of genes involved in energy metabolism and mitochondrial biogenesis such as genes encoding enzymes and proteins of the tricarboxylic acid cycle, pyruvate metabolism, oxidative phosphorylation, and electron transport [11]. Research to understand how changes in cell metabolism promote tumor growth has accelerated in recent years [12]. As a consequence, research has focused on targeting metabolic dependencies of cancer cells, an approach with the potential to have a major impact on patient care. Notably, ERRα has recently been associated with dysregulated cell metabolism and cancer progression. Accordingly, increased expression of ERRα has been shown in several cancerous tissues including breast [13], ovary [14] prostate [15] and colon [16]. Several signaling pathways, also relevant to ACC development have been shown to converge upon and regulate the expression and activity of ERRα together with its coactivators such as PGC-1α and β in others tumor types [17]. Several studies have reported that ERRα inverse agonist XCT-790 [18] can induce cell growth arrest in different tumor cell lines [19, 20]. To date, few studies have investigated the role of ERRα in adrenal gland and ACC. ERRα is expressed in normal adult adrenal and regulates the expression of enzymes involved in steroidogenesis [21]. Moreover, ERRα seems to be more expressed in ACC compared to normal adrenal and adenoma [22].

The aim of this study was to establish if ERRα depletion using XCT790 can induce growth arrest in ACC cells. The data obtained support the hypothesis that ERRα could be a promising target for the treatment of adrenocortical cancer.

RESULTS

ERRα inverse agonist XCT790 decreases ERRα protein content and inhibits ACC cells proliferation *in vitro*

First, we verified that ERRα is expressed in H295R adrenocortical cancer cells. MCF-7 breast cancer cells were used as positive control [23] (Figure 1A). Moreover, we also demonstrated that in both H295R and MCF-7 cells, XCT790 treatment decreased ERRα protein levels in a dose-dependent manner (Figure 1B). The latter results confirmed the ability of XCT790 to reduce the expression of ERRα most probably by proteasome degradation [23]. Next, we evaluated the effects of different concentrations of ERRα inverse agonist XCT790 on ACC cell growth. Results from MTT assay revealed that XCT790 treatment exerted a dose- and time-dependent inhibition on H295R cell proliferation compared to vehicle-treated cells (Figure 1C). The maximum inhibitory effect on ACC cell proliferation was seen at 10 μM XCT790 that was then used for all the following experiments.

ERRα inverse agonist XCT790 inhibits ACC cells proliferation *in vivo*

We next established H295R cell xenograft tumors in immunocompromised mice to investigate the ability of XCT790 to reduce tumor growth *in vivo*. To this aim, H295R cells were injected into the intrascapular region of mice. When tumors reached an average volume of 200 mm³, animals were randomized into two groups to be treated with either vehicle or XCT790 (2,5 mg/Kg). As shown in Figure 2A, mice treated with XCT790 displayed a significant tumor growth reduction compared to the vehicle treated control group. Accordingly, tumor reduction upon XCT790 treatment is evidenced both in terms of tumor mass (Figure 2B) and proliferation as seen in Figure 2C, showing a strong decrease in Ki67 staining (value score control: $7.2 \pm 0,46$ (SD); value score XCT790 treated cells: $4.7 \pm 0.53*$ (SD), $*p < 0.05$).

ERRα inverse agonist XCT790 blocks G1/S transition of ACC cells without inducing apoptosis

The observed effects of XCT790 on ACC cells proliferation led us to evaluate XCT790 action on H295R cell cycle progression.

First, by analyzing PI staining with FACSJazz flow cytometer, we investigated whether XCT790 treatment could affect the distribution of cells within the three major phases of the cycle. To this aim, H295R cells were grown for 24 h in 5% CS-FBS and then treated with either vehicle (DMSO) or 10 μM XCT790. 48 hours later, FACS analysis revealed that XCT790 treated cells accumulated
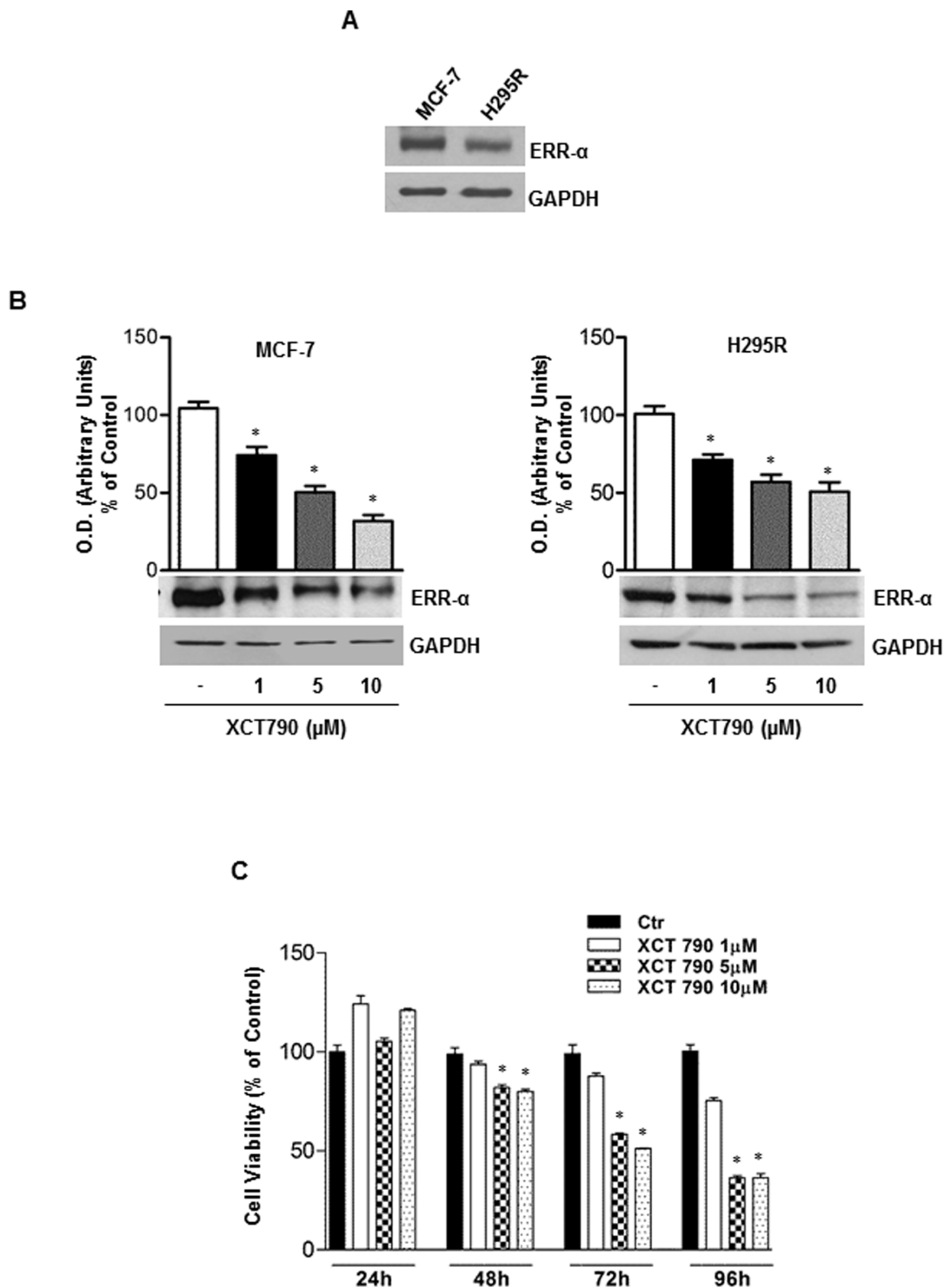
Figure 1: ERRα inverse agonist XCT790 decreases ERRα protein content and H295R cells growth *in vitro*. A. Western blot analysis of ERRα was performed on 50 μg of total proteins extracted from H295R and MCF-7 cells. Blots are representative of three independent experiments with similar results. (**B.** lower left and right panel), protein extracts from MCF-7 and H295R cells left untreated (–) or treated for 48 h with different doses of XCT790 were resolved by SDS-PAGE and subjected to immunoblot against ERRα. GAPDH served as loading control. (b, upper left and right panel), graphs represent means of ERRα optical density (O.D.) from three independent experiments with similar results normalized to GAPDH content (*$p < 0.001$ compared to untreated control sample assumed as 100). **C.** Cell viability after XCT790 treatment was measured using MTT assay. Cells were plated in triplicate in 24-well plates and were untreated (Ctr) or treated with increasing concentrations of XCT790 for the indicate times in DMEM supplemented with 2,5% Charcoal-Stripped FBS. Absorbance at 570 nm was measured on a multiwell-plate reader. Cell viability was expressed as a percentage of control, (*$p < 0.001$).
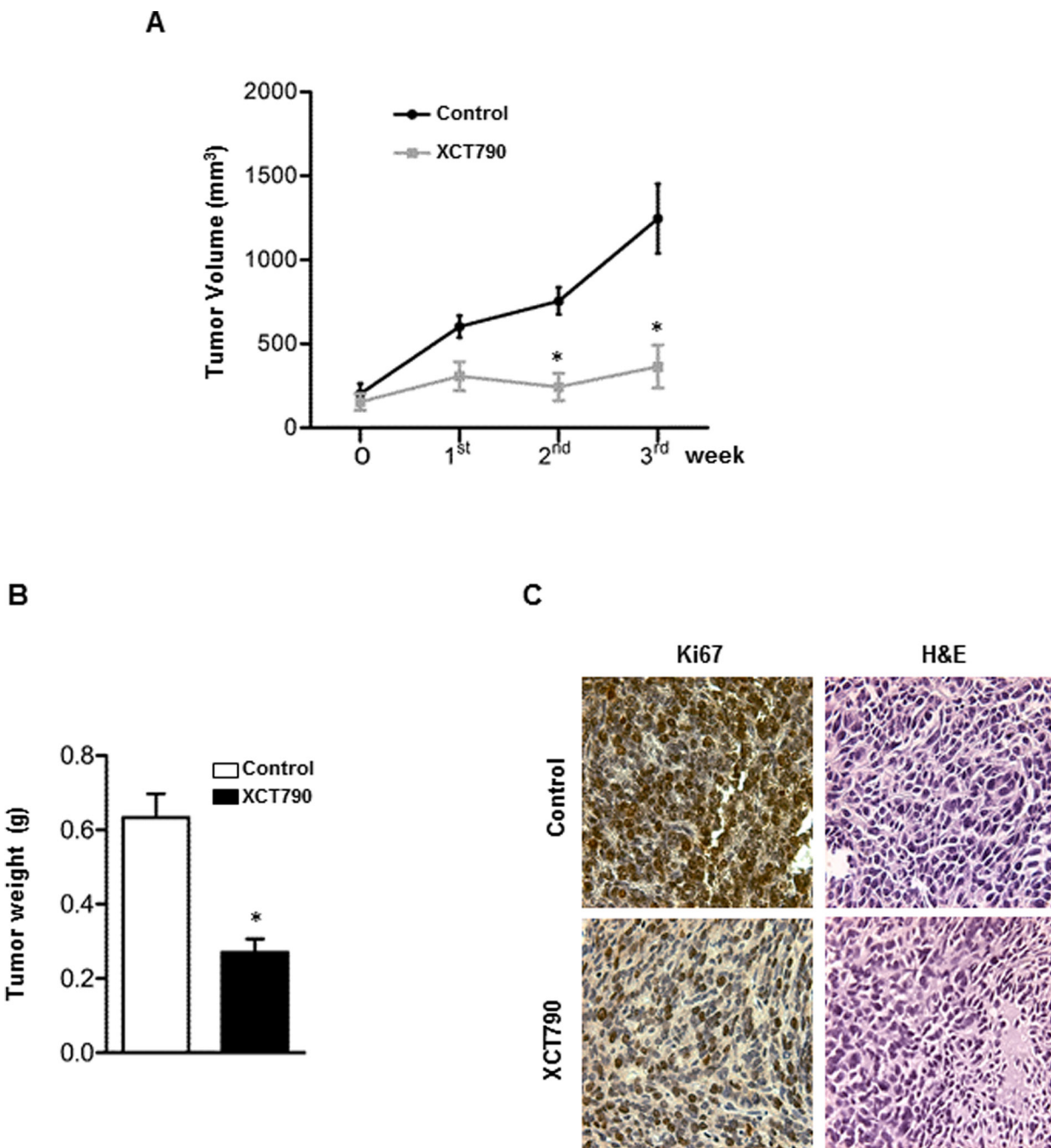
Figure 2: ERRα inverse agonist XCT790 decreases H295R cells proliferation *in vivo*. A. 6×10^6 H295R cells were injected subcutaneously onto the intrascapular region of immunocompromised mice and the resulting tumors were grown to an average of 200 mm³. The animals were randomized to vehicle controls or XCT790 treatment for twenty one days. Tumor volumes were calculated, as indicated in Materials and Methods. Values represent the mean ± SE of measured tumor volume over time in the control group (filled circles, *n* = 10) and in the XCT790-treated group (filled squares, *n* = 10). **B.** After 21 days (3 weeks) tumors were harvested and weighed. Values represent the mean ± SE of measured tumour weight (*n* = 10) *P < 0.05 versus control at the same day of treatment. **C.** Ki67 immunohistochemical and H & E staining: histologic images of H295R explanted from xenograft tumors (magnification X 400).

in the G0/G1-phase of the cell cycle while the fraction of cells in S phase decreased compared with vehicle treated cells (Figure 3A).

In order to define the molecular mechanisms involved in XCT790-dependent cell cycle arrest, changes in levels of protein involved in cell cycle regulation were investigated by Western blotting analysis. After

48 h treatment, XCT790 reduced Cyclin D1 and Cyclin E protein content while expression levels of CDK2 and CDK4 proteins were unaffected. Consistently with the observed G1/S transition arrest of the cell cycle, Rb protein showed a hypophosphorylated status (Figure 3B–3C). As the analysis of the cell cycle revealed a minimal increase of the sub-G1 fraction (Figure 3A), a known
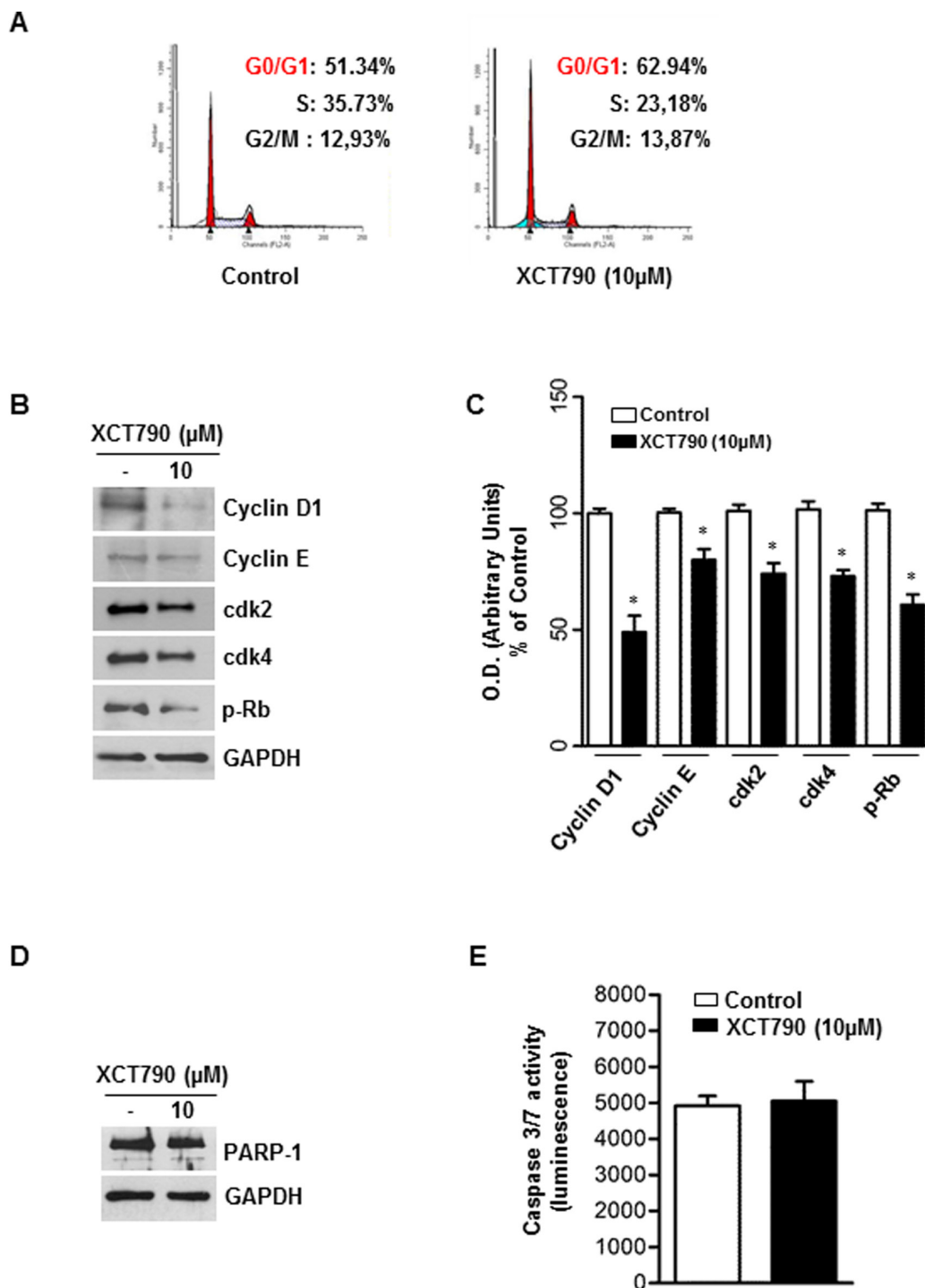
Figure 3: ERRα inverse agonist XCT790 impairs G1/S transition of ACC cells without inducing apoptosis. A. The distribution of H295R cells in the cycle was determined by Flow Cytometry using Propidium-iodide (PI) stained nuclei. The graph shows the distribution of H295R cell population (%) in the various phases of cell cycle. **B.** Total proteins from H295R cells left untreated (−) or treated with XCT790 for 48 h were resolved by SDS-PAGE and subjected to immunoblot analysis using specific antibodies against human Cyclin D1, Cyclin E, cdk2, cdk4, p-Rb. **C.** Graphs represent means of Cyclin D1, Cyclin E, cdk2, cdk4, p-Rb optical densities (O.D.) from three independent experiments with similar results normalized to GAPDH content, (*$p < 0.001$ compared to each untreated control assumed as 100); **D.** Total proteins were analyzed by Western blot for PARP-1. Blots are representative of three independent experiments with similar results. GAPDH served as loading control. **E.** Cellular caspase 3/7 activity was determined by Caspase-Glo assay system using the substrate Ac-DEVD-pNA and expressed as relative luminescence units (RLU) of treated cell to untreated control cell. Each column represents the mean ± SD of three independent experiments (*$p < 0.001$ compared to untreated control sample).

marker of apoptotic events, we next attempted to verify the presence of apoptotic features such as PARP-1cleavage and caspase 3/7 activation, all well-known biochemical markers of programmed cell death. Surprisingly, results from Western blotting analysis for PARP-1 (Figure 3D) and caspase 3/7 activity assay (Figure 3E) clearly showed that XCT790 did not activate an apoptotic pathway.

XCT-790 decreased mitochondrial mass and function in ACC cells

The activity of ERRα is highly dependent on the presence of coactivator proteins, most notably PGC-1α and PGC-1β [24], both known for their crucial role in regulating energy metabolism and mitochondrial biogenesis [24]. Moreover, it has been observed that XCT790 treatment, causing ERRα proteasome degradation, also down-regulates PGC1-α [24]. Based on these observations, we first checked if XCT790 treatment regulates PGC1-α expression in H295R cells. To this aim, ACC cells were left untreated or treated with 10 μM XCT790 for 48 h. Results from Western blotting showed (Figure 4A–4B) that XCT790 treated cells display a reduced expression of PGC1-α, with no effect on PGC-1β levels. We then asked whether reduced levels of PGC1-α would lead to reduction of mitochondrial mass. To this purpose we treated cells with MitoTracker deep red FM that stains specifically mitochondria independently of their membrane potential. Using flow cytometric analysis (Figure 4C), fluorescent imaging (Figure 4D) and fluorescent plate reader (Figure 4E), we found that XCT790 significantly decreased mitochondrial mass.

The mitochondrial citrate carrier CIC is a protein that belongs to a family of metabolites transporters embedded in the inner mitochondrial membrane [25, 26] and has been recently highlighted as important component in maintaining mitochondrial integrity and bioenergetics in normal and particularly in tumor cells [27]. We used CIC protein expression as a marker of both mitochondrial mass and function and found that XCT790 decreased mitochondrial CIC expression (Figure 4F–4G) as well as its transport activity (Figure 4H) in H295R-treated cells compared to vehicle-treated control cells.

To extend these findings, we used immunoblotting to monitor the abundance of a known reliable marker of mitochondrial mass, TOM20, in response to 10 μM XCT790 treatment. We found that XCT790 treated-H295R cells displayed a reduced expression of ERRα, as expected, concomitantly with a drastic decline of TOM20 protein expression (Figure 5A–5B). Similarly, the analysis of the expression of the mitochondrial oxidative pathway (OXPHOS) enzymes showed a substantial reduction of all the complexes (Figure 5C). In agreement with these findings, the reduction in the ATP content reveals a bioenergetics failure induced by XCT790 in treated cells (Figure 5D).

XCT790 induce cell death by necrosis in ACC cells

Very recent data revealed that low levels of CIC or its impaired expression induce mitochondrial dysfunction followed by enhanced mitochondrial turnover via autophagy/mitophagy mechanism [27]. Based on this observation and accordingly to our above reported results showing the ability of XCT790 to down-regulate CIC expression in H295R cells, we wanted to verify if autophagic features were detected in our experimental conditions. Autophagy is characterized by acidic vacuoles (AVO) formation, which can be measured by acridine orange (AO) vital staining. AO moves freely to cross biological membranes and accumulates in acidic compartment, where it is seen as bright red fluorescence [28]. As shown in Figure 6A (upper panel), AO vital staining of 48 h XCT790-treated H295R cells showed the accumulation of AVO in the cytoplasm. To quantify the accumulation of the acidific component, we performed FACS analysis of acridine orange-stained cells using FL3 mode (> 650 nm) to quantify the bright red fluorescence and FL1 mode (500–550 nm) for the green fluorescence. As shown in Figure 6A (lower panel), XCT790 treatment raised the strength of red fluorescence from 7,5% to 51%. These results corroborate the observation that XCT790, increases the formation of AVOs which suggests autophagy/mitophagy as possible mechanisms to explain the reduced mitochondrial mass. This latter event could be responsible for the inhibitory effects on cell growth elicited by XCT790 on adrenocortical cancer cells. A careful evaluation of the autophagic/mitophagic process by investigating changes in autophagic markers such as Beclin 1, LC3B, BNIP3 and Cathepsin B (Figure 6B), suggested that XCT790 treatment promotes the initial stages of the autophagic process. This is supported by the evidence of increased Beclin 1 expression and the presence of the cleaved LC3B form [29]. However, autophagy fails to terminate as indicated by decreased BNIP3, Cathepsin B and Lamp1 proteins expression [29]. Therefore, we evaluated XCT790 ability to induce H295R cells death by necrosis. To this aim, Trypan blue exclusion test was performed after 48 h of XCT790 treatment. As shown in Figure 6C, H295R displayed a significant increase in the number of positive stained cells compared to control cells indicating that membrane integrity and permeability were lost accounting for a necrotic event following a bionergetic failure triggered by ERRα depletion.

DISCUSSION

The molecular heterogeneity and complexity that characterize adrenocortical cancer biology combined with lack of an effective treatment, drive towards the discovery of new therapeutic targets. Advances in the understanding of the molecular pathogenesis of ACC have
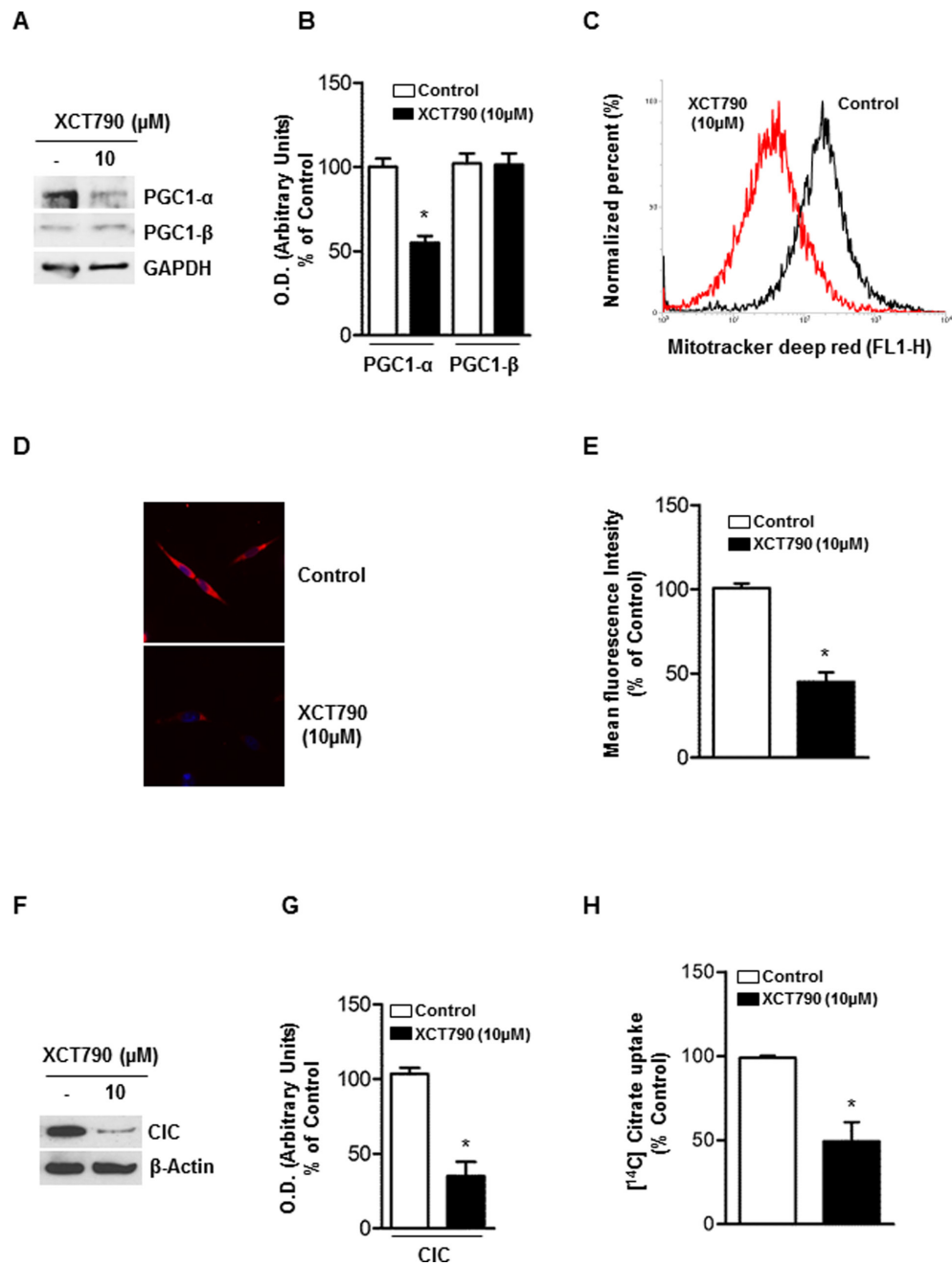
Figure 4: XCT-790 decreases mitochondrial mass and function in H295R cells. A. Total protein extracts from H295R cells, left untreated (–) or XCT790 treated in 2.5% DCC-FBS medium for 48 h were analyzed by Western blot with antibodies against PGC-1α and PGC-1β. GAPDH was used as loading control. **B.** Graphs represent means of PGC-1α and β optical densities (O.D.) from three independent experiments with similar results normalized to GAPDH content (*$p < 0.001$ compared to each untreated control sample assumed as 100). **C.** H295R cells were right untreated (control) or treated with XCT790. 48 h later, absorption of MitoTracker deep red FM was determined by FACS analysis. The uptake of MitoTracker was used as an indicator for the mitochondrial mass. **D.** Reduction in mitochondrial mass was further evaluated by fluorescence microscopy of MitoTracker-stained cells. **E.** Quantification of Mito-Tracker fluorescent signal intensity in untreated (control) or XCT790-treated H295R cells was evaluated measuring red fluorescent signal by a fluorescent plate reader (ex. 644; em. 665) *$p < 0,001$ compared to untreated control sample. **F.** Immunoblots for CIC expression from mitochondrial extracts in untreated (–) or XCT-790 treated H295R cells for 48 h. β-Actin served as loading control. Blots are representative of three independent experiments with similar results. **G.** Graph represent means of CIC density (O.D.) from three independent experiments with similar results normalized to β-Actin content (*$p < 0.001$ compared to untreated control sample assumed as 100). **H.** CIC activity was measured at 20 min as steady-state levels of citrate/citrate exchange. Transport was started by adding 0.5 mM [14C]Citrate to proteoliposomes preloaded internally with 10 mM citrate and reconstituted with mitochondria isolated from untreated H295R cells (Control; white column) and H295R-treated cells (black column). The transport reaction was stopped at 20 minutes. Results are expressed as percentage of the control. The data represent means ± SD of at least three independent experiments.
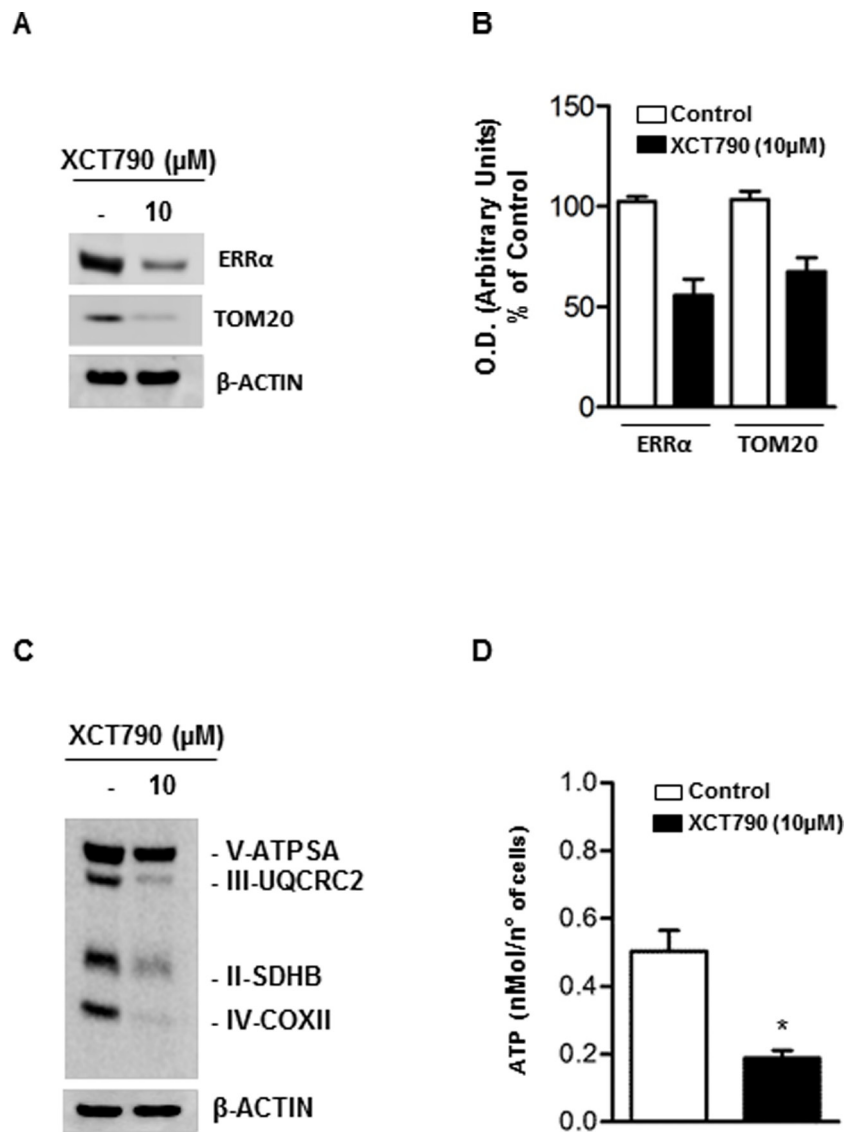
Figure 5: XCT790 decreased OXPHOS protein content and ATP concentration in H295R cells. A. Total protein extracts from H295R cells, left untreated (–) or treated for 48 h in 2.5% DCC-FBS medium with 10 μM XCT790, were analyzed by Western blot using antibodies against ERRα and TOM20. β-actin was used as loading control. **B.** Graphs represent means of ERRα and TOM20 optical densities (O.D.) from three independent experiments with similar results normalized to β-Actin content (*$p < 0.001$ compared to each untreated control sample assumed as 100). **C.** Total protein extracts from H295R cells left untreated (–) or treated for 48 h in 2.5% DCC-FBS medium with 10 μM XCT790, were analyzed by Western blot experiments using antibodies against OXPHOS subunits. β-Actin was used as loading control. Blots are representative of three independent experiments with similar results. **D.** ATP concentrations in H295R cells untreated (–) or treated with XCT790 were determined as described in Material and Methods and expressed as nmol/number of cells. Each column represents the mean ± SD of three independent experiments (*$p < 0, 001$).

been made based on studies of gene expression profiling and genetic syndromes associated with the development of ACC [30]. Results from these studies have highlighted the presence of different and important modifications such as somatic TP53 mutations, alterations at 11p15, a chromosomal locus of IGFII, H19 and cyclin-dependent kinase inhibitor 1C, β-catenin accumulation and activation of the Wnt signaling pathway and overexpression of SF-1 protein [30]. Moreover we have recently demonstrated the involvement of ESR1 in ACC cell growth regulation [5]. Genetic modifications and molecular pathways alterations

have as a common purpose the survival and proliferation of the transformed phenotype. It is currently accepted that these changes are associated with a concurrent adaptation and reprogramming of cellular metabolism [31]. In this scenario adrenocortical tumors are not an exception and the metabolic receptor ERRα represents a good therapeutic target. In fact, ERRα is a common downstream target of multiple pathways and a key factor in controlling the expression and activity of various bioenergetics processes. Indeed, it has already been observed that high ERRα gene expression correlates with unfavorable clinical outcomes
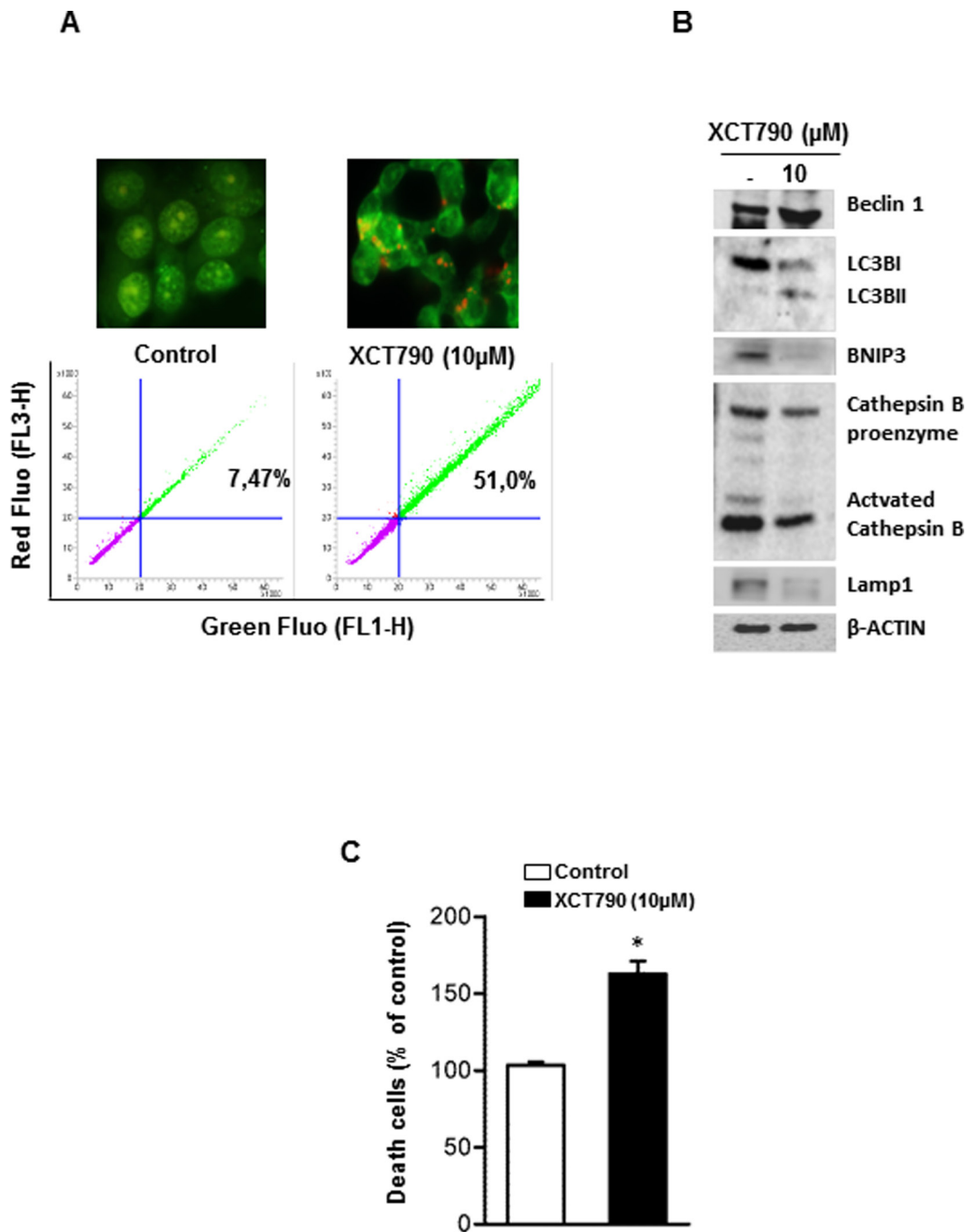
Figure 6: XCT790 induces necrosis in H295R cells. A. H295R cells were left untreated (control) or treated with XCT790 10 μM. After 48 h, cells were incubated with (1 μg/mL) acridine orange (AO) solution for 30 min at 37°C. Absorption of AO was determined by FACS analysis (lower panel). In the same experimental conditions, treated or untreated H295R cells were stained with acridine orange, mounted and immediately analyzed by fluorescent microscope (upper panel). **B.** Total protein extracts from H295R cells left untreated (–) or treated in 2.5% DCC-FBS medium with XCT790, as indicated, for 48 h were analyzed by Western blot experiments using antibodies against Beclin 1, LC3B, BNIP3, Cathepsin B, Lamp1. β-Actin was used as loading control. Blots are representative of three independent experiments with similar results. **C.** Cell death by necrosis was assessed by Trypan blue-exclusion assay in H295R cells untreated (–) or treated with XCT790. The mean ± SD of three replicates are shown. Cell death was expressed as a percentage of control, (*$p < 0.001$).

in breast [32] and ovarian cancer [14, 33] and that breast cancer cells exhibiting high ERRα activity are more sensitive to growth inhibition by an ERRα inverse agonist such as XCT790 [34]. Consistent with this findings and

with very recent data reporting high ERRα expression in adrenal tumors compared to benign and normal adrenal gland [22], here we report that ERRα is expressed in H295R cells, the most valid cell model to study ACC

biology. Moreover, our data show that pharmacological down-regulation of ERRα expression impaired H295R cell proliferation *in vitro* in a dose-dependent fashion. Most importantly, the same inhibitory effect was obtained also in *in vivo* experiments using H295R cells as xenograft model. At the molecular level, the growth inhibition is associated with a G0/G1 cell cycle arrest and by the decreased levels of G1-phase markers such as Cyclin D1 and pRb while CDKs protein levels were unaffected. Noteworthy, cell cycle arrest was not followed by any apoptotic event since we were unable to detect any morphological data (data not shown) or biochemical events such caspase activation and PARP-1 cleavage.

Accumulating data provide evidence that a caspase-independent form of programed cell death such as autophagy can be at play under certain conditions [35]. Therefore we investigated whether the inhibitory effects induced by XCT790 treatment could be linked to autophagy. Our results indicated that XCT790 caused a significant increase in autophagic vesicles. Concomitantly, we observed a drastic reduction in the expression of PGC1-α protein, which plays a key role in mitochondrial biogenesis, and of mitochondrial carrier CIC. The reduction of mitochondrial mass, also confirmed by the reduction of TOM20 protein expression, is followed by a considerable and significant decrease in the ATP concentration. Despite the presence of some autophagic markers such as the up-regulation of Beclin 1 and the cleaved form of LC3 protein, the formation of autophagolysosomes seems to be incomplete as evidenced by the reduction in LAMP1 protein, known to play an important role during the final steps of autophagy process [36]. A possible explanation could be a considerable reduction in the availability of intracellular ATP, required to drive forward the active cell death mechanism including autophagy. On the other hand, we cannot exclude that the observed initial steps of autophagy are a defense cell response to keep cells alive during energy failure to counteract the reduced expression and activity of the master bioenergetic executor ERRα. Moreover, the bioenergetics crisis following treatment with ERRα inverse agonist might be responsible for the loss of plasma membrane integrity, a key signature for a necrotic cell death, allowing the significant increase in the number of Trypan blue stained cells.

However, our most significant finding is that in ACC cells ERRα depletion after XCT790 treatment clearly caused a reduction of mitochondrial function and mass leading to the activation of a number of cellular mechanisms that result in tumor cell death.

It's now well known that mitochondria with its direct involvement in bioenergetics, biosynthesis and cell signaling are mandatory for tumorigenesis. Thus, it's not surprising that many studies have begun to demonstrate that mitochondrial metabolism and signaling is potentially a successful avenue for cancer therapy. Moreover, ACC is (in most cases) characterized by steroids producing/secreting cancer cells highly dependent on functioning mitochondria to ensure steroidogenic processes. For these reasons, strategies using mitochondrial metabolism and signaling as targets should be particularly effective for ACC treatment. Moreover, our current data obtained performing *in vivo* experiments by using H295R cells as xenograft model and according to previous *in vivo* studies performed in breast [37] and leukemia [38] tumor cells also suggest that chemical depletion of ERRα may be specific for high energy demanding cells such as tumor cells without exerting any toxic effect on other tissues.

In conclusion, our study supports the hypothesis that ERRα represents a valid innovative/alternative target for the treatment of adrenocortical cancer.

MATERIALS AND METHODS

Cell culture

H295R adrenocortical cancer cells were obtained from Dr. Antonio Stigliano (University of Rome, Italy) and cultured in DMEM/F12 supplemented with 1% ITS Liquid Media Supplement, 10% fetal bovine serum (FBS), 1% glutamine, 2% penicillin/streptomycin (complete medium) MCF7 breast cancer cells were maintained in monolayer cultures DMEM/F12. supplemented with 10% FBS, 1% glutamine, 2% penicillin/streptomycin. Both cell lines were cultured at 37°C in 5% CO_2 in a humidified atmosphere. All media and supplements were from Sigma-Aldrich, Milano, Italy.

Western blot analysis

Whole cell lysate were prepared in RIPA buffer (50 mM Tris-HCl, 150 mM NaCl, 1% NP-40, 0.5% sodium deoxycholate, 2 mM sodium fluoride, 2 mM EDTA, 0.1% SDS and a mixture of protease inhibitors) or in ice-cold lysis buffer (10 mM Tris-HCl pH 8, 150 mM NaCl, 1% Triton X-100, 60 mM octylglucoside). Samples were analyzed by 11% SDS-PAGE and blotted onto a nitrocellulose membrane. Blots were incubated overnight at 4°C with anti-ERRα polyclonal antibody, anti-cyclin D1, anti-cyclin E, anti-cdk2, anti-cdk4, anti-p-Rb, anti-PARP, anti-cathepsin B, anti-LAMP1, anti-Tom20 (all from Santa Cruz Biotechnology), anti-Beclin 1 (Novus Biological), anti-LC3B antibody, anti-BNIP3 antibody, Mitoprofile Total OXPHOS Human WB Antibody Cocktail (Abcam) and then incubated with appropriate horseradish peroxidase conjugated secondary antibodies for 1 h at room temperature. The immunoreactive products were detected by the ECL Western blotting detection system (Amersham Pharmacia Biotech, Piscataway, NJ). GAPDH antibody (Santa Cruz Biotechnology) or anti-β-Actin antibody (Sigma-Aldrich) were used as internal control.

Cell viability assay

H295R cells were seeded in 12-well plates at a density of 1×10^5 cells per well and cultured in complete medium overnight. Before treatment culture medium was switched into in DMEM F-12 supplemented with 2.5% charcoal stripped (CS) FBS and cells were untreated or treated with different concentration of XCT790 (Tocris Bioscience, Bristol, UK) for the indicated time. DMSO (Sigma-Aldrich) was used as vehicle control. Cell viability was measured using MTT assay (Sigma-Aldrich). Each experiment was performed in triplicate and the optical density was measured at 570 nm in a spectrophotometer. Experiments were repeated three times.

Trypan blue assay

Trypan blue stain was prepared freshly as a 0.4% solution in 0.9% sodium chloride before each experiment. After trypsinization, 20 µl cell suspension was added to 20 µl of Trypan blue solution and mixed thoroughly. Triplicate wells of dye positive cells from untreated or XCT790 treated were counted using a hemocytometer and the experiment was repeated three times.

Xenograft model

Athymic Nude- Foxn1^{nu} mouse 4–6 weeks old) from Charles River Laboratories [Calco (LC), Italy] were maintained in groups of five or less and quarantined for one week. Mice were kept on a 12 h light/dark cycle with ad libitum access to food and water.

6×10^6 H295R cells suspended in 100 µl of sterile PBS (*Dulbecco's* Phosphate Buffered Saline) and mixed with 100 µl of matrigel, were injected subcutaneously into the intrascapular region of each animal. When tumor size reached a volume of about 200 mm^3 mice were randomly divided in 2 groups. Animals were injected every other day with vehicle (soy oil) or XCT790 (2,5 mg/Kg) over a 21 day period. Tumors were measured with a caliper every two days, volumes were calculated using the formula $V = a\ b^2/2$ (*V:volume; a* is the length of the long axis, and *b* is the length of the short axis. At the end of the treatment period tumors were harvested and tumor weight and volumes were evaluated. All animal procedures were approved by the local Ethics Committee for Animal Research.

Immunohistochemical analysis

5 µm thick paraffin-embedded sections were mounted on slides precoated with poly-lysine, and then they were deparaffinized and dehydrated (seven to eight serial sections). Immuno-histochemical experiments were performed using rabbit polyclonal Ki67 primary antibody (Dako, Denmark) at 4°C over-night. Then, a biotinylated goat-anti-rabbit IgG was applied for

1 h at room temperature, followed by avidin biotin-horseradish peroxidase reaction (Vector Laboratories, CA). Immunoreactivity was visualized by using the diaminobenzidine chromogen (Sigma-Aldrich). Counterstaining was carried out with methylene-blue (Sigma-Aldrich). Hematoxylin and eosin Y staining was performed as suggested by the manufacturer (Bio-Optica, Milan, Italy).

Scoring system

The immunostained slides of tumor samples were evaluated by light microscopy using the Allred Score [39] which combines a proportion score and an intensity score. A proportion score was assigned representing the estimated proportion of positively stained tumor cells (0 = none; 1 = 1/100; 2 = 1/100 to <1/10; 3 = 1/10 to <1/3; 4 = 1/3 to 2/3; 5 = >2/3). An intensity score was assigned by the average estimated intensity of staining in positive cells (0 = none; 1 = weak; 2 = moderate; 3 = strong). Proportion score and intensity score were added to obtain a total score that ranged from 0 to 8. A minimum of 100 cells were evaluated in each slide. Six to seven serial sections were scored in a blinded manner for each sample.

Cell cycle analysis

H295R cells treated with different doses of XCT790 were fixed, treated with RNase A (20 µg/ml), stained with Propidium iodide (100 µg/ml) (Sigma-Aldrich) and analyzed by Flow Cytometry using BD FACSJazz™ Cell Sorter (Becton, Dickinson and Co) for DNA content and cell cycle status.

Caspases 3/7 activity assay

Caspases activity was measured with Caspase-Glo Assay Kit (Promega Italia SRL, Milano, Italy) following the manufacturer instruction. The luminescence of each sample was measured in a plate-reading luminometer (Gen5 2.01) with Synergy H1 Hybrid Reader. Each experiment was performed on triplicate wells per condition.

Mitochondrial mass determination

XCT790 treated or untreated H295R cells were incubated in serum free medium with 200 nM Mitotracker deep red (Invitrogen, USA) for 30 min at 37°C in the dark. After staining, cells were washed twice with cold PBS, trypsinized, centrifuged at 1200 rpm for 5 min and then resuspended in PBS. Absorption of MitoTracker deep red FM was determined by FACS analysis and by fluorescence microscopy. In the same experimental conditions, fluorescent signal intensity was also assessed using a fluorescent plate reader (ex. 644 nM; em. 665 nM).

Detection of acidic vesicular organelles (AVOs) with acridine orange

H295R cells were cultured on 6 well plates and treated in 2.5% CS-FBS with or without 10 μM XCT790. After 48 h, cells were washed with PBS and stained for 30 min at 37°C with 1 μg/mL acridine orange solution (Sigma-Aldrich). Cells were then washed three times with cold PBS and one drop of mounting solution was added. Cell were observed and imaged by an inverted fluorescence microscope (100X magnification). Accumulation of the acidic vacuoles was also determined by FACS analysis.

ATP Determination

1×10^5 cells were seeded in 96 white clear bottom multi-well plates in complete medium. Two days later, cells were treated in DMEM F-12 supplemented with 2.5% CS FBS containing 10 μM XCT790. After 48 h, ATP concentrations were determined using the CellTiter-Glo luminescent cell viability assay (Promega) following the manufacturer instruction. Results were normalized to the cell number evaluated by HOECHST staining (Sigma-Aldrich) and expressed as nMol/number of cells.

Mitochondria reconstitution and transport measurements

The transport activity was carried out as described previously [40]. Briefly, isolated mitochondria from untreated (control) or XCT790 treated H295R cells were solubilized in a buffer containing 3% Triton X, 114, 4 mg/ml cardiolipin, 10 mM Na2SO4, 0.5 mM EDTA, 5 mM PIPES pH 7. The mixture was incubated for 20 min and centrifuged at $138,000 \times g$ for 10 min. The supernatant was incorporated into phospholipid vesicles by cyclic removal of the detergent [41]. The reconstitution mixture consisted of 0.04 mg protein solution, 10% Triton X-114, 10% phospholipids (egg lecithin from Fluka, Milan, Italy) as sonicated liposomes, 10 mM citrate, 0.85 mg/ml cardiolipin (Sigma) and 20 mM PIPES, pH 7.0. The citrate transport was measured after external substrate removal from proteoliposomes on Sephadex G-75 columns, pre-equilibrated with buffer A (50 mM NaCl and 10 mM PIPES, pH 7.0). Transport at 25°C was started by the addition of 0.5 mM [^{14}C] citrate (Amersham) to the eluted proteoliposomes and terminated by the addition of 20 mM 1,2,3-benzene-tricarboxylate. Finally, the external radioactivity was removed from the Sephadex G-75 columns, liposomes radioactivity was measured and transport activity was calculated [41].

Statistics

All experiments were performed at least three times. Data were expressed as mean values ± standard deviation (SD), statistical significance between control and treated samples was analyzed using GraphPad Prism 5.0 (GraphPad Software, Inc.; La Jolla, CA) software. Control and treated groups were compared using the analysis of variance (ANOVA). A comparison of individual treatments was also performed, using Student's t test. Significance was defined as $p < 0.05$.

CONFLICTS OF INTEREST

The authors declare no conflicts of interest.

REFERENCES

1. Glover AR, Ip JC, Zhao JT, Soon PS, Robinson BG, Sidhu SB. Current management options for recurrent adrenocortical carcinoma. OncoTargets and therapy. 2013; 6:635–643.

2. Ronchi CL, Kroiss M, Sbiera S, Deutschbein T, Fassnacht M. EJE prize 2014: current and evolving treatment options in adrenocortical carcinoma: where do we stand and where do we want to go? European journal of endocrinology / European Federation of Endocrine Societies. 2014; 171:R1–R11.

3. Naing A, Lorusso P, Fu S, Hong D, Chen HX, Doyle LA, Phan AT, Habra MA, Kurzrock R. Insulin growth factor receptor (IGF-1R) antibody cixutumumab combined with the mTOR inhibitor temsirolimus in patients with metastatic adrenocortical carcinoma. British journal of cancer. 2013; 108:826–830.

4. Gicquel C, Bertagna X, Schneid H, Francillard-Leblond M, Luton JP, Girard F, Le Bouc Y. Rearrangements at the 11p15 locus and overexpression of insulin-like growth factor-II gene in sporadic adrenocortical tumors. The Journal of clinical endocrinology and metabolism. 1994; 78:1444–1453.

5. Sirianni R, Zolea F, Chimento A, Ruggiero C, Cerquetti L, Fallo F, Pilon C, Arnaldi G, Carpinelli G, Stigliano A, Pezzi V. Targeting estrogen receptor-alpha reduces adrenocortical cancer (ACC) cell growth *in vitro* and *in vivo*: potential therapeutic role of selective estrogen receptor modulators (SERMs) for ACC treatment. The Journal of clinical endocrinology and metabolism. 2012; 97:E2238–2250.

6. Barzon L, Masi G, Pacenti M, Trevisan M, Fallo F, Remo A, Martignoni G, Montanaro D, Pezzi V, Palu G. Expression of aromatase and estrogen receptors in human adrenocortical tumors. Virchows Archiv : an international journal of pathology. 2008; 452:181–191.

7. Montanaro D, Maggiolini M, Recchia AG, Sirianni R, Aquila S, Barzon L, Fallo F, Ando S, Pezzi V. Antiestrogens upregulate estrogen receptor {beta} expression and inhibit adrenocortical H295R cell proliferation. Journal of molecular endocrinology. 2005; 35:245–256.

8. De Martino MC, Al Ghuzlan A, Aubert S, Assie G, Scoazec JY, Leboulleux S, Do Cao C, Libe R, Nozieres C, Lombes M, Pattou F, Borson-Chazot F, Hescot S, Mazoyer C, Young J, Borget I, et al. Molecular screening for a personalized treatment approach in advanced adrenocortical cancer. The Journal of clinical endocrinology and metabolism. 2013; 98:4080–4088.

9. Cairns RA, Harris IS, Mak TW. Regulation of cancer cell metabolism. Nature reviews Cancer. 2011; 11:85–95.

10. Giguere V, Yang N, Segui P, Evans RM. Identification of a new class of steroid hormone receptors. Nature. 1988; 331:91–94.

11. Deblois G, Giguere V. Functional and physiological genomics of estrogen-related receptors (ERRs) in health and disease. Biochimica et biophysica acta. 2011; 1812:1032–1040.

12. Galluzzi L, Kepp O, Vander Heiden MG, Kroemer G. Metabolic targets for cancer therapy. Nature reviews Drug discovery. 2013; 12:829–846.

13. Ariazi EA, Jordan VC. Estrogen-related receptors as emerging targets in cancer and metabolic disorders. Current topics in medicinal chemistry. 2006; 6:203–215.

14. Fujimoto J, Alam SM, Jahan I, Sato E, Sakaguchi H, Tamaya T. Clinical implication of estrogen-related receptor (ERR) expression in ovarian cancers. J Steroid Biochem Mol Biol. 2007; 104:301–304.

15. Fujimura T, Takahashi S, Urano T, Kumagai J, Ogushi T, Horie-Inoue K, Ouchi Y, Kitamura T, Muramatsu M, Inoue S. Increased expression of estrogen-related receptor alpha (ERRalpha) is a negative prognostic predictor in human prostate cancer. International journal of cancer Journal international du cancer. 2007; 120:2325–2330.

16. Bernatchez G, Giroux V, Lassalle T, Carpentier AC, Rivard N, Carrier JC. ERRalpha metabolic nuclear receptor controls growth of colon cancer cells. Carcinogenesis. 2013; 34:2253–2261.

17. Deblois G, St-Pierre J, Giguere V. The PGC-1/ERR signaling axis in cancer. Oncogene. 2013; 32:3483–3490.

18. Busch BB, Stevens WC Jr, Martin R, Ordentlich P, Zhou S, Sapp DW, Horlick RA, Mohan R. Identification of a selective inverse agonist for the orphan nuclear receptor estrogen-related receptor alpha. Journal of medicinal chemistry. 2004; 47:5593–5596.

19. Wang J, Wang Y, Wong C. Oestrogen-related receptor alpha inverse agonist XCT-790 arrests A549 lung cancer cell population growth by inducing mitochondrial reactive oxygen species production. Cell proliferation. 2010; 43:103–113.

20. May FE. Novel drugs that target the estrogen-related receptor alpha: their therapeutic potential in breast cancer. Cancer management and research. 2014; 6:225–252.

21. Seely J, Amigh KS, Suzuki T, Mayhew B, Sasano H, Giguere V, Laganiere J, Carr BR, Rainey WE. Transcriptional regulation of dehydroepiandrosterone sulfotransferase (SULT2A1) by estrogen-related receptor alpha. Endocrinology. 2005; 146:3605–3613.

22. Felizola SJ, Nakamura Y, Hui XG, Satoh F, Morimoto R, K MM, Midorikawa S, Suzuki S, Rainey WE, Sasano H. Estrogen-related receptor alpha in normal adrenal cortex and adrenocortical tumors: involvement in development and oncogenesis. Molecular and cellular endocrinology. 2013; 365:207–211.

23. Lanvin O, Bianco S, Kersual N, Chalbos D, Vanacker JM. Potentiation of ICI182,780 (Fulvestrant)-induced estrogen receptor-alpha degradation by the estrogen receptor-related receptor-alpha inverse agonist XCT790. The Journal of biological chemistry. 2007; 282:28328–28334.

24. Chang CY, McDonnell DP. Molecular pathways: the metabolic regulator estrogen-related receptor alpha as a therapeutic target in cancer. Clinical cancer research : an official journal of the American Association for Cancer Research. 2012; 18:6089–6095.

25. Palmieri F. The mitochondrial transporter family SLC25: identification, properties and physiopathology. Molecular aspects of medicine. 2013; 34:465–484.

26. Dolce V, Rita Cappello A, Capobianco L. Mitochondrial tricarboxylate and dicarboxylate-tricarboxylate carriers: from animals to plants. IUBMB life. 2014; 66:462–471.

27. Catalina-Rodriguez O, Kolukula VK, Tomita Y, Preet A, Palmieri F, Wellstein A, Byers S, Giaccia AJ, Glasgow E, Albanese C, Avantaggiati ML. The mitochondrial citrate transporter, CIC, is essential for mitochondrial homeostasis. Oncotarget. 2012; 3:1220–1235.

28. Paglin S, Hollister T, Delohery T, Hackett N, McMahill M, Sphicas E, Domingo D, Yahalom J. A Novel Response of Cancer Cells to Radiation Involves Autophagy and Formation of Acidic Vesicles. Cancer research. 2001; 61:439–444.

29. Capparelli C, Whitaker-Menezes D, Guido C, Balliet R, Pestell TG, Howell A, Sneddon S, Pestell RG, Martinez-Outschoorn U, Lisanti MP, Sotgia F. CTGF drives autophagy, glycolysis and senescence in cancer-associated fibroblasts via HIF1 activation, metabolically promoting tumor growth. Cell Cycle. 2012; 11:2272–2284.

30. Xu Y, Qi Y, Zhu Y, Ning G, Huang Y. Molecular markers and targeted therapies for adrenocortical carcinoma. Clinical endocrinology. 2014; 80:159–168.

31. Cantor JR, Sabatini DM. Cancer cell metabolism: one hallmark, many faces. Cancer discovery. 2012; 2:881–898.

32. Deblois G, Giguere V. Oestrogen-related receptors in breast cancer: control of cellular metabolism and beyond. Nature reviews Cancer. 2013; 13:27–36.

33. Lam SS, Mak AS, Yam JW, Cheung AN, Ngan HY, Wong AS. Targeting estrogen-related receptor alpha inhibits epithelial-to-mesenchymal transition and stem cell properties of ovarian cancer cells. Molecular therapy : the journal of the American Society of Gene Therapy. 2014; 22:743–751.

34. Chang CY, Kazmin D, Jasper JS, Kunder R, Zuercher WJ, McDonnell DP. The metabolic regulator ERRalpha, a downstream target of HER2/IGF-1R, as a therapeutic target in breast cancer. Cancer cell. 2011; 20:500–510.

35. Parzych KR, Klionsky DJ. An overview of autophagy: morphology, mechanism, and regulation. Antioxidants & redox signaling. 2014; 20:460–473.

36. Eskelinen EL. Roles of LAMP-1 and LAMP-2 in lysosome biogenesis and autophagy. Molecular aspects of medicine. 2006; 27:495–502.

37. Chisamore MJ, Wilkinson HA, Flores O, Chen JD. Estrogen-related receptor-alpha antagonist inhibits both estrogen receptor-positive and estrogen receptor-negative breast tumor growth in mouse xenografts. Molecular cancer therapeutics. 2009; 8:672–681.

38. Michalek RD, Gerriets VA, Nichols AG, Inoue M, Kazmin D, Chang CY, Dwyer MA, Nelson ER, Pollizzi KN, Ilkayeva O, Giguere V, Zuercher WJ, Powell JD, Shinohara ML, McDonnell DP, Rathmell JC. Estrogen-related receptor-alpha is a metabolic regulator of effector T-cell activation and differentiation. Proceedings of the National Academy of Sciences of the United States of America. 2011; 108:18348–18353.

39. Allred DC, Harvey JM, Berardo M, Clark GM. Prognostic and predictive factors in breast cancer by immunohistochemical analysis. Modern pathology : an official journal of the United States and Canadian Academy of Pathology, Inc. 1998; 11:155–168.

40. Bonofiglio D, Santoro A, Martello E, Vizza D, Rovito D, Cappello AR, Barone I, Giordano C, Panza S, Catalano S, Iacobazzi V, Dolce V, Ando S. Mechanisms of divergent effects of activated peroxisome proliferator-activated receptor-gamma on mitochondrial citrate carrier expression in 3T3-L1 fibroblasts and mature adipocytes. Biochimica et biophysica acta. 2013; 1831:1027–1036.

41. Palmieri F, Indiveri C, Bisaccia F, Iacobazzi V. Mitochondrial metabolite carrier proteins: purification, reconstitution, and transport studies. Methods in enzymology. 1995; 260:349–369.
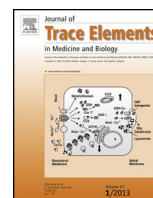
Analytical methodology

Determination of mercury in hair: Comparison between gold amalgamation-atomic absorption spectrometry and mass spectrometry

Francesco Domanico [a], Giovanni Forte [b], Costanza Majorani [b], Oreste Senofonte [b,*], Francesco Petrucci [b], Vincenzo Pezzi [a], Alessandro Alimonti [b]

[a] University of Calabria, Arcavacata di Rende (CS), Italy
[b] Italian National Institute for Health, Rome, Italy

ABSTRACT

Mercury is a heavy metal that causes serious health problems in exposed subjects. The most toxic form, i.e., methylmercury (MeHg), is mostly excreted through human hair. Numerous analytical methods are available for total Hg analysis in human hair, including cold vapour atomic fluorescence spectrometry (CV-AFS), inductively coupled plasma mass spectrometry (ICP-MS) and thermal decomposition amalgamation atomic absorption spectrometry (TDA-AAS). The aim of the study was to compare the TDA-AAS with the ICP-MS in the Hg quantification in human hair.

After the washing procedure to minimize the external contamination, from each hair sample two aliquots were taken; the first was used for direct analysis of Hg by TDA-AAS and the second was digested for Hg determination by the ICP-MS. Results indicated that the two data sets were fully comparable (median; TDA-AAS, 475 ng g^{-1}; ICP-MS, 437 ng g^{-1}) and were not statistically different (Mann-Whitney test; p = 0.44). The two techniques presented results with a good coefficient of correlation (r = 0.94) despite different operative ranges and method limits. Both techniques satisfied internal performance requirements and the parameters for method validation resulting sensitive, precise and reliable. Finally, the use of the TDA-AAS can be considered instead of the ICP-MS in hair analysis in order to reduce sample manipulation with minor risk of contamination, less time consuming due to the absence of the digestion step and cheaper analyses.

© 2016 Elsevier GmbH. All rights reserved.

1. Introduction

Mercury (Hg) is a dangerous metal and its presence in the environment and in the human food chain is a matter of increasing concern. It can occur in three forms: organic, inorganic and elemental. It is a toxic element that has not physiologic function in human body, but exposure to Hg can rise a wide range of effects, e.g., inattention, memory disturbance, learning problems, impairment of social behaviour, and low intelligence quotient [1]. Although high or repeated exposure to different forms of Hg can have serious health consequences, the most important toxicity risk that Hg poses to humans is as methylmercury (MeHg) which exposure is mainly through consumption of fish. MeHg is a neurotoxin and bioaccu-

mulates particularly in aquatic food webs. The sites where MeHg production is most intense in nature, in fact, are wetlands, lake sediments and anoxic bottom waters [2,3]. Once ingested, the 90–100% of MeHg is absorbed through the gastrointestinal tract, where it easily enters the bloodstream and distributes throughout the body. It is transported across the blood–brain barrier by an amino acid carrier and readily accumulates in the brain as well as it is able to cross the placenta and accumulates in fetal blood and brain [4]. The brain is the target where the MeHg exerts its toxic effects. Other molecular targets of MeHg exposure includes blood–brain barrier, cytoskeleton; axonal transport; neurotransmitter production, secretion, uptake and metabolism; cell signaling; protein, DNA, and RNA synthesis; respiratory and energy-generating systems [5]. In the adult, MeHg may create loss of neurons in both the visual cortex and the cerebellum, while in the developing brain MeHg affects the formation of microtubules, the neuronal migration and cell division [5–7]. The toxicity of the MeHg also depends on the degree of exposure. In particular, high level of exposure may result in a

loss of neurons in each lobe of the brain, and hyperactive reflexes, deafness, blindness, cerebral palsy, mental retardation and general paralysis. At low exposure levels deficits in language, learning and attention; motor and visual–spatial organizational impairments may be observed [8–10].

Considering the toxicity of MeHg, the United States Environmental Protection Agency (US-EPA) has set a reference dose (RfD) for ingested MeHg of 0.1 $\mu g\,kg^{-1}$ body weight per day, where the RfD represents the amount of MeHg that can be ingested over a lifetime without producing adverse health outcomes [11]. In addition, the World Health Organisation (WHO) recommended a maximum intake of MeHg of 1.6 $\mu g\,kg^{-1}$ per week [7].

The excretion of MeHg occurs through bile, feces, urine and lactation, but it is present also in hair. Generally, more than the 80% of the Hg in hair is as MeHg [7], which is taken up by the hair follicles as MeHg-cysteine complexes [12]. Considering that hair grows ca. 1 cm per month and that the half-life averages of MeHg in hair is about 65 days (range of about 35–100 days) [6,7], it would be possible to quantify the Hg load due to a long period of exposure [13]. Thus, epidemiological studies often use the total Hg concentrations in hair as biomarkers for MeHg exposure from fish consumption.

The presence of Hg in hair is generally evaluated by different techniques such as the cold vapor atomic fluorescence spectroscopy (CV-AFS) [14–16], cold vapor atomic absorption spectroscopy (CV-AAS) [17,18], inductively coupled plasma atomic emission spectrometry (ICP-AES) [19] and inductively coupled plasma mass spectrometry (ICP-MS) [20]. All these techniques are sensitive, precise and supply reliable and reproducible data, but, on the other hand, they are very time-consuming techniques due to the pretreatment of samples (e.g., acid digestion of sample, Hg reduction by adding a reducing agent, etc.). Instead, the use of the thermal decomposition amalgamation atomic absorption spectrometry (TDA-AAS) allows to decrease the preparative steps number and, consequently, to reduce the time of analysis and sample contamination risk it is necessary to quantify Hg directly on the hair. This technique gained popularity for analysis of total Hg because of its ability to analyze both liquid and solid matrices effectively, to obtain high sample throughput, and relatively low detection limits and costs. The analysis involves thermal decomposition followed by gold amalgamation and detection with atomic absorption spectrometer. In this context, a TDA-AAS instrument was adopted, in according to US-EPA 7473 method, to quantify the level of Hg directly in hair of 114 individuals. In addition, a quantification of the metal was also performed by the ICP-MS technique in the same hair samples previously digested. The performances of the two techniques were, finally, compared.

Table 1
DMA-80 TRICELL and iCAP Q instrumental setting.

DMA-80 TRICELL	
Air flow (mL min^{-1})	200
Drying	350 °C for 60 s
Decomposition and catalysis	650 °C for 180 s
Purge time 1	60 s
Amalgamator	650 °C for 12 s
Purge time 2	60 s
iCAP Q	
RF power	1550 w
Argon gas flow (L min^{-1})	Plasma gas, 14; Auxiliary, 0.8; Nebulizer gas, 1.08
KED barrier	2 V
Analytical parameters	Dwell time 80 ms per peak, 50 sweeps, 3 replicates
Analytical masses	^{202}Hg
Internal standard	^{115}In

2. Materials and methods

2.1. Study population

The population included 114 healthy individuals living in an urban area of South Italy. Subjects were interviewed to obtain detailed information on family, dietary habits, lifestyle and potential exposures and gave the informed consent. The study protocol was approved by the Institutional Ethical Committee of the Italian National Institute for Health.

2.2. Sample collection and washing

Hair samples were cut from the sub-occipital zone of the head at ca. 1 cm from the scalp, collected in individual plastic bags and stored in a desiccator kept in the dark before use. To avoid external contamination due to environmental dirt and dust, sweat and desquamation of the skin, as well as detergents and cosmetic treatments the hair samples were submitted to adequate wash intervention in order to eliminate the external metals contamination. The procedure adopted in this work is based on the following steps: i), three washes (10 min each) under continuous stirring in a mixture of 3:1 (v/v) ethyl ether/acetone (Sigma-Aldrich, St. Louis, MO, USA) to remove the sweat; ii), soaking under stirring 1 h in 5% sodium ethylenediamine tetracetic acid (Sigma-Aldrich) to bind the chemical elements present on hair surface; iii), rinse with high purity deionized water (EASY-pure UV, PBI, Milan, Italy). After drying, from each hair sample two aliquots were taken; the first was used for direct analysis of Hg in solid samples by the DMA-80 TRICELL and the second was digested for Hg determination by the ICP-MS.

2.3. Samples digestion

Approximately 100–150 mg of desiccated hair were digested with 4 ml of ultrapure HNO$_3$ (VWR, Leuven, Belgium) and 1 ml of ultrapure H$_2$O$_2$ (Romil, Cambridge, Great Britain) on heat block (ModBlock, CPI International, Palo Alto, CA, USA) at 70 °C for 3–4 h and then diluted with ultrapure deionized water (up to 10 ml). Samples were stored at 4 °C until analysis. The same approach was also conducted for reagent blanks and for the hair-based certified reference material (ERM-DB001, Human Hair, IRMM, Geel, Belgium).

2.4. Instrumental parameter

A TDA-AAS technique (DMA-80 TRICELL model, Milestone Srl, Sorisole, Italy) is based on the sample combustion, preconcentration by amalgamation with gold and quantitative determination of Hg by atomic absorption spectrometry. Briefly, samples were weighed in quartz boats, placed on the combustion tube and heated at ~650 °C with air as a carrier gas. Gaseous combustion products were carried through a heated catalyst where the Hg species are converted to elemental Hg vapor (Hg^0) whereas halogens and other species that can interfere with the analysis are trapped. Mercury vapour are carried to a glass tube gold-coated sand where Hg^0 is selectively trapped. Later, the trap is rapidly heated to release Hg^0 vapour into a single beam spectrophotometer. Mercury concentration is calculated on the absorbance measured at 253.7 nm and on the weight of the sample. Table 1 shows the instrumental parameters used. A calibration curve from 0.1 ng to 200 ng is a general method for determining Hg by DMA-80 TRICELL. A 100 mg mL^{-1} standard solution of Hg (CPAchem, Stara Zagora, Bulgaria) was used to prepare the points of the calibration curve through dilution with high purity deionized water with resistivity of 18 MΩ cm (EASY-pure UV) stabilized with a final concentration of the 1% of HCl (Romil).

Table 2
Level of Hg in hair of 114 subjects. Concentrations in $ng\,g^{-1}$.

	Mean ± SD	Median	Geometric mean	5th percentile	95th percentile
DMA-80 TRICELL					
Total population	664 ± 593	475	460	105	1834
iCAP Q					
Total population	604 ± 551	437	428	129	1606
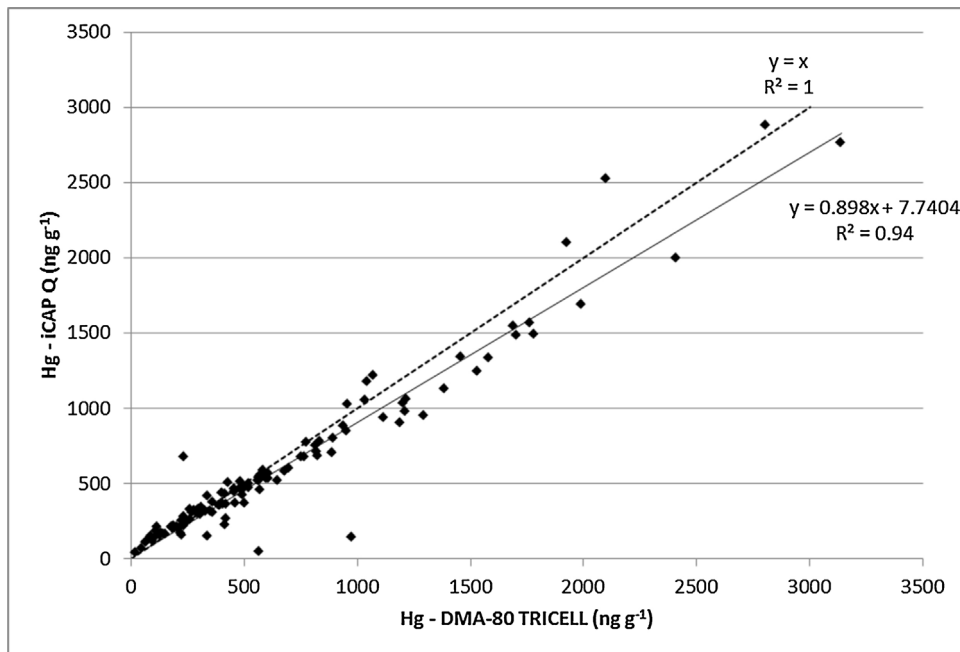
Fig. 1. Comparison between the DMA-80 TRICELL and the iCAP Q measurements.
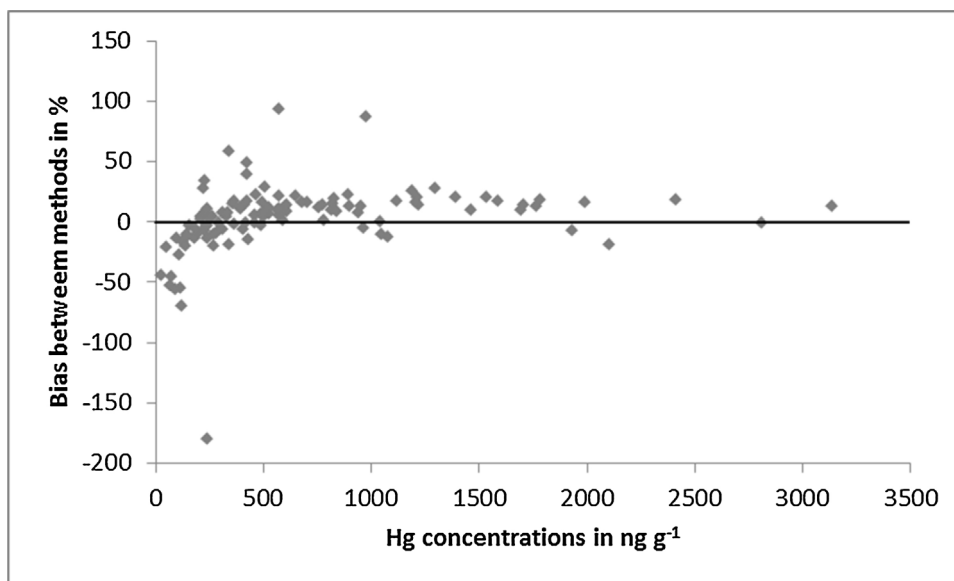
Fig. 2. Bias plot displaying the difference of the two methods in percentage.

Table 3
Precision intra-day and inter-day for the DMA-80 TRICELL expressed as CV%.

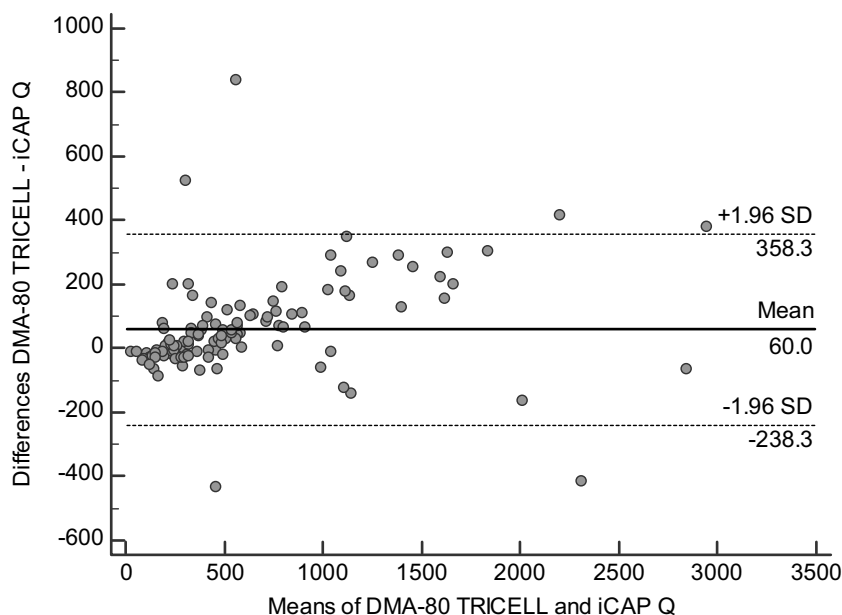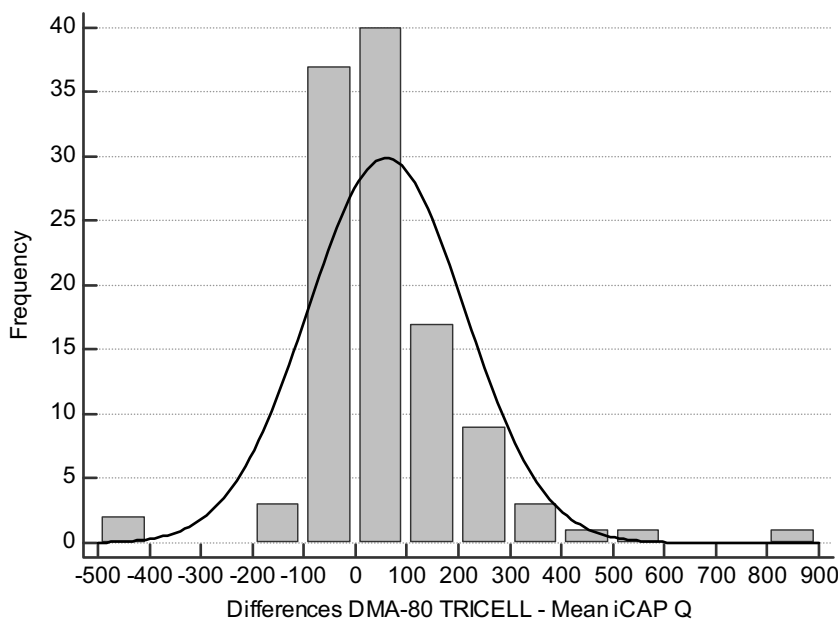|	Cell 0			Cell 1			Cell 2		
	$1\,ng\,g^{-1}$	$10\,ng\,g^{-1}$	$30\,ng\,g^{-1}$	$50\,ng\,g^{-1}$	$100\,ng\,g^{-1}$	$200\,ng\,g^{-1}$	$250\,ng\,g^{-1}$	$1000\,ng\,g^{-1}$	$2000\,ng\,g^{-1}$
Intra-day	15.5	3.83	5.54	5.92	6.32	5.49	4.17	1.04	1.47
Inter-day	25.6	2.44	3.32	2.93	5.55	3.85	2.08	2.47	2.72

Fig. 3. Bland-Altman plot.

Fig. 4. Distribution pattern of the differences between methods for each sample.

Approximately 25 mg of hair samples and of the certified reference material ERM–DB001 were weighed in a quartz boat and directly analyzed.

The ICP-MS instrument, namely an iCAP Q model (Thermo Fisher Scientific Inc., Waltham, MA, USA), was configured for routine ultra-trace elemental analysis. The instrument configuration and operation parameters are shown in Table 1. The iCAP Q used in this study was equipped with a PFA ST MicroFlow nebulizer (ESI, Omaha, NE, USA), a peltier cooled quartz cyclonic spray chamber operating at $3\,°C$, a 2.0 mm ID quartz injector, a demountable quartz torch and interface Nichel cones. Mercury was quantified with the standard addition calibration and Indium was used as the internal standard at the concentration of $1\,ng\,mL^{-1}$ in the analytical solution.

3. Results and discussion

The element concentrations, in terms of mean and standard deviation (SD), median, geometric mean, 5th and 95th percentiles, obtained with the two different techniques in 114 individuals are reported in Table 2. The two analytical methods gave results very similar each other, with a slight trend of ICP-MS to underestimate as respect to TDA-AAS, but with a smaller data spread.

The comparison of the results obtained with the two techniques was also reported in Fig. 1. The plot showed a good agreement between the two methodological approaches, the correlation coefficient, in fact, was 0.94, as also demonstrated by the data distribution close to an ideal line. To better highlight the consistency of the two methods, the bias in percentage between the DMA-80 TRICELL and the iCAP Q at the various Hg concentration

is reported in Fig. 2. In the x-axis is reported the Hg concentration and in the y-axis the per cent difference between the two methods calculated as follows: $Y\% = (Y\ DMA\text{-}80\ TRICELL - Y\ iCAP\ Q/Y\ DMA80\text{-}TRICELL)*100$, where Y DMA80-TRICELL and Y iCAP Q represented the Hg concentration observed with the two techniques for the same hair sample. From Fig. 2 it is possible to note that: *i)*, the 78% of the measures fall within the 20% bias. This means that the measures were very close each other and, thus, to the ideal line of the 0% bias; *ii)*, there was a tendency of increased bias between the two assays in the low concentration range, as expected for quantifications performed in the area with less sensitivity of the techniques leading to a greater difference between the two measurements; *iii)*, the 84% of the values provided by the DMA-80 TRICELL resulted higher than that obtained by the iCAP Q.

Furthermore, the comparison of the two datasets of measurements with the Mann-Whitney test gave a p = 0.44, indicating that the two data populations were not statistically different, as expected also considering the closeness of the Hg concentrations reported in Table 2.

Moreover, the distribution of the values was evaluated by the Bland-Altman plot, or difference plot, where the differences between the two techniques are plotted against the corresponding averages of the two techniques. The x-axis reported the average of the two measurements for each sample $(Xi = (X_{1i} + X_{2i})/2)$, while the y-axis indicated the difference $(di = X_{1i} - X_{2i})$. Horizontal lines are drawn at the mean difference and at the limits of agreement defined as the mean difference plus and minus 1.96 times the standard deviation of the differences. Information on the comparability of the two techniques are given by the position of the points in the graph. In Fig. 3 the points were randomly placed in the plot, i.e., the two techniques are interchangeable. In addition, if the two analytical methods are equivalent, the distribution of the differences has a Gaussian pattern, as well proved in Fig. 4.

The analytical performances for both methods were also determined. The limits of detection (LoD) and quantification (LoQ) were calculated using the 3σ and 10σ criteria, respectively, with a LoD = 2.60 ng g^{-1} and LoQ = 8.60 ng g^{-1} for the DMA-80 TRICELL and a LoD = 3.50 ng g^{-1} and LoQ = 11.5 ng g^{-1} for the iCAP Q.

Both analytical series exhibited an elevated grade of trueness and precision. The trueness was calculated in this case through the hair-based certified reference material ERM-DB001 obtaining a recovery of the 100% and 103% for the DMA-80 TRICELL and for the iCAP Q, respectively. The analytical precision was determined by the repeatability and by the within-laboratory reproducibility. The repeatability (intra-day) is the precision under repeatability conditions where independent results are obtained with the same method, on the same sample, in the same laboratory, by the same operator, using the same equipment, in a short interval of time. The within-laboratory reproducibility (inter-day) is the precision obtained in the same laboratory under predetermined conditions over long-term intervals [21]. In both cases, the precision was expressed as the coefficient of variation in percent (CV%). For the DMA-80 TRICELL the precision was calculated in the cells 0, 1 and 2 with ten replicate of Hg solution at three different levels of concentration for each cell analyzed in one run and in three different days, and the results are reported in Table 3. Whilst, for the iCAP Q, the precision intra-day and inter-day resulted to be the 1.8% and 1.5%, respectively. As regard the linearity, for the DMA-80 TRICELL it was evaluated for each reading cell at different Hg concentrations (ng g^{-1}): 1, 10, 30 for Cell 0; 50, 100, 200 for Cell 1 and 250, 1000, 2000 for Cell 2. The linearity for the iCAP Q was verified in the Hg concentration range of 0.1–10 ng mL^{-1}. In both cases, the linearity gave a correlation coefficient better than 0.995.

Finally, all the tests to evaluate the performances of two methods were considered satisfactory according to the internal requirements and parameters, therefore, both the DMA-80 TRICELL and the iCAP Q can be considered accurate, reproducible, sensitive and reliable techniques for the quantification of Hg in hair samples.

4. Conclusion

The Hg content of 114 hair samples was quantified by two very different techniques, namely TDA-AAS (DMA-80 TRICELL model) and ICP-MS (iCAP Q model). The analytical performances demonstrated that both techniques are sensitive, precise and supply reliable data. In addition, hair analysis indicated that the two techniques are fully consistent because gave similar results in the Hg quantification. This means that the two techniques can be used indifferently in this kind of determination. On the other hand, the use of the DMA-80 TRICELL might be preferable to the iCAP Q for a number of reasons, such as the reduction of the sample manipulation with minor risk of contamination, less time consuming due to the absence of the acid digestion cycle, cheaper analyses and the absence of matrix effects that could interfere with the measurements.

Conflict of interest

The authors have nothing to disclose.

References

[1] J. Stein, T. Schettler, D. Wallinga, M. Valenti, In harm's way: toxic threats to child development, J. Dev. Behav. Pediatr. 23 (2002) S13–S22.
[2] J.W.M. Rudd, Sources of methyl mercury to freshwater ecosystems: a review, Water Air Soil Pollut. 80 (1995) 697–713.
[3] C. Eckley, C.J. Watras, H. Hintelmann, K. Morrison, A. Kent, O. Regnell, Mercury methylation in the hypolimnetic waters of lakes with and without connection to wetlands in northern Wisconsin, Can. J. Fish. Aquat. Sci. 62 (2005) 400–411.
[4] L.E. Kerper, N. Ballatori, T.W. Clarkson, Methylmercury transport across the blood-brain barrier by an amino acid carrier, Am. J. Physiol. 262 (1992) R761–R765.
[5] A.F. Castoldi, T. Coccini, S. Ceccatelli, L. Manzo, Neurotoxicity and molecular effects of methylmercury, Brain Res. Bull. 55 (2001) 197–203.
[6] T.W. Clarkson, Mercury: major issues in environmental health, Environ. Health Perspect. 100 (1993) 31–38.
[7] WHO, Environmental Health Criteria 101: Methylmercury, World Health Organization, Geneva, 1990.
[8] L. Amin-Zaki, S. Elhassani, M.A. Majeed, T.W. Clarkson, R.A. Doherty, M. Greenwood, Intra-uterine methylmercury poisoning in Iraq, Pediatrics 54 (1974) 587–595.
[9] F. Bakir, S.F. Damluji, L. Amin-Zaki, M. Murtadha, A. Khalidi, N.Y. Al-Rawi, S. Tikriti, H.I. Dhahir, T.W. Clarkson, J.C. Smith, R.A. Doherty, Methylmercury poisoning in Iraq, Science 181 (1973) 230–241.
[10] H. Ino, K. Mizukoshi, Otorhinolaryngological findings in intoxication by organomercury compounds, in: T. Tsubaki, K. Irukayama (Eds.), Minamata Disease Methylmercury Poisoning in Minamata and Niigata, Kodanasha Ltd., Tokyo, 1977, pp. 186–208.
[11] NRC, Toxicological Effects of Methylmercury, National Research Council, Washington, 2000.
[12] E. Cernichiari, R. Brewer, G.J. Myers, D.O. Marsh, L.W. Lapham, C. Cox, C.F. Shamlaye, M. Berlin, P.W. Davidon, T.W. Clarkson, Monitoring methylmercury during pregnancy: maternal hair predicts fetal brain exposure, Neurotoxicology 16 (1995) 705–710.
[13] T. Davidson, Q. Ke, M. Costa, Selected molecular mechanisms of metal toxicity and carcinogenicity, in: G.F. Nordberg, B.A. Fowler, M. Nordberg (Eds.), Handbook on the Toxicology of Metals, Academic Press, Waltham, 2015, pp. 173–196.
[14] L. Adlnasab, H. Ebrahimzadeh, A.A. Asgharinezhad, M.N. Aghdam, A. Dehghani, S.A. Esmaeilpour, A preconcentration procedure for determination of ultra-trace mercury (II) in environmental samples eploying continuous-flow cold vapor atomic absorption spectrometry, Food Anal. Methods 7 (2014) 616–628.
[15] C.C. Brombach, B. Chen, W.T. Corns, J. Feldmann, E.M. Krupp, Methylmercury in water samples at the pg/L level by online preconcentration liquid chromatography cold vapor-atomic fluorescence spectrometry, Spectrochim. Acta B 105 (2015) 103–108.
[16] P.R. Aranda, R.A. Gil, S. Moyano, I.D. Vito, L.D. Martinez, Slurry sampling in serum blood for mercury determination by CV-AFS, J. Hazard. Mater. 161 (2009) 1399–1403.
[17] R.E. Sturgeon, J.X. Liu, M.M. Silva, Determination of mercury in gasoline by photochemical vapor generation coupled to graphite furnace atomic absorption spectrometry, Microchem. J. 117 (2014) 100–105.

[18] M.V. Balarama Khrisna, D. Karunasagar, Robust, ultrasound assisted extraction approach using dilute TMAH solutions for the speciation of mercury in fish and plant materials by cold vapor atomic absorption spectrometry (CV-AAS), Anal. Methods 7 (2015) 1997–2005.

[19] M.R. Ganjali, Y. Assadi, A. Kiani, P. Norouzi, A. Bidari, Assay of total mercury in commercial food supplements of marine origin by means of DLLME/ICP-AES, Food Anal. Methods 5 (2012) 695–701.

[20] H. Lin, D. Yuan, B. Lu, S. Huang, L. Sun, F. Zhang, Y. Gao, Isotopic composition analysis of dissolved mercury in seawater with purge and trap preconcentration and a modified Hg introduction device for MC-ICP-MS, J. Anal. At. Spectrom. 30 (2015) 353–359.

[21] Commission, Decision 2002/657/EC of 12 August 2002, Off. J. L221 (2002) 8–36.